



Universitat Autònoma de Barcelona

ADVERTIMENT. L'accés als continguts d'aquesta tesi queda condicionat a l'acceptació de les condicions d'ús establertes per la següent llicència Creative Commons:  http://cat.creativecommons.org/?page_id=184

ADVERTENCIA. El acceso a los contenidos de esta tesis queda condicionado a la aceptación de las condiciones de uso establecidas por la siguiente licencia Creative Commons:  <http://es.creativecommons.org/blog/licencias/>

WARNING. The access to the contents of this doctoral thesis it is limited to the acceptance of the use conditions set by the following Creative Commons license:  <https://creativecommons.org/licenses/?lang=en>



Universitat Autònoma de Barcelona
Facultat de Ciències
Departament de Química

New Photopharmacological Tools for the Light-Induced Control of Neuronal Signalling

Ph.D. THESIS

Ph.D. in Chemistry

Gisela Cabré Segura

2019

Supervisors:

Dr. Ramon Alibés Arqués

Dr. Félix Busqué Sánchez

Dr. Jordi Hernando Campos

Memòria presentada per aspirar al Grau
de Doctor per Gisela Cabré Segura

Gisela Cabré Segura

Vist i plau

Dr. Ramon Alibés Arqués

Dr. Félix Busqué Sánchez

Dr. Jordi Hernando Campos

Bellaterra, 17 de Juliol del 2019

“Un país només s’aixeca treballant.”

Avi Tito

A la meva família

Al Sergio

TABLE OF CONTENTS

ABBREVIATIONS.....	3
CHAPTER I: Introduction	
I.1. Glutamate receptors and their role on neuronal signalling.....	8
I.2. Light-induced control of neuronal signalling.....	11
I.2.1. Photopharmacology.....	12
I.2.1.1. Caged ligands.....	14
I.2.1.2. Photochromic ligands.....	15
I.2.1.3. Photoswitchable tethered ligands.....	18
I.2.2. Remaining challenges in photopharmacology.....	20
I.3. References.....	21
CHAPTER II: Objectives.....	25
CHAPTER III: New azobenzene-based PTLs for efficient two-photon neuronal excitation	
III.1. Introduction.....	29
III.1.1. LiGluR for the control of neuronal signalling <i>in vitro</i> and <i>in vivo</i>	29
III.1.2. Two-photon excitation of photoswitches with NIR light.....	33
III.1.3. Strategies towards two-photon absorbing MAG derivatives.....	37
III.2. Synthesis of PTLs MAG_{2P}^{slow} and MAG_{2P_F}^{slow}	40
III.2.1. Strategy towards the synthesis of target compounds MAG_{2P}^{slow} and MAG_{2P_F}^{slow}	40
III.2.2. Synthesis of azobenzene cores 16 and 17	41
III.2.3. Synthesis and incorporation of glutamate derivative 32	42
III.2.3.1. Synthesis of glutamate derivative 32	43
III.2.3.2. Introduction of glutamate derivative 32	44
III.2.4. Incorporation of the maleimide moiety and preparation of target compounds MAG_{2P}^{slow} and MAG_{2P_F}^{slow}	46
III.3. Photochemical characterisation of PTLs MAG_{2P}^{slow} and MAG_{2P_F}^{slow}	48

III.3.1. <i>Trans</i> → <i>cis</i> photoisomerisation.....	49
III.3.2. <i>Cis</i> → <i>trans</i> isomerisation.....	52
III.4. Evaluation of the light-induced biological activity of PTLs MAG_{2P}^{slow} and MAG_{2P_F}^{slow} on cultured cells.....	55
III.4.1. One-photon stimulation in cultured cells.....	57
III.4.2. Two-photon stimulation in cultured cells.....	60
III.5. Analysis of the two-photon response of MAG_{2P}^{slow} and MAG_{2P_F}^{slow} based on theoretical calculations.....	64
III.6. <i>In vitro</i> and <i>in vivo</i> evaluation of the activity of MAG_{2P_F}^{slow} in neurons.....	67
III.7. Conclusions.....	71
III.8. References.....	72

CHAPTER IV: Stilbene-based non-destructive caged ligands for the optical control of iGluRs

IV.1. Introduction.....	79
IV.1.1. Caged ligands for the photocontrol of glutamate receptors.....	79
IV.1.2. Non-destructive caged ligands: a new concept in photopharmacology..	82
IV.1.3. Stilbene photoswitches.....	83
IV.1.4. Design of novel non-destructive caged ligands for glutamate receptors..	86
IV.2. Synthesis and photochemical characterisation of GluS1	88
IV.2.1. Strategy for the synthesis of GluS1	88
IV.2.2. Synthesis of stilbene 50	89
IV.2.3. Incorporation of glutamate derivative 29	91
IV.2.4. Incorporation of the phthalimide fragment.....	93
IV.2.5. Photoisomerisation and obtention of target <i>cis</i> - and <i>trans</i> - GluS1	94
IV.2.6. Photochemical characterisation of GluS1	96
IV.3. Synthesis and photochemical characterisation of GluS2	99
IV.3.1. Synthesis of GluS2	99
IV.3.2. Photochemical characterisation of GluS2	101

IV.4. Evaluation of the light-induced biological activity of NDCLs GluS2	103
IV.5. Conclusions.....	105
IV.6. References.....	107
CHAPTER V: Synthetic photoswitchable neurotransmitters based on bridged azobenzenes	
V.1. Introduction.....	113
V.1.1. Photochromic ligands for glutamate receptors.....	113
V.1.2. C ₂ -bridged azobenzenes.....	117
V.1.3. Novel photochromic ligands based on bridged azobenzenes.....	120
V.2. Synthesis of bridged azobenzene-based PCLs.....	121
V.2.1. Synthesis of PCLs based on sulfur-bridged diazocines.....	122
V.2.2. Synthesis of PCLs based on ethylene-bridged diazocines.....	124
V.2.2.1. Synthesis of Glu_brAzo2	124
V.2.2.2. Synthesis of Glu_brAzo4 and Glu_brAzo5	126
V.3. Photochemical characterisation of PCLs Glu_brAzo4 and Glu_brAzo5	132
V.3.1. <i>Cis</i> → <i>trans</i> photoisomerisation.....	132
V.3.2. <i>Trans</i> → <i>cis</i> isomerisation.....	135
V.4. Evaluation of the light-induced biological activity of PCLs Glu_brAzo4 and Glu_brAzo5	138
V.4.1. Evaluation of the optical activity of Glu_brAzo4 and Glu_brAzo5 on cultured cells.....	138
V.4.2. Evaluation of the optical activity of Glu_brAzo4 and Glu_brAzo5 on hippocampal rat organotypic slices.....	143
V.5. Conclusions.....	145
V.6. References.....	147
CHAPTER VI: Summary and conclusions.....	153
CHAPTER VII: Experimental section.....	159
FORMULA INDEX.....	213
APPENDIX: Spectra of selected compounds.....	221

ABBREVIATIONS

1P	One-photon	eGFP	Enhanced green fluorescent protein
2P	Two-photon	EI	Electronic ionisation
1PA	One-photon absorption	ES	Extracellular solution
2PA	Two-photon absorption	ESI	Electrospray ionisation
Abs	Absorbance	Et	Ethyl
AIBN	2,2'-azobis(2-methylpropionitrile)	EtOAc	Ethyl acetate
AMPA	α -amino-3-hydroxyl-5-methyl-4-isoxazole propionic acid	EtOH	Ethanol
ATD	Amino-terminal domain	EWGs	Electron withdrawing groups
Boc	<i>tert</i> -butoxy carbonyl	exc	Excitation
Boc₂O	Di- <i>tert</i> -butyl dicarbonate	FBS	Fetal bovine serum
c	Concentration	GECI	Genetically encoded calcium indicators
<i>C. elegans</i>	<i>Caenorhabditis elegans</i>	GFP	Green fluorescent protein
CLs	Caged ligands	GIRK	G-protein-coupled inwardly rectifying potassium
CNS	Central nervous system	GluAs	AMPA ionotropic glutamate receptors
COSY	Correlation spectroscopy	GluKs	Kainate ionotropic glutamate receptors
CTD	Carboxy-terminal domain	GluNs	NMDA ionotropic glutamate receptors
DEPT	Distortionless enhancement by polarisation transfer	GluRs	Glutamate receptors
DIPEA	<i>N,N</i> -diisopropylethylamine	GPCRs	G- protein coupled receptors
DMAc	Dimethylacetamide	HEK293	Human embryonic kidney
DMAP	4-dimethylaminopyridine	HEPES	4-(2-hydroxyethyl)-1-piperazineethanesulfonic acid
DMPI	Dess-Martin periodinane	HMBC	Heteronuclear multiple bond correlation
DMF	Dimethylformamide	HOBt	1-hydroxibenzotriazole
DMSO	Dimethylsulfoxide	HRMS	High resolution mass spectrometry
EA	Electron acceptor		
EDCI	<i>N</i> -ethyl- <i>N'</i> -(3-dimethyl daminopropyl)-carbodiimide		
EDGs	Electron donating groups		

HSQC	Heteronuclear single quantum coherence	PORTLs	Photoswitchable orthogonal remotely tethered ligands
iGluRs	Ionotropic glutamate receptors	PSS	Photostationary state
IR (ATR)	Infrared spectroscopy in attenuated total reflection	PTLs	Photoswitchable tethered ligands
LBD	Ligand-binding domain	Ref.	Reference
LiHMDS	Lithium bis(trimethylsilyl)amide	rt	Room temperature
LiGluR	Light-gated ionotropic glutamate receptor	S₀	Ground electronic state
max	Maxima	S₁	First excited singlet electronic state
MCPBA	3-chloroperbenzoic acid	SEM	Standard error of mean
MeOH	Methanol	T₁	First excited triplet electronic state
mGluRs	Metabotropic glutamate receptors	TRNs	Touch receptor neurons
Mp	Melting point	TBAB	Tetrabutylammonium bromide
MS	Mass spectrometry	tBu	<i>tert</i> -butyl
nAChRs	Ionotropic acetylcholine receptors	tBuOAc	<i>tert</i> -butyl acetate
NBS	<i>N</i> -bromosuccinimide	tBuOH	<i>tert</i> -butanol
NDCLs	Non-destructive caged ligands	tBuOK	Potassium <i>tert</i> -butoxide
NIR	Near-infrared	TFA	Trifluoroacetic acid
NMDA	<i>N</i> -methyl-D-aspartate	THF	Tetrahydrofuran
NMDG⁺	<i>N</i> -methyl-D-glucamine	TLC	Thin layer chromatography
NMR	Nuclear magnetic resonance	TMD	Transmembrane domain
P	Pore	UV	Ultraviolet
PBS	Phosphate buffer solution	vis	Visible
PCLs	Photochromic ligands		
PET	Photoinduced electron transfer		
Ph	Phenyl		

CHAPTER I

Introduction

“What apparatus, in general terms, enables the brain to implement its remarkable performance? The number of components (neurons) in the brain is probably about 10^{11} . The number of synapses, or contact, between them is perhaps 10^{15} . On the average every neuron receives some thousands of distinct inputs and itself connects to many other neurons. [...] How might one make some headway through this impossible jungle? [...] It is only when we reflect on how intricate the entire system is and how complicated the many different operations it has to perform are that we realize we have a long way to go. But new methods bring new results and new results foster new ideas, and so we should not be too easily discouraged. There is no scientific study more vital to man than the study of his own brain. Our entire view of the universe depends on it.”

Francis Crick, Nobel Laureate

“Thinking about the brain” *Sci. Am.* **1979**, 241, 219-232

Neuroscience is the study of the nervous system, including the brain, spinal cord, and nerves, the basic unit of which are neurons. Unravelling how neurons interact to control physiological functions and how their malfunction leads to nervous disorders, such as multiple sclerosis or Alzheimer's disease, are therefore the main objectives of neuroscience. Nowadays, this area is being revolutionised by the use of photoresponsive biologically-active small molecules, a field known as photopharmacology. By enabling remote activation of drugs with light with high spatial and time resolution, photopharmacology seeks to tackle some of the main challenges faced by conventional pharmacology, such as poor drug selectivity and side effects. Interestingly, when applied to the investigation of neural circuits, this could allow selective manipulation of individual neurons, one of the major challenges in neuroscience.

This thesis aimed at developing new photopharmacological tools based on innovative photophysical and photochemical concepts for the control and study of neuronal signalling. To this end, new light-sensitive compounds capable of triggering neuronal activity were synthesised, fully characterised and biologically tested. As a model system to validate our novel approaches, kainate-type ionotropic glutamate receptors GluK1 and GluK2 were selected as targets, since they perform a key function in the modulation of neuronal excitability. For this reason, the first part of this introductory chapter focuses on glutamate receptors and their role and importance in neuronal circuitries. Next, the fundamentals of the manipulation of neuronal signalling with light and the different strategies developed so far are described. Finally, the remaining challenges in photopharmacology are discussed, which inspired us to design new strategies to overcome some of the limitations still persisting in this field.

I.1. GLUTAMATE RECEPTORS AND THEIR ROLE ON NEURONAL SIGNALLING

Glutamate is the primary excitatory neurotransmitter in the mammalian brain (Figure I-1) and it activates dozens of different cell surface receptors that mediate fast synaptic transmission and short-term and long-term modulation of synaptic strength.¹ Glutamate receptors (GluRs) comprise two different families: metabotropic receptors (mGluRs) and ionotropic receptors (iGluRs).¹ mGluRs are class C dimeric G protein-coupled receptors (GPCRs) broadly distributed throughout the central nervous system (CNS) and provide a mechanism by which glutamate modulates cell excitability and synaptic transmission via second messenger signalling pathways, controlling synaptic strength and plasticity.² iGluRs are a family of ligand-gated ion channels that allow the permeation of monovalent cations (sometimes even calcium) through cell membranes with little selectivity and in response to changes to the concentration of glutamate.³ They represent the major excitatory neurotransmitter pathway in the brain and consequently are essential for normal CNS functions, such as learning, memory and neuronal development.³ In addition, iGluRs are implicated in numerous neurodegenerative disorders such as multiple sclerosis and Alzheimer, Parkinson or Huntington's diseases, among others.

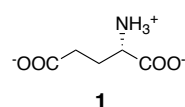


Figure I-1. Structure of glutamate, the most abundant neurotransmitter in the brain.

As depicted in Figure I-2a, iGluRs are composed of four individual subunits, which are modular structures that comprise four different domains: (i) an extracellular amino-terminal domain (ATD), which is involved in the subfamily-specific assembly and modulation of the receptor; (ii) an extracellular ligand-binding domain (LBD), which consists of two lobes D1 and D2 conforming a clamshell structure that provides the binding site for agonists and antagonists; (iii) a transmembrane domain (TMD), which forms the cation-selective pore (P); and (iv) an intracellular carboxy-terminal domain (CTD), which is involved in receptor localisation and modulation (Figure I-2b).^{4,5}

The activation cycle of iGluRs upon ligand binding comprises three different states (Figure I-3): (i) an inactive resting state where the channel is closed; (ii) an active state formed after the binding of glutamate or other agonists to the LBD of the receptor, which induces an allosteric conformational change in the TMD that allows a pore to be opened in the membrane; and (iii) an inactive desensitised state, which results in a further conformational change in the TMD that closes the channel and,

eventually, leads to agonist unbinding.⁴ Because the aperture of the pore in the active state of iGluRs provokes a flux of sodium, potassium and/or calcium ions, this causes a depolarising current and, if a large enough number of receptors are activated, an action potential in the postsynaptic neuron is triggered.

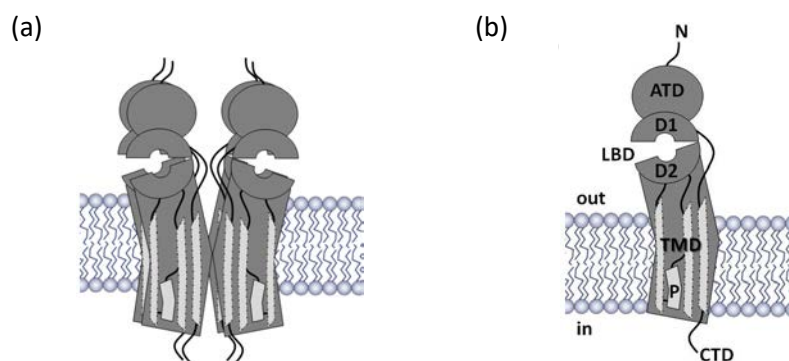


Figure I-2. (a) iGluR structure, which is made of four individual subunits. (b) Structure of these individual subunits (ATD = amino-terminal domain, LBD = ligand-binding domain, TMD = transmembrane domain, CTD = carboxy-terminal domain) and some of their more relevant parts (D1 = upper lobe of the LBD, D2 = lower lobe of the LBD, P = pore helix).^{4,5}

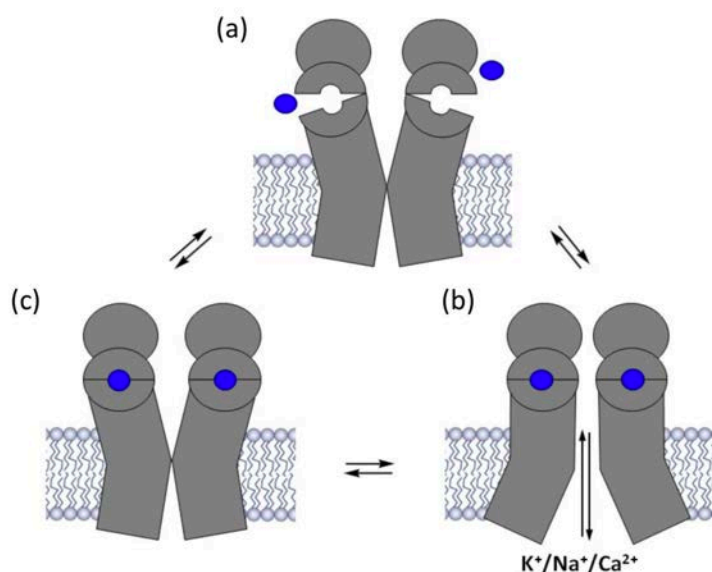


Figure I-3. Schematic representation of the activation cycle of iGluRs upon ligand (blue) binding: (a) inactive resting state where the ion channel remains closed, (b) active state formed upon binding of the ligand where the ion channel is open, and (c) inactive desensitised state where the pore is closed, and eventually leads to ligand unbinding. Only two of the four subunits of the receptor are shown for the sake of clarity.

iGluRs have been grouped according to their distinct responses to certain small molecule agonists (Figure I-4): NMDA (*N*-methyl-D-aspartate, **2**), AMPA (α -amino-3-hydroxyl-5-methyl-4-

isoxazolepropionic acid, **3**), and kainate (kainic acid, **4**). Therefore, they are divided into NMDA (GluNs), AMPA (GluAs) and kainate (GluKs) receptors. Two orphan members of the iGluR gene family, GluD1 and GluD2, are also known, but their physiological role remains somewhat mysterious.³ Since the pharmacologically defined boundary between AMPA and kainate receptors has blurred over time, now they are often grouped into the so-called *non-NMDA receptor* superfamily.^{4,5,6}

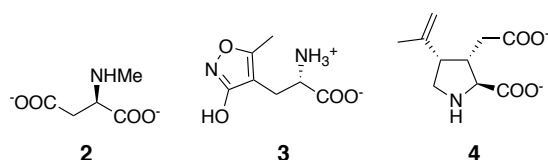


Figure I-4. Structures of the three subtype-selective agonists of iGluRs: NMDA, **2**; AMPA, **3**; and kainate, **4**.

NMDA receptors activation requires not only the simultaneous binding of glutamate and glycine (or D-serine), but also an elevated membrane potential greater than -30 mV. This renders NMDA receptors coincidence detectors at central synapses, since they are sensitive to both the release of ligands by the presynaptic neuron and changes in voltage on the postsynaptic side.⁶ AMPA receptors mediate postsynaptic depolarisation after release of glutamate from the presynaptic side and exhibit fast activation and deactivation kinetics (within a few milliseconds). This feature makes them the principle molecular component of fast excitatory synaptic transmission.⁶ By contrast, kainate receptors play a role in the modulation of neuronal excitability rather than in fast excitatory transmission. Their mode of action, however, is not as well understood as in the case of AMPA receptors.

It is due to the limited selectivity of conventional pharmacological probes when targeting kainate receptors that GluKs were the first GluRs addressed for photocontrol.⁷ In particular, kainate receptors GluK1 and GluK2 have been the object of study in multiple photopharmacological studies. Two main reasons account for this fact: (i) the wealth of structural information available for the LBD of these two receptors (Figure I-5);^{8,9} and (ii) their physiological relevance. Thus, GluK1 is mainly present in hippocampal and cortical interneurons as well as in Purkinje cells and sensory neurones,¹⁰ and fulfils important roles in plasticity mechanisms of the amygdala;³ while GluK2 is mostly expressed by hippocampal pyramidal cells, both hippocampal and cerebellar granule cells, and cortical pyramidal cells,¹⁰ and is related to several neurological disorders such as obsessive-compulsive disorder, schizophrenia or autism.³ Accordingly, GluK1 and, especially, GluK2 have been the target of the new photopharmacological tools developed along this thesis.

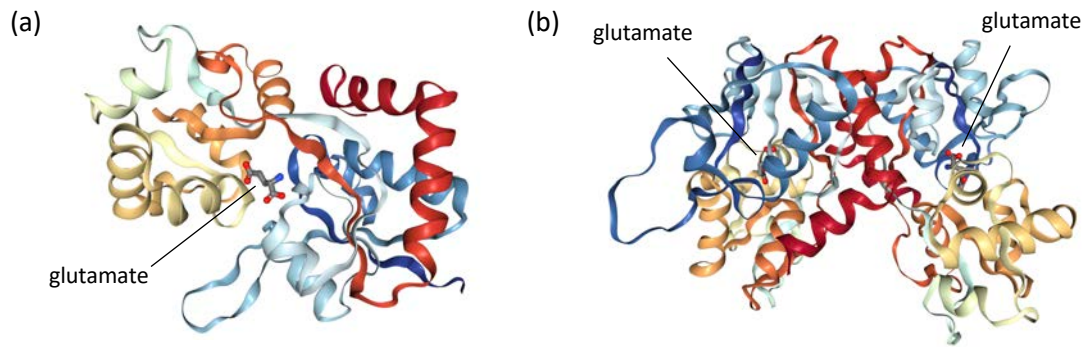


Figure I-5. Crystal structures of (a) the ligand-binding core of human GluK1 in complex with glutamate⁸, and (b) GluK2 wild-type LBD dimer in complex with glutamate.⁹

I.2. LIGHT-INDUCED CONTROL OF NEURONAL SIGNALLING

One of the main goals of neuroscience is to better understand the structure and physiology of neuronal membrane proteins, synaptic receptors and ion channels, since their function and dysfunction underlay some of the most prevalent and devastating neurodegenerative diseases, neuropsychiatric disorders and synaptopathies.¹¹

The study of neuronal systems has been extensively addressed by conventional pharmacology. However, despite the countless insights gained, this approach displays several inherent drawbacks, such as low specificity, off-targets, slow kinetics, poor spatial confinement, lack of or slow reversibility, etc. For instance, standard diffusion and partitioning of conventional drugs imply poor spatial and temporal control of their activity. Moreover, it is relatively common for the receptor or channel of interest to be expressed on multiple nearby cell types, or even on both sides of a synapse, making it difficult to isolate the effects of the target receptor within the circuit or synapse of interest.¹ Light-based techniques that operate at the intersection between chemistry, biology and neuroscience have been developed to overcome these challenges. Light allows the control of biological systems with high spatial and temporal resolution, while enabling non-invasive and remote control, reversibility, and fast and simple modulation of the excitation energy.

One of the most promising approaches developed for the study of neurons by means of light is optogenetics.^{12,13} Optogenetics relies on naturally occurring light-sensitive proteins (e.g. Channelrhodopsin-2) and repurposes them into genetically encoded light-gated cellular actuators. In other words, it involves the use of light to control cells in living tissue, typically neurons, that have been genetically modified to express exogenous light-sensitive proteins. In each case, the type of

control achieved depends on the biological function of the particular light-sensitive protein introduced.¹² Despite the enormous success of this technique, optogenetics presents several drawbacks.^{14,15} On one hand, the neuronal response generated may not perfectly match the actual endogenous behaviour. On the other hand, the expression of light-sensitive proteins *in vivo* is not specific and does not allow precise control of the level of genetic modification, thus posing some technical limitations. Moreover, the overexpression of exogenous proteins may provoke functional and morphological distortions in many cell types. Finally, optogenetics will eventually involve the use of gene therapy, which raises some issues about its therapeutic applications.

Many of these weaknesses can be overcome by photopharmacology,¹¹ also known as optopharmacology, chemical optogenetics or synthetic optogenetics. Photopharmacology also employs light to regulate the function of proteins but relies on small photoactive synthetic molecules to directly target the endogenous, or slightly genetically modified, receptors and ion channels in neurons (or in other cells). Being the field of study of this thesis, photopharmacology is further discussed in the following section.

I.2.1. PHOTOPHARMACOLOGY

Photopharmacology is an alternative light-based strategy to optogenetics that relies on the use of synthetic photoactive molecules to optically control the activity of endogenous receptors and ion channel proteins. This technique enables triggering native neural signalling processes, by employing photoactive receptor agonists, or blocking them, by using photoactive receptor antagonists or channel blockers. Photopharmacology overcomes some of the main drawbacks of optogenetics, especially when considering this technique for therapeutic applications. Hence, this novel approach may contribute to the development of personalised medicine by providing treatments that enable modulating the time a certain region is treated depending on each patient, thus reducing undesired effects. Importantly, the pharmacological activity of photopharmacological tools can be validated by means of standard procedures employed in drug development.

In recent years, several strategies in the photopharmacology field have been developed and successfully tested *in vitro* and *in vivo*. These different photopharmacological tools can be classified by their response to light and the mechanism through which they interact with their target (Figure I-6).^{1,7,16} First of all, an important categorisation criteria is whether the effect of light is irreversible or reversible. The most common irreversible photopharmacological strategies are irreversible

photoinactivation (Figure I-6a) and irreversible photoactivation of drugs (Figure I-6b). The latter, widely known as photouncaging of caged ligands, makes use of photocleavable protecting groups or *cages* that are coupled to biologically-responsive ligands and inhibit their activity until eventually removed under irradiation. Reversible photopharmacological tools are instead based on synthetic photoswitches, which can be photoconverted back and forth between different states with distinct biological activity. These compounds can be classified by their mechanism of interaction with the target. Firstly, photochromic ligands (PCLs) are freely diffusible molecules that adopt two or more different isomeric forms upon irradiation, which exhibit distinct affinities and/or efficacies towards a native target protein (Figure I-6c). These ligands can also be covalently tethered to the receptor through either a native or a genetically engineered residue, which are further divided into two subcategories depending on whether their attachment point lies close to (photoswitchable tethered ligands, PTLs, Figure I-6d) or away from (photoswitchable orthogonal remotely tethered ligands, PORTLs, Figure I-6e) the ligand binding site. Finally, photoswitches can be covalently attached to the biological target on both of their ends and, upon isomerisation, modulate its conformation and activity. These compounds are known as photoswitchable cross-linkers (Figure I-6f).

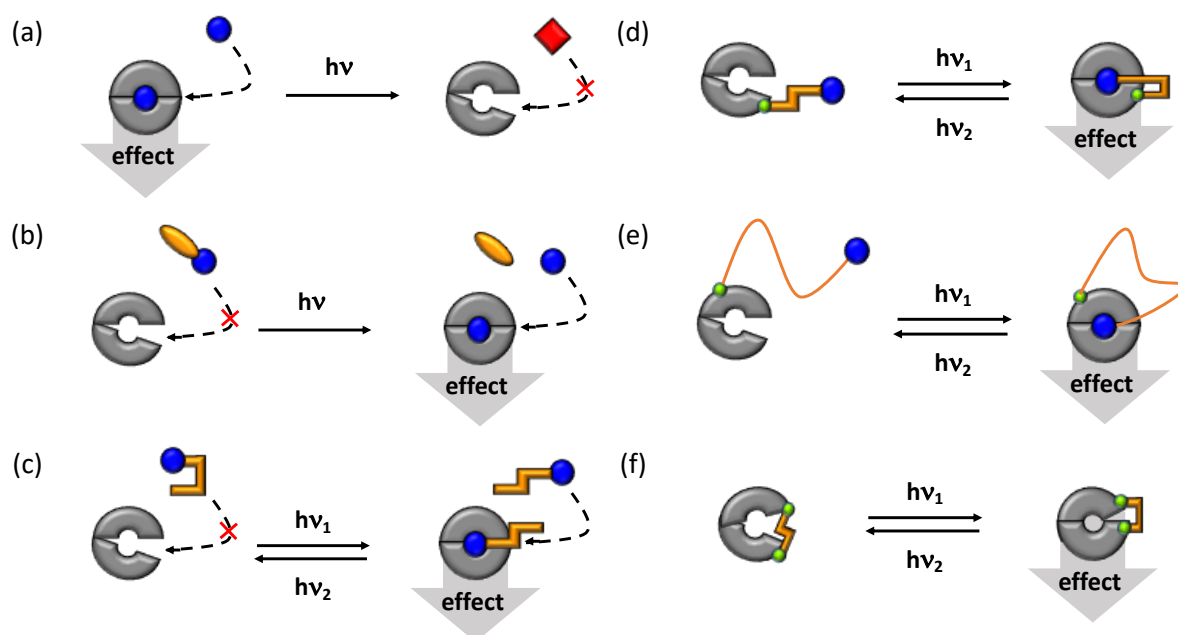


Figure I-6. Strategies in photopharmacology. (a) Irreversible photoinactivation. (b) Irreversible photouncaging of caged ligands. (c) Reversible photoactivation with a photochromic ligand (PCL). (d) Reversible photoactivation with a photoswitchable tethered ligand (PTL). (e) Reversible photoactivation with a photoswitchable orthogonal remotely tethered ligand (PORTL). (f) Reversible photoactivation with a photoswitchable cross-linker.^{1,7,16}

Among all the described photopharmacological tools, caged ligands, photochromic ligands and photoswitchable tethered ligands are the most widely used. In addition, these three strategies are the ones studied in this thesis; hence, their properties are further detailed below.

I.2.1.1. Caged ligands

Caged ligands (CLs) are the simplest approach in photopharmacology. They consist of a biologically-active molecule covalently bonded to a photolabile group (or *cage*) that can be removed (or *uncaged*) upon irradiation. The *cage* renders the biologically-active moiety inactive and, upon exposure to light, photocleavage of the protecting group releases the active substrate and triggers the desired biological effect. Thus, the release of the active drug can be focalised in terms of time and space, which is not possible with conventional pharmacology.

The performance of caged ligands depends on (i) the inertness and chemical stability of the system in the absence of light; and (ii) the efficiency and rate of release of the active ligand upon illumination. Therefore, the probe should be neither an agonist nor an antagonist when applied at useful concentrations to the biological preparations. Moreover, the higher the efficiency of uncaging, the easier to use the cage ligand. Low uncaging efficiencies may be detrimental for cell health, especially in the case of UV light-mediated uncaging.¹⁷

Nitrobenzyl groups and their derivatives are by far the most common caging groups employed due to their facile synthesis and easy installation on the molecule under study (Figure I-7).¹⁸ However, photolysis of these compounds forms potentially toxic and strongly absorbing by-products. Thus, alternative photoremovable protecting groups have been developed to overcome these disadvantages. Some of them are arylcarbonylmethyl, coumarin-4-ylmethyl and arylmethyl groups (Figure I-7).¹⁹

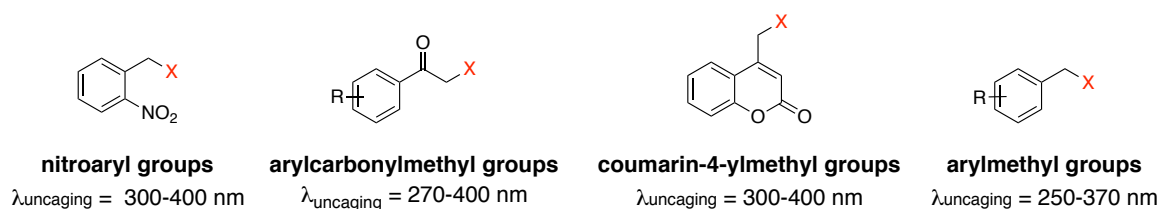
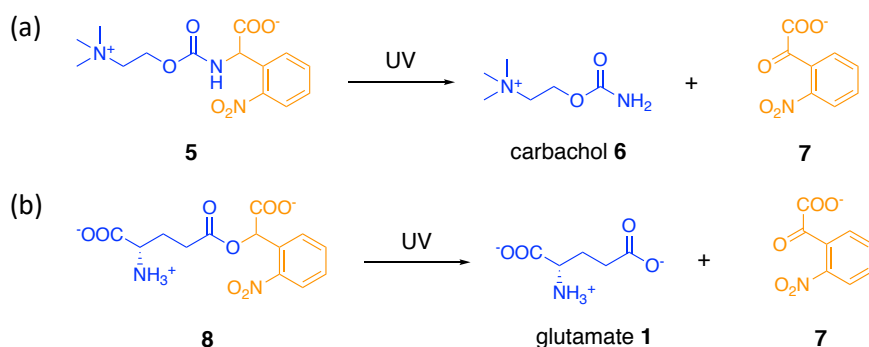


Figure I-7. Structures of the main photoremovable protecting groups used for the preparation of caged ligands.

Many different biomolecules have been caged, such as small molecules, ions, macromolecules, peptides and proteins, and even genes.^{17,18} Caged ligands have been profusely applied in neuroscience

to cage agonists for neurotransmitter receptors. The group of Hess pioneered this field by reporting the first caged neurotransmitters based on 2-nitrobenzyl derivatives of carbamoylcholine, an activator of acetylcholine receptors, which was released upon stimulation with UV-light (Scheme I-1a).²⁰ However, glutamate is the most extensively caged neurotransmitter and therefore it was the development of caged ligands based on this compound which actually revolutionised the field (Scheme I-1b).²¹



Scheme I-1. Uncaging process of (a) caged carbamoylcholine, **5**; and (b) caged glutamate, **8**. The caging group in both cases is α -carboxyl-2-nitrophenyl, a common caging group from the nitroaryl family (orange). The bioactive moieties (blue) are released upon irradiation with UV light.

Although CLs have been extensively used as photopharmacological tools, they present several disadvantages. The most important of these drawbacks are related to the photocleavage of the caging group: (i) photolysis of the caging group generates by-products, which may be toxic or present undesired effects; and (ii) since uncaging is an irreversible process, once the ligand is released, it will remain active after diffusing out of the illuminated volume and may affect non-target or undesired areas. Moreover, even though photouncaging can be readily implemented and acts on endogenously expressed receptor populations, this approach does not allow targeting specific cells.

Many of these weaknesses can be overcome by the use of reversible photopharmacological tools: photochromic ligands and photoswitchable tethered ligands.

I.2.1.2. Photochromic ligands

As caged ligands, photochromic ligands (PCLs) are free diffusing photopharmacological tools that directly target the endogenous form of cell receptors and ion channels. However, whilst caged ligands undergo irreversible activation, photochromic ligands allow the reversible manipulation of receptors using photoswitchable compounds. This can be achieved by the functionalisation of a conventional

ligand with a photochrome unit that changes its structure upon irradiation and thereby alters the binding affinity to its target receptor.

Photochromism is the reversible transformation of a chemical species between two forms with different absorption spectra induced by the absorption of electromagnetic radiation.²² Photochromic systems undergo chemical transformations upon irradiation that lead not only to a change in their optical properties but also in other physical and chemical properties (e.g. molecular geometries, redox potential or dielectric constants). For the majority of the photochromes, these chemical transformations are reversible unimolecular photoisomerisation reactions.

Photochromic systems can be classified into two groups according to the thermal stability of the photochemically generated state: T-type and P-type (Figure I-8). On one hand, T-type photochroms present a thermally unstable photochemically generated state and, hence, the initial state can be recovered either photochemically through the excited state or thermally through the ground state. On the other hand, the photochemically generated state in P-type photochroms is thermally stable, which implies that the back reaction can only take place photochemically.^{23,24}

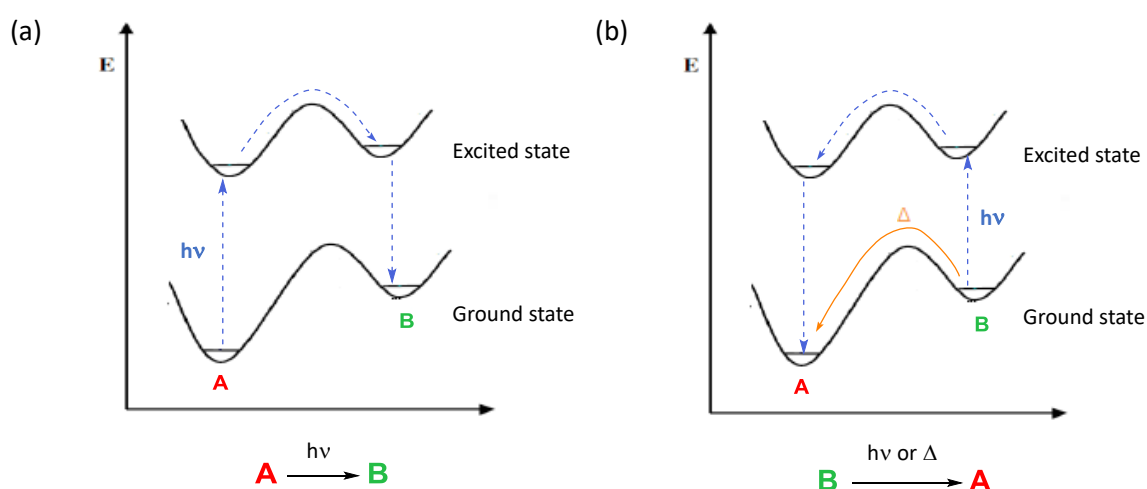


Figure I-8. Characteristic energy profile of a photochromic system. (a) Species A, the thermodynamically most stable isomer of the photochrome, turns into species B upon irradiation, which involves excitation into an electronic excited state and isomerisation through the energy barrier of this state. (b) The inverse reaction can also take place photochemically in a similar fashion, or thermally via the ground electronic state of the system. Dashed blue lines indicate isomerisation via a photochemical process whilst solid orange lines represent thermal isomerisation. This latter occurs in T-type photochromes but not in P-type photochromes.

Many strategies for the reversible control of biomolecules have been explored with a large variety of photochromes (Figure I-9). Most of these photochromes switch upon irradiation between *trans* and

cis isomers, thus resulting in a large geometrical change (e.g. azobenzenes, stilbenes and hemithioindigos), or between closed- (*c*) and open-ring (*o*) structures, which is accompanied by a significant variation in the conjugation path of the molecule (e.g. spiropyrans, diarylethenes and fulgides).²⁴

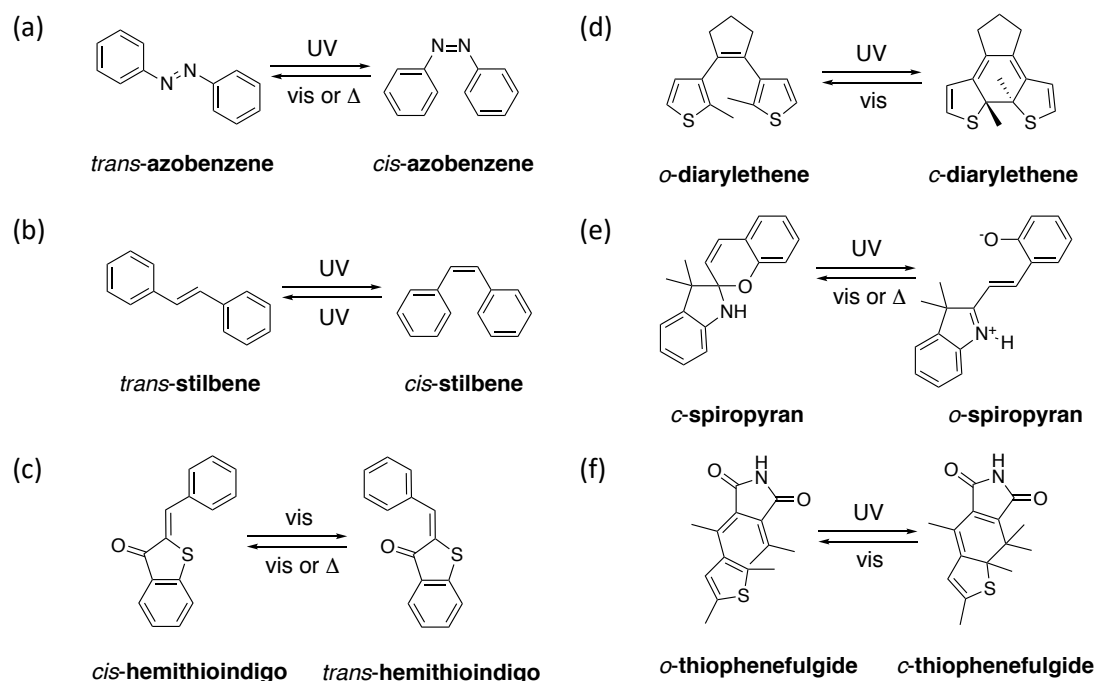
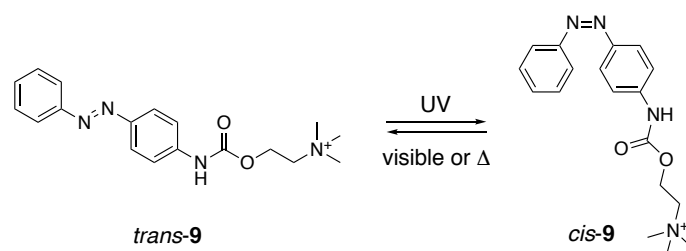


Figure I-9. Structures of the main photoswitches introduced into biomolecules for the photoinduced control of their activity.²⁴

When selecting the most appropriate synthetic photoswitch to use for the preparation of PCLs (or other photopharmacological tools), several factors must be taken into account: optimal photophysical properties (i.e. high absorbance, photoisomerisation quantum yields and photoconversions), large fatigue resistance under consecutive photoisomerisation cycles, controllable thermal stability of the photoinduced state, large geometrical changes upon isomerisation, low (photo)toxicity, and favourable pharmacokinetics and metabolic stability. Azobenzenes fulfil most of these criteria and have a great synthetic availability; as such, they are the most widely used photoswitches for the design of photochromic ligands. Actually, the first PCL developed for the control of excitable membrane receptors relied on azobenzene as the photoswitchable unit. This compound, **9**, consisted of a carbachol head group covalently linked to an azobenzene, so that the geometrical changes exhibited by the photochrome upon irradiation with UV light would enable the carbachol unit to interact differently with nicotinic acetylcholine receptors (nAChRs) and control their activity (Scheme I-2).²⁵



Scheme I-2. *Trans* and *cis* forms of the first PCL for the control of neuronal receptors with light.

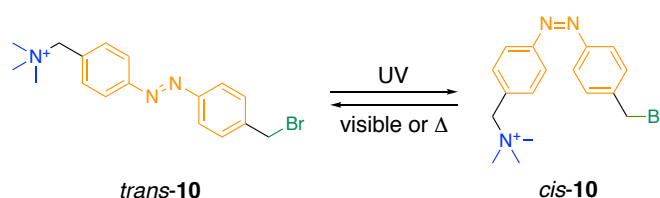
Since then, a wide range of PCLs have been successfully applied to control a variety of biological systems such as ion channels, transporters and pumps, GPCRs, enzymes or elements of the cytoskeleton.^{11,16} However, even though they improve some of the properties of CLs, they still present certain limitations: (i) the binding to the biological receptor is also governed by diffusion and can induce response in non-target areas, which poses limit to the spatial and temporal control of its activity; (ii) they are rather unspecific, since different types of receptor proteins are often sensitive to the same agonist or antagonist molecules (e.g. ionotropic and metabotropic glutamate receptors); (iii) the difference in affinity of the two photoswitch configurations and their purity at a given excitation wavelength might be rather modest; and (iv) they are normally active in their initial state, and only become inactive upon photoisomerisation within the irradiated region.

Tethering the photoisomerisable molecule with photopharmacological activity to the protein of interest would allow overcoming most of these drawbacks. Photoswitchable tethered ligands emerged based on this concept and enable surpassing some of the main deficiencies of PCLs.

1.2.1.3. Photoswitchable tethered ligands

Photoswitchable tethered ligands (PTLs) are photochromic ligands that incorporate a covalent linkage to the receptor of interest. PTLs must therefore be composed of at least three distinct functional units: (i) a biologically-active moiety, (ii) a photoisomerisable unit, and (iii) a reactive group through which the system is covalently linked to the target protein. When tethering the compound to the appropriate anchoring point, reversible isomerisation of the photoswitch leads to geometrical changes that move the biologically-active unit close or away from the binding site, thus enabling selective optical modulation of the ligand-receptor interaction on the protein of interest. Consequently, this provides further spatial control with respect to PCLs. In addition, the fact that PTLs are forced to remain tethered to the receptor and can not diffuse away ensures a high local concentration of biologically-active ligands around the binding site without requiring persistent perfusion of the compound of interest. As a result, PTLs show faster responses than PCLs and caged ligands.

The modular design of PTLs enables broadening their applicability by wisely selecting the nature of the biologically-active moiety, the optical properties of the photoswitch and the chemical behaviour of the reactive group. This has allowed the successful development of a number of PTL systems for many different biological systems.¹⁶ The first PTL developed was the cysteine-reactive QBr compound **10**, which is an azobenzene-based photoswitch that includes an additional chemical moiety to covalently bind cysteine residues in nAChRs (Scheme I-3).²⁶



Scheme I-3. *Trans* and *cis* forms of the first PTL used to control nAChRs with light. This compound consists of a quaternary ammonium ion (biologically-active moiety, blue) tethered to an azobenzene group (photoswitch, orange) bearing a bromomethylene moiety (anchor, green) to covalently attach the ligand to a native cysteine residue located near the nAChR binding site. Once attached, the agonist can bind to the receptor and activate the channel in its *trans* configuration, while in the *cis* state the tether is too short for the agonist to bind.²⁶

A key factor in the development of PTLs is the selection of the anchoring point to the target protein. Two different approaches can be followed: (i) to covalently attach the ligand to any of the groups around the binding site of the wild type form of the protein, or (ii) to selectively conjugate it to a genetically engineered chemical residue. Maleimides are the main used linkage motif for PTLs and they react to genetically engineered cysteines close to the binding site of the protein of interest. The widespread use of maleimide as anchors is due to several reasons: they are commercially available, their conjugation to thiols produces a covalent bond, and the reaction is fast, efficient and moderately specific under physiological conditions.¹¹ Moreover, from a protein engineering point of view, maleimide conjugation requires minimal protein modification, just a single amino acid substitution to cysteine. Finally, although maleimides can potentially interact with other native cysteines in the receptor, they are normally absent from sensitive areas near the ligand binding site, while they often form non-reactive disulphide bonds when found in external domains.¹

Despite the benefits of genetic-targeting, it can result in unnecessary overexpression in receptors and promiscuous cellular localisations. Thus, new PTLs using reactive groups (e.g. *N*-hydroxysuccinimide ester) capable of covalently binding to the endogenous form of the protein are also being developed.²⁷

I.2.2. REMAINING CHALLENGES IN PHOTOPHARMACOLOGY

The variety of photopharmacological tools developed so far makes it possible to explore the role and signalling mechanisms of numerous cell surface receptors, in their natural environment, *in vitro* and *in vivo*. However, there are still several barriers to cross before photopharmacology becomes widely accepted and clinically used. These remaining challenges involve:¹¹

- **Solubility, stability and toxicity:** The compounds developed need to be soluble and stable in the environment of the target, which for biological applications is mainly water. As for toxicity, it may arise from different factors: (i) the intrinsic toxicity of the photopharmacological compound due to its structure and composition; (ii) in the case of caged ligands, the release of toxic by-products during the uncaging process; and (iii) in the case of photochromic ligands, the biological response of the thermodynamically stable form administered to the tissue, which is normally the most active and therefore elicits strong tonic responses that can only be prevented under irradiation. Consequently, the development of caged ligands that do not generate toxic by-products and PCLs that are thermodynamically stable in their inactive state would be highly desirable.
- **Optical properties and irradiation conditions:** On one hand, narrower absorbing photoswitches are required, since broad absorption complicates their use with additional optical tools, such as fluorescent proteins and probes. On the other hand, in order to be able to switch quantitatively from one state of the photoswitch to the other, the absorbance spectra of both species should not overlap. Finally, it would be desirable to shift the absorbance of the photopharmacological tools to the red and near-infrared (NIR) regions. Most current compounds operate under near-UV light irradiation which is not compatible with many biomedical applications: it can cause photodamage and is efficiently absorbed and scattered by tissues, thus preventing large penetration depths from being achieved. Actually, the latter also affects light in most regions of the visible spectrum since the major absorbing species in vertebrate tissues is oxyhemoglobin, which filters off practically all wavelengths shorter than 650 nm. On the other hand, water becomes increasingly absorbant at wavelengths longer than 950 nm. These two factors define the *phototherapeutic window*, a region of larger tissue transparency that expands from 650 to 950 nm^{11,19} (i.e. red and NIR light). In addition, the use of this type of illumination reduces phototoxic effects and may allow for non-resonant two-photon (2P) excitation of photopharmaceutical tools, which enhances spatial resolution.

- **Labelling efficiency and time:** In the case of PTLs, it is difficult to determine the actual number of receptors that have been labelled. Since labelling efficiency will determine the effectiveness of the tool, methods to increase and monitor labelling efficiency are required. Furthermore, the receptor-PTL tether must be stable in time and do not degrade under physiological conditions. This is not the case of maleimides, the main motif currently used for anchoring the photoswitch to the receptor of interest, which eventually hydrolyse in tens of minutes. Finally, PTLs that target endogenous receptors need to be further developed, thus avoiding mutation of native tissues.
- **Economic issues and availability:** Most photoswitches are not commercially available; therefore, photopharmaceuticals need to be synthesised within a reasonable time frame and at a justifiable expense.

This thesis aims at giving response to some of these challenges by developing: (i) a photoswitchable tethered ligand that responds to two-photon excitation with NIR light; (ii) a non-destructive caged ligand that does not release by-products; and (iii) a photochromic ligand with a thermodynamically stable inactive form that selectively turns into the biologically-active state when irradiated.

I.3. REFERENCES

- (1) Kienzler, M. A.; Isacoff, E. Y. *Curr. Opin. Neurobiol.* **2017**, *45*, 202-209.
- (2) Niswender, C. M.; Conn, P. J. *Annu. Rev. Pharmacol. Toxicol.* **2010**, *50*, 295-322.
- (3) Bowie, D. *CNS Neurol Disord Drug Targets.* **2008**, *7*, 129–143.
- (4) Traynelis, S. F.; Wollmuth, L. P.; McBain, C. J.; Menniti, F. S.; Vance, K. M.; Ogden, K. K.; Hansen, K. B.; Yuan, H.; Myers, S. J.; Dingledine, R. *Pharmacol. Rev.* **2010**, *63*, 405-496.
- (5) Stawski, P.; Janovjak, H.; Trauner, D. *Bioorg. Med. Chem.* **2010**, *18*, 7759-7772.
- (6) Fehrentz, T.; Schönberger, M.; Trauner, D. *Angew. Chem. Int. Ed.* **2011**, *50*, 12156-12182.
- (7) Reiner, A.; Levitz, J.; Isacoff, E. Y. *Curr. Opin. Pharmacol.* **2015**, *20*, 135-143.
- (8) Unno, M.; Shinohara, M.; Takayama, K.; Tanaka, H.; Teruya, K.; Doh-Ura, K.; Sakai, R.; Sasaki, M.; Ikeda-Saito, M. *J. Mol. Biol.* **2011**, *413*, 667-683.

- (9) Nayeem, N.; Mayans, O.; Green, T. *J. Neurosci.* **2011**, *31*, 2916-2924.
- (10) Lerma, J.; Marques, J. M. *Neuron.* **2013**, *80*, 292-311.
- (11) Berlin, S.; Isacoff, E. Y. *EMBO reports* **2017**, *18*, 677-692.
- (12) Deisseroth, K. *Nat. Methods* **2011**, *8*, 26-29.
- (13) Deisseroth, K. *Nat. Neurosci.* **2015**, *18*, 1213-1225.
- (14) Kasparov, S.; Herlitze, S. *Exp. Physiol.* **2013**, *98*, 971-972.
- (15) Packer, A. M.; Roska, B.; Häusser, M. *Nat. Neurosci.* **2013**, *16*, 805-815.
- (16) Hüll, K.; Morstein, J.; Trauner, D. *Chem. Rev.* **2018**, *118*, 10710-10747.
- (17) Ellis-Davies, G. C. R. *Nat. Methods.* **2007**, *4*, 619-628.
- (18) Young, D. D.; Deiters, A. *Org. Biomol. Chem.* **2007**, *5*, 999-1005
- (19) Klán, P.; Šolomek, T.; Bochet, C. G.; Blanc, A.; Givens, R.; Rubina, M.; Popik, V.; Kostikov, A.; Wirz, J. *Chem. Rev.* **2013**, *113*, 119-191.
- (20) Milburn, T.; Matsubara, N.; Billington, A. P.; Udgaonkar, J. B.; Walker, J. W.; Carpenter, B. K.; Webb, W. W.; Marque, J.; Denk, W.; McCray J. A.; Hess, G. P. *Biochemistry* **1989**, *28*, 49-55.
- (21) Wieboldt, R.; Gee, K. R.; Niu, L.; Ramesh, D.; Carpenter, B. K.; Hess, G. P. *Proc. Natl. Acad. Sci. USA.* **1994**, *91*, 8752-6.
- (22) Rau, H. *Photochromism: Molecules and System*; Bouas-Laurent, H.; Dürr, H., Eds.; Elsevier Amsterdam, 1990; Vol. 73, pp. 639-665.
- (23) Beharry, A. A.; Woolley, G. A. *Chem. Soc. Rev.* **2011**, *40*, 4422-4437.
- (24) Szymansky, W.; Bierle, J. M.; Kistemarker, H. A. V.; Velema, W. A.; Feringa, B. L. *Chem. Rev.* **2013**, *113*, 6114-6178.
- (25) Deal, W. J.; Erlanger, B. F.; Nachmansohn, D. *Proc. Natl. Acad. Sci. USA.* **1969**, *64*, 1230-1234.
- (26) Bartels, E.; Wassermann, N. H.; Erlanger, B. F. *Proc. Natl. Acad. Sci. USA.* **1971**, *68*, 1820-1823.
- (27) Izquierdo-Serra, M.; Bautista-Barrufet, A.; Trapero, A.; Garrido-Charles, A.; Díaz-Tahoces, A.; Camarero, N.; Pittolo, S.; Valbuena, S.; Pérez-Jiménez, A., Gay, M.; García-Moll, A.; Rodríguez-Escrich, C.; Lerma, J.; de la Villa, P.; Fernández, E.; Pericàs, M. À.; Llebaria, A.; Gorostiza, P. *Nat. Commun.* **2016**, *7*, 12221.

CHAPTER II

Objectives

In this PhD thesis three different projects have been developed involving the synthesis, characterisation and biological activity evaluation of novel photopharmacological tools for the optical control of glutamate receptors. In this chapter the main goals set for this work are briefly described.

Despite the variety of photopharmacological tools developed to date for the manipulation of neuronal signalling and their successful application *in vitro* and *in vivo*, several challenges still remain in this field. In this thesis, we have developed novel photochemical and photophysical strategies to tackle some of these issues, which we have tested in kainate-type ionotropic glutamate receptors GluK1 and, mainly, GluK2 that play a key role in the modulation of neuronal excitability. In particular, three main objectives were set for this work:

OBJECTIVE 1. Synthesis, characterisation and *in vitro* and *in vivo* application of azobenzene-based photoswitchable tethered ligands that exhibit efficient two-photon (2P) activity under near-infrared light excitation (Figure II-1). Two main design concepts were exploited: (i) push-pull substitution of the azoaromatic core with electron donating (EDGs) and electron withdrawing groups (EWGs) to enhance its intrinsic 2P absorption cross-section; and (ii) rational selection of the EDGs and EWGs introduced to prevent a dramatic decrease of the thermal stability of the *cis* state of the system, which would detrimentally affect the amplitude of the light-modulated biological responses obtained. The results obtained in this area are described in Chapter III.

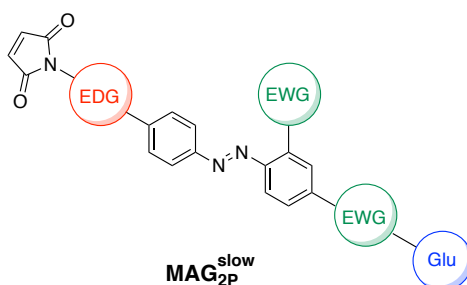


Figure II-1. General structure of the target PTLs bearing push-pull substituted azoaromatic cores that were designed to enhance their 2P activity under NIR light irradiation. They also contain a maleimide moiety as a tether to the receptor and a glutamate (Glu) derivative as agonist that can interact with the ligand-binding site of GluK2.

OBJECTIVE 2. Synthesis, characterisation and *in vitro* application of stilbene-based non-destructive photocaged ligands (Figure II-2). This new type of photopharmacological tool is based on tethering the bioactive species to a photoisomerisable group that (i) is thermally stable in the inactive state and (ii) only undergoes light-induced transformation towards the active isomer. Stilbene was chosen as the photoswitch in this study since its both isomers are thermodynamically stable and *trans*→*cis* photoisomerisation can be prevented in biological media by proper selection of its substituents. As a result, irreversible and quantitative photoconversion of the inactive *cis* state into the active *trans* isomer could be achieved without by-product generation, in contrast to conventional caged ligands. The results obtained for this topic are described in Chapter IV.

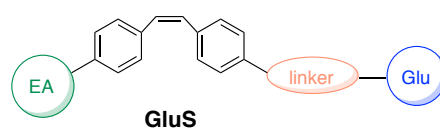


Figure II-2. General structure of the stilbene-based non-destructive photocaged ligands developed in this work, whose *cis*→*trans* isomerisation occurs with 100% efficiency and without generating any by-product. To this end, proper electron acceptor (EA) groups had to be introduced, while the linker and the glutamate (Glu) units were chosen to maximise the difference in affinity of the two states of the system with GluK1 and GluK2.

OBJECTIVE 3. Synthesis, characterisation and *in vitro* application of bridged azobenzene-based photochromic ligands (Figure II-3). In this case we replaced the common azo group employed in most PCLs with a C2 bridged azobenzene unit that also favours *trans*-active behaviour of the ligand by photoswitching between extended *trans* and bent *cis* configurations but shows larger thermodynamic stability for the *cis* isomer. This combination of properties should therefore allow direct administration of the inert *cis* form of the PCL to tissues, which could then be selectively photoactivated with time and spatial precision. The preparation and characterisation of this type of PCLs are described in Chapter V.

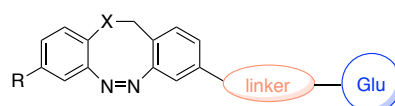


Figure II-3. General structure of the bridged azobenzene-based photochromic ligands prepared to behave as *trans*-active, *cis*-stable agonists of GluK1 and GluK2.

CHAPTER III

New azobenzene-based Photoswitchable Tethered Ligands for efficient two-photon neuronal excitation

This chapter reports our efforts towards the development of novel photoswitchable tethered ligands that enable multiphoton operation of neuronal systems upon stimulation with NIR light. The synthesis, characterisation and biological application *in vitro* and *in vivo* of these new compounds are next described.^a

^a The results reported in this chapter have been published in “Rationally designed azobenzene photoswitches for efficient two-photon neuronal excitation” Cabré, G.; Garrido-Charles, A.; Moreno, M.; Bosch, M.; Porta-de-la-Riva, M.; Krieg, M.; Gascón-Moya, M.; Camarero, N.; Gelabert, R.; Lluch, J. M.; Busqué, F.; Hernando, J.; Gorostiza, P.; Alibés, R. *Nat. Commun.* **2019**, *10*, 970.

III.1. INTRODUCTION

III.1.1. LiGluR FOR THE CONTROL OF NEURONAL SIGNALLING *IN VITRO* AND *IN VIVO*

In 2005, Trauner, Isacoff and co-workers pioneered the development of the first light-controlled ionotropic glutamate receptor, which they named LiGluR.¹ Their strategy consisted in modifying kainate-type glutamate receptor GluK2 by tethering a synthetic photochromic compound whose interaction with the ligand-binding domain could be altered by light; namely a PTL. Therefore, LiGluR functions as a light- and ligand-gated ion channel.

As described in Chapter I (see § I.1), GluK2 presents a *clamshell* ligand-binding domain that encloses around the glutamate agonist upon binding and allosterically triggers the opening of an ion channel. LBDs of this type represent an ancient module for allosteric activation and are widespread in nature. Therefore, the approach applied to the development of LiGluR could be extended to other pharmacologically important receptors, such as mGluRs, NMDA receptors, GABA_B receptors, bacterial quorum sensors or pheromone receptors.¹

The design of the PTL for LiGluR was based on extensive structure-activity relationship analysis but, mainly, on the X-ray structure of the LBD of GluK2 in complex with the agonist (2*S*,4*R*)-4-methyl glutamate. From this crystallographic structure it is evident that, upon glutamate binding, the LBD still features a narrow *exit channel*, which should enable a tether attached to the bound agonist to protrude and reach an attachment site at the surface of the protein without hampering ligand-receptor interaction. Prompted by this observation the authors

evaluated several potential candidate PTLs and finally focused on a molecule which they called **MAG**. This molecule presents (i) a cysteine-reactive maleimide for the conjugation to the exterior of the LBD (**M**), (ii) an azobenzene photoswitch that undergoes *trans-cis* photoisomerisation (**A**), and a glutamate derivative which acts as the agonist of the receptor and triggers the biological response (**G**) (Figure III-1a). At the same time, they also prepared a series of single cysteine mutants of Gluk2 by site-directed mutagenesis to find a suitable attachment site for the maleimide group of the PTL. They tested sixteen cysteine mutants around the LBD, among which eleven yielded functional channels that showed glutamate responses and three of them displayed clear responses to light. Among them, the mutant with the cysteine at position 439 (iGluR-L439, Figure III-1b) presented the larger responses.^{1,2}

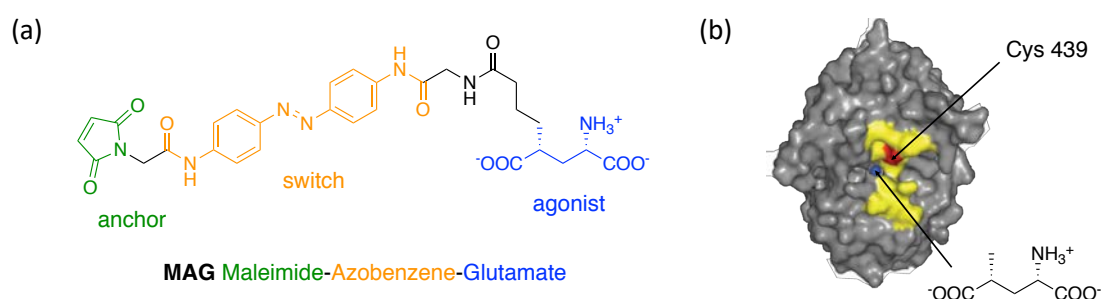


Figure III-1. (a) Structure of molecular switch **MAG**. The distinct functional units of this compound are shown in different colours (green: maleimide, orange: azobenzene core, and blue: glutamate) (b) View of the cleft of Gluk2 LBD in complex with agonist (2*S*,4*R*)-4-methyl glutamate (in blue). All the positions where cysteine residues were introduced are shown in yellow, while position 439 is depicted in red.¹

Figure III-2 displays a schematic representation of how LiGluR works under illumination. As depicted, **MAG** presents its *trans* extended structure in the dark, which is thermodynamically favoured. In this state the glutamate fragment lies far away from the binding site, and the ion channel remains closed. When **MAG** is irradiated with UV light ($\lambda_1 \sim 380$ nm), the central azobenzene unit turns into the folded *cis* configuration, which allows the interaction between the glutamate and the binding site, thus opening the ion channel for the cations to cross the membrane. Finally, this process could be reverted either through spontaneous thermal back-isomerisation to the *trans* state ($t_{1/2} \sim 18$ min at rt) or by irradiation with green light ($\lambda_2 \sim 500$ nm) to photoinduce the *cis*→*trans* interconversion.^{1,2,3}

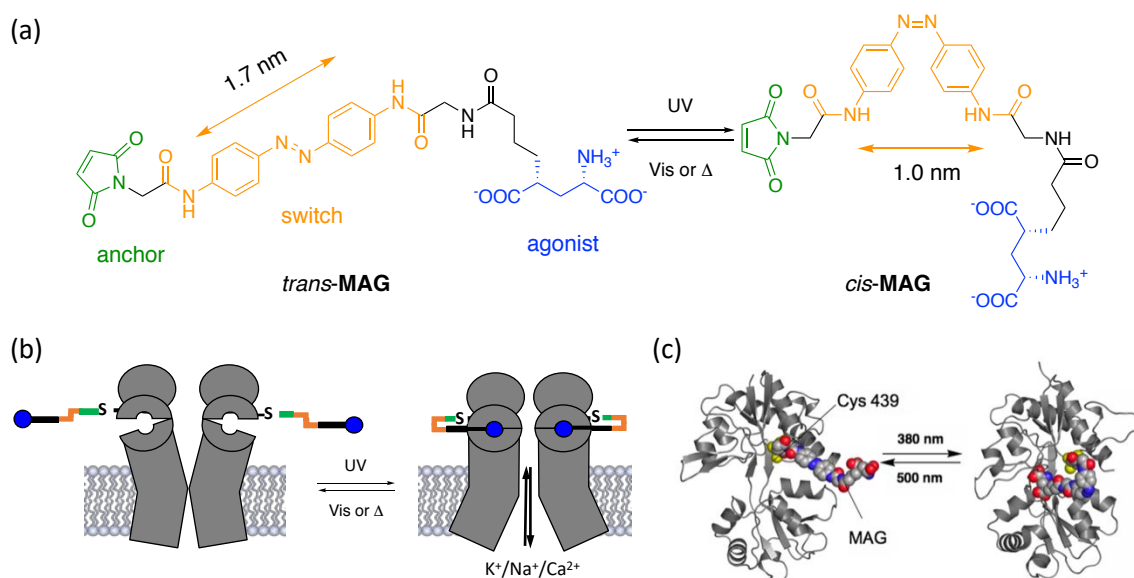


Figure III-2. (a) *Trans-cis* isomerisation of **MAG**. (b) Schematic representation of the light-induced operation of LiGluR. (c) The ribbon structure of *apo*-iGluR2 (Protein Data Bank ID code 1FTO)⁴ is depicted on the left, together with the ball-and-stick structure of *trans*-**MAG** in the extended and unbound conformation. On the right *cis*-**MAG** docked on the structure of iGluR6 in complex with methyl glutamate (Protein Data Bank ID code 1SD3)⁵ is shown.³

To assay the capability of LiGluR to trigger ion currents through cell membrane upon illumination and manipulate neuronal signalling, both *in vitro* and *in vivo* experiments were conducted. *In vitro* measurements were performed on both Human Embryonic Kidney (HEK293) cells^{1,3} and neurons^{2,6} that expressed the cysteine-mutated GluK2 receptor, and were subsequently incubated with **MAG** to induce conjugation of the photoswitch. Electrophysiological (whole-cell patch clamp, see § III.4)^{1,2,3,6} and fluorescent (calcium imaging, see § III.4)^{1,2,3} evaluation of these cells allowed registering differences in current (Figure III-3a) and fluorescence intensity (Figure III-3b) that were consistent with the light-induced aperture of LiGluR channels and the concomitant transport of ions between the extra- and intracellular media.

To test the feasibility of LiGluR to manipulate the firing of neurons *in vivo*, Isacoff, Trauner and co-workers took zebra-fish larvae as an animal model.⁶ In particular, they encoded cysteine-mutated GluK2 in the neurons that are involved in touch sensation of embryonic zebrafish, which were then incubated with **MAG**. In the dark, these organisms retained their ability to swim out after a gentle touch with a glass pipette. However, upon irradiation with UV light inducing *trans*→*cis* photoisomerisation of the LiGluR photoswitch, 28% of the larvae lost this intrinsic escape behaviour (Figure III-4a), which was recovered for 81% of them after photoexcitation with visible light (Figure III-4b).

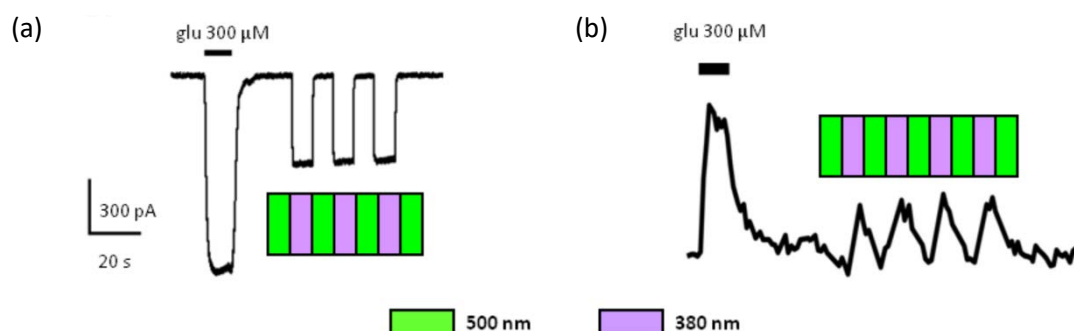


Figure III-3. Examples of (a) whole-cell patch clamp current trace and (b) calcium imaging fluorescence measurement for HEK293 cells transfected with LiGluR.¹ The first signal recorded in both traces arises from the injection of free glutamate to the sample ($c = 300 \mu\text{M}$) whilst the rest of them are induced by sequential irradiation at 380 nm and 500 nm. Photoexcitation with UV light results in activation of the channel upon *trans*→*cis* photoisomerisation, thus leading to changes in (a) current and (b) fluorescence intensity due to the transport of ions across the membrane. Subsequent photoexcitation with visible light allows the process to be reverted back, and the overall photochemical cycle can be repeated several times without apparent degradation.



Figure III-4. Zebra-fish larva expressing LiGluR in their touch sensory neurons. (a) Upon 365 nm irradiation, the intrinsic escape behavior after a gentle touch with a glass pipette is lost. (b) After illumination with 488 nm, the larva recovers its normal behavior.⁶

Despite the successful results obtained with **MAG**, this PTL suffers from several limitations, especially when applied *in vivo*. The most significant is the requirement to use UV or high energy visible light to induce azobenzene photoisomerisation, since this type of radiation (i) can produce cellular apoptosis or other photodamage processes upon prolonged exposure, and (ii) is strongly scattered and absorbed by biological media, thus significantly reducing the penetration depth in tissues (e.g. less than $300 \mu\text{m}$ in human white brain matter⁷). Isacoff,

Trauner and co-workers tried to overcome this drawback by the development of red-shifted derivatives **MAG₄₆₀**⁸ and **toCl-MAG**⁹ (Figure III-5), which undergo *trans*→*cis* photoisomerisation with visible light owing to the variation of the substitution pattern of the azobenzene core (λ_{max} = 460 nm for **MAG₄₆₀**⁸ and 560 nm for **toCl-MAG**⁹). However, the penetration depths attained in neural tissues in these spectral regions are still quite modest (e.g. about 500 μm for human white brain matter⁷).

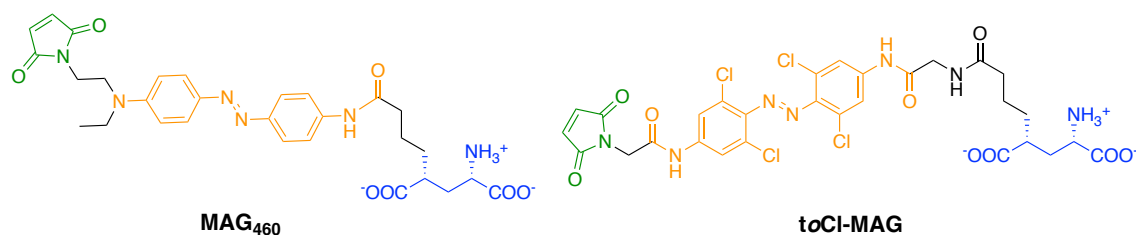


Figure III-5. Structure of red-shifted **MAG** derivatives: **MAG₄₆₀** and **toCl-MAG**.

A much better result could be reached by shifting the excitation wavelength of azobenzene-based PTLs to the near-infrared region (NIR, $\sim 700\text{-}1400$ nm), since much larger penetration depths are achieved with this radiation in biological tissues (e.g. more than 1 mm in human white brain matter⁷) with no biological photodamage. Unfortunately, the preparation of azobenzene photochromes that show regular absorption of NIR light is very challenging.^{10,11,12}

In view of this, an alternative would be to achieve NIR-induced manipulation of **MAG** derivatives via two-photon excitation,^{13,14} a strategy that provides further advantages: sub-micrometric spatial resolution in three dimensions¹⁵ and patterned illumination.^{16,17} However, in contrast to the progress made with optogenetics,^{18,19} efficient multiphoton operation of azobenzene switches still remains a challenge, mainly due to the low two-photon absorption cross-sections (σ_2 , see next section) of most of these compounds under NIR-light excitation.^{20,21}

III.1.2. TWO-PHOTON EXCITATION OF PHOTOSWITCHES WITH NIR LIGHT

Two-photon absorption (2PA) is a nonlinear process that consists in the simultaneous absorption of two photons by the same molecule. The theoretical basis for this process was set in 1931 by Maria Göppert-Mayer²² and, after the invention of the laser, it was first demonstrated experimentally in 1961 by Kaiser and Garret.²³

Unlike one-photon absorption (1PA) processes, photoexcitation of a chromophore via 2PA involves the formation of a *virtual state* with an infinitely short lifetime, with approximately half the energy of the final allowed state. Hence, it is required the nearly simultaneous absorption of two photons of this energy to excite the system. As depicted in Figure III-6, the effect of 2PA may be the same as 1PA (e.g. the excitation from a ground electronic state (S_0) to the first excited singlet electronic state (S_1) of a closed-shell organic molecule), but the mechanisms of both processes are remarkably different.

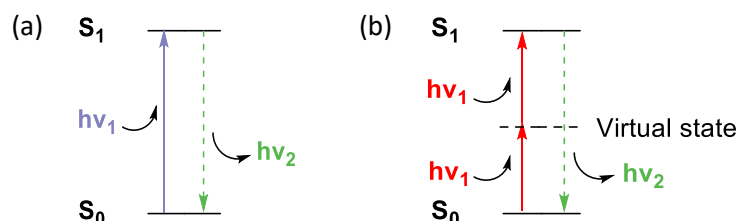


Figure III-6. Energy level diagrams for (a) 1P and (b) 2P absorption processes. As stated in the text, 2PA involves the absorption of two photons of the same energy and the formation of a short-lived *virtual state*. Once in the S_1 state, the system will undergo the same relaxation processes in both cases, such as the emission of fluorescence (shown in the figure as green dashed arrows).

Equation III-1 describes the one-photon (1P) and two-photon (2P) absorption contributions to the attenuation of a beam of light propagating through an absorbing material:¹⁴

$$-\frac{dI}{dz} = \alpha \cdot I + \beta \cdot I^2 \quad (\text{III-1})$$

In this equation I refers to the intensity of light, z is the propagation length inside the sample, and α and β describe the 1P and 2P absorption probability coefficients. Since 2PA involves the simultaneous interaction of two photons with a molecule, the absorption increases with the square of the intensity, and so, it is a nonlinear process. Moreover, $\beta \ll \alpha$, which restricts the importance of 2PA to very high excitation intensities, usually requiring the use of pulsed lasers. Hence, 2PA is an optical process several orders of magnitude weaker than 1PA, which depends linearly on the intensity.

If the intensity is expressed as a photon flux ($F = I/h\nu$) and the concentration of the sample (c) is taken into account, 2PA contribution can also be described by Equation III-2:¹³

$$-\left(\frac{dI}{dz}\right)_{2PA} = c \cdot \sigma_2 \cdot F \cdot I^2 \quad (\text{III-2})$$

In this equation, the coefficient σ_2 is known as the molecular 2PA cross-section and is usually reported in Göppert-Mayer units ($1 \text{ GM} = 10^{-50} \text{ cm}^4 \text{ s}^{-1} \text{ photons}^{-1} \text{ molecule}^{-1}$). This coefficient is the main parameter used to evaluate the efficiency of 2PA processes for any molecular material.

Even though the intrinsic lower probability of 2PA may be inconvenient in certain cases, it presents several advantages over 1PA that make it very attractive for biological imaging and the photoactivation of molecular probes. The most outstanding features of 2PA are:

- Restriction of the excitation to a small volume at the focal point of the irradiation source due to the quadratic dependence on the light intensity (Figure III-7).²⁴
- Higher penetration depth since tissue absorption and scattering are minimised. On one hand, absorption of the incident radiation takes place almost selectively at the focal point, which minimises the absorption losses throughout the material. On the other hand, 2PA occurs upon excitation with NIR light for most common organic molecules, a spectral region where biological tissues present low absorption and scattering.
- Low biological photodamage. Since 2PA absorption is less efficient than 1PA and as few biological chromophores are strong two-photon absorbers or one-photon NIR absorbers, the use of 2PA reduces photodamage.

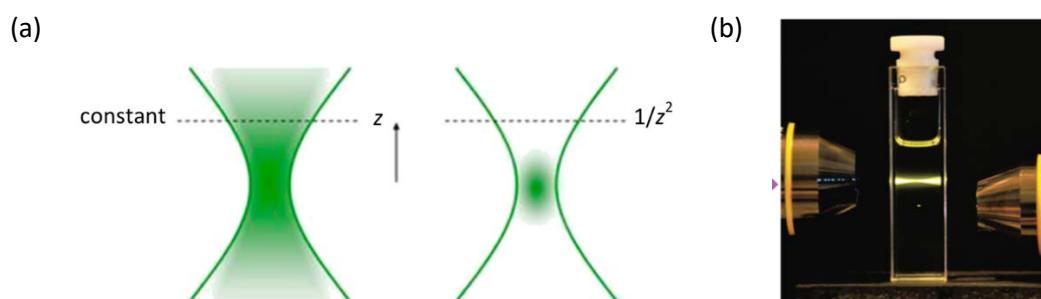


Figure III-7. (a) Schematic representation of the 1P (left) and 2P (right) absorption probability along the propagation direction (z) of a focused beam. If a light beam is focused onto sample at a wavelength only suitable for 1PA, molecules are excited throughout the beam path in the sample. By contrast, 2PA is non-linear and scales with the power of the excitation light, which makes absorption to be confined to the focal spot of the beam and its probability decays as $1/z^2$. (b) Image of a cuvette containing a fluorescent dye solution and the effect of two different laser beams on it: (i) the top beam excites the dye through 1PA, thus causing fluorescence to be emitted along all the propagation path through the cuvette; and (ii) the bottom beam induces 2P excitation of the compound, which selectively fluoresce from the focal point.²⁴

The main drawback of 2PA lies in the fact that only a few number of organic chromophores are able to absorb light efficiently via this process. As a result, σ_2 values are very low for most molecules (typically, $\sigma_2 < 10$ GM). Nevertheless, the structural factors that influence 2PA cross-section of molecules have been widely analysed¹³ and their σ_2 values can nowadays be predicted to a fairly high precision by computational calculations.²⁵ From these studies, the key structural requirements for maximising σ_2 for a chromophore have been identified to be: (i) long π -conjugation systems; (ii) the presence of strong EDGs and/or EWGs at the centre and ends of the π -conjugated system (π) to promote strong internal charge transfer upon electronic excitation; (iii) molecular symmetry, being centrosymmetric structures (e.g. EDG- π -EDG) normally preferred; (iv) molecular planarity; and (v) the incorporation of multibranching or oligomer structures which may induce *cooperative effects*. Figure III-8 clearly illustrates the effect of some of these parameters to σ_2 , taking stilbene **11** as an example.¹⁴

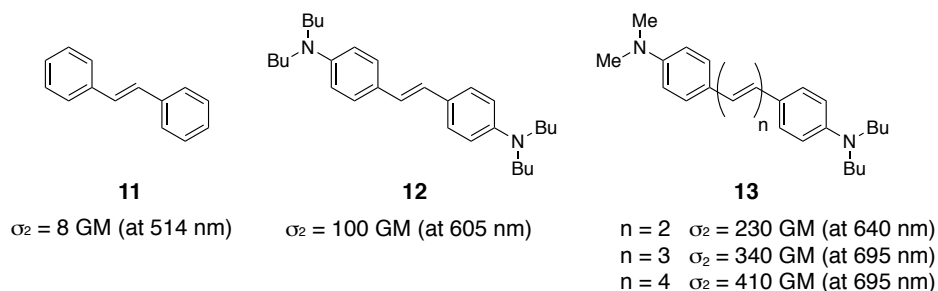


Figure III-8. The effect of the substituents and the conjugation length on the 2PA cross-section. Compound **12** presents a 14-fold increase in σ_2 value with respect to basic stilbene **11**, since it bears two dialkylamines at 4 and 4' positions which confer the system an EDG- π -EDG structure. Moreover, the extension of the conjugation in compound **13** leads to a further increase of the σ_2 value.¹⁴

Azobenzenes display rather low σ_2 values, which poses a limitation to the operation of **MAG** compounds under 2PA. Only a limited number of studies investigating the 2PA activity of azobenzenes from a fundamental point of view are found in the literature,^{20,21,26,27,28} most of them reported by Mendonça and co-workers. In these studies, a correlation between the molecular structure of azobenzenes and their σ_2 values was established. On one hand, it was observed that the increase in the conjugation path of these compounds seems to have little influence in their 2PA, whilst the addition of EDGs and EWGs provoked large variations. In addition, it was found that electronically symmetric azobenzene derivatives do not present any peak in their 2PA spectra and they display rather low σ_2 values in the NIR region (below 50 GM). By contrast, push-pull substitution by introduction of both EDGs and EWGs resulted in clear 2PA spectral peaks at twice the energy of the 1PA bands and σ_2 values up to 500 GM.

In view of these results, poor 2PA properties are expected for **MAG** as it presents an electronically symmetric azobenzene core bearing weak *p*-amido EDGs. Actually, the experimental σ_2 determined for **MAG** was 10 GM ($\lambda_{\max} = 820$ nm), while **MAG₄₆₀** displayed an 8-fold increase in this value: 80 GM ($\lambda_{\max} = 850$ nm),²⁹ thus supporting the postulation that electronically-asymmetric azobenzenes exhibit larger σ_2 .

For this reason, many efforts have been devoted to developing new **MAG** compounds that present higher σ_2 values and, thus, allow the operation of LiGluR with NIR light. In the next section, the main strategies that had been devised for this purpose are detailed.

III.1.3. STRATEGIES TOWARDS TWO-PHOTON ABSORPTING **MAG** DERIVATIVES

The multiphoton operation of LiGluR with NIR light would notably improve the applicability of this system for *in vitro* and *in vivo* studies, since it enables deeper penetration depths in biological tissues with minimal biological degradation. However, the azobenzene core present in **MAG** displays low σ_2 values and, thus, is not suitable for 2P excitation. In order to enhance the 2PA of **MAG**-type PTLs, two different strategies have been studied so far.

The first strategy is based on the incorporation of a photosensitiser unit to the ligand, which efficiently absorbs NIR light via 2P processes and transfers its electronic excitation energy to the azobenzene core to trigger isomerisation. This methodology was pioneered in our group during Marta Gascón-Moya's PhD thesis^{30,31,32} and has also been applied to accomplish 2P-induced manipulation of other azobenzene-based photochromes.^{33,34} In particular, Gascón-Moya developed two new **MAG** derivatives named **MAGA**^{31,32} where a 2P-absorbing antenna was tethered to the PTL: a pyrene group in **MAGA_{2P_pyr}**³¹ and a naphthalene derivative in **MAGA_{2P}**³² (Figure III-9). However, although this strategy works well for free **MAGA** molecules in solution and other azobenzene switches,^{33,34} when applying this approach to biological samples several problems were encountered that severely compromised the 2P sensitised photoswitching efficiency of LiGluR with NIR light: (i) poor solubility in water because of the lipophilicity of the 2P-absorbing antennas introduced; (ii) low conjugation efficiency to cysteine-tagged GluK2; and/or (iii) reduced affinity towards the receptor binding site after incorporation of the photosensitiser unit due to steric effects.^{31,32}

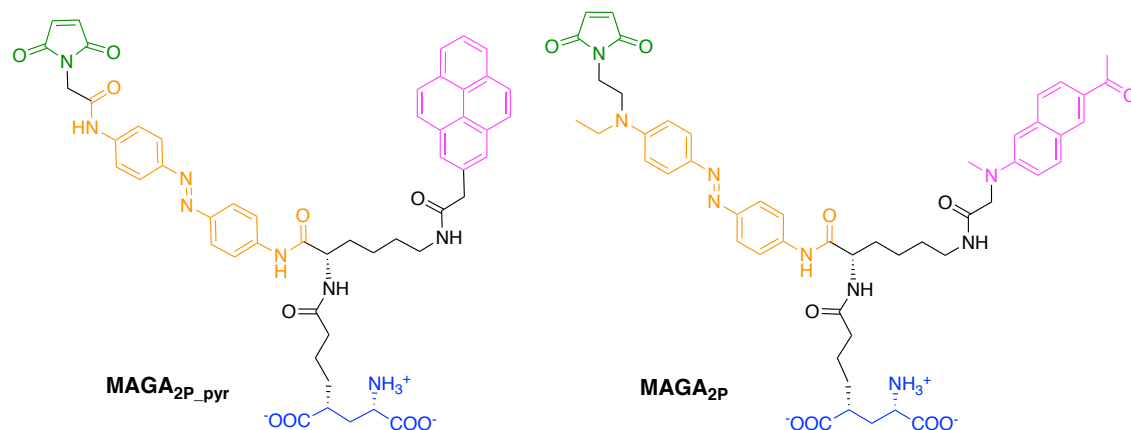


Figure III-9. Structure of the developed **MAGA** compounds by Gascón-Moya in our group.^{31,32} These molecules display the typical structure of **MAG** compounds, to which a 2P harvesting antenna (pink) is tethered. This antenna harvests NIR light via 2PA and transfers the energy to the azobenzene core for its isomerisation.

As an alternative, a second strategy was explored that involves the use of electronically-asymmetric azobenzene switches, since this type of substitution pattern has been demonstrated to enhance their 2PA cross-sections.^{20,28} For **MAG**-type PTLs, this concept was assessed both by Gascón-Moya in our group³² (**MAG_{2P}**, Figure III-10) and Isacoff and co-workers^{8,29} (**MAG₄₆₀**, Figure III-10), who introduced a strong electron-donating amino group to the azobenzene core of **MAG**. These new compounds proved to display a notable increase in their σ_2 values ($\sigma_2 = 80$ GM for *trans*-**MAG₄₆₀** at 850 nm²⁹) and 2P-induced control of LiGluR-expressing HEK293 cells and neurons with NIR light could be achieved.^{8,32} However, this was at the expense of a dramatic decrease of the thermal stability of the *cis* isomer (τ_{cis}) of the photoswitch down to the sub-second time scale. This is a well-known property of azobenzenes, where introduction of strong mesomeric EDG and/or EWG concomitantly accelerates the *cis*→*trans* thermal back-isomerisation in the dark, especially in aqueous media (e.g. with EDG = 4-NR₂ and EWG = 4-NO₂).³⁵ As a result, the *cis* isomer of **MAG_{2P}** and **MAG₄₆₀** back-isomerised as soon as the illumination ceased and prevented building up a large population of the open state of LiGluR and, hence, the generation of large biological responses.^{8,32}

It is clear then, that in order to be able to operate LiGluR via 2PA of NIR light and create large biological responses, a compromise must be met to obtain **MAG**-type PTLs with electronically-asymmetric azobenzene cores that display both large σ_2 and τ_{cis} values. Therefore, in this thesis we decided to design new **MAG** derivatives that present a push-pull substitution of the azobenzene core to enhance σ_2 , but avoiding the use of strong mesomeric EDGs and EWGs, the

presence of which dramatically decreases the thermal stability of the *cis* isomer. In particular, we devised the functionalisation of the azobenzene core of the ligand with two amides: one of them linked through its N atom, thus acting as a weak mesomeric EDG; and the other tethered through the carbonyl group, thereby performing as a weak mesomeric EWG. Moreover, we explored the incorporation of an additional F substituent in *ortho* position as a strong inductive EWG to further enhance σ_2 . Based on these principles, new **MAG**-type PTLs **MAG_{2P}^{slow}** and **MAG_{2P-F}^{slow}** were designed to achieve efficient 2P-induced control of LiGluR with NIR light (Figure III-11).

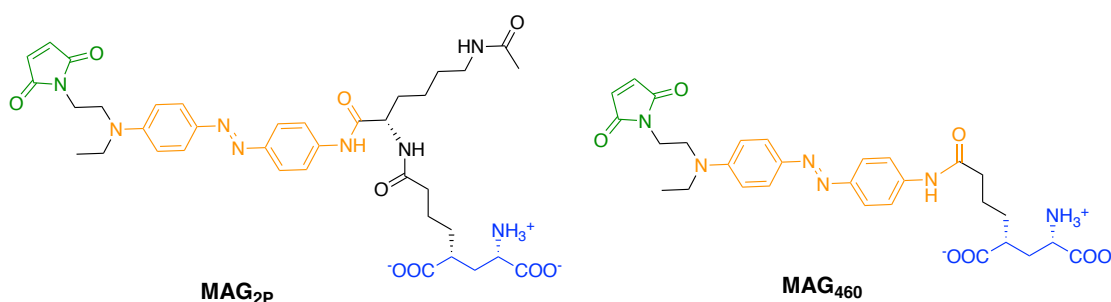


Figure III-10. **MAG**-type PTLs **MAG_{2P}** and **MAG₄₆₀** exhibiting an electronically-asymmetric azobenzene core which presents an enhanced 2PA cross-section value.^{8,32}

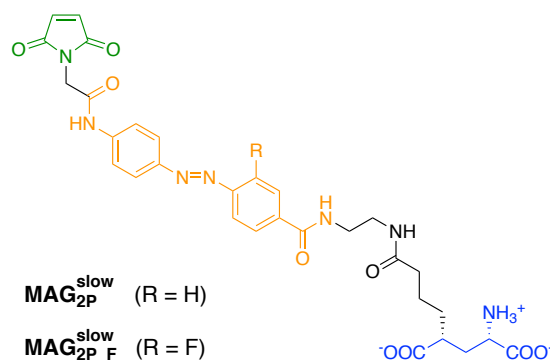


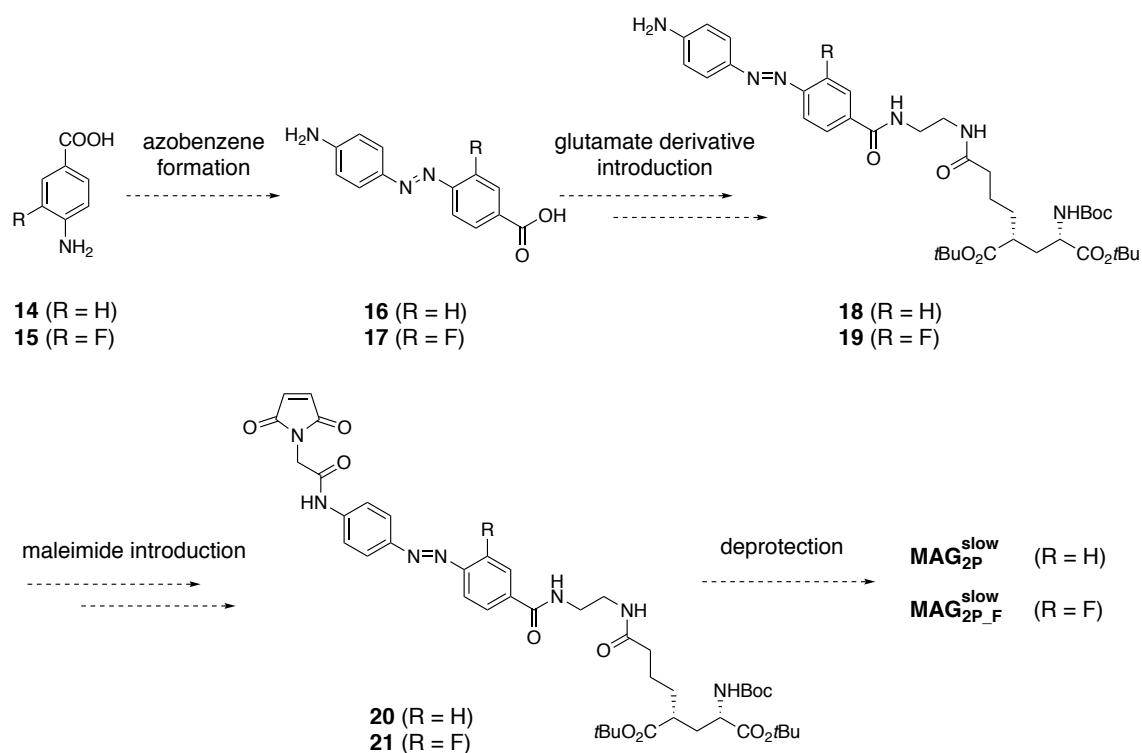
Figure III-11. Structures of the new **MAG**-type PTLs with expected large σ_2 and τ_{cis} values. Both of them present a push-pull substitution of the azobenzene core, avoiding the use of strong mesomeric EDGs and EWGs. In the case of **MAG_{2P-F}^{slow}**, an additional F substituent is introduced in *ortho* position, which should confer this ligand with a larger 2PA cross-section.

The following sections of this chapter are devoted to describing the synthesis and characterisation of these new **MAG** derivatives, as well as the studies of the activity of these compounds *in vitro* and *in vivo*.

III.2. SYNTHESIS OF PTLs $\text{MAG}_{2\text{P}}^{\text{slow}}$ AND $\text{MAG}_{2\text{P_F}}^{\text{slow}}$

III.2.1. STRATEGY TOWARDS THE SYNTHESIS OF TARGET COMPOUNDS $\text{MAG}_{2\text{P}}^{\text{slow}}$ AND $\text{MAG}_{2\text{P_F}}^{\text{slow}}$

The procedure for the synthesis of $\text{MAG}_{2\text{P}}^{\text{slow}}$ and $\text{MAG}_{2\text{P_F}}^{\text{slow}}$ was inspired on the strategy developed by Gascón-Moya in our group for the preparation of $\text{MAGA}_{2\text{P_pyr}}$, $\text{MAGA}_{2\text{P}}$ and $\text{MAG}_{2\text{P}}$.^{30,31,32} It basically consists in a modular methodology through which the different functional building blocks of the ligand (maleimide, glutamate, and if required, antenna) are tethered to the central azobenzene core, mainly via amide bond formation. Although this is the same strategy already used by Isacoff, Trauner and co-workers for their earlier synthesis of MAG ,¹ Gascón-Moya introduced an important difference by developing a new methodology for the introduction of the glutamate unit that simplifies the synthetic procedure (see § III.2.3).³¹ Based on this strategy, the synthetic pathway shown in Scheme III-1 was devised for the preparation of $\text{MAG}_{2\text{P}}^{\text{slow}}$ and $\text{MAG}_{2\text{P_F}}^{\text{slow}}$.



Scheme III-1. Synthetic pathway designed for the synthesis of target PTLs $\text{MAG}_{2\text{P}}^{\text{slow}}$ and $\text{MAG}_{2\text{P_F}}^{\text{slow}}$.

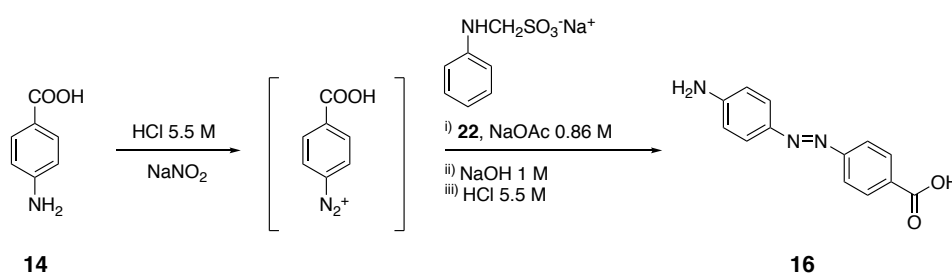
Since the azobenzene cores of our target molecules were not commercially available, the first step of our synthetic route was devoted to the obtention of azobenzenes **16** and **17** from

commercially available 4-aminobenzoic acid, **14**, and 3-fluoro-4-aminobenzoic acid, **15**, respectively. Then, a coupling reaction with a linker followed by the introduction of a glutamate derivative obtained from commercial L-pyroglutamic acid should afford intermediates **18** and **19**. Afterwards, the introduction of the maleimide moiety should furnish intermediates **20** and **21**. Finally, removal under acidic conditions of the protecting groups of the glutamate moiety should lead to target molecules **MAG_{2P}^{slow}** and **MAG_{2P-F}^{slow}**. All the synthetic steps of this pathway are described in detail in the following sections.

III.2.2. SYNTHESIS OF AZOBENZENE CORES **16** AND **17**

Coupling reactions between aryldiazonium salts and other aromatic compounds like aniline are a synthetic methodology extensively studied to obtain different types of azocompounds.³⁶ In this type of reactions, an aromatic amine is first transformed into its diazonium salt, which then reacts with another aromatic compound to furnish the azoaromatic moiety through an electrophilic aromatic substitution. We used this strategy for the preparation of azobenzene core **16** and **17**.

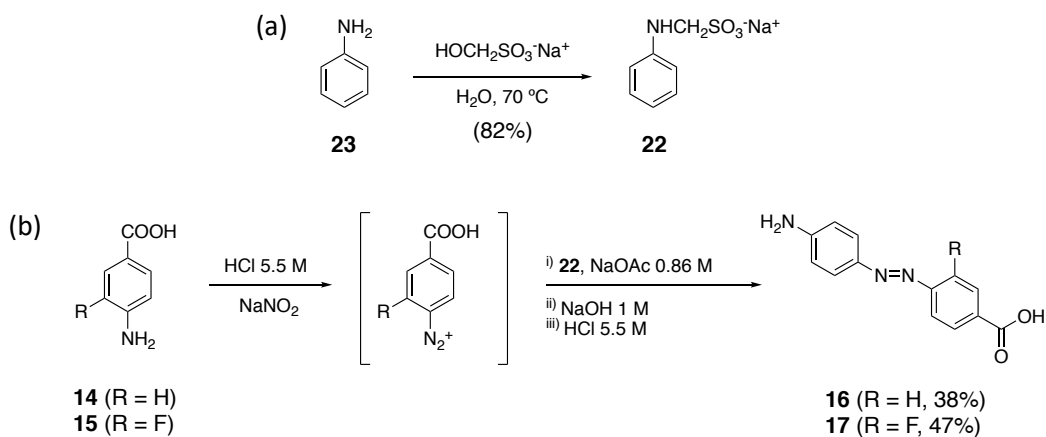
Actually, the synthesis of azobenzene **16** from compound **14** had already been studied by Morishima and co-workers (Scheme III-2).³⁷ Therefore, we decided to use the same conditions to afford both azobenzenes **16** and **17**, which had already been tested by Gascón-Moya in her Master Thesis.³⁸



Scheme III-2. Synthesis of azobenzene **16** reported by Morishima and co-workers.³⁷

Compound **22** required for azobenzene formation was synthesised as depicted in Scheme III-3a, where commercially available aniline **23** and sodium hydroxymethylsulfonate reacted in aqueous media at 70 °C.^{37,39} The procedure reported in the literature involved filtration of the solid formed, which was then washed with H₂O and Et₂O to give sulfonate **22** in 39% yield.

However, we observed that this product was highly soluble in H₂O, for which we decided to wash it only with Et₂O. This allowed obtaining compound **22** in a larger yield (82%).



Scheme III-3. (a) Synthesis of compound **22**. (b) Synthesis of azobenzene cores **16** and **17**.

Then, following the methodology described in Scheme III-3b, the diazonium salts of compounds **14** and **15** were formed with sodium nitrite under acidic conditions and were then coupled with sulfonate **22**. This procedure requires very well controlled conditions. On one hand, temperature must not exceed 10 °C and pH must be acid in order to guarantee the stability of the diazonium cation. However, pH must not be too low (pH = 2-3) in order to maintain a high enough concentration of the non-protonated form of **22**, as arylammonium ions are poorly reactive in coupling processes with diazonium salts. The solids obtained after the azocoupling reaction were filtered, recrystallised with NaOH and hydrolysed with HCl to give azobenzenes **16** and **17** as orange solids in 38% and 47% yield, respectively, which were successfully characterised by NMR and IR spectroscopy and MS. Of especial interest was the ¹³C NMR spectrum of **17**, which showed clear signal splitting due to C-F spin coupling for the aromatic carbon nuclei of the fluorosubstituted ring.

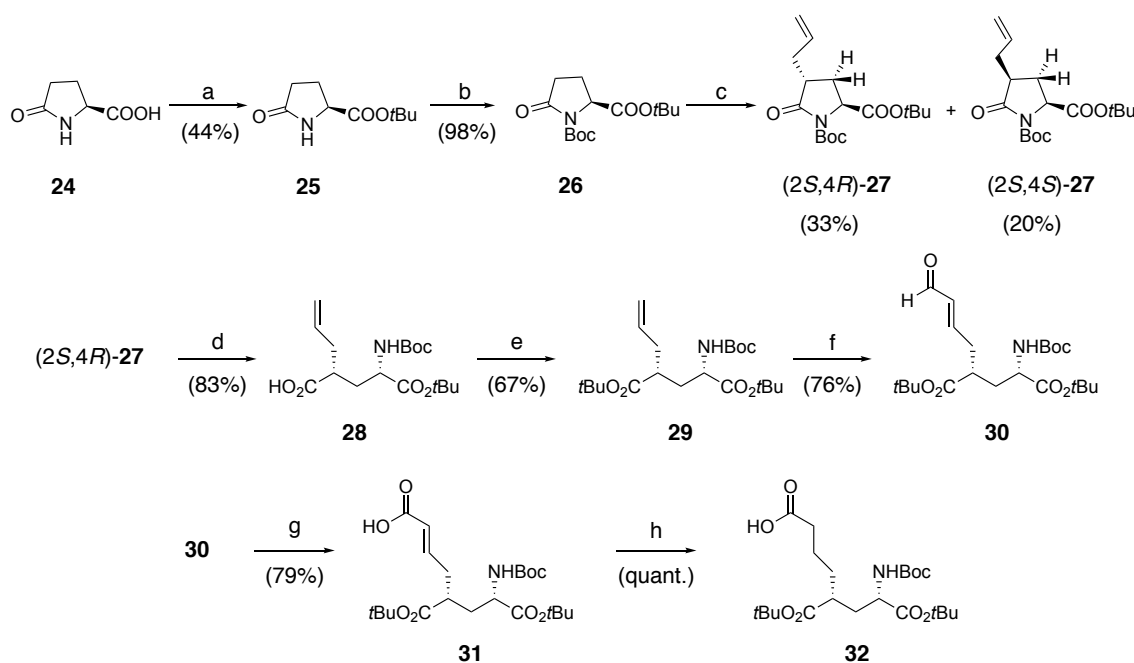
III.2.3. SYNTHESIS AND INCORPORATION OF GLUTAMATE DERIVATIVE **32**

According to the synthetic pathway designed, the next step was the introduction of the glutamate moiety to the ligand, for which we followed the methodology previously developed by Gascón-Moya in our group that relies on the use of fully protected glutamate derivative **32**.³¹ This allows overcoming some of the difficulties encountered with the cyclic pyroglutamate group normally employed in the synthesis of **MAG** compounds^{1,3,8,9}: (i) moderate stability to the

basic conditions required for the ring opening reaction of pyroglutamate of the maleimide fragment, thus requiring its introduction in a later step of the synthesis; and (ii) low solubility of the dicarboxylic acid generated from the ring opening process of the pyroglutamate precursor, which complicated its manipulation and detrimentally affected the efficiency of posterior reactions (e.g. incorporation of the maleimide group).³¹ This compound is not commercially available; thus, we first focused on the synthesis of glutamate derivative **32**.

III.2.3.1. Synthesis of glutamate derivative **32**

Glutamate derivative **32** was synthesised through the following multistep synthetic sequence previously implemented in our group (Scheme III-4).³¹



Reagents and conditions: (a) H_2SO_4 , $t\text{BuOAc}$; (b) Boc_2O , DMAP, CH_3CN ; (c) i) LiHMDS, THF, $-78\text{ }^\circ\text{C}$; ii) allyl bromide, THF, $-78\text{ }^\circ\text{C}$; (d) i) 1 M LiOH, THF/ H_2O (1:1), $0\text{ }^\circ\text{C}$; ii) 1 M HCl; (e) *tert*-butyl 2,2,2-trichloroacetimidate, $\text{BF}_3 \cdot \text{OEt}_2$, CH_2Cl_2 ; (f) Hoveyda-Grubbs II, crotonaldehyde, CH_2Cl_2 , reflux; (g) NaClO_2 , NaH_2PO_4 , 2-methyl-2-butene, $t\text{BuOH}/\text{H}_2\text{O}$ (5:1); (h) H_2 , Pd/C (10% w/w), EtOAc.

Scheme III-4. Synthesis of glutamate derivative **32**.³¹

The synthetic sequence commenced with the protection of the carboxylic acid of commercially available L-pyroglutamic acid, **24**, as the corresponding *tert*-butyl ester **25** with $t\text{BuOAc}$ and H_2SO_4 in 44% yield. Then, its nitrogen atom was protected as a *tert*-butyl carbamate to obtain known pyroglutamate **26**⁴⁰ in 98% yield. Compound **26** was treated with LiHMDS in THF at $-78\text{ }^\circ\text{C}$ to form the corresponding enolate, which was allowed to react with allyl bromide at $-78\text{ }^\circ\text{C}$

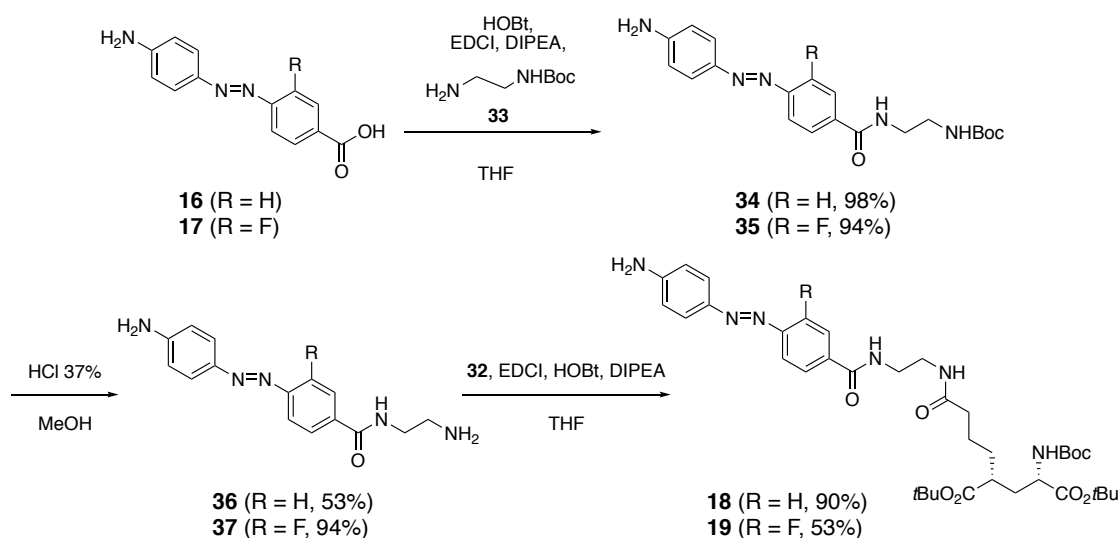
to afford a diastereoisomeric mixture of already reported allylated derivatives (2*S*,4*R*)- and (2*S*,4*S*)-**27**.⁴¹ Diastereoisomer (2*S*,4*R*)-**27** was isolated by purification by column chromatography in 33% yield and used in the following steps. The obtention of this compound is the key step of the synthetic route since: (i) the configuration of the chiral centres present in (2*S*,4*R*)-**27** will remain the same in the final glutamate derivative **32**; and (ii) is the reaction that provides the lowest yield. Actually, during my Master Thesis we studied the elements that may influence this reaction and two factors were found to detrimentally affect its yield: (i) inadequate control of the temperature during allyl bromide addition, thus leading to a higher formation of the thermodynamic enolate; and (ii) reaction time longer than 4 h, since after this time the product starts to decompose.⁴² Hence, by accurately controlling the temperature during the allyl bromide addition and the reaction time, reproducible yields can be accomplished. The assignment of the relative configuration of both isomers was confirmed by comparison with the NMR data described in the literature.⁴¹

The next step of the synthesis was the ring opening of allyl (2*S*,4*R*)-**27** by treatment with LiOH and subsequent acidification with 1 M HCl, which afforded acid **28** in 83% yield. Protection of the carboxylic acid as a *tert*-butyl ester with *tert*-butyl 2,2,2-trichloroacetimidate and catalytic BF₃·OEt₂ furnished glutamate derivative **29** in 67% yield. Afterwards, a cross-metathesis reaction of **29** with crotonaldehyde in the presence of 1% 2nd generation Hoveyda-Grubs catalyst gave aldehyde **30** in 76% yield, which was converted into the corresponding acid **31** in 79% yield following a Pinnick oxidation process.⁴³ This type of reaction uses NaClO₂ as oxidant in the presence of 2-methyl-2-butene as the scavenger of the hypochlorous acid generated. Finally, target glutamate derivative **32** was obtained quantitatively from enone **31** by standard hydrogenation using a palladium catalyst. Hence, glutamate derivative **32** was afforded through an 8-step linear synthesis from commercial L-pyroglutamic acid in 5% overall yield.

III.2.3.2. Introduction of glutamate derivative **32**

Once glutamate derivative **32** was synthesised, it had to be attached to azobenzene cores **16** and **17**. For this, we used an ethylenediamino linker, which: (i) could react with the carboxylic acid groups of both azobenzenes **16** and **17** and glutamate **32**; and (ii) allowed the separation distance between these units in the final ligands to fairly reproduce the structural features of the original **MAG** molecule.¹ Scheme III-5 shows the synthetic procedure followed to accomplish this objective in this work, for which a couple of consecutive amide bond formation reactions were required. One of the most successful approaches to undertake these reactions is the use

of coupling agents,^{44,45} which activate the carboxylic acid moiety by transformation into a new species that easier reacts with the desired amine to produce the target amide. Inspired by many amide bond formation reactions conducted in similar substrates in our group,³⁰ we decided to use EDCI as a coupling agent, HOBT as an additive to inhibit side reactions, and DIPEA as base for the introduction of glutamate **32**.



Scheme III-5. Introduction of glutamate fragment **32** to azobenzene photochromes **16** and **17**.

First, we applied these conditions to tether commercially available *tert*-butyl (2-ethylamine)carbamate, **33**, to the corresponding azobenzene derivative (**16** or **17**). The crude obtained after overnight stirring at room temperature (rt) was purified by column chromatography, providing carbamates **34** and **35** in almost quantitative yields. ¹H and ¹³C NMR spectra of both compounds revealed the success of the introduction of the linker by the appearance of new signals corresponding to the protected ethylamine fragment. Moreover, novel ¹H NMR signals corresponding to the amide formed were also detected at 8.56 ppm in **34** and at 8.62 ppm in **35**.

Afterwards, removal of the *tert*-butyl carbamate protecting group of intermediates **34** and **35** was achieved by treatment with 37% HCl in methanol, which furnished amines **36** and **37** with 53% and 94% yield, respectively. The difference in yield for these two analogous reactions was due to the lower solubility of the fluorinated compound in aqueous media. As such, when the process was quenched with a saturated solution of NaHCO₃, amine **37** immediately precipitated, which facilitated its isolation by filtration. By contrast, amine **36** was moderately soluble in the aqueous medium and could only be partially extracted from the reaction solution with CH₂Cl₂.

^1H NMR spectra of both compounds confirmed the removal of the Boc protecting group by the disappearance of the characteristic CH_3 signals at 1.38 ppm and carbamate signals at 6.94 ppm.

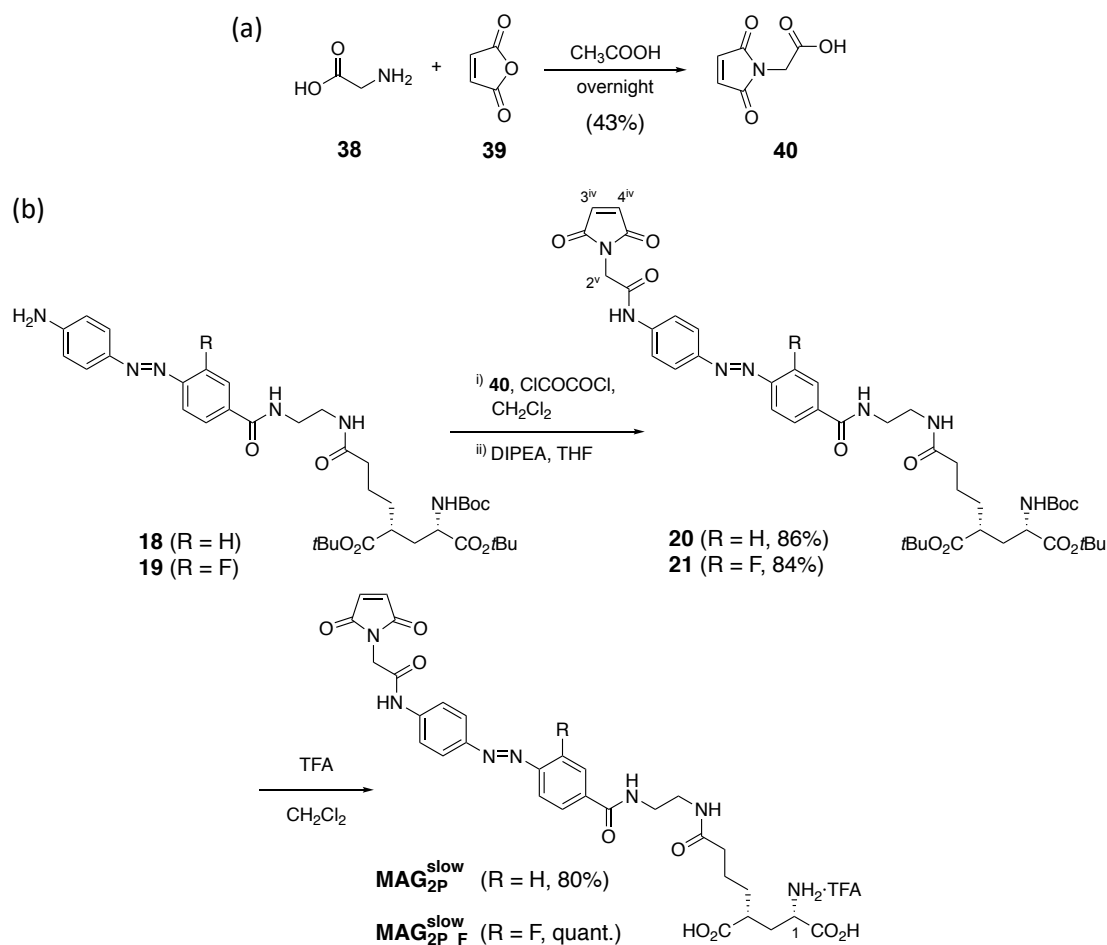
Finally, glutamate derivative **32** was attached to azobenzenes **36** and **37** through another amide bond formation reaction with EDCI, HOBt and DIPEA, delivering amines **18** and **19** as orange solids in 90% and 53% yield, respectively. These new compounds already displayed two of the three basic units of a **MAG** compound: (i) an azobenzene photoswitch; and (ii) a glutamate derivative moiety. Actually, new signals corresponding to the glutamate fragment introduced were observed in the ^1H and ^{13}C NMR spectra of molecules **18** and **19**.

III.2.4. INCORPORATION OF THE MALEIMIDE MOIETY AND PREPARATION OF TARGET COMPOUNDS **MAG**_{2P}^{slow} AND **MAG**_{2P_F}^{slow}

To culminate the synthesis of target compounds **MAG**_{2P}^{slow} and **MAG**_{2P_F}^{slow}, a maleimide moiety had to be incorporated to intermediates **18** and **19** and all the protecting groups of the glutamate unit had to be finally removed.

Following a procedure previously used in our group by Gascón-Moya,³⁰ we decided to introduce the maleimide group by reaction between carboxylic acid **40** and amines **18** and **19**. Hence, we first synthesised compound **40** by refluxing an acetic acid solution of commercially available glycine, **38**, and maleic anhydride, **39**, as reported in the literature (Scheme III-6a).⁴⁶ After purification by column chromatography, compound **40** was furnished in 43% yield.

Subsequently, acid **40** was activated by treatment with oxalyl chloride in dichloromethane and afterwards added onto an ice-cooled solution of the corresponding amine (**18** or **19**) and DIPEA in THF (Scheme III-6b). After 4 h of reaction at rt, the product was isolated and purified by column chromatography. Final intermediates **20** and **21** were afforded in 86% and 84% yield, respectively, as orange solids. Appearance of two new singlet signals at 6.82 and 4.40 ppm in **20** and 6.86 and 4.42 ppm in **21** corresponding to the olefinic protons (H-3^{IV} and H-4^{IV}) and methylene protons (H-2^{V}) evidenced successful introduction of the maleimide moiety into the ligand backbone. These crucial intermediates **20** and **21** already presented the main structure of **MAG** derivatives: (i) an azobenzene core; (ii) a glutamate derivative; and (iii) a maleimide moiety.



Scheme III-6. (a) Synthesis of maleimide derivative **40**. (b) Introduction of **40** to the ligands and final deprotection of the glutamate unit to obtain target PTLs **MAG**_{2P}^{slow} and **MAG**_{2P_F}^{slow}.

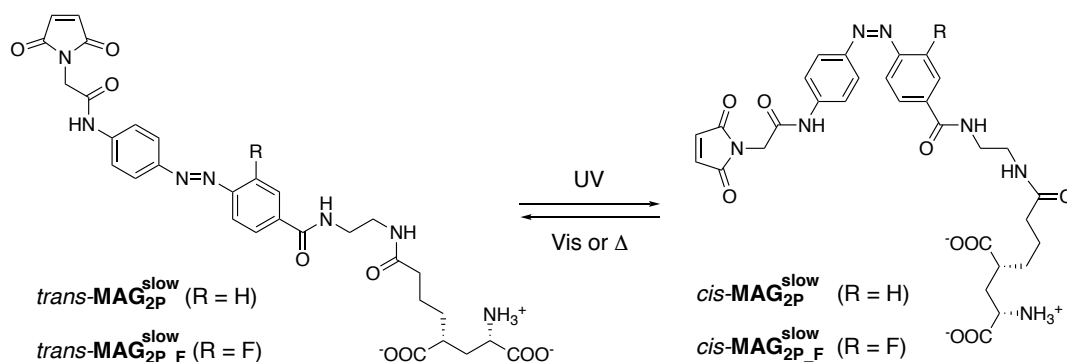
The final step of the synthetic route towards PTLs **MAG**_{2P}^{slow} and **MAG**_{2P_F}^{slow} was the removal of the protecting groups of the glutamate moiety, which we conducted using the methodology tested by Gascón-Moya for the preparation of **MAGA**_{2P_pyr}, **MAGA**_{2P} and **MAG**_{2P}.^{30,31,32} In particular, this was achieved by the treatment of products **20** and **21** with trifluoroacetic acid (TFA) in dichloromethane media, which afforded **MAG**_{2P}^{slow} in 80% yield as a lilac solid and **MAG**_{2P_F}^{slow} in a quantitative yield as an orange solid (Scheme III-6b). Both compounds were unequivocally identified from their spectroscopic data. Their ¹H NMR showed the disappearance of the characteristic *tert*-butyl signals between 1.40 and 1.50 ppm and carbamate signals around 5.05 ppm. Moreover, downfield shifts were observed for proton H-1 signals: from 4.14 ppm in **20** to 3.54 ppm in **MAG**_{2P}^{slow}, and from 4.17 ppm in **21** to 3.56 ppm in **MAG**_{2P_F}^{slow}. Finally, ¹³C NMR also confirmed the removal of the protecting groups by the disappearance of characteristic carbamate signals at 155.6 ppm and *tert*-butyl signals around 82-79 ppm and 28 ppm. Interestingly, two sets of ¹³C signals could be observed for the carbons corresponding to the

glutamate moiety, which was ascribed to conformational issues. It was determined that the presence of water enhanced the appearance of this second set of signals, while freshly prepared solutions of the compounds in DMSO- d_6 did not present these double signals.

In summary, new **MAG** derivatives **MAG**_{2P}^{slow} and **MAG**_{2P_F}^{slow} with potential activity as two-photon NIR-responsive photoswitchable tethered ligands were prepared through a 6-step linear sequence where glutamate and maleimide functions were sequentially introduced into the azoaromatic photochrome of choice. Compound **MAG**_{2P}^{slow} was afforded in 12% overall yield from aminobenzoic acid **14**, and compound **MAG**_{2P_F}^{slow} was obtained in 20% overall yield from aminobenzoic acid **15**.

III.3. PHOTOCHEMICAL CHARACTERISATION OF PTLs **MAG**_{2P}^{slow} AND **MAG**_{2P_F}^{slow}

Once target compounds **MAG**_{2P}^{slow} and **MAG**_{2P_F}^{slow} were synthesised and fully chemically characterised, we focused our attention on the investigation of their photochemical behaviour in solution. Since these molecules are azobenzene-based photoswitches, they should present two differentiated states that display different structural and physicochemical properties. These two states can be interconverted upon reversible photoinduced *trans-cis* isomerisation by direct excitation of their azoaromatic units (Scheme III-7). Moreover, the thermal instability of their *cis* isomer should result in spontaneous back isomerisation to the more stable *trans* state in the dark. These photochemical and thermal interconversion processes were investigated in detail, and the results obtained are described in this section. Most of the experiments reported herein were carried out in a phosphate buffer solution (PBS) with 1% of DMSO in order to reproduce similar conditions to those applied in the biological experiments (i.e. aqueous media with a maximum 1% in DMSO). A minimum amount of DMSO was required to favour solubility in water of **MAG**_{2P}^{slow} and **MAG**_{2P_F}^{slow}. Moreover, for comparative purposes, the photochemical behaviour of **MAG**, and even **MAG**_{2P}, was also studied. It must be noted that, since a NIR tuneable pulsed laser is not available in our laboratories, our photochemical studies were only conducted under 1P excitation conditions. 2PA properties of these potential photoswitchable tethered ligands were investigated directly in biological samples.



Scheme III-7. Photoinduced *trans-cis* isomerisation of PTLs $\text{MAG}_{2P}^{\text{slow}}$ and $\text{MAG}_{2P_F}^{\text{slow}}$ upon one-photon excitation with UV-vis light. *Cis*→*trans* back-isomerisation can also proceed thermally.

III.3.1. TRANS→CIS PHOTOISOMERISATION

We started our studies by recording the absorption spectra of the thermally stable *trans* isomers of **MAG**, $\text{MAG}_{2P}^{\text{slow}}$, $\text{MAG}_{2P_F}^{\text{slow}}$ and MAG_{2P} (Figure III-12). **MAG**, $\text{MAG}_{2P}^{\text{slow}}$ and $\text{MAG}_{2P_F}^{\text{slow}}$ present very similar absorption spectra, which are typical for azobenzene-type switches in the absence of strong mesomeric EDW and EDG.³⁵ In particular, they display: (i) an intense absorption band at $\lambda_{\text{max}} = 361, 352$ and 357 nm for **MAG**, $\text{MAG}_{2P}^{\text{slow}}$ and $\text{MAG}_{2P_F}^{\text{slow}}$, respectively, which corresponds to the allowed one-photon $S_0 \rightarrow S_2$ transition ($\pi \rightarrow \pi^*$ band) of their *trans*-azobenzene chromophore; and (ii) a broad shoulder at $\lambda \sim 450$ nm arising from the forbidden $1P S_0 \rightarrow S_1$ transition ($n \rightarrow \pi^*$ band) of these compounds. In contrast, *trans*- MAG_{2P} spectrum³² shows a red-shifted $\pi \rightarrow \pi^*$ band which overlaps with the $n \rightarrow \pi^*$ band, a typical feature for amino-substituted azobenzenes.³⁵

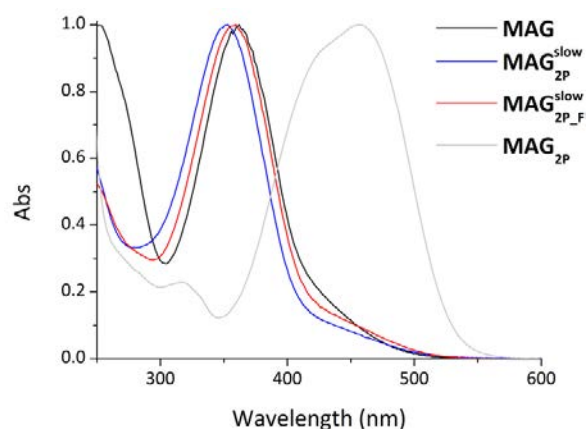


Figure III-12. Normalised absorption spectra of *trans*-**MAG**, *trans*- $\text{MAG}_{2P}^{\text{slow}}$, *trans*- $\text{MAG}_{2P_F}^{\text{slow}}$ and *trans*- MAG_{2P} in 99% PBS:1% DMSO.

When *trans*-MAG, *trans*-MAG_{2P}^{slow} and *trans*-MAG_{2P_F}^{slow} were irradiated with UV light ($\lambda_{\text{exc}} = 366$ nm; i.e. at their $\pi \rightarrow \pi^*$ band), changes were observed in absorption that are consistent with *trans*→*cis* photoisomerisation: a clear decrease and hypsochromical shift of the $\pi \rightarrow \pi^*$ absorption band, and a slight increase of the $n \rightarrow \pi^*$ absorption band (Figure III-13).³⁵ However, since the absorption spectra of the *trans* and the *cis* isomers of these compounds significantly overlap, the photoisomerisation process was not quantitative and an equilibrium state was reached. This equilibrium state is the so called photostationary state (PSS) and its composition depends on a large variety of parameters, such as the extinction coefficients (ϵ) of both isomers at the excitation wavelength, the photoisomerisation quantum yields (Φ) and the thermal back-isomerisation rate constant ($k_{\text{cis} \rightarrow \text{trans}}$).

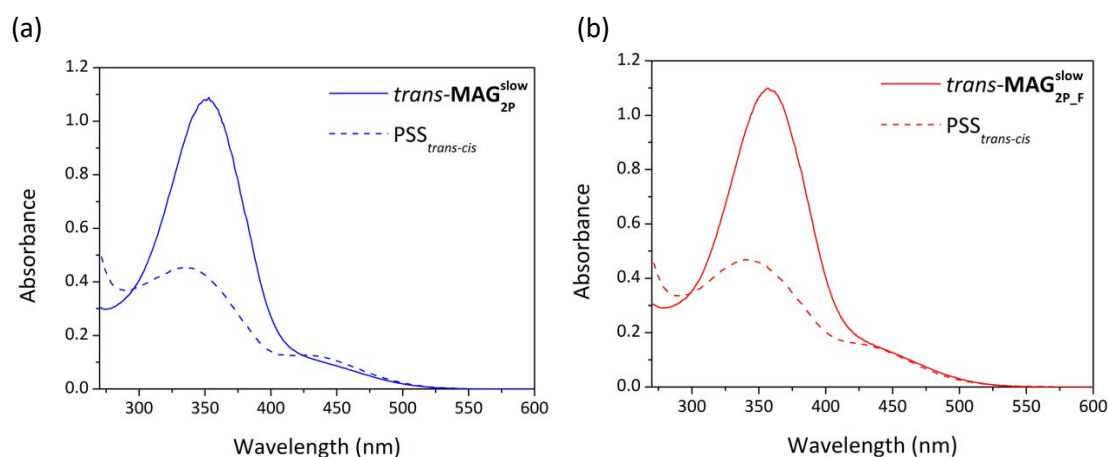


Figure III-13. (a) Absorption spectra of *trans*-MAG_{2P}^{slow} and the photostationary state mixture obtained upon irradiation at $\lambda_{\text{exc}} = 366$ nm to induce *trans*→*cis* photoisomerisation (PSS_{trans-cis}). (b) Absorption spectra of *trans*-MAG_{2P_F}^{slow} and the PSS mixture obtained upon *trans*→*cis* irradiation at $\lambda_{\text{exc}} = 366$ nm.

Trans→*cis* photoisomerisation of MAG_{2P}^{slow} and MAG_{2P_F}^{slow} upon irradiation with UV light ($\lambda_{\text{exc}} = 366$ nm) was further confirmed by ¹H NMR experiments (Figure III-14). New signals in the low-field region of the spectrum corresponding to the aromatic protons of their *cis* isomers were observed in both cases. In addition, these ¹H NMR experiments permitted the quantification of the amount of *cis* isomer present in the PSS_{trans-cis}: 72% for MAG_{2P}^{slow}, and 68% for MAG_{2P_F}^{slow} in DMSO-*d*₆. Although these experiments could not be conducted directly in aqueous media due to the higher concentrations required and the moderate solubility of MAG_{2P}^{slow} and MAG_{2P_F}^{slow} in water, the PSS_{trans-cis} compositions in 99% PBS:1% DMSO could be estimated from the ¹H NMR data in DMSO-*d*₆ and the UV-vis absorption measurements in 99% PBS:1% DMSO: 71% and 69%

of *cis* isomer content for **MAG_{2P}^{slow}** and **MAG_{2P_F}^{slow}**, respectively (Table III-1). Interestingly, these values are very similar to that found for **MAG** in aqueous media (70%).

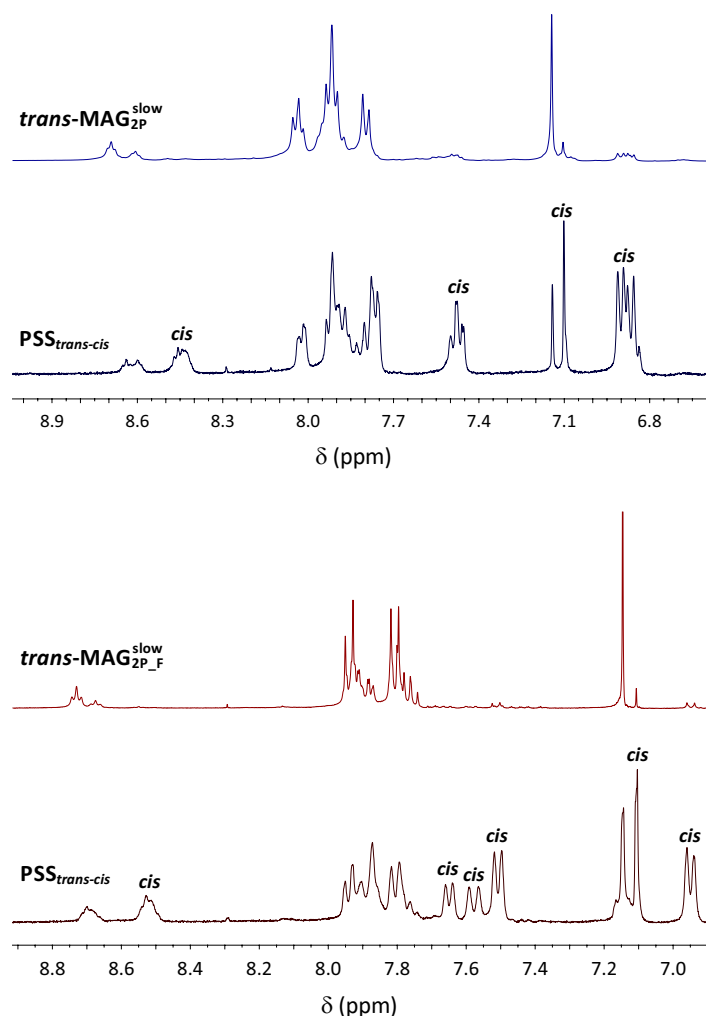


Figure III-14. ¹H NMR spectra (400 MHz, DMSO-*d*₆) of *trans*-MAG_{2P}^{slow} and *trans*-MAG_{2P_F}^{slow} and the corresponding *trans*→*cis* photostationary state mixtures prepared by irradiation at λ_{exc} = 366 nm.

Furthermore, *trans*→*cis* photoisomerisation quantum yields ($\Phi_{trans \rightarrow cis}$) of **MAG_{2P}^{slow}** and **MAG_{2P_F}^{slow}** were determined by comparison of the experimental behaviour of these compounds with that of azobenzene as a reference. Clearly, very similar results were obtained for both ligands ($\Phi_{trans \rightarrow cis} \sim 0.15$, Table III-1), which very much resemble the value encountered for **MAG**. This, together with the equivalent PSS_{trans-cis} determined for the three compounds confirms that the push-pull substitution introduced in the azobenzene cores of **MAG_{2P}^{slow}** and **MAG_{2P_F}^{slow}** does not affect the *trans*→*cis* photoisomerisation process with respect to parent PTL **MAG**.

Table III-1. Results of the *trans*→*cis* photoisomerisation process of *trans*-**MAG**, *trans*-**MAG**_{2P}^{slow} and *trans*-**MAG**_{2P_F}^{slow} in 99% PBS:1% DMSO.

Compound	$\lambda_{\text{max}}^{\text{abs}}$ (nm) ^a	<i>cis</i> PSS (%) ^b	$\Phi_{\text{trans} \rightarrow \text{cis}}$ ^c
MAG	361	70	0.18
MAG _{2P} ^{slow}	352	71	0.13
MAG _{2P_F} ^{slow}	357	69	0.16

(a) $\pi \rightarrow \pi^*$ absorption band; (b) $\lambda_{\text{exc}} = 366$ nm; (c) $\lambda_{\text{exc}} = 355$ nm and using azobenzene as a reference ($\Phi_{\text{trans} \rightarrow \text{cis}} = 0.15$ in acetonitrile³⁵).

III.3.2. CIS→TRANS ISOMERISATION

As mentioned above, *cis*→*trans* isomerisation of compounds *cis*-**MAG**_{2P}^{slow} and *cis*-**MAG**_{2P_F}^{slow} could occur both photochemically and thermally. Thus, both processes were studied in detail.

Photochemical *cis*→*trans* back-isomerisation was investigated by irradiation of a PSS_{trans-cis} mixture of compounds **MAG**_{2P}^{slow} and **MAG**_{2P_F}^{slow} at $\lambda_{\text{exc}} = 473$ nm. At this wavelength, their $n \rightarrow \pi^*$ absorption bands were excited and typical spectral features accounting for *cis*→*trans* photoisomerisation were observed: (i) a sharp increase of their $\pi \rightarrow \pi^*$ absorption bands; and (ii) a slight decrease in their $n \rightarrow \pi^*$ absorption bands. Once again, since the absorption spectra of the *trans* and the *cis* isomers significantly overlap, the photoisomerisation process was not quantitative and PSS_{cis-trans} were obtained (Figure III-15). ¹H NMR experiments permitted the determination of the composition of these PSS_{cis-trans}: 88% and 80% of *trans* isomer content for **MAG**_{2P}^{slow} and **MAG**_{2P_F}^{slow}, respectively, in 99% PBS:1% DMSO (Table III-2). These results are very similar to that found for **MAG** (%*trans* PSS_{cis-trans} = 91%). *Cis*→*trans* photoisomerisation quantum yields ($\Phi_{\text{cis} \rightarrow \text{trans}}$) of **MAG**_{2P}^{slow} and **MAG**_{2P_F}^{slow} in aqueous media were also determined using azobenzene as a reference. Both compounds showed the same behaviour ($\Phi_{\text{cis} \rightarrow \text{trans}} = 0.26$, Table III-2), which is very similar to that of **MAG** ($\Phi_{\text{cis} \rightarrow \text{trans}} = 0.30$, Table III-2). This further demonstrates the similarity in photochemical properties of the two new PTLs developed by us with respect to **MAG** under 1P excitation.

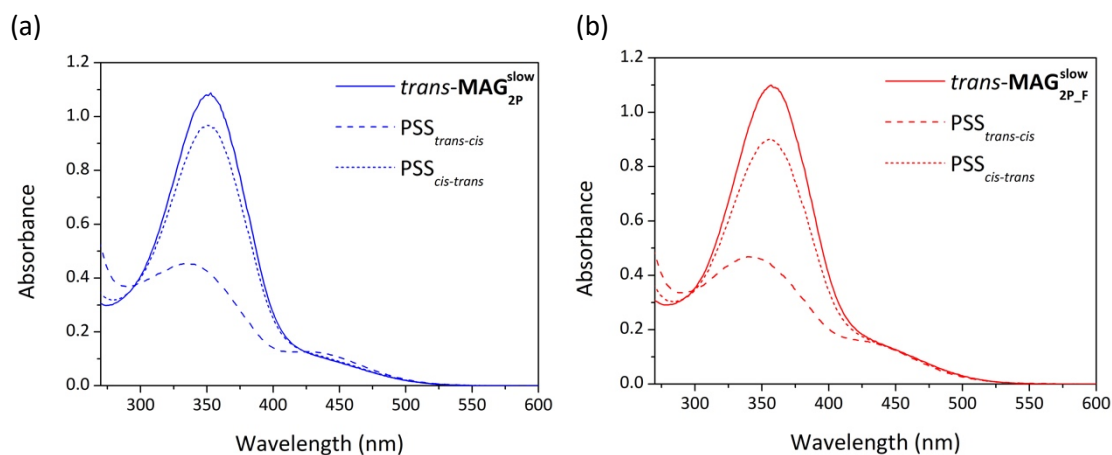


Figure III-15. (a) Absorption spectra of $trans\text{-MAG}_{2P}^{\text{slow}}$, the photostationary state mixture obtained upon irradiation at $\lambda_{\text{exc}} = 366$ nm to induce $trans \rightarrow cis$ photoisomerisation ($PSS_{trans-cis}$), and the photostationary state mixture obtained upon irradiation at $\lambda_{\text{exc}} = 473$ nm to induce $cis \rightarrow trans$ photoisomerisation ($PSS_{cis-trans}$) in 99% PBS:1% DMSO. (b) Absorption spectra of $trans\text{-MAG}_{2P_F}^{\text{slow}}$, the photostationary state mixture obtained upon irradiation at $\lambda_{\text{exc}} = 366$ nm to induce $trans \rightarrow cis$ photoisomerisation, and the photostationary state mixture obtained upon irradiation at $\lambda_{\text{exc}} = 473$ nm to induce $cis \rightarrow trans$ photoisomerisation in 99% PBS:1% DMSO.

Table III-2. Results of the $cis \rightarrow trans$ photoisomerisation process of **MAG**, $\text{MAG}_{2P}^{\text{slow}}$ and $\text{MAG}_{2P_F}^{\text{slow}}$ upon irradiation at $\lambda_{\text{exc}} = 473$ nm and thermal stability values of $cis\text{-MAG}$, $cis\text{-MAG}_{2P}^{\text{slow}}$ and $cis\text{-MAG}_{2P_F}^{\text{slow}}$ at rt.

Compound	$transPSS$ (%)	$\Phi_{cis \rightarrow trans}$	τ_{cis} (min)
MAG	91	0.30	25.5 ³
$\text{MAG}_{2P}^{\text{slow}}$	88	0.26	10.5
$\text{MAG}_{2P_F}^{\text{slow}}$	80	0.26	11.9

(a) All the results shown were measured in 99% PBS:1% DMSO.

The thermal $cis \rightarrow trans$ back-isomerisation process was studied by recording the spectral changes in a $trans\text{-cis}$ mixture of $\text{MAG}_{2P}^{\text{slow}}$ and $\text{MAG}_{2P_F}^{\text{slow}}$ over time and in the dark by UV-vis absorption spectroscopy. A continuous increase in the $\pi \rightarrow \pi^*$ absorption bands of both compounds was observed in these experiments, which clearly indicated that $cis \rightarrow trans$ back-isomerisation was taking place in the absence of illumination. By plotting the changes registered at the λ_{max} of the $\pi \rightarrow \pi^*$ absorption bands of these compounds and fitting the traces obtained with a monoexponential growth function (Figure III-16a), we determined that: (i) their thermal $cis \rightarrow trans$ back-isomerisation follows a first order kinetics, as expected; and (ii) the lifetimes of

cis-**MAG**_{2P}^{slow} and *cis*-**MAG**_{2P_F}^{slow} at rt in the dark are $\tau_{cis} = 10.5$ and $\tau_{cis} = 11.9$ min, respectively (Figure III-16b, Table III-2).

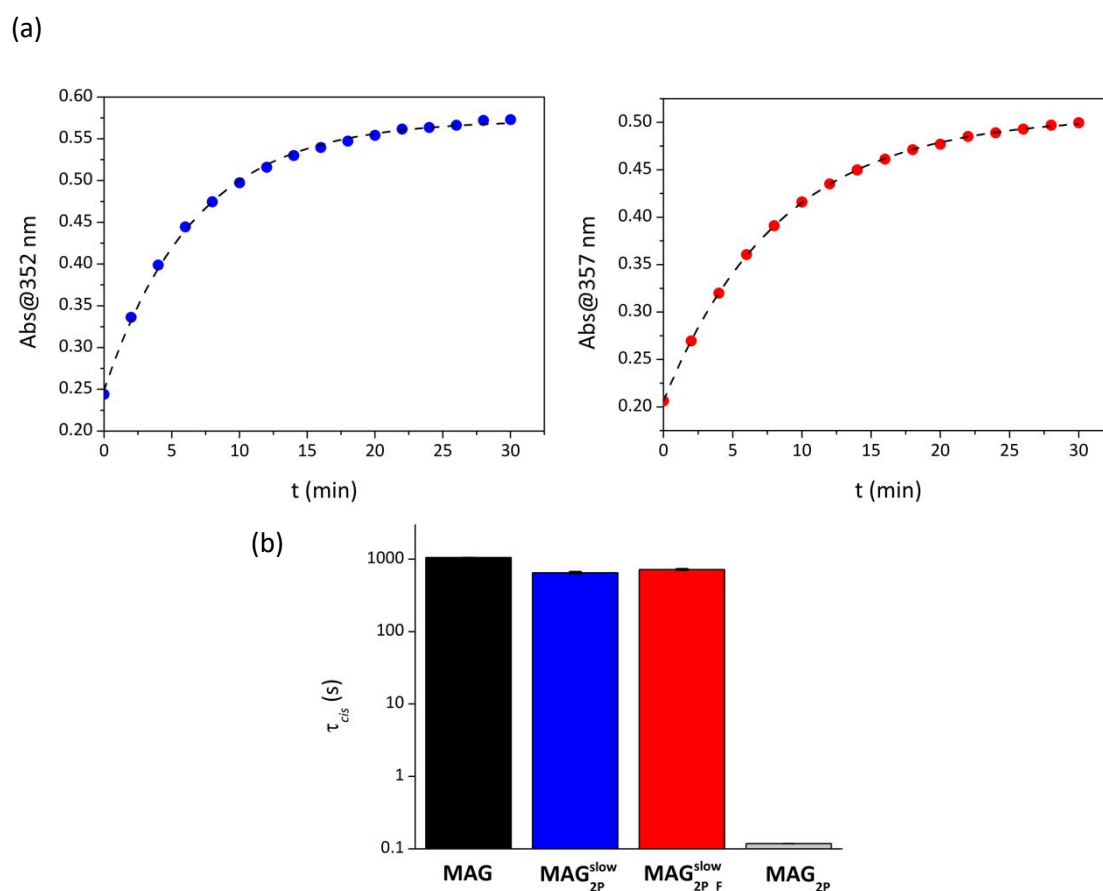


Figure III-16. (a) Variation of the absorption of the *trans-cis* mixture of **MAG**_{2P}^{slow} (blue) and **MAG**_{2P_F}^{slow} (red) in the dark at 25 °C in 99% PBS:1% DMSO. At these conditions, thermal *cis-trans* back-isomerisation takes place, thus restoring the initial concentration of the *trans* state of the ligands, which presents a larger extinction coefficient at $\lambda_{abs} = 352$ nm and $\lambda_{abs} = 357$ nm. Points correspond to the experimental data, while lines were obtained from monoexponential fits. (b) Thermal lifetimes of *cis*-**MAG**, *cis*-**MAG**_{2P}^{slow}, *cis*-**MAG**_{2P_F}^{slow}, and *cis*-**MAG**_{2P} at rt in 99% PBS:1% DMSO. Errors from the monoexponential fits to obtain τ_{cis} are shown.

As depicted in Figure III-16b, the thermal *cis* lifetimes of the new synthesised PTLs **MAG**_{2P}^{slow} and **MAG**_{2P_F}^{slow} are similar to the value reported for **MAG** and clearly surpass the thermal stability of other electronically-asymmetric **MAG** derivatives with strong mesomeric groups proposed for the 2P-induced control of LiGluR with NIR light (e.g. **MAG**_{2P}³²). Thus, one of the objectives set for the new ligands developed in this work had been accomplished: long *cis*-state thermal stability.

III.4. EVALUATION OF THE LIGHT-INDUCED BIOLOGICAL ACTIVITY OF PTLs $\text{MAG}_{2\text{P}}^{\text{slow}}$ AND $\text{MAG}_{2\text{P}_F}^{\text{slow}}$ ON CULTURED CELLS

In view of the optimal photochemical properties of our new molecules $\text{MAG}_{2\text{P}}^{\text{slow}}$ and $\text{MAG}_{2\text{P}_F}^{\text{slow}}$, which fairly reproduced those of **MAG**, we decided to explore their ability to photocontrol LiGluR channels in living cells under 1P and 2P stimulation. These experiments were conducted in collaboration with Aida Garrido-Charles in the laboratories of the research group of Pau Gorostiza at *Institut de Bioenginyeria de Catalunya* (IBEC) and in the *Parc Científic de Barcelona*.

First biological experiments were performed *in vitro* on cultured HEK293 cells which expressed GluK2 receptors bearing a cysteine residue at position L439C (GluK2-L439C) and were then incubated with the PTL of interest. In order to obtain HEK293 cells expressing the desired receptors, transfection protocols were carried out. Transfection is the process of artificially introducing nucleic acids (DNA or RNA) into cells, using means other than viral infection, such as plasmids: double-stranded extra chromosomal and generally circular DNA sequences that are capable of replication using the host cell's replication machinery. Such introductions of foreign nucleic acid can result in a change of the properties of the cell. Transfection of HEK293 cells was performed by Aida Garrido-Charles using expression plasmids for GluK2-L439C and GluK2-L439C-eGFP kindly provided by Ehud Y. Isacoff (University of California).

Two different techniques were employed to record the changes in the cells photoinduced by the ligands: whole-cell patch clamp and calcium imaging. Both methodologies are briefly described in Figure III-17. With the kind assistance of Aida Garrido-Charles, I could perform myself the calcium imaging experiments reported in this thesis. However, the whole-cell patch clamp technique is a much more complicated methodology that requires a lot of experience to be operated. For this reason, all the electrophysiological measurements described were performed by Aida Garrido-Charles.

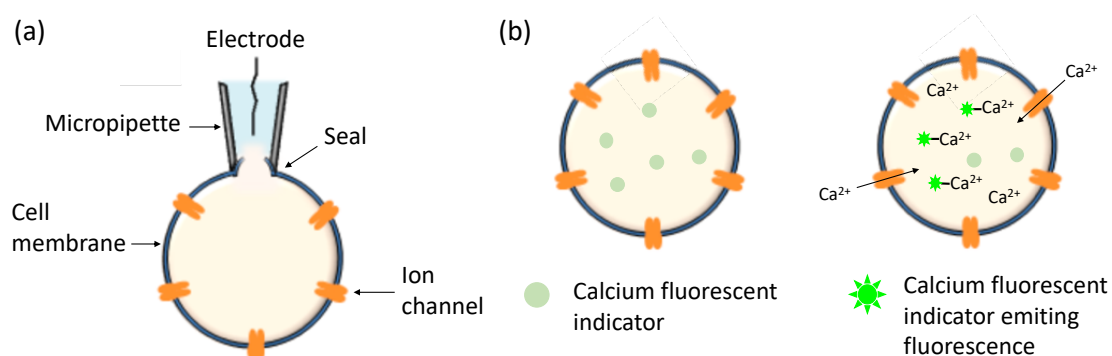


Figure III-17. (a) Schematic representation of whole-cell patch clamp, a neurophysiology technique that enables high-resolution recording of the ionic currents flowing through a cell's plasma membrane.⁴⁷ This method relies on the use of a thin electrode (usually a chloride silver electrode) located in the interior of a glass micropipette filled with a buffer solution resembling the intracellular media. The pipette displays an open tip, with a diameter around 1 μm , with which a small membrane surface area or *patch* can be enclosed. Strong suction ruptures the membrane patch, thus providing access to the intracellular space of the cell. Then, two different operation modes can be used: (i) voltage-clamp, where the voltage is maintained constant and the electrical current between the intra- and extra-cellular media is monitored; or (ii) current-clamp, where the current is the one that remains invariable and the feature recorded is the difference in membrane potential. (b) Schematic representation calcium imaging, a fluorescence imaging technique that consists in the use of fluorescent dyes (or calcium fluorescent indicators) with which Ca^{2+} can be specifically labelled. Hence, when there is an increase in Ca^{2+} concentration inside the cells, an increase of their fluorescence emission at the detection wavelength can be observed. There are two main classes of calcium indicators: (i) chemical indicators, small molecules that can chelate calcium ions; and (ii) genetically encoded calcium indicators (GECI), fluorescent proteins derived from green fluorescent protein (GFP) or its variants. In our experiments, we took advantage of the permeability of GluK2 channels for Ca^{2+} , which is a major second intracellular messenger that mediates neuronal activity.

It must be noted that even though whole-cell patch clamp is a much more sensitive technique which provides high resolution recordings of the ionic currents flowing through a single cell's plasma membrane, calcium imaging displays other features which make this technique also advantageous: (i) simplicity of operation; (ii) ability to simultaneously record the response of multiple cells in a non-invasive manner, thus facilitating statistical studies; and (iii) it enables solely optical study of cells. In both cases, however, several common conditions were applied:

- LiGluR expressing cells incubated with the **MAG** compound of interest (either **MAG**, **MAG_{2P}^{slow}** or **MAG_{2P}^{slow_F}**) were sequentially illuminated with different excitation wavelengths to induce reversible *trans*→*cis* and *cis*→*trans* photoisomerisation of the PTL. As described in Figure III-2 for **MAG**, this should result in geometrical changes

between the *trans* and *cis* states, which trigger the opening and closing of the ion channel by bringing the glutamate moiety close to (*cis* state) or far away from (*trans* state) the binding pocket where it must bind. The aperture and closure of the ion channel triggered by the corresponding **MAG** derivative can be recorded as a variation of either (i) membrane current by whole-cell calcium imaging; or (ii) fluorescence emission of the cells, in the case of calcium imaging.

- Either at the beginning or at the end of the experiment, cells were exposed to 300 μM concentration of free glutamate. This was performed to: (i) demonstrate no inhibition of the endogenous behaviour of the cells caused by our PTLs; and (ii) quantify the relative response of our **MAG** compounds.
- Cells were also incubated with Concanavalin A, a tetrameric lectin which binds to specific carbohydrate residues and inhibits desensitisation of glutamate receptors upon prolonged binding,⁴⁸ in order to elongate the time the ion channel was open, thus permitting the recording of larger biological responses.

III.4.1. ONE-PHOTON STIMULATION IN CULTURED CELLS

We started our set of *in vitro* experiments by evaluating the ability of our new PTLs **MAG**_{2P}^{slow} and **MAG**_{2P}^{slow_F} to photocontrol LiGluR channels under one-photon stimulation. For comparative issues, we also performed the same experiments with **MAG**. The following conditions were applied in these experiments: (i) the biological samples incubated with the compound of interest were irradiated with UV-violet light ($\lambda_{\text{exc}} = 360 \text{ nm}$) to induce the opening of the ion channels and with green light ($\lambda_{\text{exc}} = 500 \text{ nm}$) to trigger their closure; and (ii) GCaMP6s⁴⁹ was used as a calcium imaging indicator for the fluorescence measurements (Figure III-18).

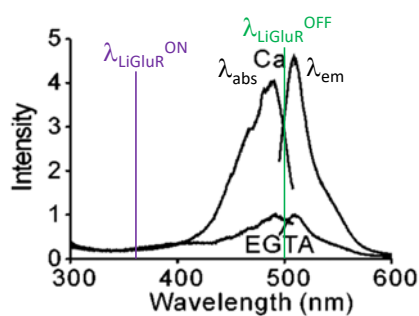


Figure III-18. Absorption and emission spectrum of GCaMP6s in the presence of 1 mM Ca^{2+} or 5 mM ethyleneglycol tetracetic acid (EGTA).⁴⁹ Excitation wavelengths of LiGluR are shown.

As plotted in Figure III-19, large, repetitive and reproducible electrophysiological signals and fluorescent responses in GluK2-L439C-expressing cells upon repetitive illumination with sequential pulses of UV-violet and green light were recorded for **MAG**, **MAG_{2P}^{slow}** and **MAG_{2P_F}^{slow}**. As such, this demonstrates that the capacity to light-control the operation of LiGluR was not lost for new PTLs **MAG_{2P}^{slow}** and **MAG_{2P_F}^{slow}** despite the changes introduced in the substitution pattern of their azoaromatic core.

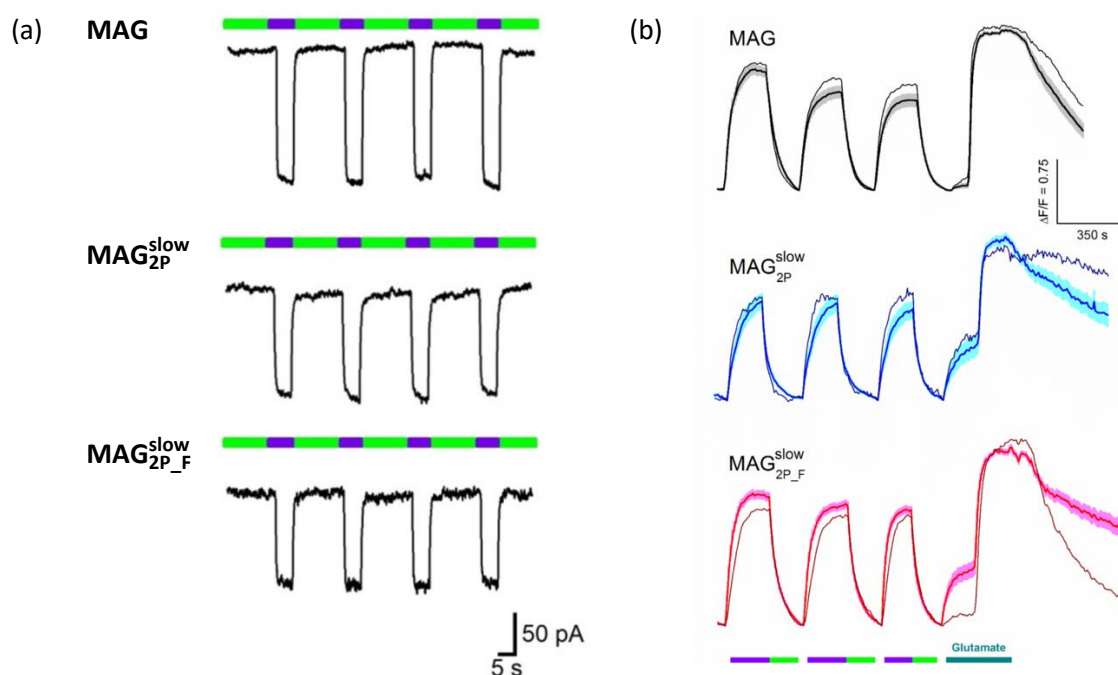


Figure III-19. (a) Whole-cell patch clamp current traces from cells expressing GluK2-L439C after conjugation to **MAG**, **MAG_{2P}^{slow}** and **MAG_{2P_F}^{slow}**. (b) Individual (thin lines) and average (thick lines) calcium imaging fluorescence traces registered for HEK293 cells co-expressing GluK2-L439C and GCaMP6s after conjugation to **MAG** ($n = 31$ cells), **MAG_{2P}^{slow}** ($n = 20$ cells) and **MAG_{2P_F}^{slow}** ($n = 45$ cells) (50 μ M each photoswitch). After three photoinduced opening-closing cycles, LiGluR activation was achieved by addition of 300 μ M free glutamate. The bands around average traces plot the corresponding standard errors of the mean (SEM). For both experiments (a) and (b), 1P excitation at 360 nm (violet) was applied to open LiGluR, while 1P excitation at 500 nm (green) was applied to revert back the process.

To identify the irradiation conditions for achieving maximal biological responses, we recorded the action spectra of **MAG**, **MAG_{2P}^{slow}** and **MAG_{2P_F}^{slow}** by scanning the excitation wavelength used to induce LiGluR channel aperture. For comparison purposes, the action spectrum of **MAG_{2P}** was also recorded by whole-cell patch clamp experiments. Calcium imaging was not suitable for this due to the low τ_{cis} of **MAG_{2P}**, which impedes obtaining large responses before the *cis* isomer back-isomerises thermally. Figure III-20 depicts the action spectra obtained in this way from

electrophysiology and calcium imaging experiments. As expected from their analogous photochemical properties, **MAG**, **MAG_{2P}^{slow}** and **MAG_{2P-F}^{slow}** exhibited very similar spectral responses, with maximal signal at $\lambda_{\text{exc}} \sim 360$ nm. By contrast, a broader red-shifted action spectrum was obtained for **MAG_{2P}**, with maximum response at $\lambda_{\text{exc}} \sim 425$ nm. Noticeably, for all PTLs investigated, their action spectra recorded nicely correlated with the absorption spectra of their *trans* isomer (see Figure III-12).

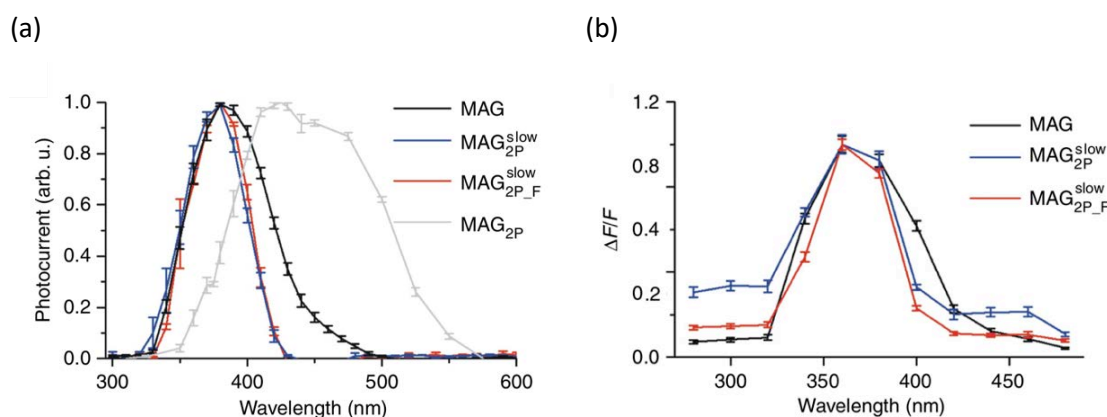


Figure III-20. (a) Normalised 1P action spectra recorded using whole-cell patch-clamp in HEK293 cells expressing GluK2-L439C after conjugation with **MAG**, **MAG_{2P}^{slow}**, **MAG_{2P-F}^{slow}** and **MAG_{2P}** ($n = 5, 7, 3$ and 8 biologically independent cells, respectively). (b) Normalised 1P action spectra recorded using calcium imaging in HEK293 cells co-expressing GluK2-L439C and GCaMP6s after conjugation with **MAG**, **MAG_{2P}^{slow}** and **MAG_{2P-F}^{slow}** ($n = 33, 20$ and 25 biologically independent cells, respectively). For both figures, errors are SEM.

Finally, we quantified the relative response of the **MAG** derivatives by comparing their maximal photoinduced response with that triggered by endogenous glutamate at $300 \mu\text{M}$. Noticeably, **MAG**, **MAG_{2P}^{slow}** and **MAG_{2P-F}^{slow}** presented nearly equivalent behaviours, exhibiting a 69.5%, 62.5% and 65.5% responses, respectively, under identical illumination conditions (Figure III-21). Together with the results shown previously, this proves that the 1P biological activity of **MAG** in LiGluRs is preserved for **MAG_{2P}^{slow}** and **MAG_{2P-F}^{slow}** PTLs bearing electronically-asymmetric azobenzene cores, both in terms of amplitude and spectral response.

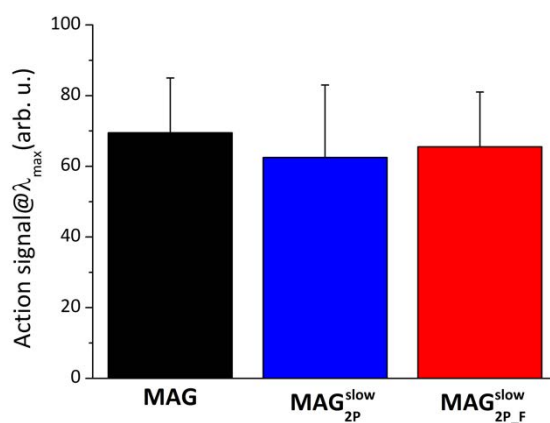


Figure III-21. One-photon responses of **MAG**, **MAG_{2P}^{slow}** and **MAG_{2P_F}^{slow}** after conjugation to GluK2-L439C-expressing HEK293 cells (50 μ M each photoswitch). Photoresponses were measured by means of calcium imaging measurements using GCaMP6s as fluorescence indicator. Before averaging over different cells, the one-photon responses of each cell were normalised with respect to the free glutamate response (300 μ M) ($n = 81$ cells, $n = 63$ cells, and $n = 76$ cells, respectively). Errors are SEM.

III.4.2. TWO-PHOTON STIMULATION IN CULTURED CELLS

After assessing the biological responses triggered under one-photon excitation, we focused our efforts on the evaluation of the ability of our new **MAG_{2P}^{slow}** and **MAG_{2P_F}^{slow}** PTLs to photocontrol LiGluR channels under two-photon stimulation with NIR light. The 2P operation of LiGluR in HEK293 cells was only investigated by calcium imaging experiments. These experiments were conducted in a confocal fluorescence microscope equipped with both continuous-wave visible lasers and a femtosecond pulsed Ti: Sapphire laser. This allowed for sequential and independent 1P and 2P stimulation of cells by raster-scanning the focused laser beam of choice over the sample while detecting the fluorescence signal of the calcium ion indicator for the whole field of view.

In a first step, we conducted calcium imaging measurements using GCaMP6s as a fluorescent indicator, in a similar way to previous experiments performed under 1P excitation. However, the only UV source available in the equipment used for these new experiments was a laser of $\lambda_{exc} = 405$ nm and GCaMP6s was stimulated under these irradiation conditions, thus providing non-specific responses. For this reason, we employed R-GECO1⁵⁰ as a fluorescent probe instead because it exhibits a red-shifted absorption spectrum and therefore was not stimulated under the experiment's conditions (Figure III-22).

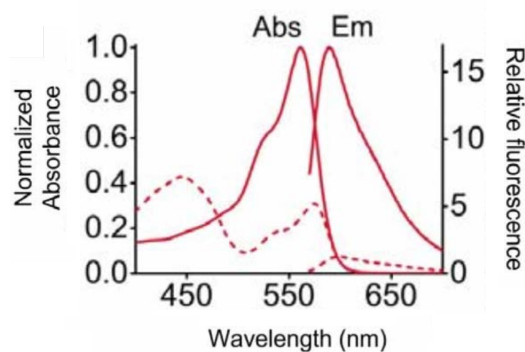


Figure III-22. Absorption and emission spectrum of R-GECO1. Dotted lines represent the Ca^{2+} -free state and solid lines represent Ca^{2+} -bound state.⁵⁰

Under these conditions, we first performed experiments consisting in two consecutive cycles of 1P photostimulation of LiGluR with violet light ($\lambda_{\text{exc}} = 405 \text{ nm}$), followed by two cycles of 2P photostimulation with NIR light ($\lambda_{\text{exc}} = 780 \text{ nm}$). In agreement with the 1P experiments reported in the previous section, LiGluR channels were closed upon irradiation with green light ($\lambda_{\text{exc}} = 514 \text{ nm}$) after every 1P or 2P stimulation. Figure III-23a shows the responses obtained along these experiments after conjugation with **MAG**, **MAG_{2P}^{slow}** and **MAG_{2P-F}^{slow}**. As clearly observed, whilst **MAG** exhibited almost no response under 2P stimulation, **MAG_{2P}^{slow}** and **MAG_{2P-F}^{slow}** displayed clear 2P signals with NIR light. This fact highlights the poor efficiency of 2P *trans*→*cis* photosomerisation of **MAG**, as already pointed out by Isacoff and co-workers.²⁹ Moreover, **MAG_{2P-F}^{slow}** 2P responses obtained were larger than for **MAG_{2P}^{slow}**, thus confirming that an increase in the electronic asymmetry of the azobenzene core due to the presence of an additional F substituent provokes an enhancement in σ_2 and, therefore, more efficient 2PA. Actually, the 1P and 2P calcium imaging responses measured for **MAG_{2P-F}^{slow}** presented similar intensities.

We also determined whether the 2P stimulation of the cells with **MAG_{2P-F}^{slow}** was reproducible, repetitive and occurred with minimal photodegradation. For this purpose, the cells were subjected to four consecutive cycles of 2P excitation with NIR light ($\lambda_{\text{exc}} = 780 \text{ nm}$) to trigger the opening of the channels followed by 1P stimulation with green light ($\lambda_{\text{exc}} = 514 \text{ nm}$) to induce the closing of the channels. As illustrated in Figure III-23b, negligible variation in calcium imaging responses was observed after four consecutive light-gating cycles for different individual cells, thus confirming that compound **MAG_{2P-F}^{slow}** shows neither phototoxicity nor photodegradation.

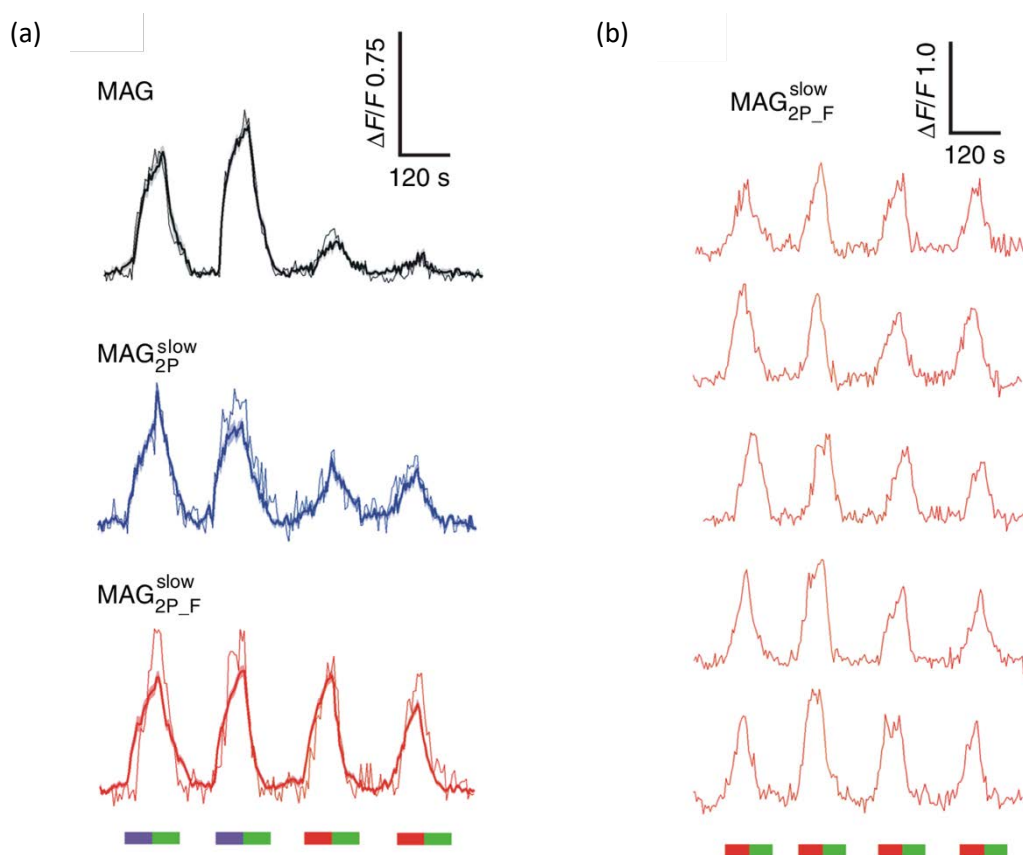


Figure III-23. (a) Individual (thin lines) and average (thick lines) calcium imaging fluorescence traces recorded for HEK293 cells co-expressing GluK2-L439C and R-GECO1 after conjugation to **MAG**, **MAG_{2P}^{slow}**, **MAG_{2P_F}^{slow}** ($n = 16, 14$ and 34 biologically individual cells, respectively). The bands around average traces plot the corresponding SEM. Both 1P (violet, 405 nm, power density = $0.37 \text{ mW } \mu\text{m}^{-2}$) and 2P (red, 780 nm, power density = $2.8 \text{ mW } \mu\text{m}^{-2}$) excitation scans were used to open LiGluR channels and trigger calcium-induced R-GECO1 fluorescence enhancement, while 1P scans (green, 514 nm, power density = $0.35 \text{ mW } \mu\text{m}^{-2}$) were applied to induce the closing of the channels. (b) Repetitive 2P induced calcium imaging responses of 5 individual HEK293 cells co-expressing GluK2-L439C and R-GECO1 after conjugation to **MAG_{2P_F}^{slow}**.

Next, we recorded the action spectra of **MAG**, **MAG_{2P}^{slow}** and **MAG_{2P_F}^{slow}** under 2P illumination by scanning the excitation wavelength used to induce LiGluR channel aperture (Figure III-24). The spectra obtained exhibit similar spectral distribution, being rather broad and presenting a maximum at $\sim 780 \text{ nm}$. It must be noted that this spectral maximum occurs at almost twice the wavelength of the 1P absorption band corresponding to the 2P allowed $S_0 \rightarrow S_2$ transition of the *trans*-azobenzene core of these compounds ($\sim 360 \text{ nm}$), as expected for most 2P-induced absorption in azobenzenes.²⁰

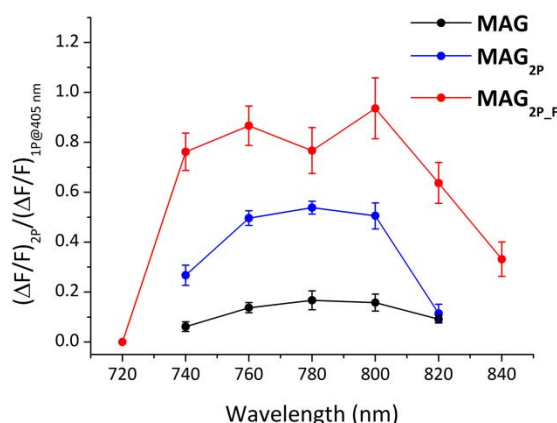


Figure III-24. Two-photon action spectra recorded for **MAG**, **MAG_{2P}^{slow}**, **MAG_{2P_F}^{slow}** after conjugation to HEK-239 cells co-expressing GluK2-L439C and R-GECO1. Before averaging over different cells, the 2P responses of each cell were normalized with respect to the 1P response at 405 nm (**MAG**: 740, 760, 780, 800, and 820 nm; $n = 28, 33, 40, 7,$ and 12 biologically independent cells, respectively; **MAG_{2P}^{slow}**: 740, 760, 780, 800, and 820 nm; $n = 20, 9, 12, 16,$ and 17 biologically independent cells, respectively; and **MAG_{2P_F}^{slow}**: 720, 740, 760, 780, 800, 820, and 840 nm; $n = 14, 17, 18, 86, 15, 23,$ and 17 biologically independent cells, respectively). Errors are SEM.

Having established the conditions for the optimal 2P-excitation of the PTLs, we aimed at quantitatively assessing the difference in multiphoton activity of **MAG**, **MAG_{2P}^{slow}** and **MAG_{2P_F}^{slow}** to control LiGluR. For this, we first determined the ratio between 1P and 2P responses on the same cells (2P/1P ratio) when irradiating at the maximum of the 2P action spectra of these compounds. By comparing these ratios after averaging over a large number of cells ($n > 25$ cells), we could observe an outstanding increase in the 2P activity of **MAG_{2P}^{slow}** and **MAG_{2P_F}^{slow}** compared to that of **MAG** (Figure III-25a). Specifically, 3.5- and 6-fold increase in the 2P/1P ratio was recorded for **MAG_{2P}^{slow}** and **MAG_{2P_F}^{slow}** with respect to **MAG**, respectively. Second, we investigated the reliability of conducting the 2P stimulation of LiGluR with **MAG_{2P}^{slow}** and **MAG_{2P_F}^{slow}** in comparison to **MAG**. Whilst 2P photoresponses of LiGluR upon conjugation with **MAG_{2P}^{slow}** and **MAG_{2P_F}^{slow}** were observed for all the cells analysed that exhibited 1P signals, this only occurred for about ~70% of the cells incubated with **MAG** (Figure III-25b).

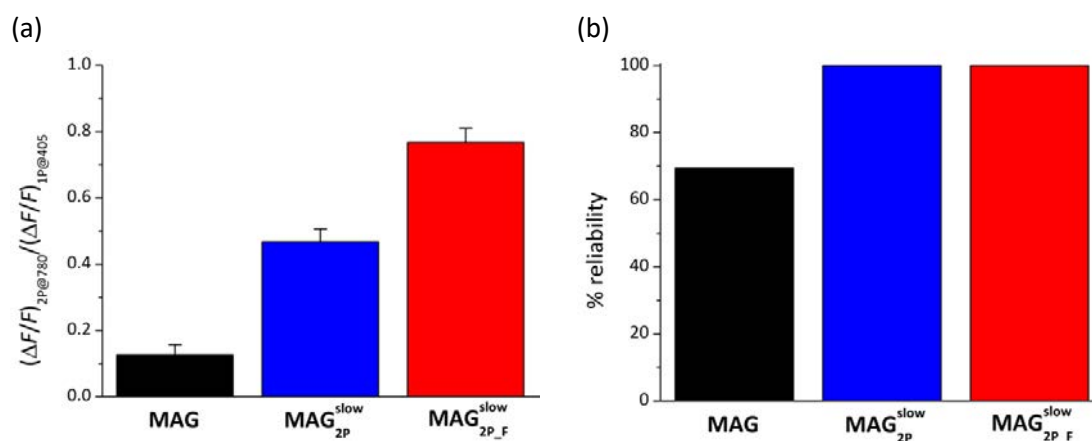


Figure III-25. (a) Ratio between the 2P and 1P responses of **MAG**, MAG_{2P}^{slow} and $MAG_{2P_F}^{slow}$ for the same cells excited at $\lambda_{exc} = 780$ and 405 nm, respectively ($n = 72$, 25 and 86 cells, respectively). Errors are SEM. (b) Reliability of the 2P calcium imaging responses obtained for HEK-239 cells co-expressing GluK2-L439C and R-GECO1 upon conjugation with **MAG**, MAG_{2P}^{slow} and $MAG_{2P_F}^{slow}$ ($n = 75$, 25 and 86 biologically independent cells, respectively). Errors are SEM.

Overall, the results obtained for the operation of HEK293 cells expressing GluK2-L439C under 2P stimulation of **MAG**, MAG_{2P}^{slow} and $MAG_{2P_F}^{slow}$ clearly indicate that our new PTLs, and especially $MAG_{2P_F}^{slow}$, are efficient and reliable tools to control LiGluR in neurotransmission studies under 2P irradiation with NIR light.

III.5. ANALYSIS OF THE TWO-PHOTON RESPONSE OF MAG_{2P}^{slow} AND $MAG_{2P_F}^{slow}$ BASED ON THEORETICAL CALCULATIONS

The photochemical studies and biological experiments described in the previous sections confirmed that MAG_{2P}^{slow} and $MAG_{2P_F}^{slow}$ possess the features which we devised when designing their azobenzene cores: large *cis* state thermal stability and enhanced 2PA. In view of these results, we explored the possibility to computationally predict and rationalise their properties thus providing with a tool to design even more efficient PTLs for the 2P manipulation of cellular receptors.

Accordingly, theoretical calculations based on density functional theory were performed by Miquel Moreno, Ricard Gelabert and Josep M^a Lluçh from the *Universitat Autònoma de Barcelona* on a series of model azobenzene photochromes that, for simplicity, were considered

in these studies instead of the full PTL systems. In particular, the following azobenzenes were analysed: (i) compounds **41** and **42** as the azobenzene cores of **MAG** and **MAG_{2P}/MAG₄₆₀**, respectively; (ii) azoaromatic compounds **43** and **44** as the photoswitches of new PTLs **MAG_{2P}^{slow}** and **MAG_{2P_F}^{slow}**, respectively; and (iii) azobenzene **45**, which exhibits a similar push-pull structure to compound **44**, but bearing a strong mesomeric EWG in *ortho* position instead of the F substituent (Figure III-26). For these compounds the following parameters were computed at the CAM-B3LYP/6-31G(d) level and accounting for solvent (water) effects with a self-consistent PCM continuum method (Table III-3):

- The energy barrier of the thermal *cis*→*trans* isomerisation reaction ($\Delta E^{\ddagger}_{cis-trans}$) from which the *cis* isomer lifetime at rt was estimated using Eyring equation.⁵¹
- The 2PA cross-section of the $S_0 \rightarrow S_2$ transition of the *trans* and *cis* isomers which is the most allowed for azobenzenes under two photon stimulation.

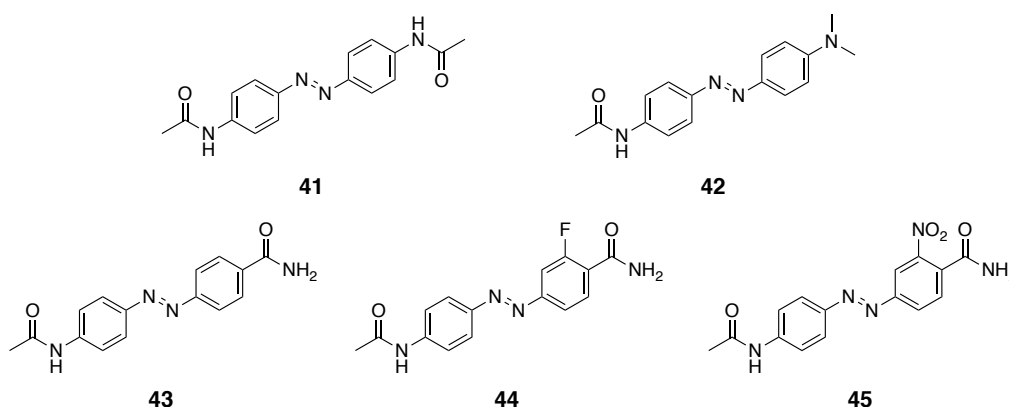


Figure III-26. Structures of the azobenzene cores whose properties were predicted by computational studies.

As shown in Table III-3, null 2PA was predicted for *trans*-**41**, which is consistent with the behaviour expected for centrosymmetric azobenzenes^{20,21} and the experimental σ_2 obtained for **MAG**.²⁹ On the other hand, a much higher σ_2 was determined for *trans*-**42**, in agreement with the value experimentally measured for *trans*-**MAG₄₆₀**.²⁹ Furthermore, larger σ_2^{trans} values were computed for azobenzenes **43**, **44** and **45**, and clear proofs of the dependence of σ_2^{trans} on the electronic asymmetry of the azobenzene core were observed. The introduction of *ortho*-fluoro and *ortho*-nitro EWGs in one of the aromatic rings of the azobenzene (**44** and **45**, respectively) resulted in a remarkable increase in σ_2 with respect to the *ortho*-unsubstituted *trans*-**43**. The 2PA properties of the *cis* isomers were also predicted since they also affect the efficiency of the photoisomerisation process of azobenzenes. Moreover, higher $\sigma_2^{trans}/\sigma_2^{cis}$ ratios were

determined for compounds **43**, **44** and **45** with respect to **41** and **42**, which favour selective 2P excitation of the *trans* state. Finally, the enhancement of σ_2^{trans} in compounds **43** and **44** was not found to have a detrimental effect on their *cis* state thermal stability. By contrast, notably lower τ_{cis} were computed for azobenzenes **42** and **45**, both bearing strong mesomeric EDGs and EWGs.

Table III-3. Two-photon absorption cross-sections and *cis* thermal stabilities computed for model azo compounds in water.^a

Compound	σ_2^{trans} (GM) ^b	σ_2^{cis} (GM) ^b	$\Delta E^\ddagger_{cis-trans}$ (kJ mol ⁻¹) ^c	τ_{cis} ^d
41	0 ^e	23	91.2 ^h	25.5 min ³
42	56 ^f	- ^g	67.7 ^h	118 ms ³²
43	58	81	97.2	4.9 h
44	69	91	98.1	7.0 h
45	112	32	46.0	18.6 μ s

(a) CAM-B3LYP/6-31G(d) level and accounting for solvent (water) effects with a self-consistent PCM continuum method. (b) 2PA cross-sections for the $S_0 \rightarrow S_2$ transition. (c) In all the cases, the lowest-energy barrier height for the thermal *cis* \rightarrow *trans* isomerisation was found to correspond to an inversion mechanism. (d) Thermal *cis* isomer lifetime estimated using Eyring equation and the barrier height computed for the thermal *cis* \rightarrow *trans* isomerisation. (e) $\sigma_2 = 10 \text{ GM}^{29}$ for *trans*-**MAG** containing a **41** core. (f) $\sigma_2 = 80 \text{ GM}^{29}$ for *trans*-**MAG**₄₆₀ containing a **42** core. (g) Calculation did not converge. From the σ_2 value computed in the gas phase an estimation in water was made ($\sigma_2 = 100 \text{ GM}$). (h) Estimated from the experimental τ_{cis} values reported for **MAG**³ and **MAG**_{2p}³² at rt using Eyring equation.

Therefore, the results obtained by computational studies clearly demonstrate that a compromise can be met between large σ_2 and high τ_{cis} by using electronically-asymmetric azobenzene cores with weak mesomeric EDGs and EWGs as well as strong inductive EWGs. Compounds designed based on these principles will emerge as excellent candidates for the preparation of azobenzene-based switches with high 2P activity for biological applications.

III.6. *IN VITRO* AND *IN VIVO* EVALUATION OF THE ACTIVITY OF $\text{MAG}_{2\text{P}_F}^{\text{slow}}$ IN NEURONS

The excellent results obtained for $\text{MAG}_{2\text{P}_F}^{\text{slow}}$ when photocontrolling HEK293 cells expressing GluK2-L439C under 2P stimulation encouraged us to test this compound in two relevant biological systems: in hippocampal rat organotypic slices *in vitro*, and in *Caenorhabditis elegans* (*C. elegans*) animal models *in vivo*. These experiments were conducted by Aida Garrido-Charles, in collaboration with Miquel Bosch and Núria Camarero in *Parc Científic* of Barcelona for the hippocampal rat organotypic slices, and in collaboration with Montserrat Porta de la Riva and Michael Krieg in *Institut de Ciències Fotòniques* (ICFO) of Barcelona, for the *in vivo C. elegans* experiments.

First, the experiments in hippocampal rat organotypic slices were carried out. The purpose of these experiments was to assess the ability of $\text{MAG}_{2\text{P}_F}^{\text{slow}}$ to control by means of multiphoton excitation with NIR light the operation of neuronal cells embedded in their physiological environment. In this way, the efficiency of $\text{MAG}_{2\text{P}_F}^{\text{slow}}$ in neurons with mature synapses naturally containing endogenous glutamate could be evaluated. With this purpose, organotypic slice cultures from neonatal rat hippocampi were prepared and biolistically transfected with GluK2-L439C-eGFP and RCaMP2,⁵² another genetically encoded calcium imaging indicator that provided better results in these experiments than R-GECO1. This transfection enabled to localise the cells expressing LiGluR within the slices by the green fluorescence of the expressed enhanced green fluorescent protein (eGFP), while simultaneously recording their activity after 1P and 2P stimulation by the calcium-sensitive red fluorescence of RCaMP2 (Figure III-27). In these experiments no Concanavalin A was used to inhibit GluK2 desensitisation, thus these measurements truly reported on intact neuronal gating and connectivity.

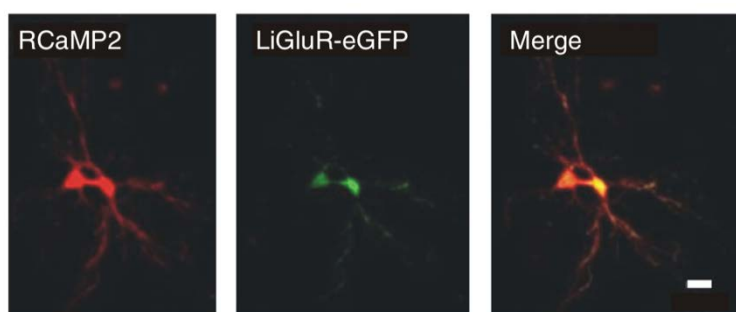


Figure III-27. Microphotograph of a neuron expressing both RCaMP2 (red) and GluK2-L439C-eGFP (green) (scale bar = 20 μm).

The illumination protocols carried out were similar to those used in cultured cells. As observed in these cells, slices incubated with **MAG** displayed clear photoresponses under 1P stimulation ($\lambda_{\text{exc}} = 405 \text{ nm}$), but almost no responses upon 2P excitation ($\lambda_{\text{exc}} = 780 \text{ nm}$) (Figure III-28a). In contrast, slices incubated with **MAG_{2P_F}^{slow}** presented clear photoresponses upon 2P stimulation at 780 nm, with comparable intensities to the responses obtained under 1P illumination at 405 nm (Figure III-28b). The 2P/1P ratio was also determined for both compounds and, as previously demonstrated in cultured cells, **MAG_{2P_F}^{slow}** presented an outstanding enhancement of its multiphoton activity with respect to **MAG** (Figure III-28c). This behaviour was proven robust, reproducible and reliable in many different cells ($n = 6$ cells) located at different depths of the brain tissue (0-100 μm).

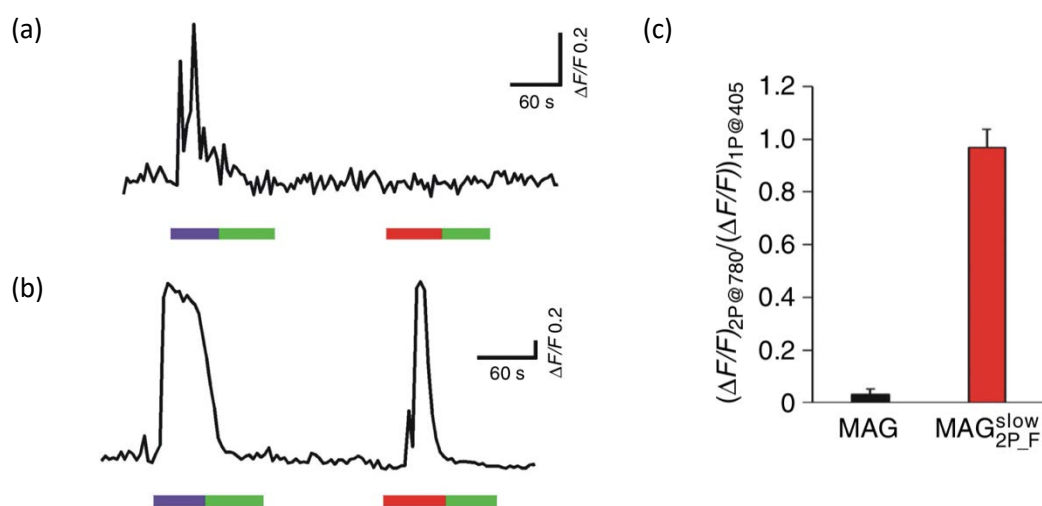


Figure III-28. (a-b) Real time traces of a single-cell neuronal activity of slices incubated with (a) **MAG** and (b) **MAG_{2P_F}^{slow}**. In both cases, 1P stimulation (violet, $\lambda_{\text{exc}} = 405 \text{ nm}$) is first applied to trigger the opening of the channel, followed by irradiation with green light ($\lambda_{\text{exc}} = 514 \text{ nm}$) to induce its closure. Then, the cells are stimulated with 2P irradiation (red, $\lambda_{\text{exc}} = 780 \text{ nm}$), followed again by illumination at 514 nm. (c) Ratio between 2P and 1P responses of **MAG** and **MAG_{2P_F}^{slow}** for the same cells ($n = 5$ and 6 biologically independent cells, respectively). Errors are SEM.

Encouraged by these excellent results, we decided to test the ability of **MAG_{2P_F}^{slow}** to control the operation of neuronal activity *in vivo* by means of 2P excitation. The model of choice to analyse neuronal circuits was *C. elegans*, since the morphology and function of its 302 neurons have been characterised in detail. Therefore, GluK2-L439C-mCherry and GCaMP6s were co-expressed in touch receptor neurons (TRNs) of *C. elegans* individuals. This transfection again enabled to localise the cells expressing LiGluR by the red fluorescence of mCherry, while simultaneously

recording their activity after 1P and 2P stimulation by the green fluorescence of the GCaMP6s, the calcium imaging indicator used in this case (see Figure III-18).

C. elegans presents six TRNs, and among them, the experiments were focused on the single pair located near the tail (Figure III-29a). Like in other neurons within the nervous system, pairs of TRNs can be selectively stimulated in the anterior and posterior part of the animal by means of spatial light patterning. However, it is very difficult to distinguish between neurons when they are overlapping along the optical axis (Figure III-29b) or are closely packed as in the head. 2P excitation would be highly beneficial in those cases, since it enables the activation of cells with a 10 μm axial plane selectivity.⁵³

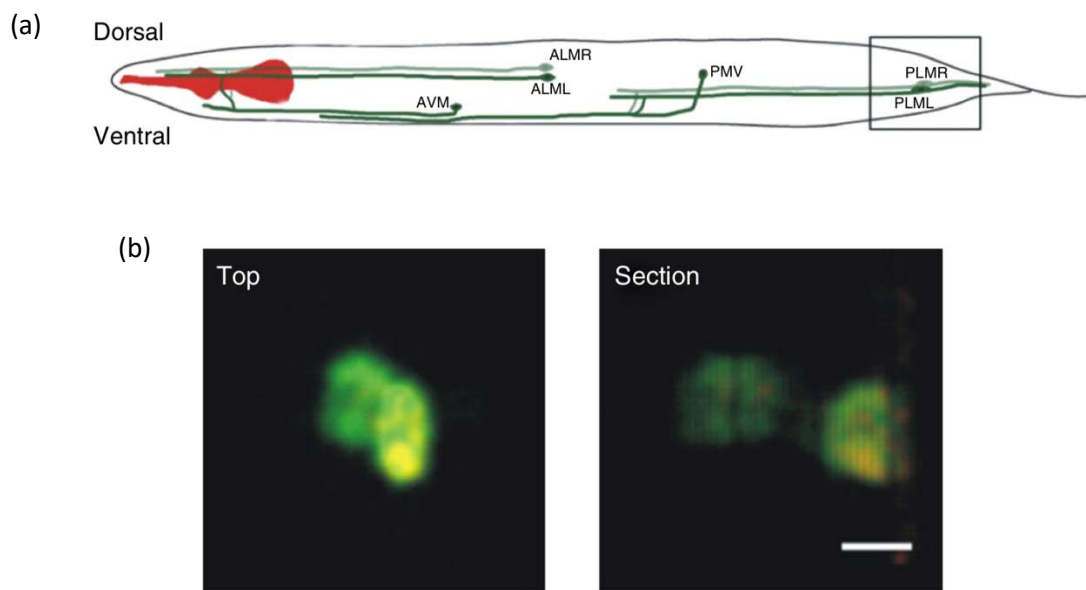


Figure III-29. (a) Schematic picture of *C. elegans* where the TRNs are depicted. (b) Microphotograph of the region squared in (a) of a *C. elegans* co-expressing LiGluR-mCherry (red) and GCaMP6s (green). (scale bar = 5 μm).

Therefore, $\text{MAG}_{2\text{P}_F}^{\text{slow}}$ was delivered to living individuals and the calcium imaging responses triggered in posterior TRNs expressing GluK2-L439C-mCherry and GCaMP6s were monitored using a confocal fluorescence microscope. Clear 2P responses were observed in every animal responding to 1P excitation ($n = 5$ neurons from 4 different individuals, Figure III-30a), which displayed a 2P/1P efficiency of 100% (Figure III-30c), while no response was observed for control animals ($n = 5$ neurons from 4 different individuals, Figure III-30b). Moreover, no signs of toxicity were observed after injection of $\text{MAG}_{2\text{P}_F}^{\text{slow}}$ or during recovery and imaging.

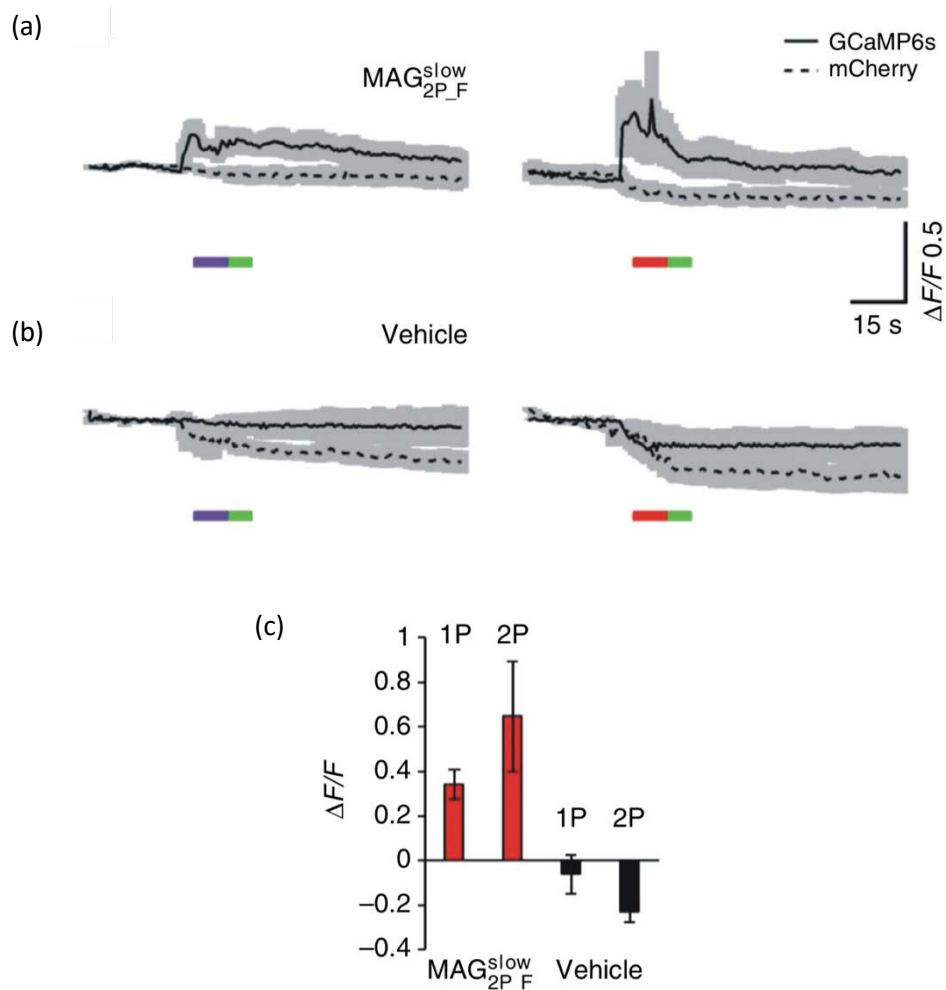


Figure III-30. (a-b) Average traces of 1P- (violet, $\lambda_{exc} = 405 \text{ nm}$, $15 \mu\text{W mm}^{-2}$) and 2P-induced (red, $\lambda_{exc} = 780 \text{ nm}$, $2.8 \mu\text{W mm}^{-2}$) photoactivation of TRNs in animals treated with (a) $MAG_{2P_F}^{slow}$ ($n = 5$ and 6 cells from 4 different animals experiments for 1P and 2P traces, respectively) or (b) with vehicle ($n = 5$ and 6 cells from 4 different animals experiments for 1P and 2P traces, respectively). Continuous line trace indicates GCaMP6s fluorescence signal and dashed trace mCherry fluorescence. In both cases, the channel closure was induced under green illumination ($\lambda_{exc} = 514 \text{ nm}$, $1.21 \mu\text{W mm}^{-2}$). (c) Quantification of the photoresponses obtained in animals injected with vehicle (black bars, $n = 5$ cells from 4 different animals) and $MAG_{2P_F}^{slow}$ (red bars, $n = 5$ cell from 4 different animals). Errors are SEM.

These experiments altogether confirm that $MAG_{2P_F}^{slow}$ presents excellent 2P properties that enable its use as a photopharmacological tool to manipulate neuronal activity in light-scattering tissue *in vitro* and *in vivo*, such as in brain slices under nearly physiological conditions and *C. elegans* touch receptor neurons, with high efficacy and selectivity.

III.7. CONCLUSIONS

In this chapter, the synthesis, photochemical properties, computational analysis and biological application of novel photoswitchable tethered ligands **MAG**_{2P}^{slow} and **MAG**_{2P-F}^{slow} have been described. These compounds were designed as optical tools to control the operation of ionotropic glutamate receptors by means of 2P stimulation with NIR light based on the structure of the well-known **MAG** PTL. Thus, the molecules prepared display the three main parts of this parent system: (i) an azobenzene core that acts as a molecular switch interconverting between from its *trans* and *cis* isomers upon illumination; (ii) a glutamate derivative as an agonist of receptor GluK2; and (iii) a maleimide moiety that acts as an anchor covalently linking the molecule to a cysteine close to the binding site of the receptor (Figure III-31). The key feature of these new **MAG** derivatives is the push-pull substitution of their azobenzene cores, for which we introduced weak mesomeric EWG and EDG and inductive EWG that enhance their 2PA cross sections without detrimentally affecting the long *cis* state thermal lifetime.

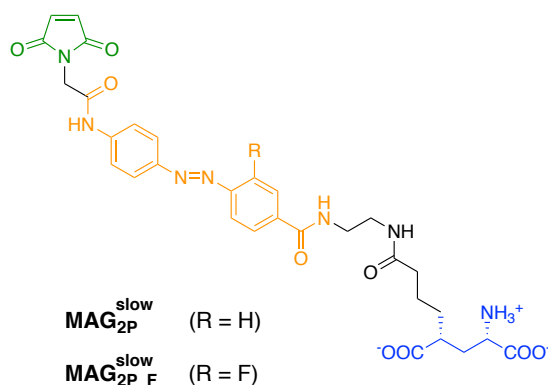


Figure III-31. Structure of new PTLs **MAG**_{2P}^{slow} and **MAG**_{2P-F}^{slow} that enable the operation of light-gated ionotropic glutamate receptors by means of 2P excitation with NIR light. These compounds display the three main building blocks of **MAG** compounds: (i) azobenzene core (orange); (ii) glutamate moiety (blue); and (iii) maleimide anchor (green).

The main conclusions obtained from the studies conducted in **MAG**_{2P}^{slow} and **MAG**_{2P-F}^{slow} are:

- The modular synthetic strategy developed in our group by Gascón-Moya to grant access to new **MAG** derivatives proved to be broadly applicable to the synthesis of other PTLs bearing electronically-asymmetric azobenzene cores. Following this synthetic pathway, compound **MAG**_{2P}^{slow} was prepared in 12% overall yield from aminobenzoic acid **14** and compound **MAG**_{2P-F}^{slow} was obtained in 20% overall yield from aminobenzoic acid **15**.

- Our design approach based on the substitution of the azobenzene core with weak mesomeric and strong inductive EDGs and EWGs proved to be successful for the obtention of PTLs that display: (i) long τ_{cis} , as proven by the measures in solution; and (ii) high σ_2 , as proven by the 2P-stimulation biological experiments. This was corroborated by theoretical calculations, which confirm the possibility to computationally predict and rationalise the properties of these compounds, thus providing with a tool to design even more efficient PTLs for the 2P manipulation of cellular receptors.
- Compound **MAG_{2P_F}^{slow}** is able to efficiently trigger LiGluR under 2P-excitation with NIR light, which we evidenced for two relevant biological systems: hippocampal organotypic slices and *C. elegans* touch receptor neurons.

In view of these, we have demonstrated that new **MAG** derivatives exhibiting push-pull azobenzene cores with weak mesomeric and strong inductive EDGs and EWGs are synthetically accessible and display excellent properties to emerge as new photopharmacological tools for the optical control by means of 2P- stimulation with NIR light of neuronal circuits. Therefore, the results presented in this chapter constitute a proof of concept that paves the way toward all-optical experiments of neuronal activity imaging and manipulation *in vivo* using azobenzene photoswitches, which ultimately require the use of multiphoton excitation with NIR light.

III.8. REFERENCES

- (1) Volgraf, M.; Gorostiza, P.; Numano, R.; Kramer, R. H.; Isacoff, E. Y.; Trauner, D. *Nat. Chem. Biol.* **2006**, *2*, 47-52.
- (2) Numano, R.; Szobota, S.; Laud, A. Y.; Gorostiza, P.; Volgraf, M.; Roux, B.; Trauner, D.; Isacoff, E. Y. *Proc. Natl. Acad. Sci. USA* **2009**, *106*, 6814–6819.
- (3) Gorostiza, P.; Volgraf, M.; Numano, R.; Szobota, S.; Trauner, D.; Isacoff, E. Y. *Proc. Natl. Acad. Sci. USA* **2007**, *104*, 10865-10870.
- (4) Armstrong, N.; Gouaux, E. *Neuron* **2000**, *28*, 165-181.
- (5) Mayer, M. L. *Neuron* **2005**, *45*, 486-493.

- (6) Szobota, S.; Gorostiza, P.; Del Bene, F.; Wyart, C.; Fortin, D. L.; Kolstad, K. D.; Tulyathan, O.; Volgraf, M.; Numano, R.; Aaron, H. L.; Scott, E. K.; Kamer, R. H.; Flannery, J.; Baier, H.; Trauner, D.; Isacoff, E. Y. *Neuron* **2007**, *54*, 535-545.
- (7) Yaroslavsky, A. N.; Schulze, P. C.; Yaroslavsky, I. V.; Schober, R.; Ulrich, F.; Schwarzmaier, H. J. *Phys. Med. Biol.* **2002**, *47*, 2059–2073.
- (8) Kienzler, M. A.; Reiner, A.; Trautman, E.; Yoo, S.; Trauner, D.; Isacoff, E. Y. *J. Am. Chem. Soc.* **2013**, *135*, 17683-17686.
- (9) Rullo, A.; Reiner, A.; Reiter, A.; Trauner, D.; Isacoff, E. Y.; Woolley, G. A. *Chem. Commun.* **2014**, *50*, 14613-14615.
- (10) Dong, M.; Babalhavaeji, A.; Collins, C. V.; Jarrah, K.; Sadovski, O.; Dai, Q.; Woolley, G. A. *J. Am. Chem. Soc.* **2017**, *139*, 13483-13486.
- (11) Yang, Y.; Hughes, R. P.; Aprahamian, I. *J. Am. Chem. Soc.* **2016**, *136*, 13190-13193.
- (12) Hammerich, M.; Schütt, C.; Stähler, C.; Lentjes, P.; Röhrich, F.; Höppner, R.; Herges, R. *J. Am. Chem. Soc.* **2016**, *138*, 13111-13114.
- (13) Pawlicki, M.; Collins, H. A.; Denning, R. G.; Anderson, H. L. *Angew. Chem. Int. Ed.* **2009**, *48*, 3244-3266.
- (14) Bort, G.; Gallavardin, T.; Ogden, D.; Dalko, P. I. *Angew. Chem. Int. Ed.* **2013**, *52*, 4526-4537.
- (15) Denk, W.; Strickler, J. H.; Webb, W. W. *Science* **1990**, *248*, 73-76.
- (16) Oron, D.; Papagiakoumou, E.; Anselmi, F.; Emiliani, V. *Prog. Brain Res.* **2012**, *196*, 119-143.
- (17) Watson, B. O.; Nikolenko, V.; Yuste, R. *Front. Neural Circuits* **2009**, *3*, 6.
- (18) Packer, A. M.; Peterka, D. S.; Hirtz, J. J.; Prakash, R.; Deisseroth, K.; Yuste, R. *Nat. Methods* **2012**, *9*, 1202-1205.
- (19) Rowlands, C. J.; Park, D.; Bruns, O. T.; Piatkevich, K. D.; Fukumura, D.; Jain, K. J.; Bawendi, M. G.; Boyden, E. S.; So, P. T. S. *Light Sci. Appl.* **2017**, *6*, e16255.
- (20) de Boni, L.; Misoguti, L.; Zilio, S. C.; Mendonça, C. R. *ChemPhysChem* **2005**, *6*, 1121-1125.

- (21) Silva, D. L.; Krawczyk, P.; Bartkowiak, W.; Mendonça, C. R. *J. Chem. Phys.* **2009**, *131*, 244516.
- (22) Göppert-Mayer, M. *Ann. Phys.* **1931**, *401*, 273-294.
- (23) Kaiser, W.; Garret, C. G. B. *Phys. Rev. Lett.* **1961**, *7*, 229-231.
- (24) Andrade, C. D.; Yanez, C. O.; Rodriguez, L.; Belfield, K. D. *J. Org. Chem.* **2010**, *75*, 3975-3982.
- (25) Dreuw, A.; Polkehn, M. A.; Binder, R.; Heckel, A.; Knippenberg, S. *J. Comput. Chem.* **2012**, *33*, 1797-1805.
- (26) de Boni, L.; Jr, J. J. R.; Jr, D. S. S.; Silva, C. H. T. P.; Balogh, D. T.; Jr, O. N. O.; Zilio, S. C.; Misoguti, L.; Mendonça, C. R. *Chem. Phys. Lett.* **2002**, *361*, 209-213.
- (27) Andrade, A. A.; Yamaki, S. B.; Misoguti, L.; Zilio, S. C.; Atvars, T. D. Z.; Oliveira, O. N.; Mendonça, C. R. *Opt. Mater.* **2004**, *27*, 441-444.
- (28) Antonov, L.; Kamada, K.; Ohta, K.; Kamounah, F. S. *Phys. Chem. Chem. Phys.* **2003**, *5*, 1193-1197.
- (29) Carroll, E. C.; Berlin, S.; Levitz, J.; Kienzler, M. A.; Yuan, Z.; Madsen, D.; Larsen, D. S.; Isacoff, E. Y. *Proc. Natl. Acad. Sci. USA* **2015**, *112*, E776-E785.
- (30) Gascón-Moya, M. Doctoral Thesis, Universitat Autònoma de Barcelona, 2014.
- (31) Gascón-Moya, M.; Pejoan, A.; Izquierdo-Serra, M.; Pittolo, S.; Cabré, G.; Hernando, J.; Alibés, R.; Gorostiza, P.; Busqué, F. *J. Org. Chem.* **2015**, *80*, 9915-9925.
- (32) Izquierdo-Serra, M.; Gascón-Moya, M.; Hirtz, J. J.; Pittolo, S.; Poskanzer, K. E.; Ferrer, E.; Alibés, R.; Busqué, F.; Yuste, R.; Hernando, J.; Gorostiza, P. *J. Am. Chem. Soc.* **2014**, *136*, 8693-8701.
- (33) Croissant, J.; Maynadier, M.; Gallud, A.; N'Dongo, H. P.; Nyalosaso, J. L.; Derrien, G.; Charnay, C.; Durand, J-O.; Raehm, L.; Serein-Spirau, F.; Cheminet, N.; Jarrosson, T.; Mongin, O.; Blanchard-Desce, M.; Gary-Bobo, M.; Garcia, M.; Lu, J.; Tamanoi, F.; Tarn, D.; Guardado-Alvarez, T. M.; Zink, J. I. *Angew. Chem. Int. Ed.* **2013**, *52*, 13813-13817.
- (34) Moreno, J.; Gerecke, M.; Grubert, L.; Kovalenko, S. A.; Hecht, S. *Angew. Chem. Int. Ed.* **2016**, *55*, 1544-1547.

- (35) Bandara, H. M. D.; Burdette, S. C. *Chem. Soc. Rev.* **2012**, *41*, 1809-1825.
- (36) Hegarty, A. *The Chemistry of the Diazonium and Diazo Group*. VCH, Wiley, New York, **1978**.
- (37) Kamachi, M.; Seki, M.; Tsuji, M.; Morishima, Y. *Macromolecules* **1993**, *26*, 3299-3305.
- (38) Gascón-Moya, M. Màster en Experimentació en Química, Universitat Autònoma de Barcelona, 2010.
- (39) Supuran, C.; Vullo, D.; Scozzafava, A.; Maresca, A.; Carta, F. *Bioorg. Med. Chem.* **2009**, *17*, 7093-7099.
- (40) Ezquerra, J.; Pedregal, C.; Rubio, A.; Yruretagoyena, B.; Escribano, A.; Sánchez-Ferrando, F. *Tetrahedron* **1993**, *49*, 8665-8678.
- (41) Steger, M.; Young, D. W. *Tetrahedron* **1999**, *55*, 7935-7956.
- (42) Cabré, G. Master in Industrial Chemistry and Introduction to Chemical Research, Universitat Autònoma de Barcelona, 2015.
- (43) Bal, B. S.; Childers, W. E.; Pinnick, H. W. *Tetrahedron* **1981**, *37*, 2091-2096.
- (44) König, W.; Geiger, R. *Chem. Ber.* **1970**, *103*, 788-798.
- (45) Han, S. Y.; Kim, Y. A. *Tetrahedron* **2004**, *60*, 2447-2467.
- (46) Pearson, R. J.; Kassianidis, E.; Slawin, A. M. Z.; Philip, D. *Org. Biomol. Chem.* **2004**, *2*, 3434-3441.
- (47) Zhao, Y.; Inayat, S.; Dikin, D. A.; Singer, J. H.; Ruoff, R. S.; Troy, J. B. *Proc. Inst. Mech. Eng. Part N J. Nanoeng. Nanosyst.* **2008**, *222*, 1-11.
- (48) Mathers, D. A.; Usherwood, P.N. R. *Nature* **1976**, *259*, 409-411.
- (49) Nakai, J.; Ohkura, M.; Imoto, K. *Nat. Biotechnol.* **2001**, *19*, 137-141.
- (50) Zhao, Y.; Araki, S.; Wu, J.; Teramoto, T.; Chang, Y-F.; Nakano, M.; Abdelfattah, A. S.; Fujiwara, M.; Ishihara, T.; Nagai, T.; Campbell, R.E. *Science* **2011**, *333*, 1888-1891.
- (51) Eyring, H. *J. Chem. Phys.* **1935**, *3*, 107-115.
- (52) Bosch, M.; Castro, J.; Saneyoshi, T.; Matsuno, H.; Sur, M.; Hayashi, Y. *Neuron* **2014**, *16*, 444-459.

- (53) Prakash, R.; Yizhar, O.; Grewe, B.; Ramakrishnan, C.; Wang, N.; Goshen, I.; Packer, A. M.; Peterka, D. S.; Yuste, R.; Schnitzer, M. J.; Deisseroth, K. *Nat. Methods* **2012**, *9*, 1171-1179.

CHAPTER IV

Stilbene-based non-destructive caged ligands for the optical control of iGluRs

This chapter reports our efforts towards the development of the first example of non-destructive caged ligands (NDCLs), a novel concept in photopharmacology that surpasses the main drawback of caged ligands and enables photocontrol of ionotropic glutamate receptors. The synthesis, characterisation and biological application *in vitro* of these new compounds are next detailed.

IV.1. INTRODUCTION

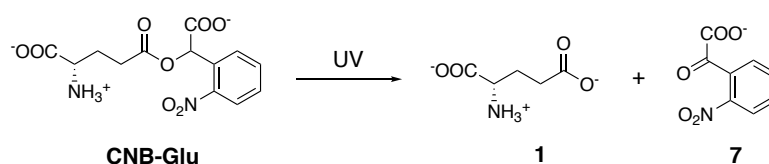
IV.1.1. CAGED LIGANDS FOR THE PHOTOCONTROL OF GLUTAMATE RECEPTORS

In the field of photopharmacology, caged compounds are biologically-active molecules rendered inactive by covalent attachment to photolabile protecting groups. Hence, when irradiated with light of the appropriate wavelength, photocleavage of the protecting group releases the active substrate and triggers the desired biological effect. Since the synthesis of the first caged compound in 1978 (a 2-nitrobenzyl-based caged ATP¹), this strategy has been applied to many different biomolecules, such as small molecules, ions, macromolecules, peptides and proteins, and even genes.^{2,3}

Hess and co-workers revolutionised the field of neuroscience with the development of the first caged neurotransmitters.^{4,5,6} Since then, the light-induced uncaging of neurotransmitters has become an active topic of research and this approach has been widely exploited for the study of neuronal circuitries.⁷ Caged glutamate is the most extensively employed caged neurotransmitter by neurobiologists and many compounds of this type have been described using different chromophores and caging strategies.⁸ However, very few of them are actually suitable for their application in biological tissues due to slow uncaging kinetics, low stability and/or toxicity.⁸

A first milestone in this area was set by Hess and co-workers⁵ and Callaway and Katz⁹ in the early 90s when they pioneered the use of caged glutamates based on 2-nitrobenzyl chromophores

(e.g. **CNB-Glu** in Scheme IV-1) to conduct whole-cell patch clamp experiments in rat hippocampal neurons. Upon UV light stimulation, these compounds released free glutamate moieties that induced rapid onset of transmembrane currents. However, they were not sensitive to neither visible light nor two-photon stimulation with NIR light, which would be highly desirable to reduce phototoxicity and increase penetration into tissues¹⁰ and even excitation resolution¹¹ (see § III.1.2). Therefore, many efforts have been put since then in the development of new caged glutamates that are not only suitable for biological applications, but also respond to visible light and, even better, to two-photon excitation.



Scheme IV-1. Structure of **CNB-Glu** and its uncaging process. This compound was one of the first successful caged glutamate developed for practical use on neurons under UV light stimulation.^{5,9}

In 2000, Ellis-Davies and co-workers developed the first caged glutamate that could be successfully applied to the photocontrol of glutamate receptors by two-photon excitation: methoxynitroindolin-glutamate, **MNI-Glu**¹² (Figure IV-1). This compound was found to be highly soluble in physiological media and, though it presented a rather modest two-photon absorption cross-section ($\sigma_2 = 0.06 \text{ GM}$ at 730 nm),¹² it underwent 2P-induced uncaging with NIR light without apparent phototoxicity. For these reasons, **MNI-Glu** has been widely applied for neuronal excitation, functional mapping and *in vivo* uncaging.^{13,14} Inspired by **MNI-Glu** structure, Ellis-Davies and co-workers later developed analogous caged ligands with higher σ_2 values: (i) **MDNI-Glu**,¹⁵ which exhibited outstanding efficiency in astrocytes in brain slices (Figure IV-1); and (ii) **CDNI-Glu**,¹⁶ whose additional acid residue allowed preventing the solubility issues encountered for **MNI-Glu** in aqueous media (Figure IV-1).

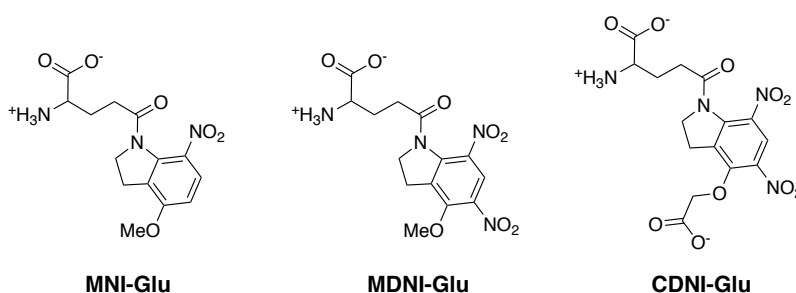


Figure IV-1. Structures of the first caged glutamates developed that enabled neuronal operation upon 2P stimulation.^{12,15,16}

Despite the good results obtained with the caged glutamates previously described, these compounds exhibit a high antagonistic effect on GABAergic transmission, which hampers their use in the study of neural circuits. To overcome this problem, Yuste and co-workers synthesised **RuBi-Glu**,¹⁷ a caged glutamate based on a ruthenium-bipyridine complex (Figure IV-2). This new ligand features a relatively high absorption cross-section in the visible (blue) light, and high quantum efficiency of uncaging. As such, it could be used at lower concentrations than other caged ligands, thus reducing the off-target effects on GABAergic transmission. Moreover, **RuBi-Glu** showed efficient 2P absorption, which enabled successful mapping studies in mouse frontal cortex.¹⁸ Another attempt to improve the performance of caged glutamates was the synthesis of **DEAC450-Glu**¹⁹ by Ellis-Davies and co-workers (Figure IV-2). **DEAC450-Glu** is a coumarin-based caged ligand that releases glutamate upon 2P irradiation with rather long-wavelength NIR light (900 nm). Therefore, the combination of other caged ligands with this compound enabled orthogonal uncaging of different neurotransmitters within the same experiment.²⁰

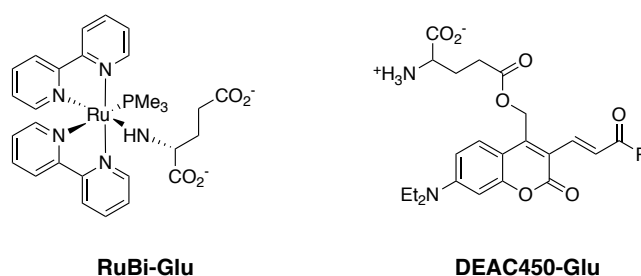


Figure IV-2. Structure of **RuBi-Glu**¹⁷ and **DEAC450-Glu**¹⁹, new types of caged glutamates with improved biological and/or optical properties.

One common weakness of caged glutamates is their lack of specificity on different glutamate receptors, which poses some limitations on the study of neural circuitries. One strategy to overcome this drawback is the use of caged ligands that exclusively target certain GluR subtypes. Hence, the replacement of glutamate in caged ligands with subtype-specific GluR agonists such as kainate, NMDA or AMPA, would enable selective activation of GluR subtypes without requiring the presence of selective antagonists, as needed when using caged glutamates. Palma-Cerda and co-workers, reported the first caged subtype-specific iGluR agonists: **MNI-kainate**, **MNI-NMDA** and **NPEC-AMPA** (Figure IV-3),²¹ with which selective activation of different iGluRs subtypes was achieved with good time resolution and spatial localisation.

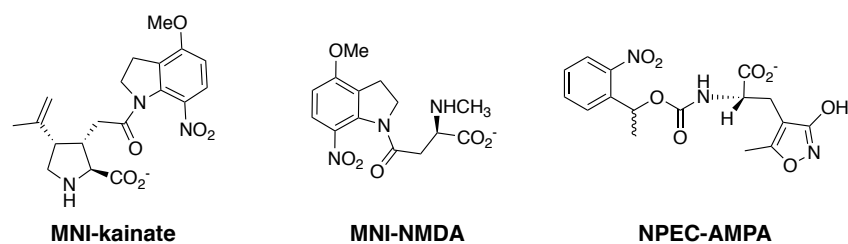


Figure IV-3. Structure of caged iGluR agonists **MNI-kainate**, **MNI-NMDA** and **NPEC-AMPA** that enable subtype-specificity.²¹

Despite the multiple improvements in the development of new caged ligands for iGluRs and their successful application *in vitro* and *in vivo*, these compounds still suffer from several disadvantages with respect to photochromic ligands: (i) their photoinduced activation is irreversible and can not be switched off; and (ii) the release of by-products upon photocleavage, which might be toxic or present undesired biological effects. To overcome the latter, a new photopharmacological strategy based on photoswitches has been explored in this thesis, which we called non-destructive caged ligands.

IV.1.2. NON-DESTRUCTIVE CAGED LIGANDS: A NEW CONCEPT IN PHOTOPHARMACOLOGY

Non-destructive caged ligands (NDCLs) are a new class of photopharmacological compounds that have been conceived in our group in order to overcome one of the drawbacks of current caged ligands, namely the generation of by-products. This new concept originates from the combination of the properties of caged ligands and photochromic ligands, with which we aim to achieve the efficient, irreversible photoactivation of CLs by means of the use of non-photolysable light-responsive switches as in PCLs. To reach this goal, NDCLs must be composed of a bioactive species tethered to a photoisomerisable group which (i) must render the ligand inactive in its thermally stable state; and (ii) must undergo unidirectional light-induced transformation towards the active form of the system by somehow inhibiting the back-isomerisation reaction of the photoswitch (Figure IV-4). Under such circumstances, the light-promoted inactive-to-active state transition of the ligand should be irreversible and quantitative, in a similar fashion as in caged ligands but without the generation of by-products.

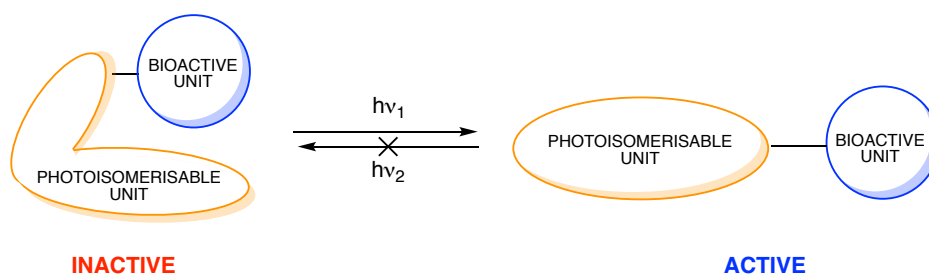
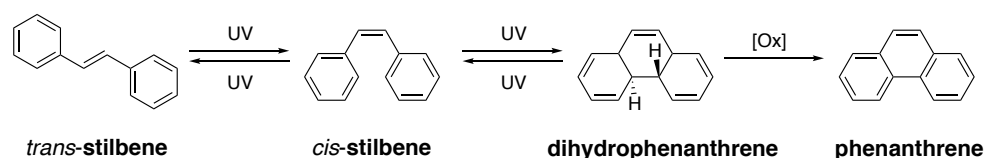


Figure IV-4. General structure and behaviour of non-destructive caged ligands (NDCLs).

Stilbenes could be good candidates as light-responsive building blocks for the preparation of NDCLs due to their synthetic accessibility, their ability to photoswitch between *trans* and *cis* configurations, the large geometrical change between them, the thermal stability of both isomers, and finally, the capacity to selectively block the *trans*→*cis* photoisomerisation reaction upon wise choice of the substituents. The following section deeper describes these interesting properties of stilbene photowitches.

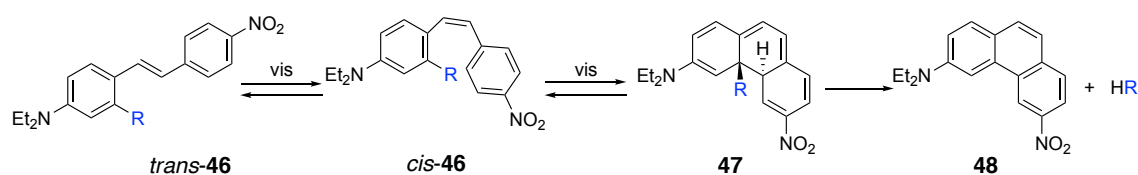
IV.1.3. STILBENE PHOTOSWITCHES

Stilbenes are constituted by a carbon-carbon double bond in conjugation with two phenyl ring substituents. In a similar way to azobenzenes, stilbenes can undergo reversible photoinduced *trans-cis* isomerisation reactions, which result in large geometrical changes in their structure (Scheme IV-2).²² However, they present an additional advantage that could be exploited in many applications: stilbenes are P-type photochromes, since the energy barrier of their thermal *cis*→*trans* back-isomerisation is quite high (typically, about 45 kcal/mol), which implies that thermal isomerisation is negligible at rt.²³ Unfortunately, the photochemical performance of stilbenes suffers from several drawbacks that ultimately limit their use:²² (i) photoisomerisation requires excitation of their π - π^* absorption band with rather high energy UV radiation ($\lambda_{\text{abs,max}} \sim 300$ and 280 nm for unsubstituted *trans*- and *cis*-stilbenes, respectively²²), although bathochromical shifts can be induced upon substitution with EDGs and/or EWGs; (ii) because of the spectral overlap between the π - π^* absorption band of both isomers, photoisomerisation efficiencies are moderate and usually lower than for other *trans-cis* photoswitches; and (iii) *cis*-stilbenes are often photochemically unstable and they can undergo an electrocycloisomerisation reaction to produce dihydrophenanthrenes under irradiation, which can irreversibly convert into the corresponding phenanthrenes in the presence of oxidants²⁴ (e.g. O₂, Scheme IV-2).



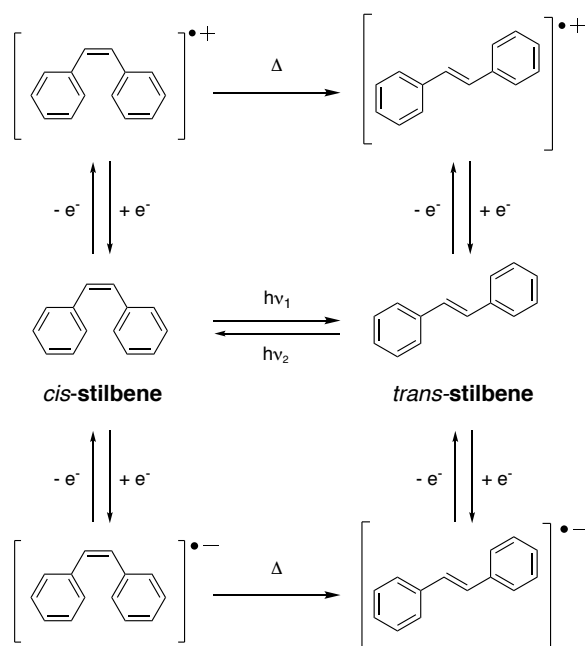
Scheme IV-2. *Trans-cis* photoisomerisation process of stilbene and photocyclisation reaction of its *cis* isomer, which irreversibly leads to phenanthrene upon oxidation.

Because of these disadvantages over azobenzenes, stilbenes have been seldom used in photopharmacology. Only a few examples of stilbene-based photopharmacological tools can be found in the literature, such as heterostilbene-based PCLs for the reversible photoregulation of gene expression²⁵ or for the photoinduced inhibition of kinases,²⁶ or stilbene-based PCLs for the allosteric photocontrol of GPCRs.²⁷ Recently, a caged ligand based on stilbene has been reported by Singh and co-workers.²⁸ They developed push-pull-substituted stilbene **46** which displayed the $\pi-\pi^*$ absorption band in the visible region of the spectrum and exploited the photocyclisation reaction of *cis*-stilbene and the subsequent formation of phenanthrene to release different caged compounds with high efficiency and moderate photochemical quantum yields ($\Phi_{\text{uncaging}} \sim 0.1$). Basically, by introducing a leaving group at the point of cyclisation, spontaneous thermally driven non-oxidative elimination process took place, thus releasing the desired caged compound (Scheme IV-3). The authors reported successful *in vitro* uncaging of an anticancer agent in MCF-7 breast cancer cell line upon stimulation with $\lambda_{\text{exc}} \geq 410$ nm. It must be noted that, in contrast to stilbenes, diarylethene photoswitches (which are structurally related to stilbenes) have been widely used in the photopharmacological field, specially by the groups of König^{29,30,31,32} and Branda.^{29,33,34}



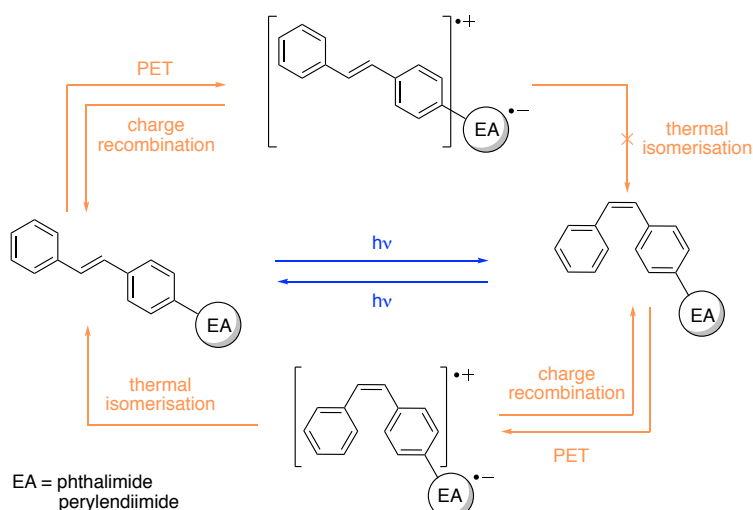
Scheme IV-3. Photoinduced release of caged compounds (R) from stilbene-based caged ligand **46**.²⁸

In addition to photoinduced switching, electrochemical *cis*→*trans* isomerisation of stilbenes has also been reported. In particular, it was described that both the radical cations³⁵ and radical anions³⁶ of *cis*-stilbenes obtained upon oxidation and reduction, respectively, undergo spontaneous thermal isomerisation. Subsequent reduction or oxidation of the isomerised radical ions finally furnish the corresponding neutral *trans* isomers (Scheme IV-4).



Scheme IV-4. Proposed mechanism for the *cis*-stilbene cations and anions isomerisation process.

In our group it has been shown that the electrochemical *cis*→*trans* isomerisation of stilbenes can be photoinduced. On one hand, Marc Padilla demonstrated that electron-rich *cis*-stilbenes could be isomerised by hole transfer from nearby photoexcited gold nanoparticles.³⁷ On the other hand, Rafael Sánchez showed that, by covalently tethering stilbene groups to good electron acceptor moieties (e.g. phthalimide, perylendiimide), photoinduced electron transfer (PET) processes took place upon irradiation that resulted in selective isomerisation of the transient *cis*-stilbene^{•+} species formed (Scheme IV-5).³⁸ Several additional relevant features were observed in the latter case: (i) PET in stilbene-electron acceptor dyads occurred for both isomers of the system and it could completely inhibit direct *trans*→*cis* and *cis*→*trans* photoisomerisation; (ii) no thermal isomerisation was observed for the *trans*-stilbene^{•+} species generated under such circumstances, which led to quantitative PET-induced *cis*→*trans* photoconversion; (iii) the efficiency of the PET processes could be controlled by solvent polarity, which allowed switching between regular reversible *trans*-*cis* stilbene photoisomerisation (in non-polar solvents) to selective electropromoted *cis*→*trans* transformation (in polar solvents); and (iv) PET could take place both upon photoexcitation of the stilbene and electron acceptor groups, thus opening the door for triggering *cis*→*trans* isomerisation with a visible-absorbing electron acceptor unit (e.g. with green light in the case of perylendiimide-stilbene derivative).³⁸ Actually, a similar behaviour has been recently reported for the *cis*→*trans* isomerisation of azobenzenes by Hecht and co-workers.^{39,40}



Scheme IV-5. Photoisomerisation process of stilbene-electron acceptor (EA) dyads in non-polar solvents (blue) and polar solvents (orange). In non-polar solvents switching between both isomers takes place through regular reversible photoisomerisation, whilst in polar solvents PET completely inhibits direct photoisomerisation and *cis*→*trans* conversion is selectively electropromoted.

In this work, we aimed to exploit the precedents in our group about the PET-induced isomerisation of *cis*-stilbenes to develop the new concept of non-destructive caged ligands.

IV.1.4. DESIGN OF NOVEL NON-DESTRUCTIVE CAGED LIGANDS FOR GLUTAMATE RECEPTORS

As a proof of concept of our novel approach, we decided to develop a NDCL for the photocontrol of ionotropic glutamate receptors. For the design of its structure, we sought inspiration in **GluAzo**,⁴¹ a well-known PCL that targets GluK1 and GluK2 (Figure IV-5a).

GluAzo was developed in 2007 by Isacoff, Trauner and co-workers. It was designed based on the crystal structure of the complex of 4-(*R*)-methylglutamate with the clamshell-like ligand-binding domain of kainate receptor GluK2, which shows that a side chain can be attached to the bound glutamate molecule and stick out through an *exit channel* between the lips of the clamshell. By introducing a photoisomerisable azobenzene group in such chain, the authors aimed to modulate the agonist-binding site interaction under irradiation, which should decrease for the bent *cis* configuration of the ligand due to steric effects. In practice, this required a very short linker between the azo and glutamate moieties and, eventually, **GluAzo** was prepared with a vinyl tether. By means of electrophysiological measurements, this compound was proven to

function as a partial agonist for kainate receptors GluK1 and GluK2 in its dark-adapted *trans* form and to majorly lose its activity in its *cis* state upon 380 nm stimulation (Figure IV-5b). This result, which was exploited to light-induce action potentials in neurons,⁴¹ was fully rationalised in 2013, when Trauner and co-workers successfully crystallised the LBD of GluK2 bound to *trans*-**GluAzo**.⁴² As illustrated in Figure IV-5c, the structure obtained shows how the LBD of this receptor can take a closed conformation around the photochromic ligand by allowing the *trans*-azobenzene unit of the molecule to stick out from the binding site cavity via an exit tunnel. However, this cannot occur for the folded *cis* isomer of **GluAzo**, thus interfering with the closing of the clamshell and accounting for the difference in biological activity for the two states of the ligand.

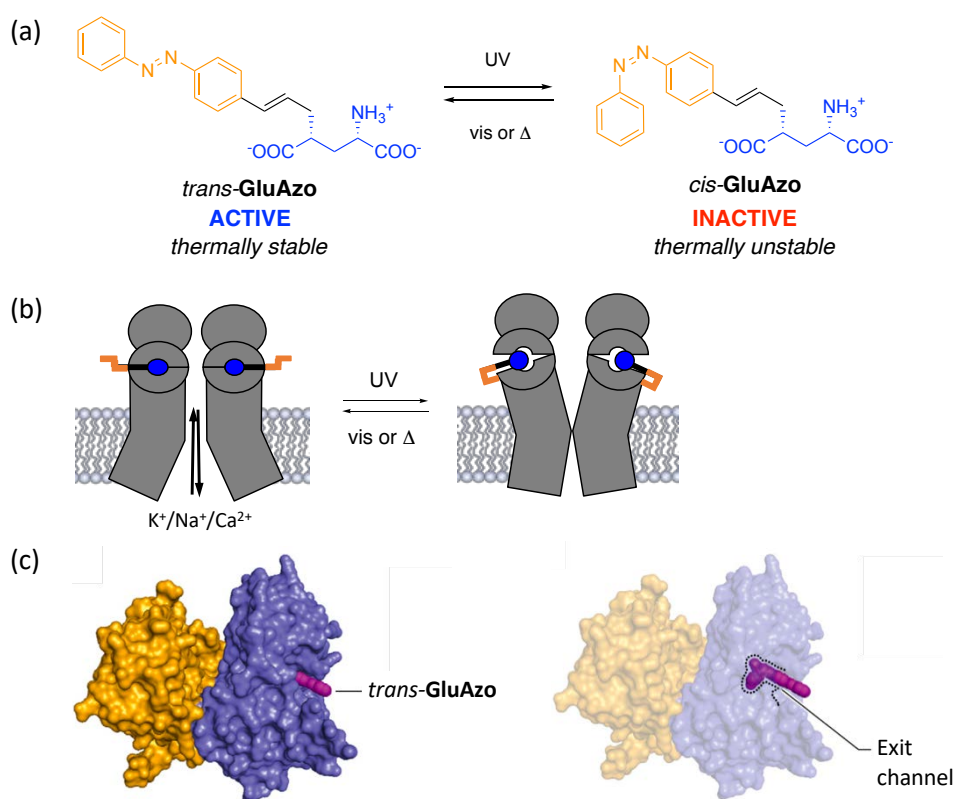
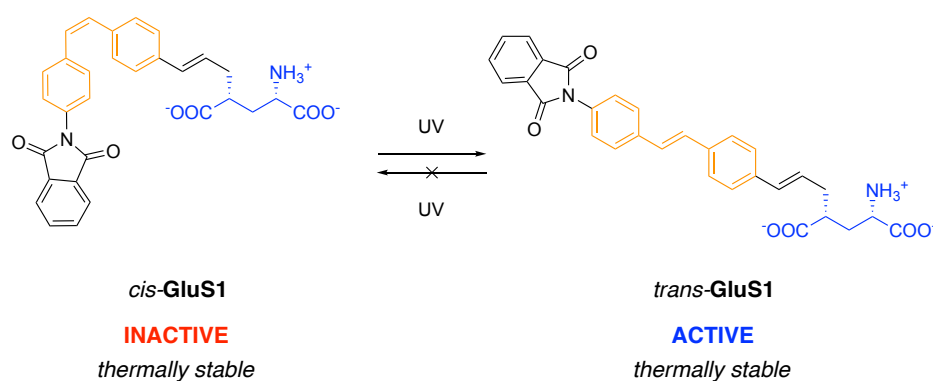


Figure IV-5. (a) Structure and *trans-cis* isomerisation of **GluAzo**. (b) Schematic representation of the light-induced operation of iGluRs with **GluAzo**. In its thermodynamically stable extended *trans* structure, the glutamate moiety of **GluAzo** can interact with the binding site of the receptor, triggering the opening of the channel. Upon irradiation with UV light, the folded *cis* structure is formed, and the glutamate fragment poorly interacts with the binding site, thereby rendering the channel closed. Back-isomerisation to the *trans* state upon irradiation with visible light or thermally allows this process to be reverted. (c) Crystal structure of the LBD of a kainate receptor bound to *trans*-**GluAzo** (the structure comes from PDB: 4H8I). Left: surface representation of GluK2-LBD dimers in complex with **GluAzo** (magenta). Right: Transparent view of the dimer, depicting the partially embedded **GluAzo** within the LBD (dashed line) and the exit tunnel through which the azobenzene protrudes.⁴³

In view of the successful performance of **GluAzo** to photocontrol iGluRs and the results previously obtained in our group for stilbene-electron acceptor dyads, we devised **GluS1**, the first example of NDCL, on the basis of the following design concepts (Scheme IV-6): (i) the photoisomerisable azobenzene group of **GluAzo** was replaced by a stilbene photochrome bearing a phthalimide substituent to inhibit *trans*→*cis* photoconversion in biological media and allow selective PET-induced *cis*→*trans* transformation; (ii) the stilbene and glutamate moieties of **GluS1** were tethered through a vinyl linker, as in **GluAzo**; and (iii) taking advantage of the *cis* stability of stilbene photochromes, **GluS1** was synthesised in its *cis* state, which should present no (or low) activity due to steric effects, by analogy with *cis*-**GluAzo**. As a result, the agonist behaviour of **GluS1** on GluK1 and GluK2 should be phototriggered upon quantitative light-induced conversion to its *trans* isomer.



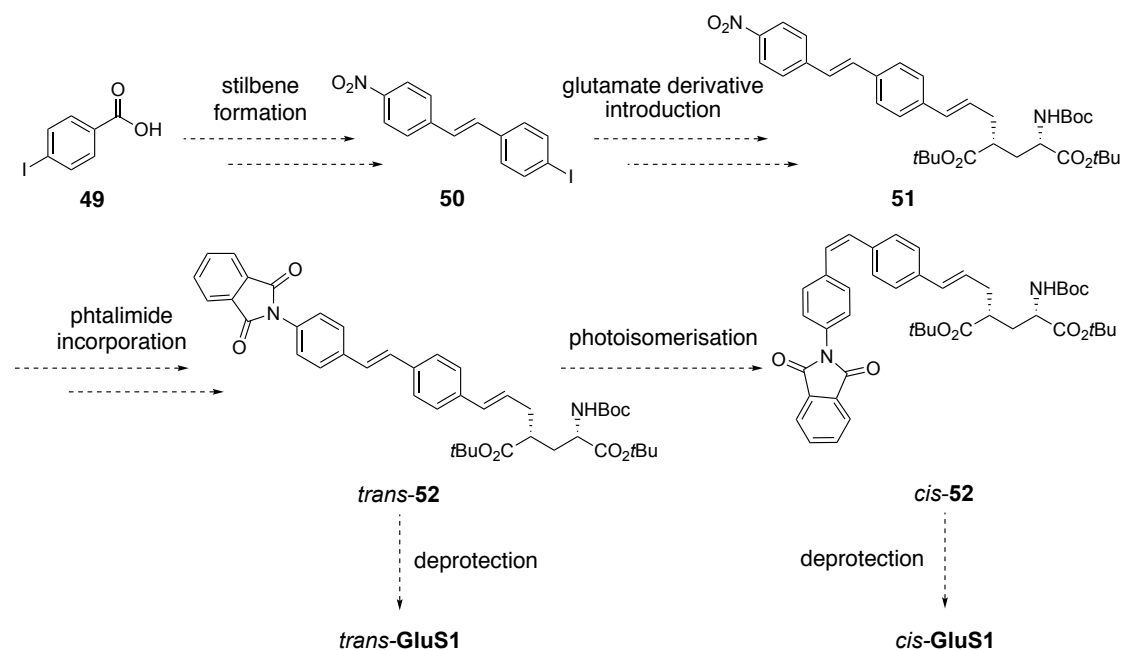
Scheme IV-6. Structure and photoinduced response devised for **GluS1**, the first case of NDCL inspired on photocromic ligand **GluAzo**.

IV.2. SYNTHESIS AND PHOTOCHEMICAL CHARACTERISATION OF **GluS1**

IV.2.1. STRATEGY FOR THE SYNTHESIS OF **GluS1**

The synthesis of **GluS1** was devised as depicted in Scheme IV-7. The first step of the synthetic pathway proposed focused on the preparation of *trans*-stilbene **50** from commercially available 4-iodobenzoic acid, **49**. Subsequently, a carbon-carbon coupling reaction with a glutamate derivative afforded from commercial L-pyroglutamic acid should furnish compound **51**. Then, the introduction of the phthalimide moiety should give compound *trans*-**52**. The key step of this synthetic route was devoted to the obtention of the *cis* isomer of **GluS1**. As stated in the introduction of this chapter for previous phthalimide-stilbene dyads prepared in our group (see

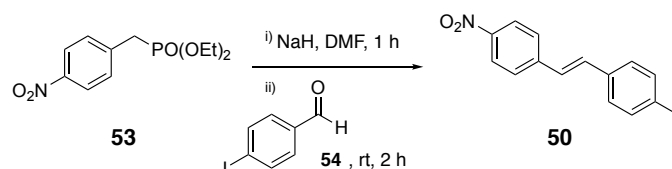
§ IV.1.3), *trans*-**GluS1** should only photoisomerise in non-polar media. Therefore, the photoisomerisation reaction to afford the *cis* configuration of the target ligand should take place before the removal of the protecting groups of the glutamate moiety, since this would make the final compound be soluble only in polar media. Hence, *trans*→*cis* photoisomerisation had to be performed in advance for lipophobic intermediate **52**. Finally, removal under acidic conditions of the protecting groups of the glutamate moiety should lead to target molecule *cis*-**GluS1** and its stereoisomer *trans*-**GluS1**.



Scheme IV-7. Synthetic pathway designed towards target NDCL *cis*-**GluS1** and its geometrical isomer *trans*-**GluS1**.

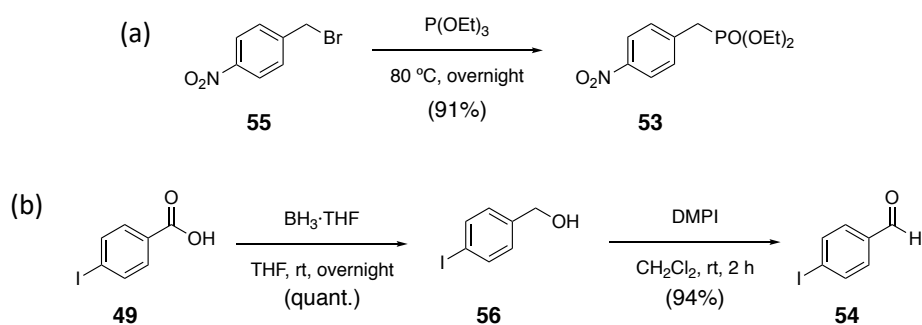
IV.2.2. SYNTHESIS OF STILBENE **50**

The first part of the synthetic route towards **GluS1** aimed at the preparation of stilbene **50**. Wu and co-workers had already reported the synthesis of this compound through a Horner-Wadsworth-Emmons reaction between phosphonate **53** and aldehyde **54** in 75% yield,⁴⁴ as depicted in Scheme IV-8. The Horner-Wadsworth-Emmons procedure is a well-known reaction between phosphonate carbanions and aldehydes to afford predominantly *trans*-alkenes.⁴⁵ We decided to use the same procedure to achieve *trans*-stilbene **50** and, thus, we first focused on the obtention of phosphonate **53** and aldehyde **54**.



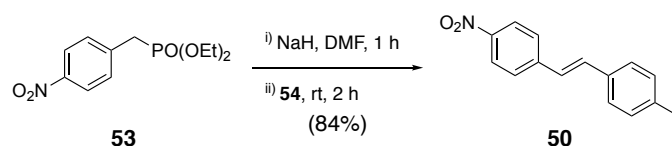
Scheme IV-8. Synthesis of stilbene **50** reported by Wu and co-workers.⁴⁴

Phosphonate **53** was readily prepared through an Arbuzov reaction with commercially available 4-nitrobenzyl bromide, **55**, and triethyl phosphite at 80 °C overnight.⁴⁶ The desired product was obtained in 91% yield. Aldehyde **54** was then easily prepared through the reduction of commercially available 4-iodobenzoic acid, **49**, with borane-tetrahydrofuran complex to furnish alcohol **56** in quantitative yield, followed by partial oxidation of this compound with Dess-Martin periodinane to give the desired aldehyde in 94% yield.



Scheme IV-9. Synthesis of (a) phosphonate **53** and (b) aldehyde **54**.

Finally, *trans*-stilbene **50** was synthesised following the methodology reported by Wu and co-workers. The synthesis commenced with the formation of the phosphonate-stabilised carbanion using sodium hydride as a base. Then, reaction with aldehyde **54** to *trans*-stilbene **50**, which could be readily isolated after its precipitation upon water addition. In this way, stilbene **50** was obtained in 84% yield and its ¹H NMR spectrum confirmed the selective obtention of its *trans* isomer.

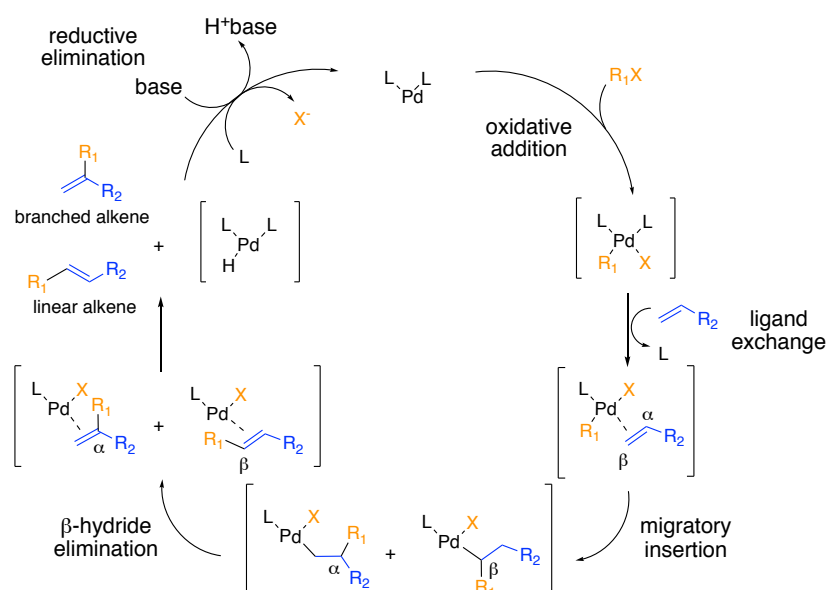


Scheme IV-10. Synthesis of stilbene **50** through a Horner-Wadsworth-Emmons reaction.

IV.2.3. INCORPORATION OF GLUTAMATE DERIVATIVE 29

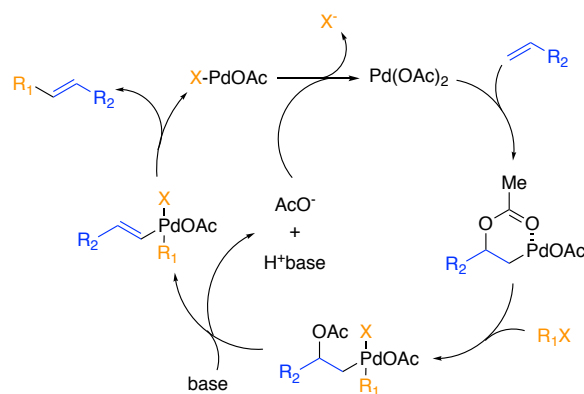
The subsequent step of our synthetic route was the incorporation of the glutamate moiety. A Heck-type carbon-carbon coupling reaction between stilbene **50** and allyl **29** was proposed in order to obtain target compound **51**. It must be noted that glutamate derivative **29** was synthesised from commercially available L-pyroglutamic acid as described in Chapter III (see § III.2.3.1).

The Heck reaction⁴⁷ is one of the main tools employed for C-C bond formation in organic synthesis. It is a palladium-catalysed coupling of olefins with aryl and vinyl halides that enables the obtention of C-C bonds at unfunctionalized olefinic carbons employing a wide variety of aryl and vinyl halide substrates. It is a robust process that tolerates almost any sensitive functionality. The mechanism of the Heck reaction has been widely studied^{48,49,50} (Scheme IV-11). It starts with the oxidative addition of the halide to a coordinatively unsaturated Pd⁰ complex followed by ligand exchange with the olefinic compound. Then, formation of a Pd-C single bond via migratory insertion takes place. Finally, β -hydride elimination affords the desired product and Pd^{II} hydride, which eventually regenerates the catalytically active Pd⁰ species upon base-induced reductive elimination. As shown in Scheme IV-11, this mechanism may lead to two different constitutional isomers depending on the regioselectivity of the migratory insertion step (linear vs branched alkenes); however, insertion in the β -position to yield the linear alkene is normally favoured due to steric effects. It must be noted that the *trans* isomer of product **51** was selectively obtained, which is one of the advantages of the Heck reaction.⁵¹

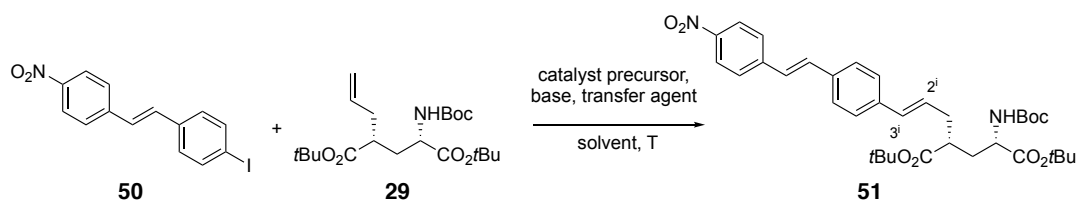


Scheme IV-11. General mechanism of the Heck reaction.⁵⁰

The performance of the Heck reaction depends on many factors, such as the catalyst, the solvent or the base employed. Thus, several conditions were screened to optimise the coupling reaction between stilbene **50** and allyl **29** (Table IV-1). In a first step, we tested the conditions previously used in our group for this type of reaction (entry 1): a tetracoordinated Pd^{II} complex (PdCl₂(PPh₃)₂) as a catalyst precursor, sodium carbonate as a base, anhydrous DMF as a solvent, tetrabutylammonium bromide as a transfer agent to enhance base solubility, and heating at 90 °C.⁵² However, these conditions achieved compound **51** in a low yield (6%). Therefore, two other different catalyst precursors were investigated (entries 2 and 3): a tetracoordinated Pd⁰ complex (Pd(PPh₃)₄) and a dicoordinated Pd^{II} complex (Pd(OAc)₂) in combination with PPh₃, while the remaining conditions were kept constant. Eventually, palladium(II) acetate was found to be the best catalyst precursor, affording coupling product **51** albeit in 30% yield. To enhance the efficiency of the reaction, Pd(OAc)₂ was tested together with triethanolamine, which played the triple role of reductive ligand, base and solvent⁵³ (entries 4 and 5). However, lower yields were obtained regardless of the reaction temperature. For this reason, a different set of reaction conditions were assayed that had been reported to be especially suitable for the coupling between aryl halides and styrene derivatives to generate the corresponding *trans*-stilbenes: Pd(OAc)₂ as a catalyst, K₃PO₄ as a base, dimethylacetamide (DMAc) as a solvent, heating at 140 °C and in the absence of auxiliary ligand (entry 6).⁵⁴ Indeed, rather good results were obtained in this case and target compound **51** was furnished in 78% yield. It must be noted that, under these reaction conditions, the classical Pd⁰-Pd^{II} catalytic cycle of the Heck reaction shown in Scheme IV-11 is highly unlikely to occur and, instead, an alternative Pd^{II}-Pd^{IV} catalytic cycle has been proposed (Scheme IV-12).⁵⁴ According to this mechanism, the reaction between the olefinic compound and Pd(OAc)₂ forms the initial transient palladacycle, which undergoes an oxidative addition of the halide to form the Pd^{IV} species. Afterwards, base-promoted elimination of the acetate ion and subsequent formation of the Pd^{II} species releases the coupling product. Finally, the acetate ion regenerates the initial Pd(OAc)₂.



Scheme IV-12. Proposed mechanism for the Heck reaction catalysed by Pd(OAc)₂.⁵⁴

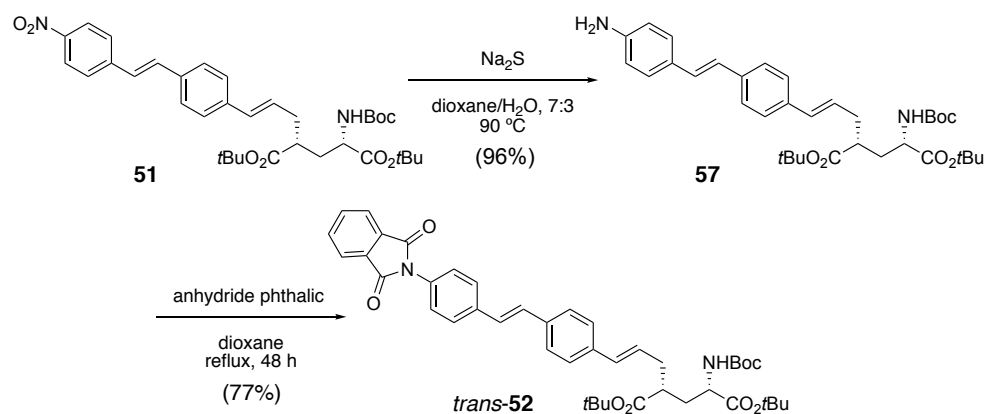
Table IV-1. Heck reaction conditions assayed for the preparation of **51**.

	Catalyst precursor	Ligand	Base	Solvent	Transfer agent	T (°C)	Yield
1	PdCl ₂ (PPh ₃) ₂	-	Na ₂ CO ₃	DMF	TBAB	90	6%
2	Pd(PPh ₃) ₄	-	Na ₂ CO ₃	DMF	TBAB	90	-
3	Pd(OAc) ₂	PPh ₃	Na ₂ CO ₃	DMF	TBAB	90	30%
4	Pd(OAc) ₂		Triethanolamine		-	100	20%
5	Pd(OAc) ₂		Triethanolamine		-	85	15%
6	Pd(OAc) ₂	-	K ₃ PO ₄	DMAc	-	140	78%

Compound **51** was unambiguously identified by ¹H and ¹³C NMR spectroscopy and HR-MS. Thus, new signals corresponding to the glutamate fragment introduced were observed in the spectra, while new ¹H NMR doublet at 6.43 ppm and multiplet at 6.15 ppm related to the protons of the C=C double bond created (H-3ⁱ and H-2ⁱ, respectively) appeared. In addition, the coupling constant of the ¹H NMR doublet corresponding to H-3ⁱ ($J_{3^i,2^i} = 15.8$ Hz) confirmed the obtention of the *trans* isomer.

IV.2.4. INCORPORATION OF THE PHTHALIMIDE FRAGMENT

Once the glutamate moiety was appended to the stilbene core, we then had to introduce the phthalimide fragment. To this end, we first reduced the nitro group of compound **51** with sodium sulfide to afford amine **57** in almost quantitative yield. ¹H NMR spectrum of the product showed downfield shifts of the protons of the aromatic ring bearing the amino group, thus confirming successful reduction of the substrate. Afterwards, amine **57** and anhydride phthalic were refluxed in dioxane for 48 h to give *trans*-**52** in 77% yield through a condensation reaction. New signals corresponding to the phthalimide moiety introduced were observed in the ¹H and ¹³C NMR spectra.

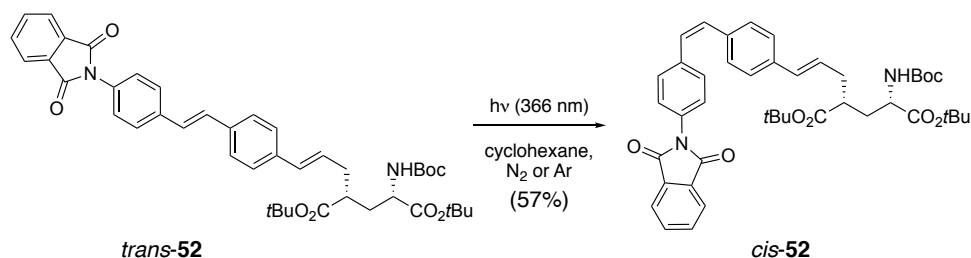


Scheme IV-13. Introduction of phthalimide to stilbene photochrome **51**.

IV.2.5. PHOTOISOMERISATION AND OBTENTION OF TARGET *cis*- AND *trans*-GluS1

As previously stated, the photoisomerisation reaction is the key step of this synthetic pathway to obtain **GluS1**. Based on previous studies in our group, the *trans* isomer of stilbene-phthalimide dyad should only isomerise in non-polar media, in which the formation of the charged species resulting from photoinduced electron transfer (i.e. stilbene radical cation and phthalimide radical anion) is known to be disfavoured.³⁸ Since *trans*-**GluS1** should only be soluble in polar media due to the presence of unprotected amino and carboxylic acid groups, the photoisomerisation reaction had to be conducted before the removal of the protecting groups of the glutamate moiety; i.e. for *trans*-**52**. In view of this, *trans*-**52** was irradiated at $\lambda_{\text{exc}} = 366$ nm in cyclohexane until a photostationary state was reached and no change was observed in the ^1H NMR spectra of the illuminated sample. Several aspects must be noted about the experimental conditions that were applied to perform the photoisomerisation reaction: (i) it was carried out under inert atmosphere to minimise the irreversible formation of the phenanthrene photodegradation product (see Scheme IV-2); (ii) *trans*-**52** was not excited at its absorption spectral maximum ($\lambda_{\text{abs,max}} = 333$ nm in cyclohexane) but in the long-wavelength fall of its $\pi \rightarrow \pi^*$ absorption band, with which we aimed to enhance the difference in absorptivity relative to the *cis* isomer and, consequently, further displace the PSS; and (iii) although the solubility of *trans*-**52** was found to be moderate in cyclohexane, this solvent was chosen because of its optical transparency at the irradiation wavelength and very low dielectric constant ($\epsilon_s = 2.02$), which resulted in better results for the photoisomerisation process than when other good solvents were used. In this way, a *cis*-enriched mixture was obtained under irradiation ($\% \text{PSS}^{\text{cis-52}} = 67\%$), which was then separated using flash column chromatography to isolate the desired product

cis-**52** in 57% yield. A clear downfield shift of some of the protons of the stilbene core in the ^1H NMR spectrum confirmed the obtention of the *cis* configuration. Particularly, a notorious difference could be observed in the protons of the stilbene C=C double bond, which for this compound appeared as two doublets at 6.62 and 6.57 ppm with $J_{cis} = 12.0$ Hz.

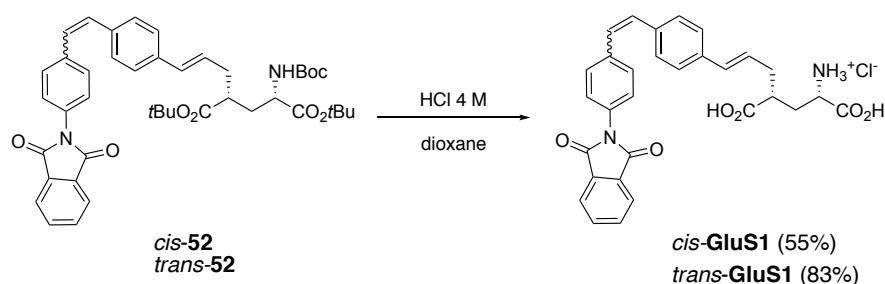


Scheme IV-14. Photoisomerisation of *trans*-**52** to obtain *cis*-**52**.

Once obtained and separated the *trans* and *cis* isomers of **52**, the removal of their glutamate moiety protecting groups under acidic conditions had to take place to culminate the synthetic route. The first conditions tested were those employed in the last step of the synthetic sequence of **MAG** derivatives (see § III.2.4). However, when treating both *cis*- and *trans*-**52** with trifluoroacetic acid in CH₂Cl₂, the ^1H NMR signals of the protons corresponding to the C=C double bond linking the stilbene and glutamate units disappeared, probably due to the nucleophilic addition of TFA.⁵⁵ Hence, we decided to use a non-nucleophilic acid instead. Accordingly, *cis*- and *trans*-**52** were treated with HCl in diethyl ether. Although no degradation of the initial substrate was observed, full removal of the *tert*-butyl groups was not achieved. Then, HCl in dioxane was tested, which turned to be most the appropriate conditions for the deprotection step.

Therefore, *cis*-**52** was treated with HCl 4 M in dioxane and stirred for 24 h (Scheme IV-15). Purification with reverse phase flash column chromatography furnished target NDCL *cis*-**GluS1** in 55% yield. Its ^1H NMR spectrum showed the disappearance of the characteristic *tert*-butyl signals at 1.44 ppm and carbamate signals at 5.00 ppm. Moreover, its ^{13}C NMR spectrum also confirmed the removal of the protecting groups by the disappearance of characteristic carbamate signals at 155.3 ppm and *tert*-butyl signals around 82-79 ppm and at 28 ppm.

Trans-**52** was also treated with HCl 4 M in dioxane for 40 h to achieve glutamate deprotection (Scheme IV-15). In this case, however, the product obtained precipitated in the reaction medium and could be easily isolated, thus affording *trans*-**GluS1** in 83% yield. The ^1H NMR and ^{13}C NMR spectra of this compound also showed the disappearance of the characteristic *tert*-butyl signals.

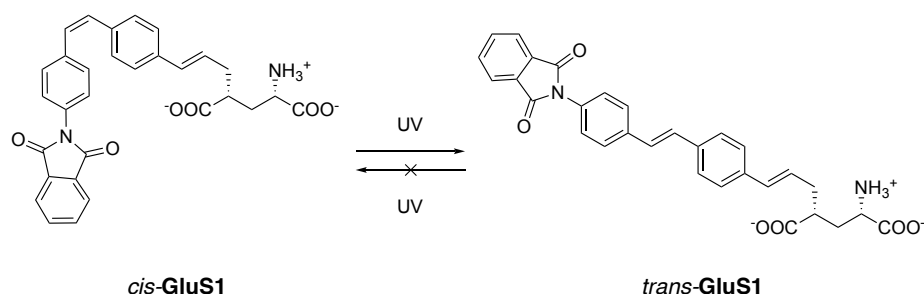


Scheme IV-15. Removal of the protecting groups of the glutamate moiety under acidic conditions to obtain target NDCL *cis-GluS1* and *trans-GluS1*.

To sum up, the first example of NDCL, *cis-GluS1* was afforded in 14% overall yield from commercially available 4-iodobenzoic acid, **49**, through an 8-step synthetic sequence where the glutamate moiety and the phthalimide were sequentially introduced to the stilbene core. Its geometrical isomer *trans-GluS1* was also prepared in 7 steps through the same synthetic pathway in 38% overall yield.

IV.2.6. PHOTOCHEMICAL CHARACTERISATION OF **GluS1**

After synthesising NDCL *cis-GluS1* and its geometrical *trans* isomer, their photochemical properties were investigated in solution at ambient atmosphere. According to our design principles, *cis-GluS1* should afford *trans-GluS1* quantitatively upon irreversible PET-induced *cis*→*trans* photoisomerisation upon direct excitation of its stilbene unit in polar solvents. By contrast, *trans-GluS1* photoinduced isomerisation should be inhibited in such media and no changes should be observed upon irradiation (Scheme IV-16). In addition, both isomers should be thermally stable at rt, and therefore, no *cis*→*trans* isomerisation should occur in the absence of light.



Scheme IV-16. Photoinduced *cis*→*trans* isomerisation of novel NDCL *cis-GluS1* upon stilbene excitation with UV light. According to our design principles, the *trans*→*cis* photoisomerisation of this compound should be inhibited in polar media.

Figure IV-6 shows the absorption spectra of *cis*- and *trans*-**GluS1** in MeOH. Both compounds present typical absorption features of stilbene-type switches. On one hand, *trans*-**GluS1** shows a very intense $\pi \rightarrow \pi^*$ absorption band in the UV region of the spectrum ($\lambda_{\text{abs,max}} = 335$ nm). On the other hand, *cis*-**GluS1** absorption spectrum displays a spectral blue shift ($\lambda_{\text{abs,max}} = 304$ nm) and an important decrease in the intensity of the $\pi \rightarrow \pi^*$ band, which is related to the loss of planarity of the stilbene moiety. Importantly, no changes in these spectral properties were observed in time for both solution and solid-state samples of *cis*- and *trans*-**GluS1**. This demonstrates the thermal stability of the two isomers of the compound.

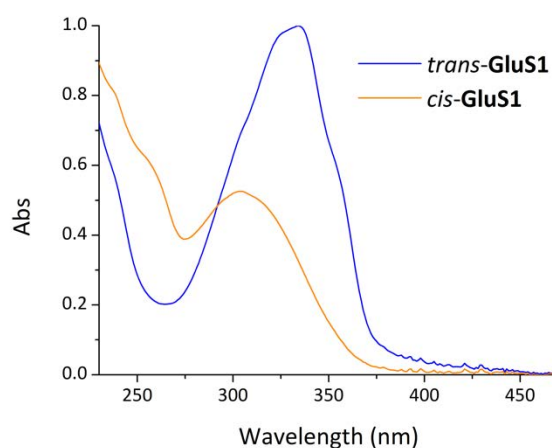


Figure IV-6. Absorption spectra of *cis*-**GluS1** and *trans*-**GluS1** in MeOH.

Next, we investigated the photoinduced *cis-trans* isomerisation of **GluS1** upon irradiation of its $\pi \rightarrow \pi^*$ absorption band. First, these studies were conducted in MeOH, where both isomers of the compound were irradiated with UV light at $\lambda_{\text{exc}} = 355$ nm. When irradiating *cis*-**GluS1**, spectral changes accounting for *cis* \rightarrow *trans* photoisomerisation were observed: a red shift of the $\pi \rightarrow \pi^*$ absorption band and a sharp increase of its intensity (Figure IV-7a). Importantly, irradiation of *cis*-**GluS1** led to *trans*-**GluS1** in a quantitative way: the absorption spectrum of the $\text{PSS}_{\text{cis-trans}}$ reached perfectly matched that of *trans*-**GluS1** and, when monitoring this process in CDCl_3 , complete conversion of one isomer into the other was formed. On the contrary, when irradiating a solution of *trans*-**GluS1** in MeOH no change in the absorption spectra could be observed over time (Figure IV-7b). These results are in agreement with the photochemical behaviour expected for **GluS1** in polar media, the excited state dynamics must be controlled by PET between the stilbene and phthalimide units for both isomers of this compound which should result in quantitative *cis* \rightarrow *trans* photoconversion and inhibition of *trans* \rightarrow *cis* photoisomerisation.

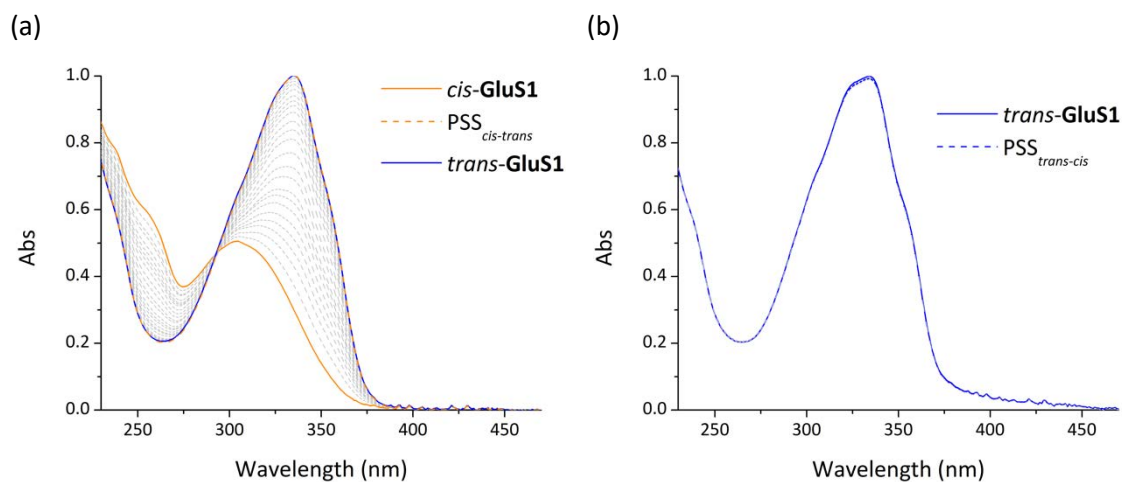


Figure IV-7. (a) Changes registered in the absorption spectra of *cis*-GluS1 in MeOH upon irradiation at $\lambda_{\text{exc}} = 355$ nm until a photostationary state (PSS_{*cis-trans*}) was achieved. For sake of comparison, the absorption spectrum of *trans*-GluS1 is also shown. (b) Absorption spectra of *trans*-GluS1 upon irradiation at $\lambda_{\text{exc}} = 355$ nm, which suffered no changes in time.

Afterwards, we decided to test the photochemical behaviour of **GluS1** in aqueous media, where strikingly different results were obtained with respect to MeOH solution (Figure IV-8). Although *cis*-GluS1 seemed to isomerise to the *trans* compound at short irradiation times, a fast decrease and broadening of the intensity of the $\pi \rightarrow \pi^*$ absorption band was subsequently observed. Interestingly, the same behaviour was found when directly irradiating *trans*-GluS1, and after testing several solvent mixtures and temperatures. In addition, although this phenomenon could be ascribed to very low solubility of *trans*-GluS1 in aqueous media, it was not possible to recover the initial absorption spectrum after addition of good solvents to the irradiated sample. This observation pointed towards the formation of an irreversible degradation species upon irradiation of *trans*-GluS1 in aqueous media. According to precedents in the literature,^{56,57} this could hardly be ascribed to phenanthrene generation, since this photodegradation product is formed by electrocyclisation reaction of *cis*-stilbenes (and not *trans*-stilbenes) and must produce an intense colouration of the sample (which was not observed in our case). A more plausible explanation would be the dimerisation of *trans*-GluS1 via a [2+2] photocycloaddition reaction, a low probability process in stilbenes that is however favoured in aqueous media due to intermolecular aggregation via hydrophobic interactions (Scheme IV-17).^{56,57} To corroborate this hypothesis, new irradiation measurements were performed where surfactants were added to prevent molecular aggregation in aqueous media, which allowed recovering the regular photochemical behaviour registered for *cis*-GluS1 and *trans*-GluS1 in MeOH. Unfortunately, the amount of surfactant required to avoid photodimerisation was too high to be used in biological

experiments and thus, **GluS1** was not a good candidate to test on cells. Therefore, we considered synthesising a new **GluS** derivative that displayed higher solubility in water.

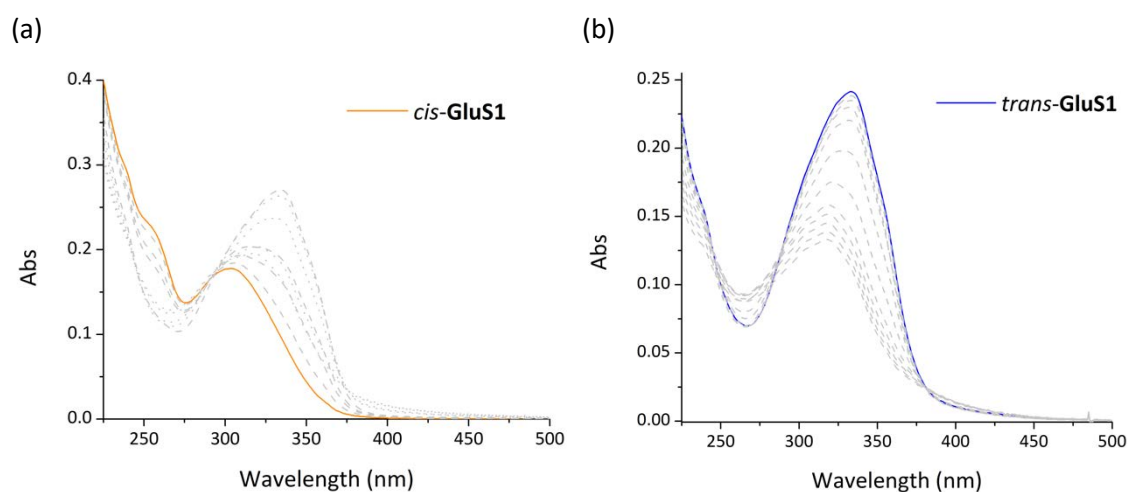
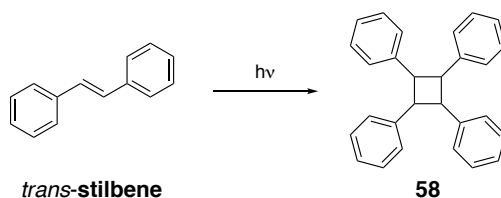


Figure IV-8. (a) Changes registered in the absorption spectra of *cis*-**GluS1** in PBS:MeOH upon irradiation at $\lambda_{\text{exc}} = 355$ nm. At short irradiation times, the photoisomerisation seems to proceed as in MeOH (dashed grey lines); however, a fast decrease and broadening of the intensity of the absorption band is observed at longer irradiation times (pointed grey lines). (b) Changes registered in the absorption spectra of *trans*-**GluS1** in PBS:MeOH upon irradiation at $\lambda_{\text{exc}} = 355$ nm. A clear decrease and broadening of the intensity of the absorption band is observed, which indicates photodegradation.



Scheme IV-17. Photodimerisation product of *trans*-stilbene.^{56,57}

IV.3. SYNTHESIS AND PHOTOCHEMICAL CHARACTERISATION OF **GluS2**

IV.3.1. SYNTHESIS OF **GluS2**

In order to avoid **GluS** photodimerisation due to low solubility, we devised the incorporation of a carboxylic group in the phthalimide aromatic ring of **GluS1**, which should be ionised at physiological pH and, therefore, enhance its solubility in aqueous media. This led to the design of new NDCL **GluS2** (Figure IV-9).

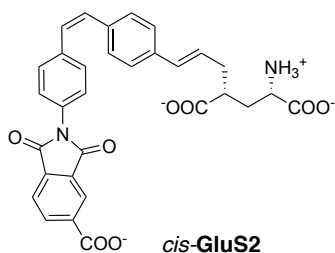
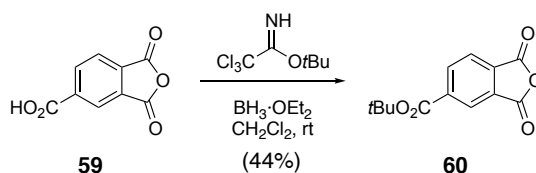


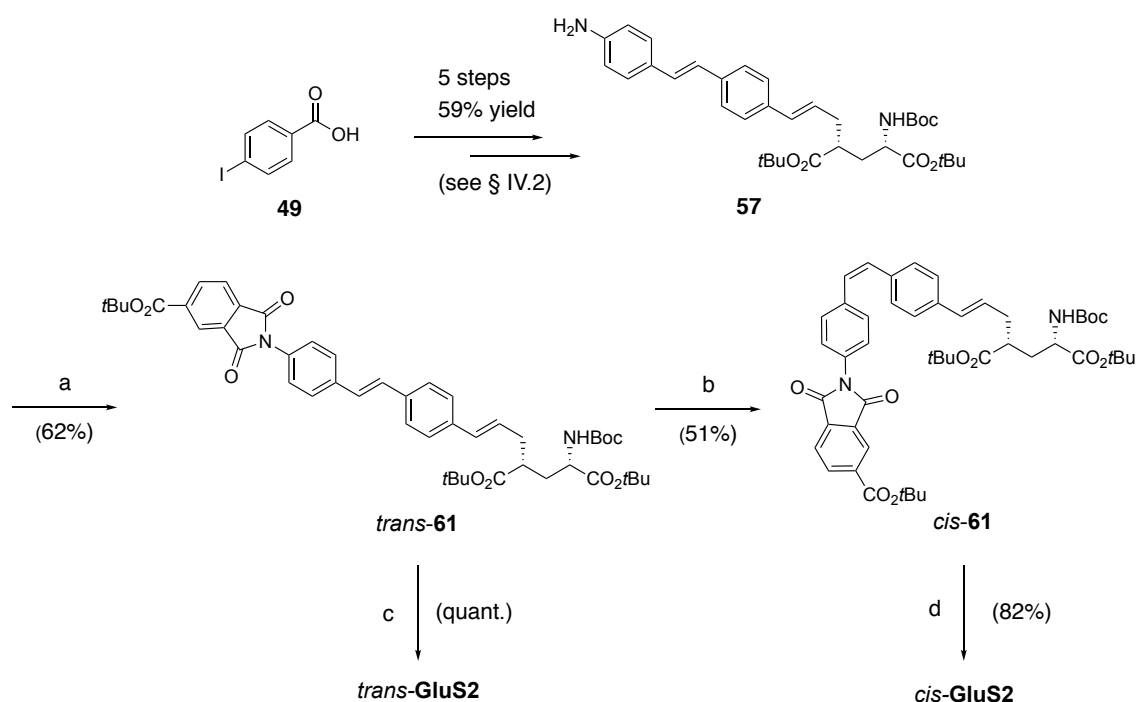
Figure IV-9. Structure of new potential NDCL **GluS2**, a modification of **GluS1** intended to show higher solubility in aqueous media and avoid photodimerisation.

The synthetic pathway devised for **GluS2** was inspired on that employed to achieve **GluS1**, though phthalic anhydride derivative **59** bearing a carboxylic group had to be used in this case to obtain the desired phthalimide fragment. In addition, this commercially available compound had to be previously protected as *tert*-butyl ester **60** before being introduced into the synthetic sequence (Scheme IV-18).



Scheme IV-18. Synthesis of protected phthalic anhydride derivative **60**.

Scheme IV-19 illustrates the synthetic route followed for the obtention of *cis*- and *trans*-**GluS2**. First, common intermediate **57** was synthesised as previously described (see § IV.2). This compound was reacted with anhydride **60** in dioxane under reflux conditions to give *trans*-**61** in 62% yield. Subsequently, *trans*-**61** was photoisomerised to *cis*-**61** in cyclohexane affording the desired *cis* isomer in 51% yield. Finally, both **61** isomers were treated with HCl 4 M in dioxane to furnish target compounds *trans*- and *cis*-**GluS2** in quantitative and 82% yield, respectively. Both isomers were unambiguously identified by ^1H and ^{13}C NMR spectroscopy and HR-MS. Their ^1H and ^{13}C spectra were very similar to the respective isomers of **GluS1**, although clear desymmetrisation of the phthalimide unit signals due to the presence of the carboxylic acid substituent could be observed. Compound *cis*-**GluS2** was prepared in 8 steps in 15% yield and *trans*-**GluS2** was afforded in 7 steps in 37% yield.



Reagents and conditions: (a) **60**, dioxane, reflux, 48 h; (b) hv (366 nm), cyclohexane; (c) and (d) HCl 4 M in dioxane, dioxane.

Scheme IV-19. Synthetic pathway followed towards target NDCL *cis*-GluS2 and its geometrical isomer *trans*-GluS2.

IV.3.2. PHOTOCHEMICAL CHARACTERISATION OF GluS2

Figure IV-10 shows the absorption spectra of *cis*-GluS2 and *trans*-GluS2 in aqueous media (PBS:MeOH 2:1), where very similar spectral features to those of GluS1 were found: a large $\pi \rightarrow \pi^*$ absorption band for the *trans* isomer ($\lambda_{\text{abs,max}} = 334$ nm) that blue-shifts and decreases in intensity for the *cis* state ($\lambda_{\text{abs,max}} = 304$ nm). Moreover, no changes were observed either in the absorption spectra of both isomers of GluS2 over time, thus confirming their thermal stability. Finally, when monitoring the irradiation of aqueous solutions of this compound with UV light, much better results were obtained than for GluS1. As illustrated in Figure IV-10 neither photodegradation nor photoisomerisation was observed for *trans*-GluS2 in PBS:MeOH 2:1, while selective and quantitative *cis* \rightarrow *trans* photoconversion was found for *cis*-GluS2. Therefore, GluS2 showed the photochemical behaviour devised for NDCLs based in stilbene-electron acceptor dyads even in aqueous media.

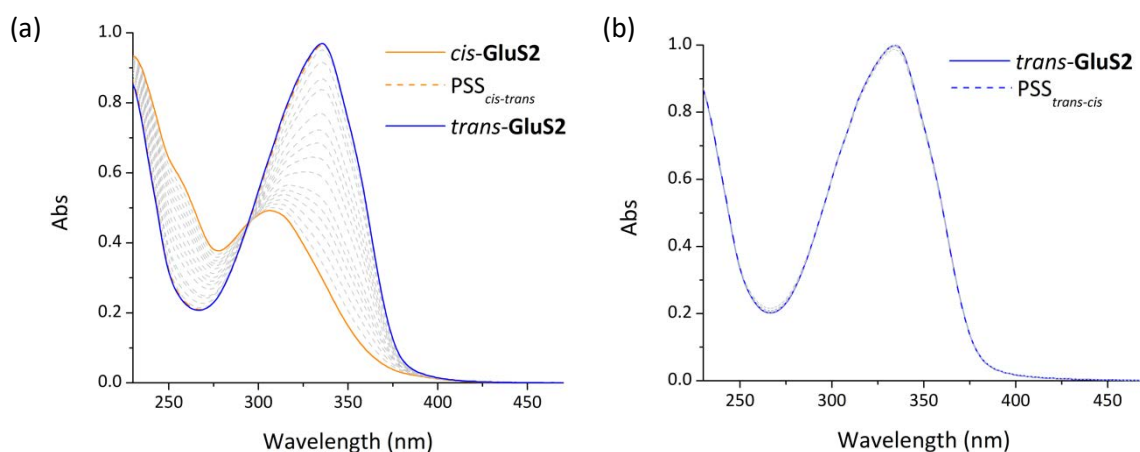


Figure IV-10. (a) Changes in the absorption spectra of *cis*-**GluS2** upon irradiation at $\lambda_{\text{exc}} = 355$ nm in PBS:MeOH 2:1. Clear *cis*→*trans* photoisomerisation occurred, leading quantitatively to the *trans* isomer. (b) Absorption spectra of *trans*-**GluS2** upon irradiation of the *trans* isomer at $\lambda_{\text{exc}} = 355$ nm in PBS:MeOH 2:1. Neither *trans*→*cis* photoisomerisation nor photodegradation can be observed.

To further investigate *cis*→*trans* photoconversion of **GluS2**, two additional experiments were performed. First, the *cis*→*trans* photoisomerisation quantum yield of **GluS2** was determined in PBS:MeOH 2:1 ($\Phi_{\text{cis} \rightarrow \text{trans}} = 0.1$), which was found to be similar to that reported for commonly used caged glutamates, such as **CNB-Glu** ($\Phi_{\text{uncaging}} = 0.14$)⁵ or **MNI-Glu** ($\Phi_{\text{uncaging}} = 0.085$).² Second, UV light-induced isomerisation of *cis*-**GluS2** was monitored by ¹H NMR, a measurement that was conducted in DMSO-*d*₆ because of the higher concentration needed. As shown in Figure IV-11, complete conversion of *cis*-**GluS2** ¹H NMR signals into *trans*-**GluS2** ¹H NMR resonances were observed, thus confirming the large efficiency of the photoconversion process.

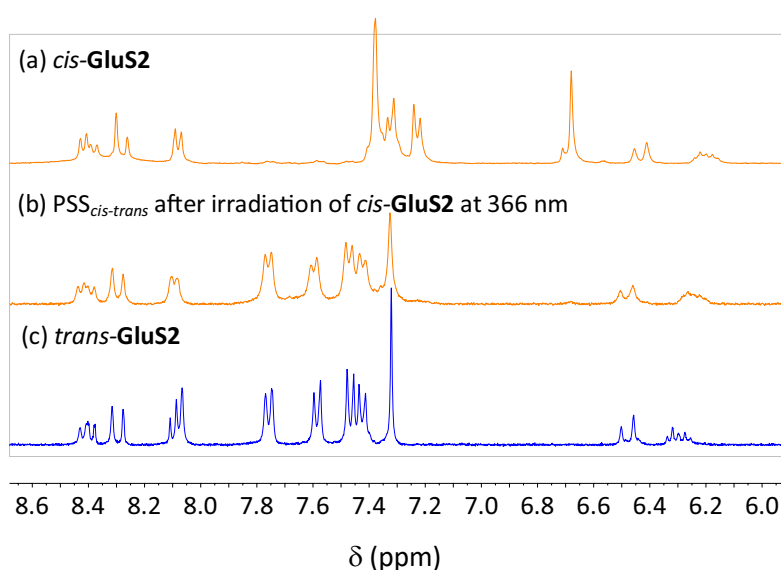


Figure IV-11. Low-field region of the ¹H NMR spectra (400 MHz, DMSO-*d*₆) of (a) *cis*-**GluS2**; (b) the PSS_{*cis-trans*} obtained after irradiation of *cis*-**GluS2** at $\lambda_{\text{exc}} = 366$ nm; and (c) *trans*-**GluS2**.

IV.4. EVALUATION OF THE LIGHT-INDUCED BIOLOGICAL ACTIVITY OF NDCLs

GluS2

In view of the optimal photochemical behaviour established for **GluS2** in solution, we decided to explore its ability to photocontrol iGluR channels in living cells under one-photon stimulation. These experiments were conducted in collaboration with Aida Garrido-Charles in the laboratories of the research group of Prof. Pau Gorostiza at the *Institut de Bioenginyeria de Catalunya* (IBEC). The experiments were performed on human embryonic kidney 293 cells (HEK293) overexpressing GluK2 receptors. In order to record the response of these receptors to our photoresponsive ligand and measure the flux of ions from the extra- to the intracellular medium upon channel activation, whole-cell patch clamp technique (see § III.4) was used.

The experiments carried out consisted in illuminating GluK2-expressing cells administrated with either the *cis* or *trans* isomer of the ligand. As illustrated in Figure IV-5b, extended *trans*-**GluS** should interact more efficiently with the ligand-binding domain of GluK2, thus evoking larger inward currents than its folded *cis* isomer. Upon illumination with UV light, quantitative PET-induced photoisomerisation of *cis*-**GluS** should occur, which should lead to an increase in the ligand-receptor binding site affinity and subsequently trigger an increase in the biological response. By contrast, no changes should be observed when irradiating *trans*-**GluS2**. It must be noted, that in order to determine the cell maximum response and demonstrate no inhibition of the endogenous behaviour of the receptor caused by our ligand, cells were administered with 300 μ M solution of free glutamate either at the beginning or at the end of the recording. Moreover, they were previously incubated with Concanavalin A to inhibit endogenous desensitisation of the receptors after ligand-binding site interaction and so to obtain larger responses.

Despite the inconvenient photochemical behaviour in aqueous media observed for **GluS1**, we performed a first set of experiments with this compound by treating GluK2-expressing HEK293 cells with 30 μ M solution of both **GluS1** isomers. Clear inward currents indicating an efficient opening of the channels and, thus, an influx of cations could be observed for cells administered with *trans*-**GluS1** (Figure IV-12a). By contrast, apparently no electrophysiological difference was triggered upon perfusion of a solution of the same concentration of *cis*-**GluS1** (Figure IV-12b). These results are in agreement with the expected behaviour for this ligand: extended *trans* state displays a more efficient interaction with GluK2 binding site than its bent *cis* geometrical isomer.

Unfortunately, no changes in current could be evoked upon irradiation of *cis*-**GluS1** with $\lambda_{\text{exc}} = 350$ nm, which confirmed the inability of **GluS1** to photoisomerise in polar medium.

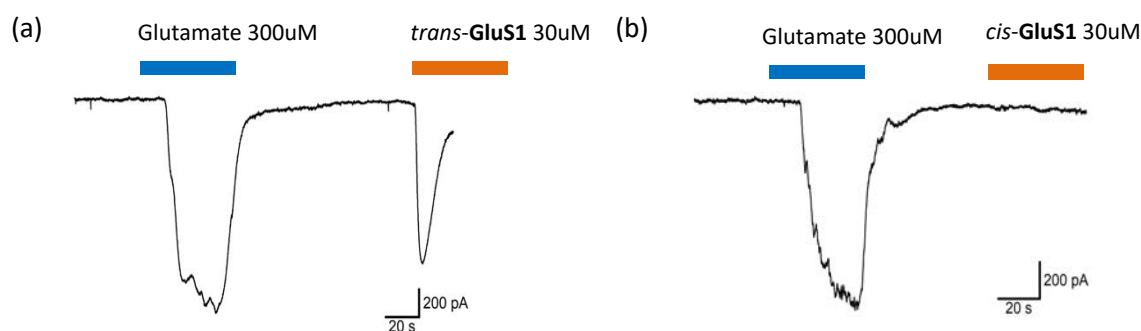


Figure IV-12. (a) Inward currents measured for HEK293 cells expressing GluK2 perfused with (a) a 300 μM solution of glutamate and 30 μM solution of *trans*-**GluS1** and (b) a 300 μM solution of glutamate and 30 μM solution of *cis*-**GluS1**. No current change can be observed upon administration of *cis*-**GluS1**.

The same experiments were then conducted with 3 μM solutions of both isomers of **GluS2**. As expected from **GluS1** results, large electrophysiological responses could be recorded upon administration of *trans*-**GluS2** (Figure IV-13a), while almost no inward currents could be observed when perfusing the cells with *cis*-**GluS2** (Figure IV-13b). However, when cells containing *cis*-**GluS2** were illuminated at $\lambda_{\text{exc}} = 350$ nm, a sharp increase in the inward current could be observed (Figure IV-13c), which confirmed the highly efficient photoconversion to the more biologically active *trans* isomer that was determined in solution. Finally, cells treated with *trans*-**GluS2** were exposed to several pulses of $\lambda_{\text{exc}} = 350$ nm and no change in the electrophysiological response was recorded (Figure IV-13d). This is in agreement with the inhibition of *trans* \rightarrow *cis* photoisomerisation in aqueous media determined by the photochemical studies in solution. Importantly, **GluS2** was found to enable high photoinduced modulation of GluK2 channels and maximal electrophysiological signals could be recorded for a 3 μM solution of *trans*-**GluS2** that were around 65% of those triggered by a 300 μM solution of endogenous free glutamate.

The results obtained for the experiments conducted in HEK293 cells expressing GluK2 confirm that **GluS2** exhibits the photochemical behaviour devised for NDCLs based in stilbene-electron acceptor dyads in biological media (i.e. quantitative *cis* \rightarrow *trans* PET-induced photoconversion and inhibited *trans* \rightarrow *cis* photoisomerisation) and enables a high modulation of GluK2 activity upon simple photoconversion from its *cis* to its *trans* isomer.

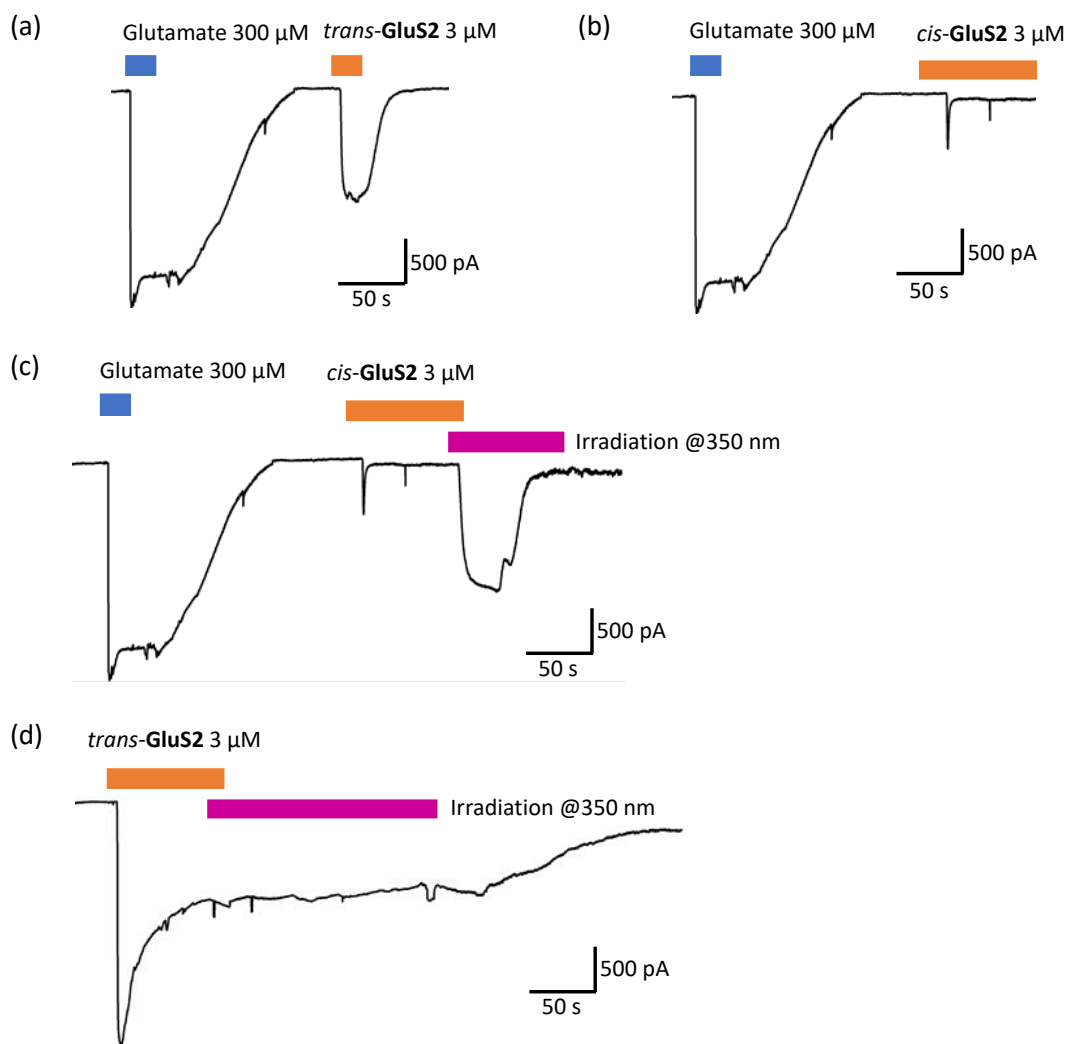


Figure IV-13. (a) Inward currents measured for HEK293 cells expressing GluK2 perfused with (a) a 300 μM solution of glutamate and 3 μM solution of *trans*-GluS2; (b) a 300 μM solution of glutamate and 3 μM solution of *cis*-GluS2; (c) a 300 μM solution of glutamate and 3 μM solution of *trans*-GluS2.

IV.5. CONCLUSIONS

In this chapter a new photopharmacological strategy was explored to tackle one of the main drawbacks of caged ligands: the generation of by-products upon ligand uncaging. This led us to develop **GluS1** and **GluS2**, the first examples of non-destructive caged ligands (NDCLs), which were designed to target ionotropic glutamate receptors GluK1 and GluK2. To this end, we sought inspiration in the structure of the well-known PCL of these receptors **GluAzo**, and the particular photochemical properties of stilbene-phthalimide dyads, which undergo unidirectional and quantitative *cis*→*trans* photoisomerisation in polar solvents. (Figure IV-14).

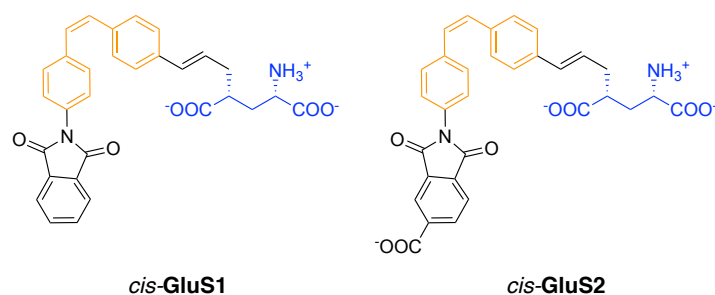


Figure IV-14. Structure of the new NDCLs **GluS1** and **GluS2** developed in this work, which are composed of a phthalimide-stilbene dyad tethered through a vinyl linker to a glutamate unit.

The main conclusions obtained from the studies conducted on **GluS1** and **GluS2** are:

- The linear synthetic strategy designed to afford **GluS1** and **GluS2** proved to be robust and reproducible. Compounds *cis*-**GluS1** and *cis*-**GluS2** were synthesised in 8 steps in 14% and 15% overall yield, respectively, and their geometrical isomers *trans*-**GluS1** and *trans*-**GluS2** were afforded in 7 steps in 38% and 37% overall yield, respectively.
- The photochemical properties of **GluS1** and **GluS2** have been investigated and it has been determined that in polar media photoinduced electrochemical *cis*→*trans* isomerisation takes place, which completely inhibits regular direct photoisomerisation. Consequently, these compounds exhibit (i) quantitative *cis*→*trans* PET-induced photoconversion under UV light stimulation; and (ii) prevented *trans*→*cis* photoisomerisation. However, **GluS1** low solubility in aqueous media led to photodegradation reactions due to intermolecular aggregation via hydrophobic interactions, which impeded *cis*→*trans* photoconversion in these conditions and, thus, was not suitable for biological purposes.
- Anhydride **60** was readily prepared in one step and 44% yield from commercially available anhydride **59** and was successfully incorporated to **57** to afford the desired phthalimide bearing a carboxylic acid residue present in **GluS2**. Introduction of this carboxylic acid residue in the phthalimide moiety of **GluS** compounds did not modify their photochemical properties and provided **GluS2** with higher solubility in water, thus preventing undesired photodimerisation reactions and making this compound suitable for biological applications.
- **GluS2** enables the successful modulation of the activity of GluK2 with UV light through irreversible *cis*→*trans* photoconversion, in a similar fashion than CLs but without the generation of by-products.

In summary, this chapter reports the first example of a novel photopharmacology strategy based on non-destructive caged ligands. As a proof of concept, we prepared **GluS** derivatives, whose operation relies on the particular photochemical behaviour of stilbene-electron acceptor dyads. Interestingly, these novel compounds could be further modified to incorporate an electron acceptor at the phthalimide position which enables photosensitising the stilbene core isomerisation with visible light or even with 2P-absorption of NIR light.

IV.6. REFERENCES

- (1) Kaplan, J. H.; Forbush, B.; Hoffman, J. F. *Biochemistry* **1978**, *17*, 1929-1935.
- (2) Ellis-Davies, G. C. R. *Nat. Methods*. **2007**, *4*, 619-628.
- (3) Young, D. D.; Deiters, A. *Org. Biomol. Chem.* **2007**, *5*, 999–1005
- (4) Wilcox, M.; Viola, R. W.; Johnson, K. W.; Billington, A. P.; Carpenter, B. K.; McCray, J. A.; Guzikowski, A. P.; Hess, G. P. *J. Org. Chem.* **1990**, *55*, 1585-1589.
- (5) Wiebolt, R.; Gee, K. R.; Niu, Li.; Ramesh, D.; Carpenter, B. K.; Hess, G. P. *Proc. Natl. Acad. Sci. USA* **1994**, *91*, 8752-8756.
- (6) Niu, L.; Gee, K. R.; Schaper, K.; Hess, G. P. *Biochemistry* **1996**, *35*, 2030-2036.
- (7) Shepherd, G. M. *Cold Spring Harb Protoc.* **2012**, *9*, 998-1004.
- (8) Ellis-Davies, G. C. R. *Caged Glutamate for Use in the CNS*; New Encyclopedia of Neuroscience. Elsevier: Oxford, **2009**; pp 639-645.
- (9) Callaway, E. M.; Katz, L. C. *Proc. Natl. Acad. Sci. USA* **1993**, *90*, 7661-7665.
- (10) Papagiakoumou, E.; Bègue, A.; Leshem, B.; Schwartz, O.; Stell, B. M.; Bradley, J.; Oron, D.; Emiliani, V. *Nat. Photon.* **2013**, *7*, 274-278.
- (11) Denk, W.; Strickler, J. H.; Webb, W. W. *Science* **1990**, *248*, 73-76.
- (12) Matsuzaki, M.; Ellis-Davies, G. C. R.; Nemoto, T.; Miyashita, Y.; Iino, M.; Kasai, H. *Nat. Neurosci.* **2001**, *4*, 1086-1092.
- (13) Nikolenko, V.; Poskanzer, K. E.; Yuste, R. *Nat. Methods* **2007**, *4*, 943-950.

- (14) Noguchi, J.; Nagaoka, A.; Watanabe, S.; Ellis-Davies, G. C. R.; Kitamura, K.; Kano, M.; Matsuzaki, M.; Kasai, H. *J. Physiol.* **2011**, *589*, 2447-2457.
- (15) Fedoryak, O. D.; Sul, J. Y.; Haydon, P. G.; Ellis-Davies, G. C. R. *Chem. Commun.* **2005**, *29*, 3664-3666.
- (16) Ellis-Davies, G. C. R.; Matsuzaki, M.; Paukert, M.; Kasai, H.; Bergles, D. E. *J. Neurosci.* **2007**, *27*, 6601-6604.
- (17) Fino, E.; Araya, R.; Peterka, D. S.; Salierno, M.; Etchenique, R.; Yuste, R. *Front. Neural Circuits* **2009**, *3*, 1-9.
- (18) Fino, E.; Yuste, R. *Neuron* **2011**, *69*, 1188-1203.
- (19) Olson, J. P.; Kwon, H. B.; Takasaki, K. T.; Chiu, C. Q.; Higley, M. J.; Sabatini, B. L.; Ellis-Davies, G. C. R. *J. Am. Chem. Soc.* **2013**, *135*, 5954-5957.
- (20) Amatrudo, J. M.; Olson, J. P.; Agarwal, H. K.; Ellis-Davies, G. C. R. *Eur. J. Neurosci.* **2015**, *41*, 5-16.
- (21) Palma-Cerda, F.; Auger, C.; Crawford, D. J.; Hodgson, A. C. C.; Reynolds, S. J.; Cowell, J. K.; Swift, K. A. D.; Cais, O.; Vyklicky, L.; Corrie, J. E. T.; Ogden, D. *Neuropharmacology* **2012**, *63*, 624-634.
- (22) Waldeck, D. H. *Chem. Rev.* **1991**, *91*, 415-436.
- (23) Han, W. G.; Lovell, T.; Liu, T. Q.; Noodleman, L. *ChemPhysChem* **2002**, *3*, 167-178.
- (24) Rodier, J.-M.; Myers, A. B. *J. Am. Chem. Soc.* **1993**, *115*, 10791-10795.
- (25) Osagawara, S.; Maeda, M. *Bioorg. Med. Chem.* **2011**, *21*, 5457-5459.
- (26) Schmidt, D.; Rodat, T.; Heintze, L.; Weber, J.; Horbert, R.; Girreser, U.; Raeker, T.; Bußmann, L.; Kriegs, M.; Hartke, B.; Peifer, C. *ChemMedChem* **2018**, *13*, 2415-2426.
- (27) Jones, B. J.; Scopelliti, R.; Tomas, A.; Bloom, S. R.; Hodson, D. J.; Broichhagen, J. *ChemistryOpen* **2017**, *6*, 501-505.
- (28) Paul, A.; Biswas, A.; Sinha, S.; Shah, S. S.; Bera, M.; Mandal, M.; Singh, N. D. P. *Org. Lett.* **2019**, *21*, 2968-2972.
- (29) Vomasta, D.; Högner, C.; Branda, N. R.; König, B. *Angew. Chem. Int. Ed.* **2008**, *47*, 7644-7647.

- (30) Reisinger, B.; Kuzmanovic, N.; Löffler, P.; Merkl, R.; König, B.; Sterner, R. *Angew. Chem. Int. Ed.* **2014**, *53*, 595-598.
- (31) Wutz, D.; Gluhacevic, D.; Chakrabarti, A.; Schmidtkunz, K.; Robaa, D.; Erdmann, F.; Romier, C.; Sippl, W.; Jung, M.; König, B. *Org. Biomol. Chem.* **2017**, *15*, 4882-4896.
- (32) Kneuttinger, A. C.; Winter, M.; Simeth, N. A.; Heyn, K.; Merkl, R.; König, B.; Sterner, R. *ChemBioChem* **2018**, *19*, 1750-1757.
- (33) Al-Atar, U.; Fernandes, R.; Johnsen, B.; Baillie, D.; Branda, N.R. *J. Am. Chem. Soc.* **2009**, *131*, 15966-15967.
- (34) Wilson, D.; Li, J. W.; Branda, N. R. *ChemMedChem* **2017**, *12*, 284-287.
- (35) Majima, T.; Tojo, S.; Ishida, A.; Takamuku, S. *J. Org. Chem.* **1996**, *61*, 7793-7800.
- (36) Ward, T. A.; Levin, G.; Swarc, M. *J. Am. Chem. Soc.* **1975**, *97*, 258-261.
- (37) Padilla, M.; Peccati, F.; Bourdelande, J. L.; Solans-Monfort, X.; Guirado, G.; Sodupe, M.; Hernando, J. *Chem. Commun.* **2017**, *53*, 2126-2129.
- (38) Sánchez, R. Doctoral Thesis, Universitat Autònoma de Barcelona, **2011**.
- (39) Goulet-Hanssens, A.; Utecht, M.; Mutruc, D.; Titov, E.; Schwarz, J.; Grubert, L.; Bléger, D.; Saalfrank, P.; Hecht, S. *J. Am. Chem. Soc.* **2017**, *139*, 335-341.
- (40) Goulet-Hanssens, A.; Rietze, C.; Titov, E.; Abdullahu, L.; Grubert, L.; Saalfrank, P.; Hecht, S. *Chem.* **2018**, *4*, 1740-1755.
- (41) Volgraf, M.; Gorostiza, P.; Szobota, S.; Helix, M. R.; Isacoff, E. Y.; Trauner, D. *J. Am. Chem. Soc.* **2007**, *129*, 260-261.
- (42) Reiter, A.; Skerra, A.; Trauner, D.; Schiefner, A. *Biochemistry* **2013**, *52*, 8972-8974.
- (43) Berlin, S.; Isacoff, E. Y. *EMBO reports* **2017**, *18*, 677-692.
- (44) Wu, C.; Wei, J.; Tian, D.; Feng, Y.; Miller, R. H.; Wang, Y. *J. Med. Chem.* **2008**, *51*, 6682-6688.
- (45) Wadsworth, W. *Org. React.* **1977**, *25*, 73.
- (46) Hong, M. C.; Kim, Y. K.; Choi, J. Y.; Yang, S. Q.; Rhee, H.; Ryu, Y. H.; Choi, T. H.; Cheon, G. J.; An, G. I.; Kim, H. Y.; Kim, Y.; Kim, D. J.; Lee, J-S.; Chang, Y-T.; Lee, K. C. *Bioorg. Med. Chem.* **2010**, *18*, 7724-7730.

- (47) Heck, R. F. *Acc. Chem. Res.* **1979**, *12*, 146-152.
- (48) Beletskaya, I. P.; Cheprakov, A. V. *Chem. Rev.* **2000**, *100*, 3009-3066.
- (49) Amatore, C.; Jutand, A. *Acc. Chem. Res.* **2000**, *33*, 314-321.
- (50) Fristrup, P.; Le Quement, S.; Tanner, D.; Norrby, P. **2004**, *23*, 6160-6165.
- (51) Ouellette, R. J.; Rawn, J. D. *Organic Chemistry. Structure, Mechanism, and Synthesis*; Elsevier, 2004; pp 567-593.
- (52) Alibés, R.; Ballbé, M.; Busqué, F.; De March, P.; Elias, L.; Figueredo, M.; Font, J. *Org. Lett.* **2004**, *6*, 1813-1816.
- (53) Li, H. J.; Wang, L. *Eur. J. Org. Chem.* **2006**, *22*, 5099-5102.
- (54) Yao, Q.; Kinney, E. P.; Yang, Z. *J. Org. Chem.* **2003**, *68*, 7528-7531.
- (55) Peterson, P. E.; Allen, G. *J. Org. Chem.* **1962**, *27*, 51505-1509.
- (56) Syamala, M. S.; Ramamurthy, V. *J. Org. Chem.* **1986**, *51*, 3712-3715.
- (57) Ito, Y.; Kajita, T.; Kunimoto, K.; Matsuura, T. *J. Org. Chem.* **1989**, *54*, 587-591.

CHAPTER V

Synthetic photoswitchable neurotransmitters based on bridged azobenzenes

This chapter reports the development of novel photochromic ligands based on bridged azobenzenes for the control of neuronal signalling. The synthesis, characterisation and biological application *in vitro* of these new compounds are described herein.^a

^a The results reported in this chapter have been published in “Synthetic photoswitchable neurotransmitters based on bridged azobenzenes” Cabré, G.; Garrido-Charles, A.; González-Lafont, A.; Moormann, W.; Langbehn, D.; Egea, D.; Lluch, J. M.; Herges, R.; Alibés, R.; Busqué, F.; Gorostiza, P.; Hernando, J. *Org. Lett.* **2019**, *21*, 3780-3784.

V.1. INTRODUCTION

V.1.1. PHOTOCHROMIC LIGANDS FOR GLUTAMATE RECEPTORS

As discussed in Chapter I, photochromic ligands are freely diffusible molecules that consist of a photoswitch chemically attached to a biologically active moiety. The photoswitch selected for this application must display different isomeric forms upon irradiation with light that make the ligand exhibit distinct affinities towards the biological target. As it has been mentioned, among all the existing photoswitches, azobenzenes (and other azoaromatic compounds) have emerged as the photochromes of choice for the preparation of most PCLs (Figure V-1).¹ This can be accounted to many of their features: (i) fast photoswitching; (ii) large geometrical changes between their *trans* and *cis* isomers; (iii) relatively high photostationary states and photoisomerisation quantum yields; (iv) lack of phototoxicity; (v) fatigue resistance; (vi) tunability; (vii) easy synthetic accessibility; and (viii) biocompatibility.^{2,3}

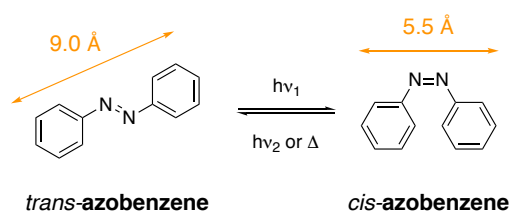


Figure V-1. *Trans* and *cis* isomers of azobenzene, which display a difference in distance between their 4 and 4' positions of 3.5 Å.

Another interesting property of azobenzenes is that they are relatively small (e.g. the parent azobenzene molecule has a molecular weight of 182 Da), which facilitates their incorporation into low molecular weight compounds. Two different strategies are mainly employed to integrate this photoswitch and develop azobenzene-based PCLs: *azo-attachment* (Figure V-2a) and *azo-integration* (or *azologization*, Figure V-2b). The first approach relies on covalently appending an azobenzene unit to a well-known biologically-active ligand, while the second approach directly integrates the azoaromatic photoswitch into the structure of such ligand.

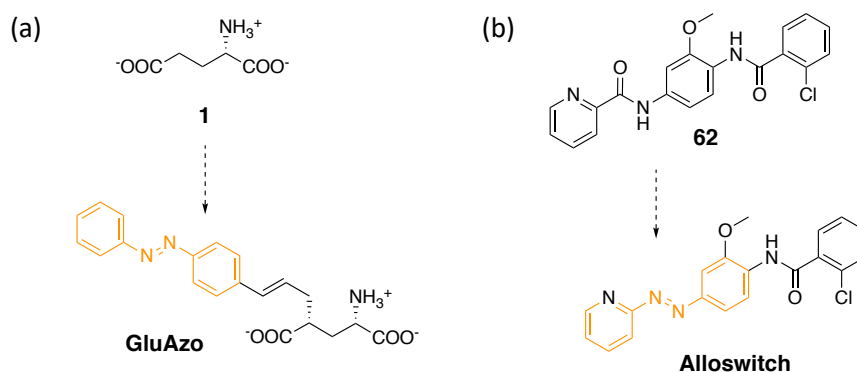


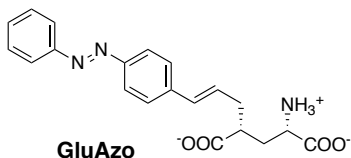
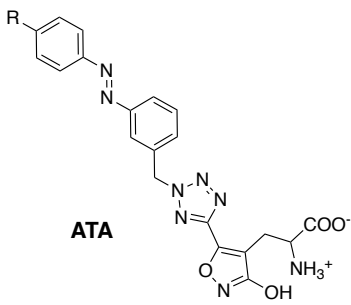
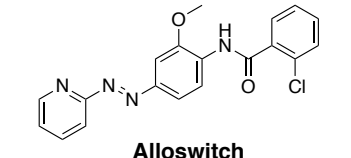
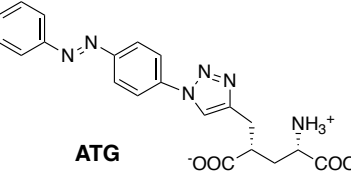
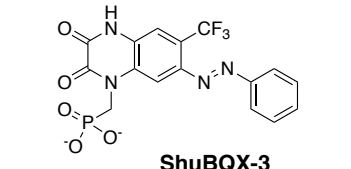
Figure V-2. (a) PCL **GluAzo**,⁴ a photochromic agonist of GluK1 and GluK2, was obtained following the *azo-attachment* approach: an azobenzene moiety was covalently linked to a glutamate unit. (b) PCL **Alloswitch**⁵ was derived by *azologization*; i.e. by replacing a fragment of the structure of **62**, a known positive allosteric modulator of mGluR₄, with an azoaromatic switch.

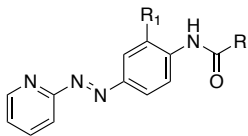
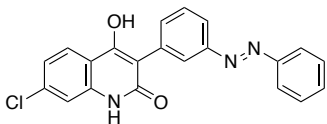
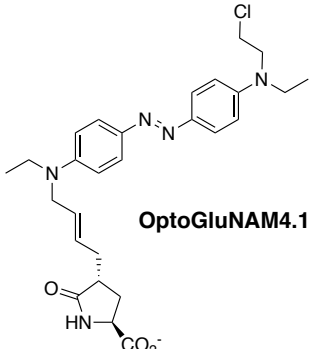
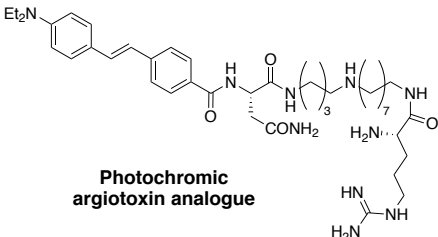
The first PCL for the control of glutamate receptors was developed in 2007 by Trauner, Isacoff and co-workers: **GluAzo** (see § IV.1.4), which consisted of an azobenzene moiety attached to a glutamate ligand through a vinyl linker.⁴ This compound showed partial agonist activity for kainate receptors GluK1 and GluK2 in the dark (i.e. in its *trans* isomer), while displayed much lower activity in its *cis* state formed upon irradiation with UV light. This allowed trains of action potentials to be generated in rat hippocampal neurons under illumination. The successful performance of this PCL inspired the development of other compounds for the optical control of glutamate receptors. Table V-1 summarises the main PCLs developed to date for this purpose.

As clearly shown in Table V-1, all the PCLs developed so far for the photocontrol of glutamate receptors rely on azoaromatic switches. Except from **ATG**, another common feature of these compounds is that they are biologically active in its more extended *trans* state (i.e. *trans* active) and lose activity upon irradiation and photoisomerisation to its folded *cis* isomer, where affinity to the receptor is reduced due to steric effects. Because of the inherent photochemical properties of azoaromatic compounds,⁶ this fact poses an important limitation to azobenzene-

based PCLs: most of them are active in the dark, where they lie in the more thermodynamically stable *trans* isomer (i.e. *trans* stable). Therefore, these compounds exert their pharmacological effects in the absence of illumination (e.g. receptor activation, blocking or modulation), which can only be inhibited upon irradiation. Unfortunately, this severely hampers their use since the opposite behaviour would be preferred for most applications; namely, PCLs should remain in their inactive state when administered to tissues, and be selectively photoactivated on demand with both spatial and temporal precision.

Table V-1. PCLs for glutamate receptors developed to date. Their target receptor, activity and active isomer are specified, as well as the strategy followed to incorporate the azobenzene photoswitch to the biologically-active ligand.

PCL	Target receptor	Activity	Active isomer	Strategy	Ref.
 <p>GluAzo</p>	GluK1 and GluK2	agonist	<i>trans</i>	Azo-attached	4
 <p>ATA</p>	GluA2 (AMPA)	agonist	<i>trans</i>	Azo-attached	7
 <p>Alloswitch</p>	mGluR	modulator	<i>trans</i>	Azo-integrated	5
 <p>ATG</p>	NMDAR	agonist	<i>cis</i>	Azo-attached	8
 <p>ShuBQX-3</p>	AMPA	antagonist	<i>trans</i>	Azo-attached	9

PCL	Target receptor	Activity	Active isomer	Strategy	Ref.
 <p>Phenylazopyridine derivatives</p>	mGluR	modulator	<i>trans</i>	Azo-integrated	10
 <p>PNRA</p>	NMDAR	antagonist	<i>trans</i>	Azo-integrated	11
 <p>OptoGluNAM4.1</p>	mGluR	antagonist	<i>trans</i>	Azo-attached	12
 <p>Photochromic argitoxin analogue</p>	AMPAR	antagonist	<i>trans</i>	Azo-attached	13

To overcome this important drawback, C_2 -bridged azobenzenes could be used as photoswitches. As for azoaromatic compounds, bridged azobenzenes may display *trans*-active behaviour towards the receptor by switching between their extended *trans* and bent *cis* isomers. However, given the bridge is short enough (i.e. C_2), the ring strain leads *cis* to be the most thermodynamically stable isomer at room temperature.^{14,15,16,17,18,19,20,21,22,23} Therefore, C_2 -bridged azobenzenes (i.e. diazocines) exhibit a *trans*-active, *cis*-stable behaviour, in contrast to azobenzene and other azoaromatic compounds (Figure V-3). Interestingly, diazocines isomerise with visible light,¹⁴⁻²³ which is a further advantage to azobenzenes, which respond to potentially harming UV light.⁶ The structure and main properties of C_2 -bridged azobenzenes are detailed in the following section.

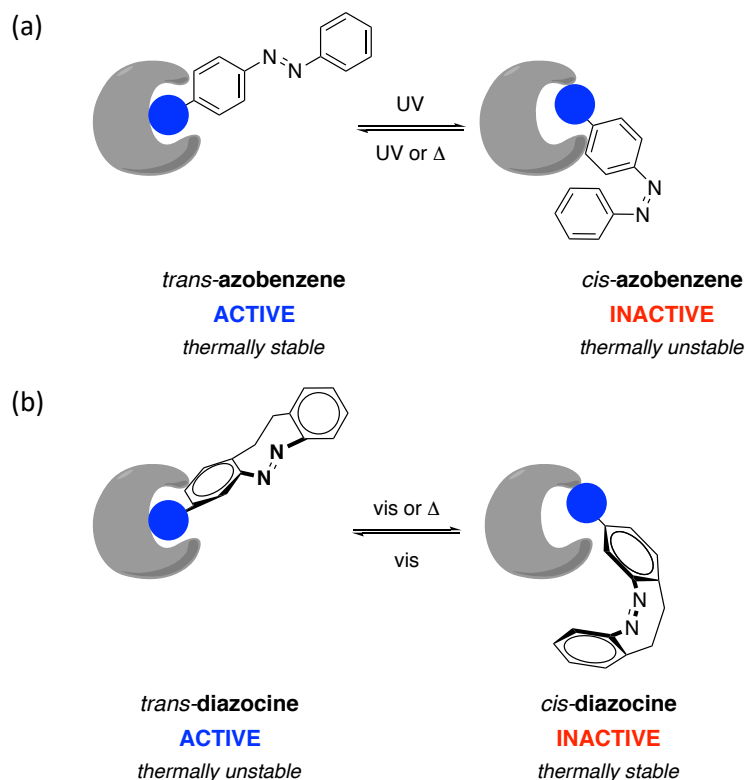


Figure V-3. Schematic representation of the interaction of (a) azobenzene and (b) diazocine (i.e. C₂-bridged azobenzene) isomers with the receptor. Both compounds exhibit *trans*-active behaviour towards the receptor, however, azobenzenes are *trans*-stable while diazocines display *cis*-stable behaviour.

V.1.2. C₂-BRIDGED AZOBENZENES

C₂-bridged azobenzenes or diazocines are azobenzene derivatives where the diazene unit is embedded in an eight-membered ring. The first diazocine was reported by Duval in 1910 (**63**, Figure V-4),²⁴ and its synthesis was later improved by Paudler and Zeiler in 1969²⁵ and by Tauer and Machinek in 1996.²⁶ However, it was not until 2009 when Temps, Herges and co-workers reported the behaviour of this compound as a molecular photoswitch.¹⁴

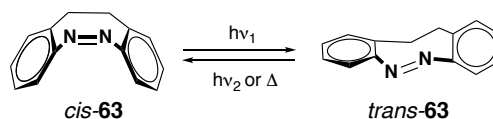


Figure V-4. *Cis-trans* isomerisation of the first described C₂-bridged azobenzene **63**. The *cis* state is the most thermodynamically stable and can be isomerised to the *trans* form upon irradiation with visible light. Then, the *trans* isomer can back-isomerise either upon illumination with visible light or thermally.¹⁴

In their seminal work, Temps, Herges and co-workers reported the absorption spectra of *cis*- and *trans*-**63** and the photostationary state obtained upon irradiation at 385 nm (Figure V-5a).¹⁴ Because of the non-planar structure of these two isomers deriving from the short C₂ bridge, they showed especially intense n→π* bands in the visible region of the spectrum that were fairly separated: λ_{max} = 404 nm and 490 nm for *cis*-**63** and *trans*-**63**, respectively. This enabled *cis*-**63** to be converted into *trans*-**63** with an efficiency higher than 90% by using violet light, while *trans*-**63** could be switched back quantitatively upon irradiation with green light. Moreover, this bridged azobenzene proved to have high fatigue resistance: it underwent repeated isomerisation cycles without any signs of degradation (Figure V-5b). Finally, the most interesting feature of diazocine **63** was that, due to the ring strain caused by the ethylenic bridge, its *cis* state was the thermodynamically stable isomer at room temperature, which strikingly contrasts to the behaviour of common azobenzenes. The thermal lifetime of the *trans* isomer was found to be 4.5 h at 28.5 °C.¹⁴

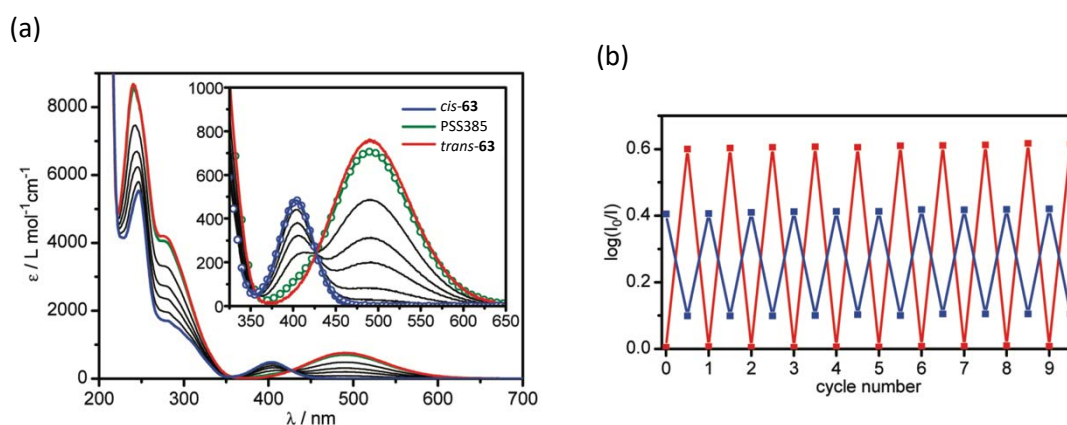


Figure V-5. (a) UV-vis absorption spectra of *cis*-**63**, *trans*-**63** and the photostationary state at λ_{exc} = 385 nm (PSS385) in *n*-hexane. The inset shows the n→π* bands on an enlarged scale. (b) Repeated photoswitching cycles of **63**. The graph shows the absorbances measured for a solution of **63** at 400 nm (blue) and 490 nm (red) after alternating irradiation at λ_{exc} = 385 nm and 520 nm.¹⁴

Inspired by the interesting photochemical properties of diazocines, Herges and co-workers recently reported for the first time the preparation of heterodiazocines, C₂-bridged azobenzenes where the bridge contains either an O or S atom (Figure V-6).¹⁷ Heterodiazocines emerged a modified version of diazocines that display two interesting properties: (i) their n→π* bands are shifted to the red-NIR region of the spectrum; and (ii) the *trans* state thermal lifetime can be modulated: *S*-heterodiazocines exhibit long *trans* lifetimes while *O*-heterodiazocines present short *trans* lifetimes.

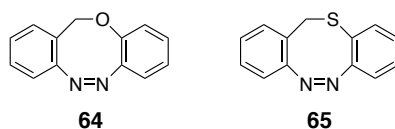


Figure V-6. First heterodiazocines reported by Herges and co-workers, where the bridge contains an O (**64**) or S (**65**) atom.¹⁷

These novel compounds could be obtained through a short (two or three steps) and reliable synthesis compared to that of parent compound **63**. Their absorption spectra were measured to be very similar to that of **63** (Figure V-7a): the *cis* isomer $n \rightarrow \pi^*$ bands were located at around 400 nm, while the *trans* isomers exhibited $n \rightarrow \pi^*$ bands at $\lambda_{\text{max}} = 525$ nm. Interestingly, the latter were found to be rather broad and extend up to 700 nm, which enabled back-isomerisation to the *cis* state with red light. The PSS reached from *cis*-**64** and *cis*-**65** upon irradiation at 385 nm and 405 nm contained 80% and 70% of the *trans* isomers, respectively, and back-isomerisation at 530 nm (**64**) and 660 nm (**65**) was achieved quantitatively. Moreover, the fatigue resistance of heterodiazocines was tested and no signs of photodegradation were observed (Figure V-7b). Finally, an important difference with respect to diazocines was observed: thermal stability of the *trans* isomer could be modulated upon variation of the heteroatom in the C₂-bridge. The *trans* isomer lifetime of heterodiazocine **64** bearing an O atom was found to be 89 s at 20 °C while a very different value was determined for heterodiazocine **65**, 3.5 days at 27 °C.¹⁷

Many C₂-bridged azobenzenes have been developed during the last years,^{15,16,18-23,27} however, their applications have been rather limited due to the difficulty of their synthesis, which proceeds with low yields and lack of reproducibility, especially when trying to obtain substituted diazocines. Actually, very few examples of their use in biological systems can be found in the literature. By the beginning of this thesis, diazocines had only been applied to the photocontrol of peptide conformation²⁰ and oligonucleotides.²¹⁻²³

Interestingly, even though diazocines exhibit convenient photophysical properties which may make them advantageous over other commonly used photochromes, at the beginning of the preparation of this manuscript no photopharmacological applications had been described using these compounds as photoswitch. Hence, we devised the preparation of PCLs for the control of iGluRs based on C₂-bridged azobenzenes, which would display the inactive state in the dark, thus enabling direct administration of the compound, and only after irradiation the active isomer would be obtained.

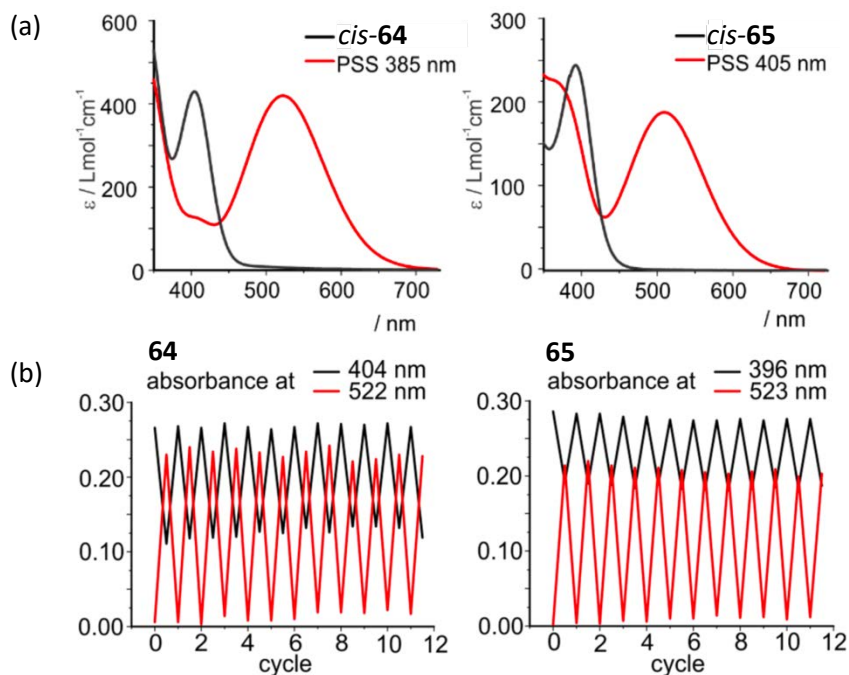


Figure V-7. (a) UV-vis absorption spectra of *cis*-**64** (in THF at $-80\text{ }^{\circ}\text{C}$) and *cis*-**65** (in acetonitrile at room temperature) and of their photostationary states at $\lambda_{\text{exc}} = 385\text{ nm}$ and 410 nm , respectively. (b) Repeated photoswitching cycles of **64** and **65**. The graph shows the absorbances measured for solutions of **64** and **65** at 404 nm and 522 nm after alternating irradiation at $\lambda_{\text{exc}} = 396\text{ nm}$ and 523 nm .¹⁷

V.1.3. NOVEL PHOTOCHROMIC LIGANDS BASED ON BRIDGED AZOBENZENES

As a proof of concept, in this thesis we devised the development of novel bridged azobenzene-based PCLs for the control of iGluRs, which we named **Glu_brAzo**. These compounds were designed inspired in the structure of **GluAzo** (Table V-1),⁴ an effective PCL for GluK1 and GluK2 optical modulation (see § IV.1.4). Hence, they consisted of a diazocine unit covalently linked to a glutamate moiety through a vinyl group (Figure V-8a). The glutamate moiety should act as an agonist of the receptor, while the bridged azobenzene photoswitch should enable affinity modulation towards the binding site with *trans*-active and *cis*-stable behaviour. Therefore, when in their dark-adapted *cis* bent configuration, **Glu_brAzo** PCLs should not be able to interact efficiently with the binding site of ionotropic glutamate receptors and thus, their ion channel should remain closed. By contrast, when isomerised to their *trans* state with extended geometry, ligand-receptor interaction should be favoured, thus triggering the opening of the channels and the ion flux through the cell membrane (Figure V-8b). In other words, **Glu_brAzo**

compounds should be able to be administered in its inactive form and be subsequently activated upon irradiation with the appropriate wavelength.

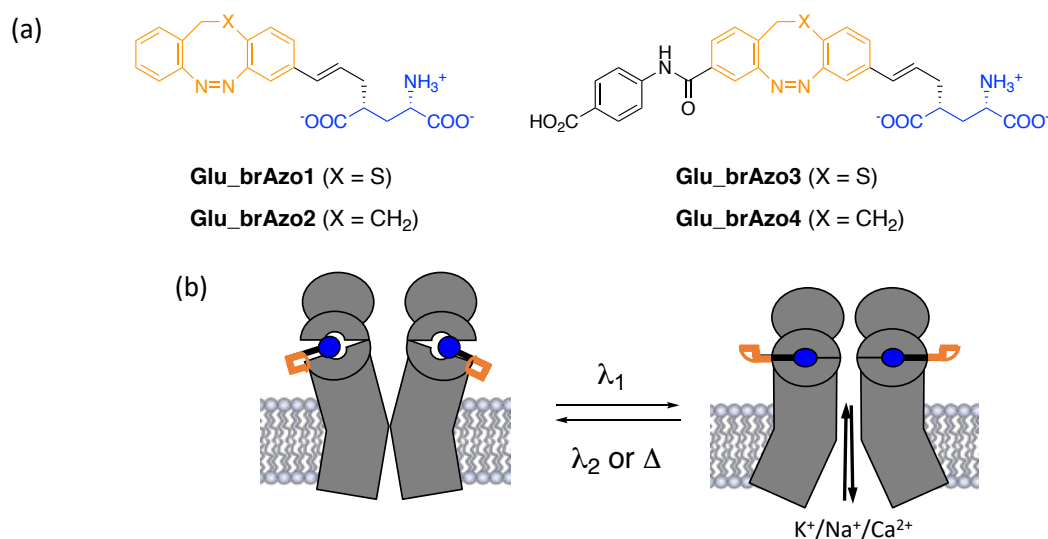


Figure V-8. (a) Structures of bridged azobenzene-based PCLs devised for the optical control of iGluRs. (b) Schematic representation of the light-induced operation of iGluRs with **Glu_brAzo**, which should behave as a *trans*-active, *cis*-stable agonist of these receptors.

Two different bridged azobenzene cores were devised for **Glu_brAzo** PCLs in this work: sulfur-bridged (**Glu_brAzo1-3**) and ethylene-bridged (**Glu_brAzo2-4**) diazocines, since both types of photochromes present large *trans* state thermal stability.^{14,17} This is not the case of oxygen-based heterodiazocines,¹⁷ which could impede obtaining large biological responses under irradiation. Accordingly, their use was not considered for this thesis. Moreover, inspired by the results obtained in Chapter IV for non-destructive caged ligands, the addition of a lateral ionic bulky group to the diazocine unit was also proposed (**Glu_brAzo3** and **Glu_brAzo4**), with which we aimed to: (i) enhance solubility in aqueous media, and (ii) further hinder the interaction of the *cis* isomer with the receptor by increasing the steric congestion around the glutamate moiety, thus enhancing the difference in activity between the two states of the PCL.

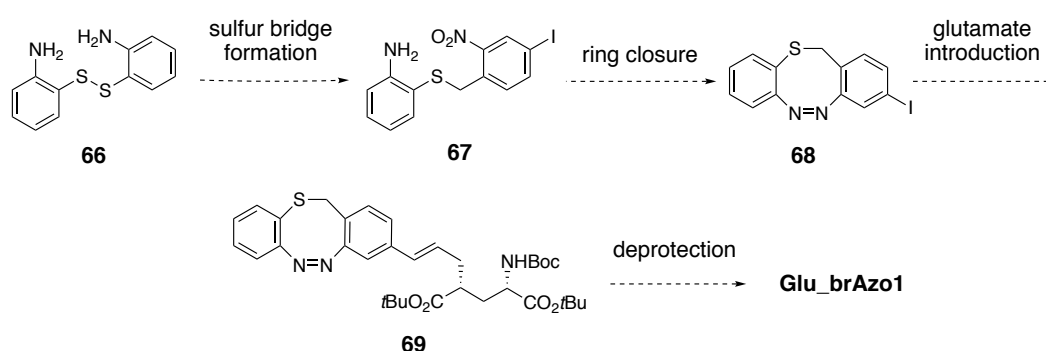
V.2. SYNTHESIS OF BRIDGED AZOBENZENE-BASED PCLs

The synthesis of the bridged azobenzene photochromes of target PCLs **Glu_brAzo1-4** was conducted during a 3-month research training stay in the group of Prof. Herges at Christian-Albrechts University in Kiel (Germany), one of the pioneers in the field of diazocine-based

switches. Because of the more efficient and reproducible synthesis described for heterodiazocines,¹⁷ our attention first focused on the preparation of **Glu_brAzo1** and **Glu_brAzo3** bearing a *S*-diazocine core.

V.2.1. SYNTHESIS OF PCLs BASED ON SULFUR-BRIDGED DIAZOCINES

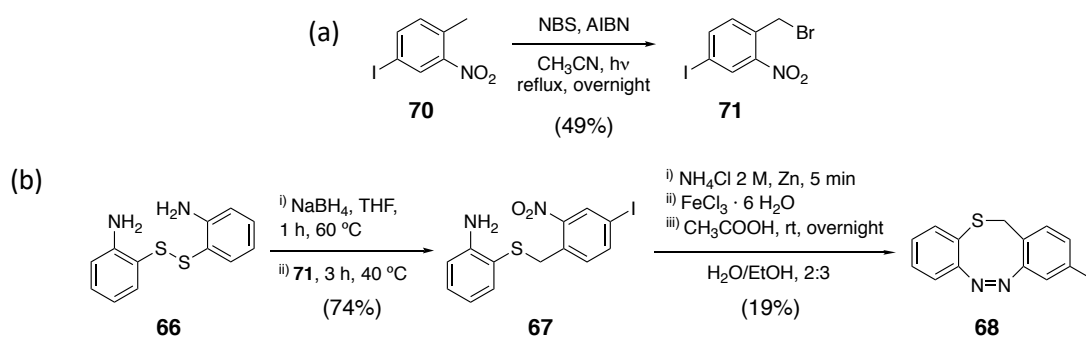
The synthesis of **Glu_brAzo1**, the simplest PCL bearing a sulfur-bridged diazocine as a photoswitch, was devised as depicted in Scheme V-1. From commercially available 2,2'-disulfanediyl dianiline, **66**, thioether **67** should be obtained, which should lead to heterodiazocine **68** through a ring closure reaction. Then, a carbon-carbon coupling reaction with glutamate derivative **29** should lead to key intermediate **69**, from which target **Glu_brAzo1** should be obtained by simple removal of the protecting groups of the glutamate moiety.



Scheme V-1. Synthetic pathway designed for the synthesis of target PCL **Glu_brAzo1**.

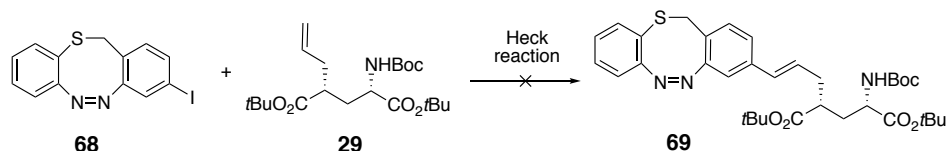
According to the synthetic pathway conceived, our first goal was the preparation of the heterodiazocine core **68**. The synthesis of this compound had already been described by Herges and co-workers,²⁷ so we decided to follow the reported procedure (Scheme V-2). Therefore, benzyl bromide **71**, which would be used in the sulfur bridge formation, was first prepared. This compound was obtained by the radical bromination of commercially available 4-iodo-2-nitrotoluene, **70**, with *N*-bromosuccinimide (NBS) as a bromine source and 2,2'-azobis(2-methylpropionitrile) (AIBN) as a radical initiator in dry CH₃CN (Scheme V-2a). The reaction mixture was stirred overnight under reflux and illumination. After purification by column chromatography and recrystallisation with petroleum ether, compound **71** was obtained in 49% yield. Afterwards, commercially available disulfide **66** was reduced with sodium borohydride and *in situ* reacted with **71** to deliver **67** in 74% yield (Scheme V-2b). Compound **67** should undergo a ring closing reaction; however, neither reductive nor oxidative conditions could be

used since they were not compatible with its thioether group. Thus, a milder alternative had to be used: the condensation between nitrosoarenes and anilines under weakly acidic conditions. This reaction is known as the Baeyer-Mills reaction and was discovered by Baeyer in 1874²⁸ and further studied by Mills²⁹ and Bamberger.³⁰ Therefore, compound **67** was first treated with zinc powder to reduce its nitro group to the corresponding hydroxylamine, which was subsequently *in situ* oxidised to its nitroso derivative using iron(III) chloride. Finally, acetic acid was added, and the reaction mixture was stirred overnight at room temperature (Scheme V-2b).²⁷ Purification by column chromatography led to target heterodiazocine **68** albeit in only 19% yield. The comparison of its ¹H NMR spectrum with that reported in the literature confirmed the obtention of the desired product.



Scheme V-2. (a) Bromination reaction of **70** for the preparation of compound **71**. (b) Synthesis of monosubstituted heterodiazocine **68**.

The subsequent step of the synthesis was the carbon-carbon coupling reaction between heterodiazocine **68** and glutamate derivative **29**, which was obtained from L-pyroglutamic acid as reported in Chapter III (see § III.2.3.1). For this, we decided to perform a Heck reaction, as previously done for the coupling between glutamate derivative **29** and stilbene **50** (see § IV.2.3). Thus, the conditions that gave the best yield in that case were first tested: Pd(OAc)₂ as a catalyst, K₃PO₄ as a base, DMAc as a solvent, and heating at 140 °C overnight. However, no product was obtained and only glutamate derivative **29** could be recovered, since bridged azobenzene **68** underwent complete degradation. Several milder conditions were tested: lower temperatures, less reaction times and lower amounts of base, as well as alternative bases and solvents. All the attempts performed were completely unsuccessful due to the low stability of sulfur-bridged diazocines in basic media or at high temperatures, which are common conditions in Heck reactions (Scheme V-3).



Scheme V-3. Introduction of glutamate moiety **29** to heterodiazocine core **68**.

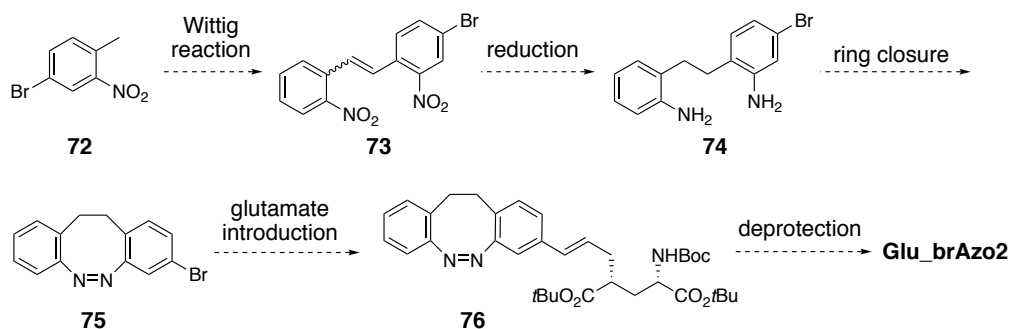
In view of the low stability of compound **68**, which could also be an issue in the final step towards **Glu_brAzo1** where acid conditions would be required for glutamate fragment deprotection, we decided to set aside the synthesis of *S*-diazocine-based PCLs and focus on ethylene-bridged diazocines, which should exhibit higher thermal and chemical stability.

V.2.2. SYNTHESIS OF PCLs BASED ON ETHYLENE-BRIDGED DIAZOCINES

The synthesis of ethylene-bridged azobenzenes has been further studied than that of heterodiazocines.^{15,16,18-23} However, most of the procedures reported by the beginning of this work were related to symmetrically-substituted diazocines, while our target molecules displayed either monosubstituted (**Glu_brAzo2**) or unsymmetrically-disubstituted (**Glu_brAzo4**) C₂-bridged azobenzene cores, which made the preparation of these compounds more challenging. Moreover, the diazocines described in the literature had been afforded in low yields. Thus, we were interested in the development of a new method for the preparation of non-symmetric C₂-bridged azobenzenes through a robust, efficient and reproducible synthesis.

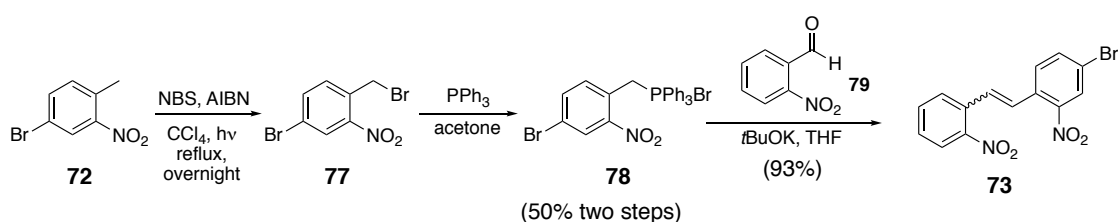
V.2.2.1. Synthesis of **Glu_brAzo2**

Scheme V-4 depicts the synthetic strategy conceived for the synthesis of PCL **Glu_brAzo2**. From commercially available 4-bromo-2-nitrotoluene, **72**, stilbene **73** should be obtained through a Wittig reaction. Then, reduction of the nitro groups and hydrogenation of the double bond should lead to diamine **74**. Ring closing reaction between the amino groups should lead to diazocine core **75**, to which glutamate unit should be incorporated through a carbon-carbon coupling reaction. Finally, removal of the glutamate moiety protecting groups on **76** should give target PCL **Glu_brAzo2**.



Scheme V-4. Synthetic pathway designed for the synthesis of target PCL **Glu_brAzo2**.

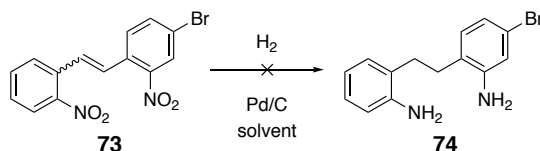
Our first goal was the preparation of stilbene **73** from compound **72** (Scheme V-5). As stated above, we devised the synthesis of this compound through a Wittig reaction.³¹ First, we focused on the preparation of the phosphonium salt of compound **72**. A radical bromination reaction on **71** with NBS and AIBN in CCl_4 was performed as reported in the literature.³² After stirring overnight under reflux and illumination, the reaction mixture was treated and the residue obtained was directly reacted with PPh_3 in acetone without previous purification. Phosphonium salt **78** was obtained in 50% overall yield. Then, the Wittig reaction was performed with commercially available aldehyde **79** in the presence of potassium *tert*-butoxide in THF. Stilbene **73** was achieved in 93% yield as a 1:3 mixture of *trans* and *cis* isomers, which were not further separated since the subsequent hydrogenation reaction led to the same product. The ^1H NMR spectrum of the product showed clear doublets at 7.59 and 7.48 ppm ($J_{\text{trans}} = 16.0$ Hz) and at 7.13 and 7.00 ppm ($J_{\text{cis}} = 11.8$ Hz) which correspond to the protons of the new central C=C double bond formed of both isomers.



Scheme V-5. Synthesis of stilbene **73** from commercially available 4-bromo-2-nitrotoluene, **72**.

The following step was the hydrogenation of the double bond to afford the ethylene bridge between both arene moieties and concomitant reduction of the nitro groups to give diamine **74** (Scheme V-6). For that purpose, stilbene **73** was treated with H_2 in the presence of Pd/C catalyst. Unfortunately, the reaction was not successful, since the nitro groups were only partially reduced and no signs of hydrogenation of the double bond could be observed. Different amounts of Pd/C catalyst, reaction times and solvents were tested, but results did not improve.

Most probably, this was due to the presence of the bromide group in **73**, which must have suffered Pd insertion into the C-halogen bond. Hence, another synthetic strategy had to be designed. However, since we were working on the synthesis of **Glu_brAzo4** in parallel and obtained more promising results, we decided to abandon the obtention of **Glu_brAzo2** and focus on the preparation of disubstituted diazocine-based PCL **Glu_brAzo4**.

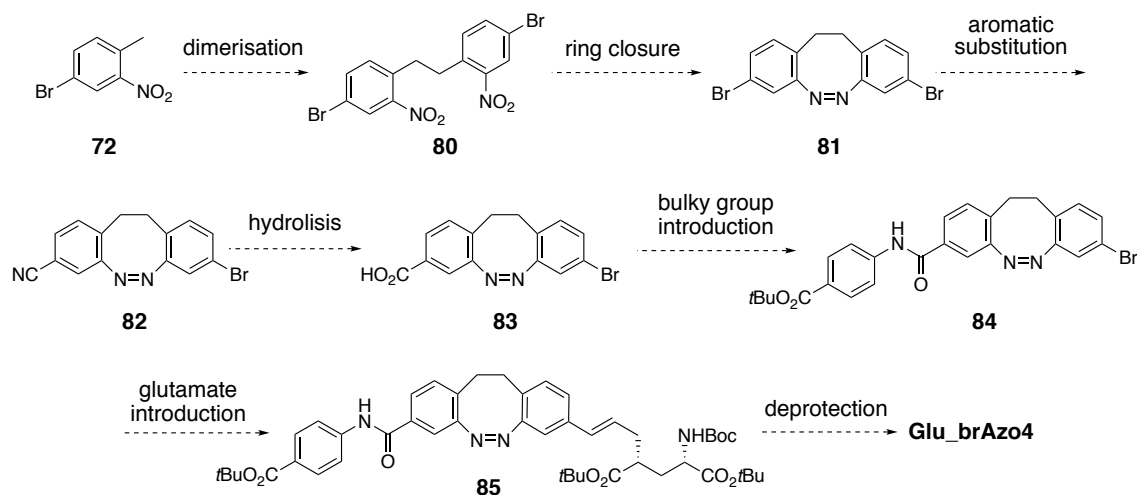


Scheme V-6. Reduction of the double bond and nitro groups of **73** to give intermediate **74**.

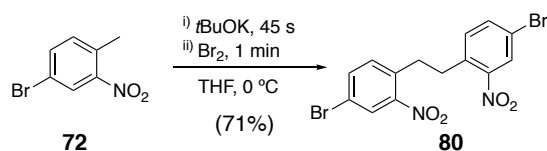
V.2.2.2. Synthesis of **Glu_brAzo4** and **Glu_brAzo5**

The preparation of **Glu_brAzo4** was devised following the synthetic strategy depicted in Scheme V-7. It is a linear synthetic sequence through which the different functional building blocks of the ligand (i.e. bulky group and glutamate) are consecutively tethered to the central diazocine core. This route should commence by the dimerisation of commercially available **72** to give compound **80**, where the ethylene bridge is already present. Afterwards, a ring closing reaction should lead to symmetrically-substituted diazocine **81**. An aromatic substitution reaction should then be performed to replace one bromine atom for a nitrile group to give unsymmetrically-substituted diazocine **82**. Subsequent hydrolysis of the nitrile group should lead to acid **83**, through which the desired bulky group could be introduced. Then, a carbon-carbon coupling reaction between diazocine **84** and glutamate derivative **29** should give key intermediate **85**, which should directly afford **Glu_brAzo4** by removal of the glutamate unit protecting groups.

The synthesis of the photochromic unit started by the obtention of compound **80** through a radical-mediated dimerisation as previously described by Herges and co-workers.¹⁸ With this aim, commercially available **72** was treated with *t*BuOK in dry THF, followed by the addition of Br₂ (Scheme V-8). The reaction occurred extremely fast (1.75 min) and, upon the addition of ice, dinitro derivative **80** precipitated and could be easily isolated in 71% yield. The ¹H NMR spectrum of the product showed a new signal at 3.10 ppm corresponding to the ethylene bridge formed.

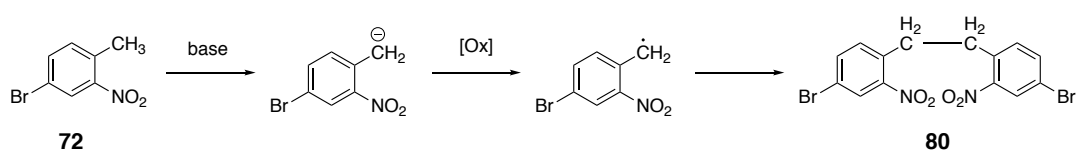


Scheme V-7. Synthetic pathway designed for the synthesis of target PCL **Glu_brAzo4**.



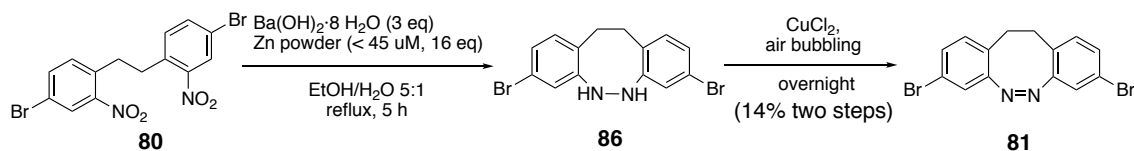
Scheme V-8. Radical-mediated dimerisation reaction for the synthesis of compound **80**.

In 1980 Chaudhuri and Ball reported the mechanism for this radical-mediated dimerisation.³³ As clearly illustrated in Scheme V-9, treatment of the nitrotoluene derivative with a base produces the corresponding benzyl anion. Then, the benzyl radical is obtained by oxidation of this anion. Finally, the radical dimerisation takes place and gives the desired ethylene-bridged compound.



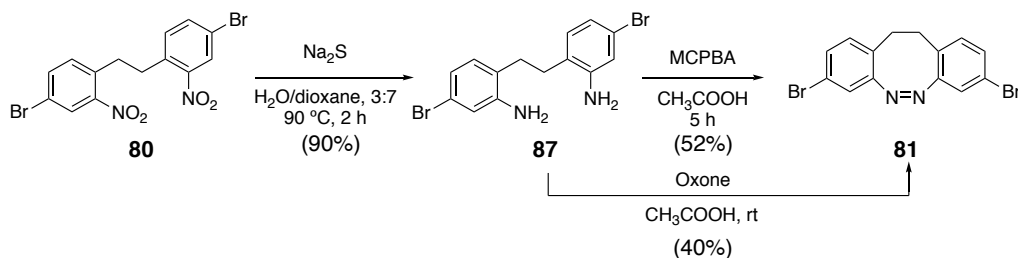
Scheme V-9. Mechanism of the radical-mediated dimerisation of 4-bromo-2-nitrotoluene, **72**.³³

The next step of the synthetic procedure was the ring closing reaction, for which common reductive conditions reported for the synthesis of diazocines were used.¹⁴⁻¹⁹ Therefore, compound **80** was reduced to the corresponding hydrazine derivative with Zn and Ba(OH)₂, and further oxidised to the azo compound by bubbling air into the reaction mixture in the presence of CuCl₂. Bridged azobenzene **81** was finally obtained in very low yield (14%) using this procedure, which we ascribed to the formation of dimers and higher oligomers in the first reductive step.¹⁸



Scheme V-10. Ring closing reaction for the obtention of bridged azobenzene **81**.

The low yield in which diazocine **81** was obtained prompted us to develop an alternative methodology for the ring closure reaction of **80**. For this, we decided to explore the use of Mills coupling reaction, commonly used in the formation of azo compounds.³⁴ With this aim, we first reduced the nitro groups of **80** with sodium sulfide to furnish amine **87** in 90% yield.³⁵ Then, oxidative coupling was undertaken using 3-chloroperbenzoic acid (MCPBA) in acetic acid, which afforded bridged azobenzene **81** in 52% yield (Scheme V-11). In this intramolecular process, one of the aniline groups of the compound must be oxidised to the corresponding nitrosoarene, which must then react with the other unaltered amine. Importantly, the reaction needed to be performed at very low concentration conditions in order to avoid polymerisation. The ¹H NMR spectrum of the product showed three sets of signals in the low field region of the spectra corresponding to the aromatic protons and a clear multiplet at 2.82 ppm which indicated the presence of the ethylene bridge.

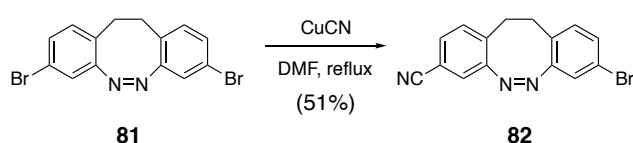


Scheme V-11. Reduction and ring closing reactions for the obtention of C₂-bridged azobenzene **81**.

This novel methodology developed for the ring closing reaction of **80** enabled the obtention of diazocines in a better yield than those previously reported^{15-18,20-23} following a more convenient procedure that could be easily reproduced, which was one of the main issues regarding the current diazocine formation reactions. In view of the success of this new methodology, other oxidative conditions were tested for the intramolecular ring closing reaction. Oxone[®] mediated oxidation was found to be an alternative method that also afforded **81** in good yield (Scheme V-11).

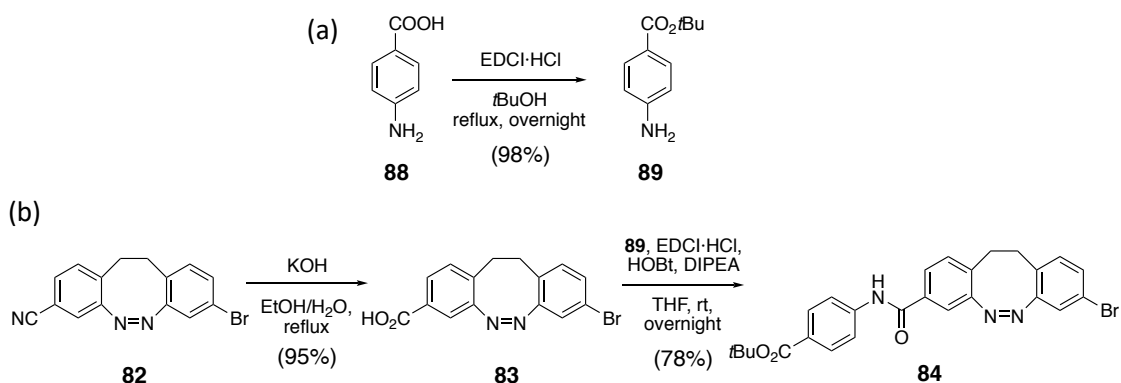
Once symmetrically substituted diazocine **81** was obtained, an aromatic substitution reaction was performed to replace one bromine atom for a nitrile group. This reaction was performed by

heating a solution of **81** in DMF under reflux in the presence of 1 equivalent of CuCN (Scheme V-12). To prevent full disubstitution of the bromine atoms of **81**, the reaction time needed to be monitored carefully. Hence, when little presence of the disubstituted compound was appreciated by TLC analysis, the reaction was immediately quenched. This somewhat limited the efficiency with which compound **82** could be obtained (51% yield after purification). However, it must be mentioned that non-reacted **81** could be recovered and reused (78% yield considering recovered **81**). The ^1H NMR spectrum of diazocine **82** showed clear desymmetrisation of the aromatic protons, which confirmed the selective substitution of one bromine atom to form an unsymmetrically-substituted diazocine.



Scheme V-12. Monocyanation of **81** to give the unsymmetrically-substituted diazocine **82**.

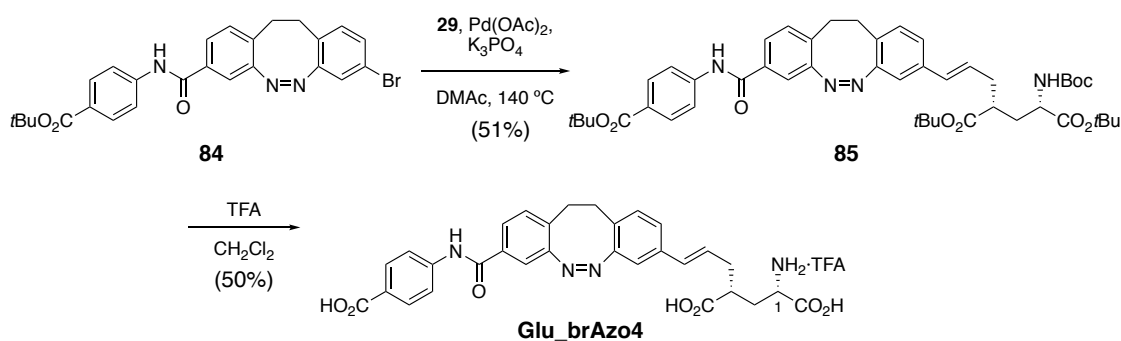
In order to introduce the bulky group to the bridged azobenzene core, amine **89** was prepared almost quantitatively through the protection as a *tert*-butyl ester of commercially available **88** as reported in the literature³⁶ (Scheme V-13a). Then, nitrile **82** was treated with basic conditions at reflux temperature to give the corresponding acid **83** in 95% yield (Scheme V-13b). Afterwards, an amide bond formation reaction using EDCI and HOBT as coupling agents enabled tethering amine **89** to the bridged azobenzene core **83** to give compound **84** in 78% yield (Scheme V-13a). New signals corresponding to the aromatic ring introduced were observed in the ^1H and ^{13}C NMR spectra of the product.



Scheme V-13. (a) Synthesis of **89** by the protection of acid **88** as a *tert*-butyl ester. (b) Introduction of **89** to give compound **84**.

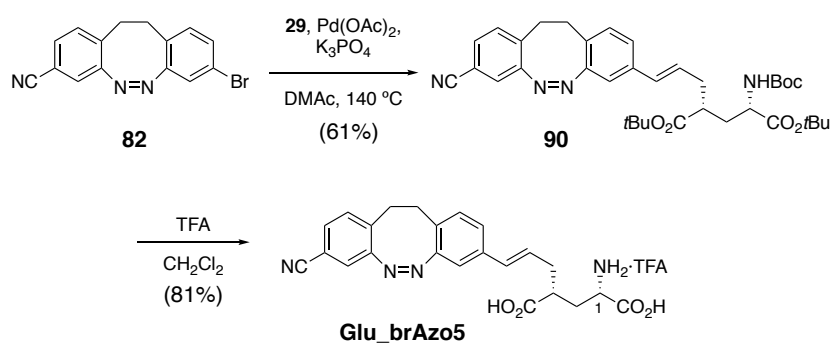
The final part of the synthetic sequence towards PCL **Glu_brAzo4** was devoted to the introduction of the glutamate moiety and final removal of its protecting groups to afford the target compound. In order to introduce the glutamate unit, a carbon-carbon coupling Heck reaction was devised. Hence, the optimal conditions used for the coupling between glutamate derivative **29** and iodostilbene **50** (see § IV.2.3) were tested: Pd(OAc)₂ as a catalyst, K₃PO₄ as a base, DMAc as a solvent, and heating at 140 °C overnight (Scheme V-14). The reaction was successful and, after purification by column chromatography, compound **85** was obtained in 51% yield. New signals corresponding to the glutamate fragment introduced were observed in the ¹H and ¹³C NMR spectra of molecule **85**. It is worth mentioning that this compound already presented the three basic units of the designed PCL: (i) a C₂-bridged azobenzene photoswitch, (ii) a glutamate derivative moiety, and (iii) a bulky group.

To culminate the synthesis of **Glu_brAzo4**, the protecting groups had to be removed under acid media. For that purpose, we first treated **85** with HCl 4 M in dioxane, as previously done for the obtention of **GluS** (see § IV.2.4) bearing a similar structure. However, these conditions were not suitable in this case since no complete removal of the protecting groups was achieved. Therefore, we decided to test the deprotection conditions used in the synthesis towards **MAG** compounds: TFA in CH₂Cl₂ (see § III.2.4). Complete removal of the protecting groups was observed and, after purification, **Glu_brAzo4** was achieved in 50% yield. The target compound was unequivocally identified from its spectroscopic data. Its ¹H NMR spectrum showed the disappearance of the characteristic *tert*-butyl signals between 1.40 and 1.60 ppm and carbamate signal around 4.99 ppm. Furthermore, downfield shifts were observed for proton H-1 signals: from 4.21 ppm in **85** to 3.29 ppm. Lastly, ¹³C NMR also confirmed the removal of the protecting groups by the disappearance of characteristic carbamate signals at 155.4 ppm and *tert*-butyl signals around 82-79 ppm and 28 ppm.



Scheme V-14. Introduction of glutamate derivative **29** and removal of the protecting groups for the obtention of target PCL **Glu_brAzo4**.

Prompted by our success in the synthesis of **Glu_brAzo4**, we decided to prepare an analogous compound to **Glu_brAzo2** using a similar procedure. In particular, we aimed to synthesise a diazocine-glutamate dyad that did not bear the bulky group appended to **Glu_brAzo4** and, hence, could be used as a reference compound to rationalise the effect of such group in the light-controlled biological activity of **Glu_brAzo** PCLs. With this in mind, we designed **Glu_brAzo5** ligand (Scheme V-15), where the bulky carboxylaryl pending group was replaced by a less sterically demanding nitrile moiety. The preparation of this compound was conceived by simply coupling glutamate derivative **29** to diazocine **82**, followed by removal of the glutamate unit protecting groups (Scheme V-15).



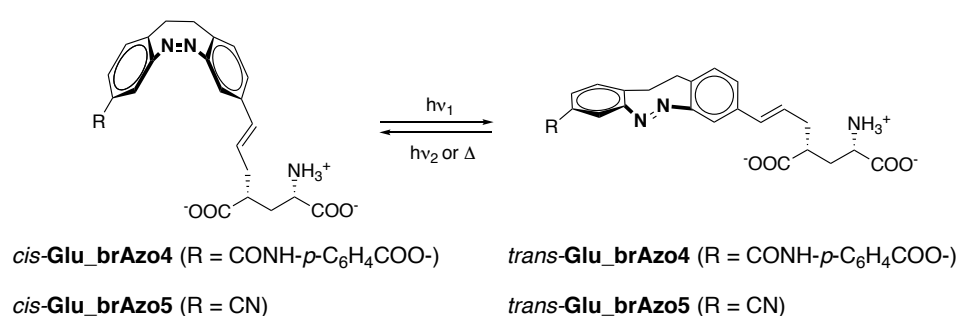
Scheme V-15. Introduction of glutamate derivative **29** and removal of the protecting groups for the obtention of PCL **Glu_brAzo5**.

Glutamate derivative **29** was successfully tethered to bridged azobenzene **82** through a Heck reaction using the same conditions applied in the synthesis of **Glu_brAzo4**. The desired compound **90** was achieved in 61% yield and clear signals corresponding to the glutamate unit introduced could be observed in its ^1H and ^{13}C NMR spectra. Subsequently, **90** was treated with TFA in CH_2Cl_2 media, which gave **Glu_brAzo5** in 81% yield (Scheme V-15). The target compound was unequivocally identified from its spectroscopic data, which showed similar features to those previously found for **Glu_brAzo4**.

In summary, new diazocine derivatives **Glu_brAzo4** and **Glu_brAzo5** with potential activity as photochromic ligands for iGluRs were prepared through a linear sequence where the different functional building blocks of the ligand were tethered to the central bridged azobenzene core. Compound **Glu_brAzo4** was achieved in 8 steps in 3% overall yield from 4-bromo-2-nitrotoluene **72**, and compound **Glu_brAzo5** was afforded in 6 steps in 8% overall yield from **72**. It must be noted that the novel methodology introduced for the preparation of diazocines based on an oxidation-mediated ring closure reaction provides a procedure to furnish diazocines in good yields in a robust and reproducible manner.

V.3. PHOTOCHEMICAL CHARACTERISATION OF PCLs **Glu_brAzo4** AND **Glu_brAzo5**

Once target **Glu_brAzo4** and **Glu_brAzo5** compounds were synthesised and fully characterised, we focused our attention on the investigation of their photochemical behaviour in solution. Since they are composed of bridged azobenzene-based photoswitches, these molecules should present two differentiated states that display distinctive structural and physicochemical properties and can be interconverted upon reversible photoinduced *cis-trans* isomerisation (Scheme V-16). Additionally, the thermal instability of their *trans* isomer should result in spontaneous back isomerisation to the more stable *cis* state in the dark. These photochemical and thermal interconversion processes were investigated in detail, and the results obtained are described in this section. The experiments reported herein were mainly carried out in PBS:DMSO 1:1 mixtures due to the limited solubility of **Glu_brAzo4** and, especially, **Glu_brAzo5** in aqueous media.



Scheme V-16. Photoinduced *cis-trans* isomerisation of **Glu_brAzo4** and **Glu_brAzo5** upon stimulation with light. *Trans*→*cis* back-isomerisation can also proceed thermally.

V.3.1. CIS→TRANS PHOTOISOMERISATION

Figure V-9 shows the absorption spectra registered for **Glu_brAzo4** and **Glu_brAzo5** in PBS:DMSO 1:1. Both compounds present similar spectral features that are typical for the *cis* isomer of C₂-bridged azobenzene photoswitches:^{14-16,18-23} a strong $\pi\rightarrow\pi^*$ absorption band in the UV region of the spectrum and a weaker $n\rightarrow\pi^*$ absorption band in the high-energy visible region (λ_{\max} = 395 nm for **Glu_brAzo4** and 392 nm **Glu_brAzo5**).

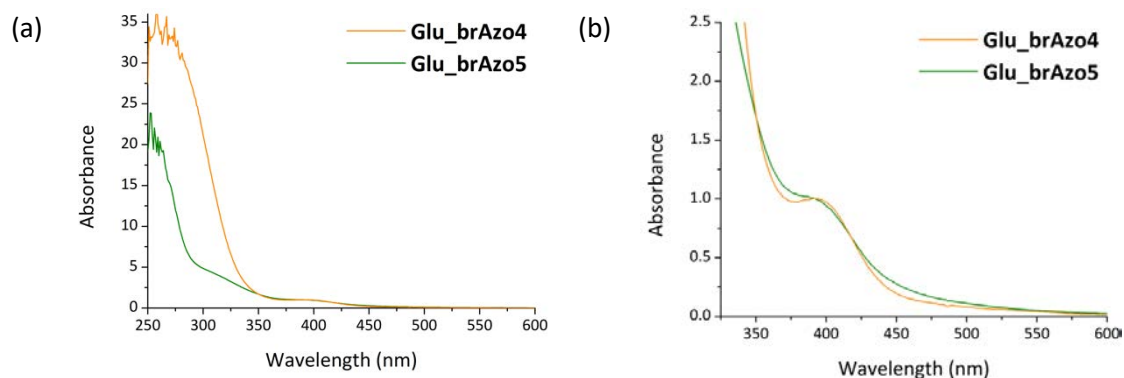


Figure V-9. (a) Absorption spectra of *cis*-Glu_brAzo4 and *cis*-Glu_brAzo5 in PBS:DMSO 1:1 normalised at the maximum of the $n \rightarrow \pi^*$ absorption band. (b) Inset of the $n \rightarrow \pi^*$ absorption band region of *cis*-Glu_brAzo4 and *cis*-Glu_brAzo5 in PBS:DMSO 1:1.

According to the literature,^{14-16,18-23} the *cis* isomer of C₂-bridged azobenzenes can isomerise to the *trans* state upon photoexcitation of its $n \rightarrow \pi^*$ absorption band. Actually, when *cis*-Glu_brAzo4 and *cis*-Glu_brAzo5 were irradiated with violet light ($\lambda_{\text{exc}} = 405$ nm), spectral changes could be observed that were consistent with *cis*→*trans* photoisomerisation (Figure V-10). Specifically, a new red-shifted absorption band was found at $\lambda_{\text{max}} \sim 480$ nm in both cases, which is a distinctive spectral feature of the *trans* isomer of diazocines due to its non-planar geometry.^{14-16,18-23} However, the absorption spectra of the *cis* and *trans* isomers of these compounds overlapped at the excitation wavelength ($\lambda_{\text{exc}} = 405$ nm), and thus, quantitative *cis*→*trans* photoisomerisation was not expected to take place.

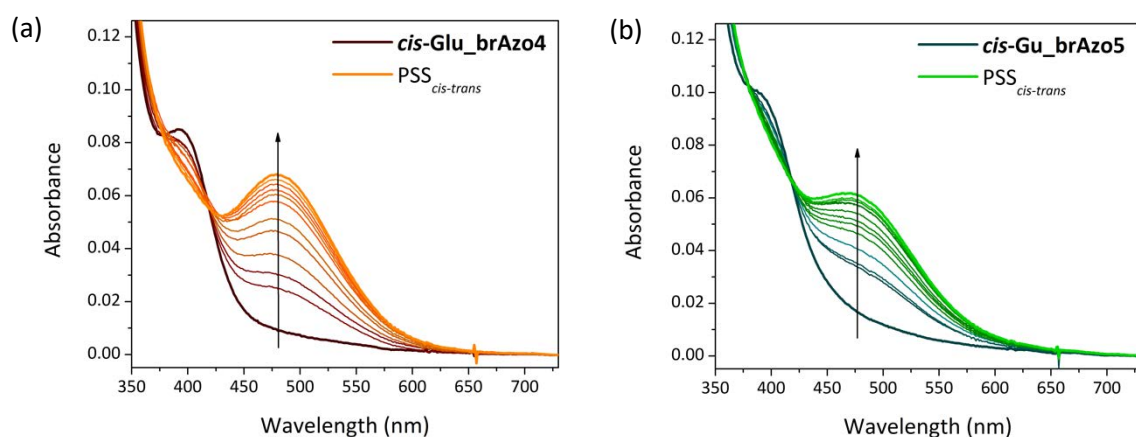


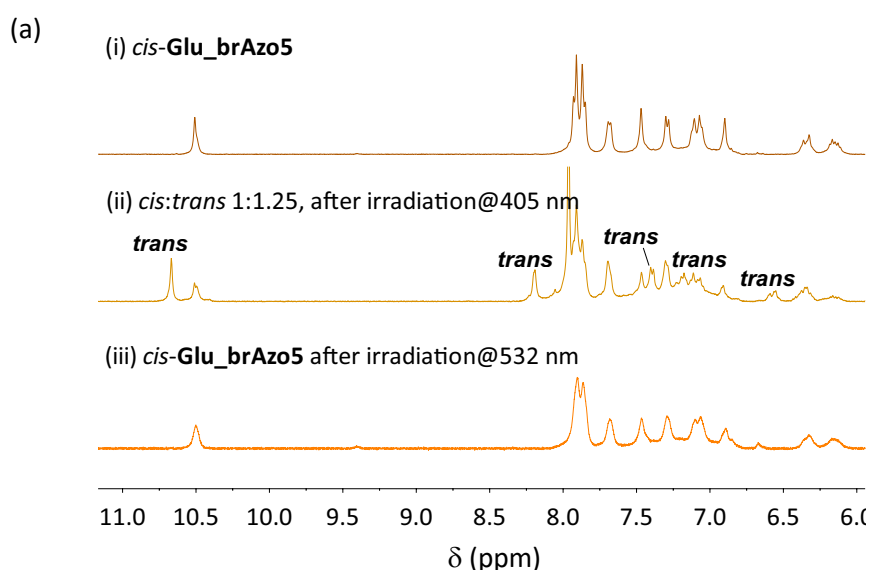
Figure V-10. Variation of the absorption spectra of (a) Glu_brAzo4 and (b) Glu_brAzo5 in PBS:DMSO 1:1 upon irradiation of their *cis* isomer at $\lambda_{\text{exc}} = 405$ nm. The arrows indicate the direction of the changes observed.

Cis→*trans* photoisomerisation of **Glu_brAzo4-5** with violet light was further investigated by ¹H NMR experiments (Figure V-11). In both cases, new signals in the low-field region of the spectrum were observed upon irradiation that were assigned to the aromatic protons of their *trans* isomers, which confirmed the expected isomerisation process. Moreover, these experiments enabled the determination of the composition of the photostationary states obtained. The amount of *trans* isomer in the PSS_{*cis-trans*} was found to be 60% for **Glu_brAzo4** and 47% for **Glu_brAzo5** (Table V-2). It must be noted that these experiments were not directly conducted in aqueous media due to the higher concentrations required and the moderate solubility of **Glu_brAzo4** and **Glu_brAzo5**. However, the PSS_{*cis-trans*} compositions in PBS:DMSO 1:1 could be estimated from the ¹H NMR data in DMSO-*d*₆ and the UV-vis absorption measurements in PBS:DMSO 1:1. In addition, *cis*→*trans* photoisomerisation quantum yields ($\Phi_{cis\rightarrow trans}$) of **Glu_brAzo4-5** in PBS:DMSO 1:1 were also determined. Very similar, moderate values were found for both ligands: $\Phi_{cis\rightarrow trans} = 0.13$ and 0.11 for **Glu_brAzo4** and **Glu_brAzo5**, respectively (Table V-2).

Table V-2. Results of the *cis*→*trans* photoisomerisation process of *cis*-**Glu_brAzo4-5** in PBS:DMSO 1:1.

Compound	$\lambda_{abs,max}^{cis}$ (nm) ^a	$\lambda_{abs,max}^{trans}$ (nm) ^a	<i>trans</i> PSS (%) ^b	$\Phi_{cis\rightarrow trans}$ ^c
Glu_brAzo4	395	481	60	0.13
Glu_brAzo5	392	471	47	0.11

(a) $n\rightarrow\pi^*$ absorption band; (b) $\lambda_{exc} = 405$ nm; (c) $\lambda_{exc} = 405$ nm and using 1,2-bis(5-chloro-2-methyl-3-thienyl)perfluorocyclopentene as a reference ($\Phi_{ring\ opening} = 0.13$ in hexane³⁷).



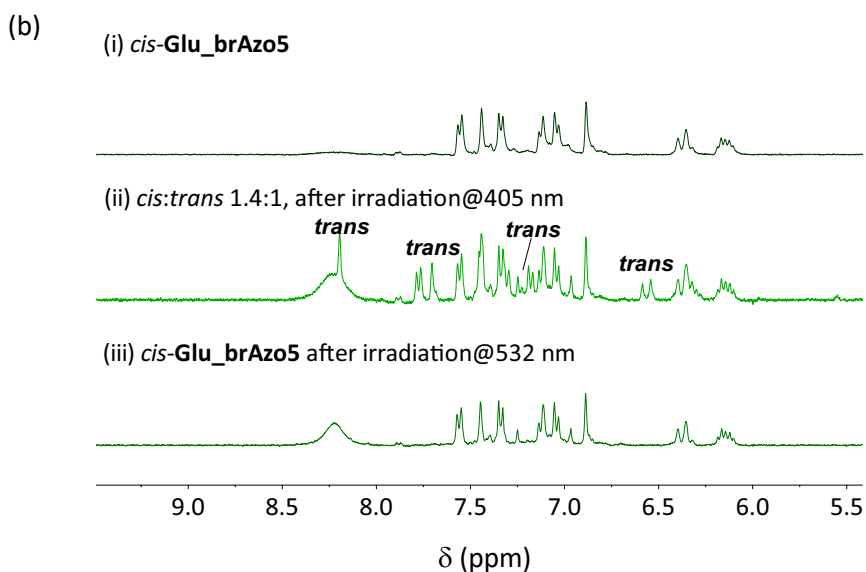


Figure V-11. (a) Low field region of the ^1H NMR spectra (360 MHz, $\text{DMSO-}d_6$) of **Glu_brAzo4**: (i) freshly prepared (*cis* isomer); (ii) after irradiation at $\lambda_{\text{exc}} = 405$ nm for 3 h (*cis:trans*, 1:1.25 mixture); (iii) after irradiation of (ii) at $\lambda_{\text{exc}} = 532$ nm for 3 h (*cis* isomer). (b) Low field region of the ^1H NMR spectra (400 MHz, $\text{DMSO-}d_6$) of **Glu_brAzo5**: (i) freshly prepared (*cis* isomer); (ii) after irradiation at $\lambda_{\text{exc}} = 405$ nm for 3 h (*cis:trans*, 1.4:1 mixture); (iii) after irradiation of (ii) at $\lambda_{\text{exc}} = 532$ nm for 3 h (*cis* isomer).

V.3.2. *TRANS*→*CIS* ISOMERISATION

The *trans*→*cis* isomerisation of diazocine-based PCLs **Glu_brAzo4-5** can proceed either photochemically or thermally. Therefore, both processes were fully investigated.

The photochemical *trans*→*cis* back-isomerisation was studied by irradiation at $\lambda_{\text{exc}} = 532$ nm of the $\text{PSS}_{\text{cis-trans}}$ mixtures obtained for compounds **Glu_brAzo4-5**. The spectral changes in absorption observed were consistent with *trans*→*cis* photoisomerisation: the red-shifted $n\rightarrow\pi^*$ band characteristic of the *trans* isomer disappeared, while that corresponding to the *cis* state was recovered (Figure V-12). In this case, the *cis* isomer did not absorb at the excitation wavelength and, thus, photoisomerisation proceeded quantitatively to fully regenerate the initial *cis* isomer, as demonstrated ^1H NMR experiments (Figure V-11). In addition, *trans*→*cis* photoisomerisation quantum yields ($\Phi_{\text{trans}\rightarrow\text{cis}}$) of **Glu_brAzo4-5** were also found to be very large (0.86 for **Glu_brAzo4** and 0.89 for **Glu_brAzo5**, Table V-3) in contrast to the values determined for the light-induced *cis*→*trans* conversion.

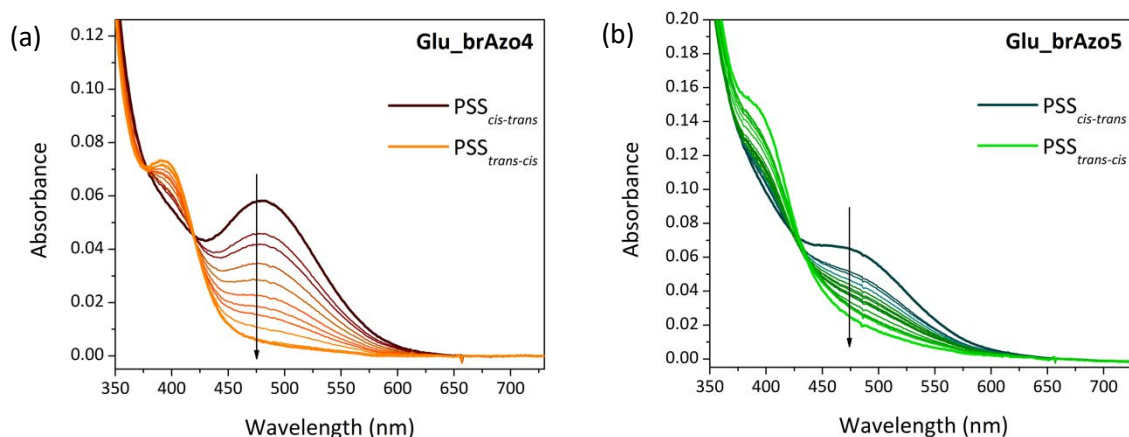


Figure V-12. Variation of the absorption spectra of (a) **Glu_brAzo4** and (b) **Glu_brAzo5** in PBS:DMSO 1:1 upon irradiation at $\lambda_{\text{exc}} = 532$ nm of the *cis-trans* photostationary mixture previously prepared $\lambda_{\text{exc}} = 405$ nm. The arrows indicate the direction of the changes observed.

Table V-3. Results of the *trans*→*cis* isomerisation process of **Glu_brAzo4-5** in PBS:DMSO 1:1.

Compound	<i>cis</i> PSS (%) ^a	$\Phi_{\text{trans} \rightarrow \text{cis}}^{\text{b}}$	$\tau_{\text{trans}}^{\text{c}}$ (h)
Glu_brAzo4	100	0.86	5.6
Glu_brAzo5	100	0.89	6.8

(a) $\lambda_{\text{exc}} = 532$ nm. (b) $\lambda_{\text{exc}} = 532$ nm and using 1,2-bis(5-chloro-2-methyl-3-thienyl)perfluorocyclopentene as a reference. (c) Measured at room temperature.

Because of the reversible photoinduced switching observed for **Glu_brAzo4-5**, the fatigue resistance of both compounds was investigated. For this, they were submitted to 10 consecutive irradiation cycles at $\lambda_{\text{exc}} = 405$ nm (to induce *cis*→*trans* photoisomerisation) and 532 nm (to induce *trans*→*cis* photoisomerisation), and the variation of the $n \rightarrow \pi^*$ absorption band of the *trans* isomer was recorded (Figure V-13). As clearly shown, no photodegradation was observed for any of the compounds under study.

As reported for other C_2 -bridged azobenzenes,¹⁴⁻²³ the *trans* isomer of **Glu_brAzo4-5** generated under irradiation could also back-isomerise to the initial *cis* state thermally in the dark. Therefore, we investigated the thermal *trans*→*cis* back-isomerisation process of these compounds by recording the spectral changes in a *cis-trans* mixture of **Glu_brAzo4-5** over time in the dark by UV-vis absorption spectroscopy. A clear decrease in the intensity of the characteristic red-shifted *trans* isomer band could be observed in time, which was plotted and fitted with a monoexponential growth function (Figure V-14). In this way we could prove the first order rate kinetics of *trans*-**Glu_brAzo4-5** back-isomerisation and determine the lifetimes

of these isomers at room temperature in the dark: $\tau_{trans} = 5.6$ h and 6.8 h for **Glu_brAzo4** and **Glu_brAzo5**, respectively (Figure V-14, Table V-3).

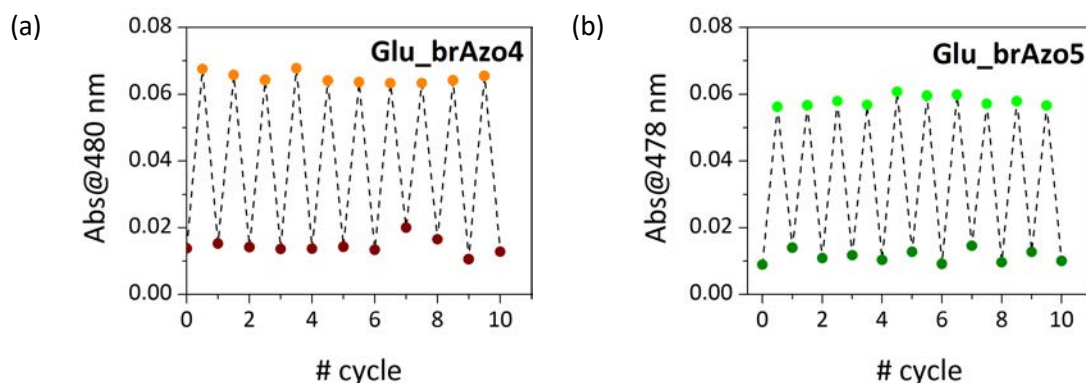


Figure V-13. Variation of the absorption at 480 nm and 478 nm of (a) **Glu_brAzo4** and (b) **Glu_brAzo5** in PBS:DMSO 1:1 upon consecutive cycles of *cis-trans* ($\lambda_{exc} = 405$ nm) and *trans-cis* photoisomerisation ($\lambda_{exc} = 532$ nm).

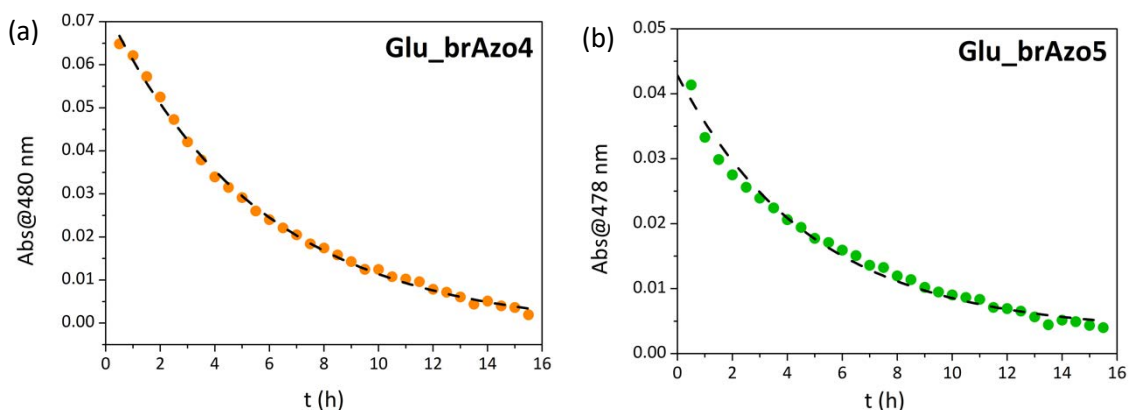


Figure V-14. Variation of the absorption of the *cis-trans* photostationary state mixture of (a) **Glu_brAzo4** and (b) **Glu_brAzo5** in the dark at 25 °C in PBS:DMSO 1:1. At these conditions, thermal *trans-cis* back-isomerisation takes place, thus restoring the initial concentration of the *cis* state of the ligands, which presents a smaller extinction coefficient at $\lambda_{abs} = 480$ nm and $\lambda_{abs} = 478$ nm for **Glu_brAzo4** and **Glu_brAzo5**, respectively. Points correspond to the experimental data, while dashed lines were obtained from monoexponential fits.

In conclusion, our spectroscopic experiments in solution demonstrated that **Glu_brAzo4-5** preserve the photochemical properties of their diazocine photochrome: (i) they can efficiently photoswitch between their *cis* and *trans* isomers without apparent degradation, and (ii) the *cis* state is their thermodynamically stable isomer, while their *trans* state spontaneously back-isomerises in the dark, although at a rather low rate at room temperature in aqueous media. In

view of this, **Glu_brAzo4-5** should be capable to behave as photoresponsive agonists of iGluRs that can be administered in their inactive form and be selectively activated upon irradiation.

V.4. EVALUATION OF THE LIGHT-INDUCED BIOLOGICAL ACTIVITY OF PCLs **Glu_brAzo4** AND **Glu_brAzo5**

After evaluating the photochemical properties of novel diazocine-based PCLs **Glu_brAzo4** and **Glu_brAzo5**, we assessed their capability to control ionotropic glutamate receptors in living cells under illumination. For that purpose, we conducted electrophysiological experiments on cultured cells and on hippocampal rat organotypic slices. These experiments were performed in collaboration with Aida Garrido-Charles in the laboratories of the research group of Prof. Pau Gorostiza at the *Institut de Bioenginyeria de Catalunya* (IBEC). The results obtained are described in this section.

V.4.1. EVALUATION OF THE OPTICAL ACTIVITY OF **Glu_brAzo4** and **Glu_brAzo5** ON CULTURED CELLS

In order to evaluate the capacity of **Glu_brAzo4** and **Glu_brAzo5** to light-gate iGluRs, electrophysiological experiments were conducted in HEK293 cells expressing either GluK1 or GluK2 receptors. In particular, whole-cell voltage clamp measurements were conducted (see § III.4) to record the variation of currents through cell membrane triggered by our compounds, whose activation should cause iGluR channel opening and ion flux from the extra- to the intracellular medium.

In general, the experiments consisted in perfusing different concentrations of the compound of interest to the cell culture and applying variable illumination conditions to induce reversible *cis*→*trans* and *trans*→*cis* photoisomerisation of the PCL. As depicted in Figure V-8b, this should result in geometrical changes between the *cis* and *trans* states, which should interact differently with the binding site of the receptor and elicit changes in the electrophysiological signals measured. Moreover, all the experiments performed had two additional common features: (i) cells were exposed to 300 μM concentration of free glutamate either at the beginning or at the end of the recording, which allowed us to determine the cell maximum response and

demonstrate no inhibition of the endogenous behaviour of iGluRs caused by our PCLs; and (ii) cells were previously incubated with Concanavalin A to inhibit endogenous desensitisation of the receptors after ligand-binding site interaction, which resulted in larger responses evoked.

Our first set of experiments was focused on the assessment of the ability of **Glu_brAzo4-5** to control iGluRs activity by simply switching between their *cis* and *trans* isomers. For this we chose a constant 100 μM concentration of the PCLs and irradiation with violet light ($\lambda_{\text{exc}} = 390 \text{ nm}$, to induce *cis*→*trans* photoisomerisation) and green light ($\lambda_{\text{exc}} = 530 \text{ nm}$, to trigger *trans*→*cis* back-isomerisation). As plotted in Figure V-15, clear repetitive and reproducible electrophysiological signals were recorded in this way for GluK1- and GluK2-expressing cells perfused either with **Glu_brAzo4** or **Glu_brAzo5**. It must be noted that more negative signals in these measurements correspond to larger inward currents (i.e. to more efficient ion channel opening). Therefore, our results indicate preferential interaction between the receptors binding site of GluK1 and GluK2 and the *trans* state of the ligands generated under photoexcitation with violet light. Consequently, **Glu_brAzo4-5** preserve the *trans*-active agonist behaviour reported for **GluAzo** despite replacing its azobenzene photochrome with a diazocine. By contrast, they show *cis* stability, which allows to minimise biological responses in the dark.

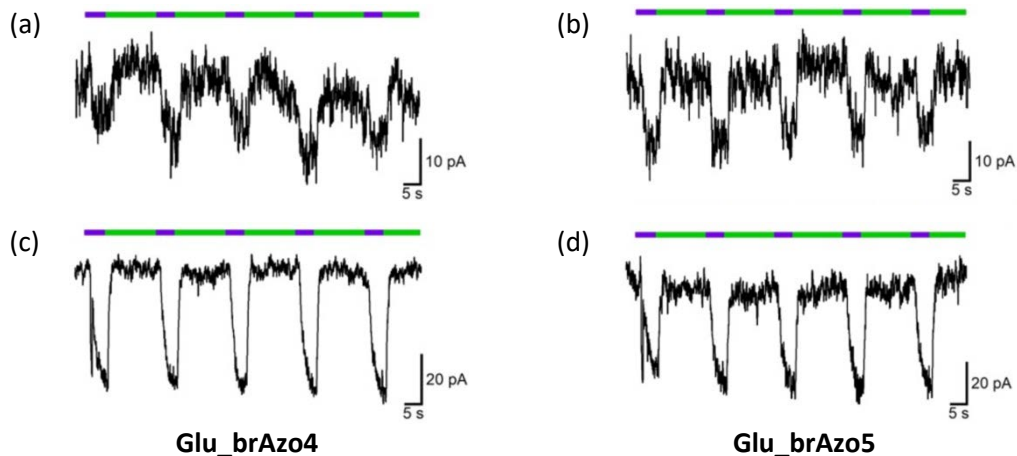


Figure V-15. Light-dependent inward currents measured for HEK293 cells expressing GluK1 and GluK2. (a-b) HEK293 cells transfected with GluK1 and perfused with (a) *cis*-**Glu_brAzo4** and (b) *cis*-**Glu_brAzo5** (100 μM). (c-d) HEK293 cells transfected with GluK2 and perfused with (c) *cis*-**Glu_brAzo4** and (d) *cis*-**Glu_brAzo5** (100 μM). Light pulses at $\lambda_{\text{exc}} = 390 \text{ nm}$ (purple bars) were employed to induce *cis*→*trans* photoisomerisation, which in all the cases resulted in larger electrophysiological currents (i.e. receptor activation and channel opening). Irradiation at $\lambda_{\text{exc}} = 530 \text{ nm}$ (green bars) was used to trigger *trans*→*cis* back-isomerisation and recover the initial signal (i.e. receptor deactivation and channel closing).

Afterwards, we recorded the activation and deactivation spectra of **Glu_brAzo4** and **Glu_brAzo5** by scanning the excitation wavelength used to *cis*→*trans* and *trans*→*cis* photoisomerisation, respectively (Figure V-16). These experiments were performed to identify the irradiation conditions that permitted achieving maximal biological responses. Maximal inward currents arising from receptor activation were measured at $\lambda_{\text{exc}} = 390\text{-}400$ nm and minimal signals due to receptor deactivation were recorded at $\lambda_{\text{exc}} > 450$ nm. As expected, the activation and deactivation spectra determined nicely correlated to the absorption spectra recorded in solution.

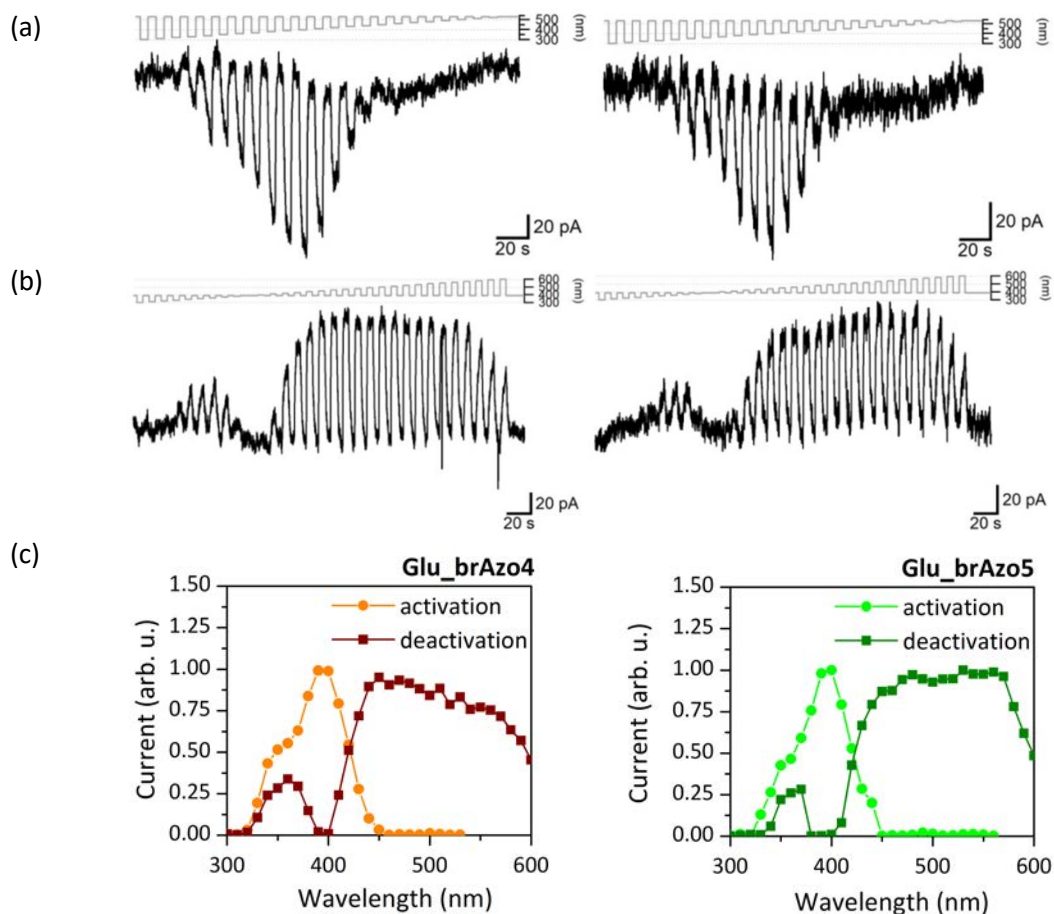


Figure V-16. (a) Light-dependent inward currents measured for **Glu_brAzo4** (left, 100 μM) and **Glu_brAzo5** (right, 100 μM) in HEK293 cells transfected with GluK2, where wavelength excitation to promote *cis*→*trans* photoisomerisation and receptor activation ranges from 300 nm to 530 nm. In all the cases, *trans*→*cis* back-isomerisation was achieved with pulses at $\lambda_{\text{exc}} = 530$ nm. (b) Light-dependent inward currents measured for **Glu_brAzo4** (left, 100 μM) and **Glu_brAzo5** (right, 100 μM) in HEK293 cells transfected with GluK2, where wavelength excitation to promote *trans*→*cis* photoisomerisation and receptor deactivation ranges from 300 nm to 600 nm. In all the cases, *cis*→*trans* isomerisation was previously conducted with pulses at $\lambda_{\text{exc}} = 390$ nm. (c) Activation and deactivation spectra of **Glu_brAzo4** (left, orange) and **Glu_brAzo5** (right, green) in GluK2-expressing HEK293 cells derived from the measurements in (a) and (b).

Finally, dose-response experiments were conducted to quantify the difference in activity of both isomers of **Glu_brAzo4-5** in GluK1- and GluK2-expressing cells. With this aim, solutions of four different concentrations of each compound (10, 30, 100 and 300 μM) were perfused to these cells and the responses evoked in the dark (i.e. for *cis*-**Glu_brAzo4-5**) or upon stimulation at $\lambda_{\text{exc}} = 390 \text{ nm}$ (i.e. for PSS_{*cis-trans*} of **Glu_brAzo4-5**) were recorded (Figure V-17). As expected from previous experiments, larger inward currents arose from the PSS_{*cis-trans*} mixture generated from the irradiation of the initial *cis* isomer. However, low-to-moderate photoinduced modulation (ca. 10-35% current increase with respect to the dark) was observed and the maximal values obtained were only about 20-40% of those triggered by free glutamate at 300 μM . These results can be attributed to three main factors. First, incomplete photoconversion into the more active *trans* isomer upon irradiation at $\lambda_{\text{exc}} = 390 \text{ nm}$, as previously determined in solution (< 60%, Table V-2). As a result, lower signals with reduced photomodulation were obtained than if *cis*→*trans* photoisomerisation occurred quantitatively. Second, steric hindrance of the diazocine group with respect to free glutamate even in its extended *trans* configuration, which lowers the affinity towards the receptor binding site. Third, limited modification of the glutamate-binding site affinity upon *cis*→*trans* isomerisation. This is somewhat surprising in light of the results obtained for **GluS** compounds in Chapter IV: *cis*→*trans* photoisomerisation in these disubstituted stilbene derivatives did lead to large changes in biological response in GluK2-expressing HEK293 cells (see § IV.4). Structural differences between the stilbene and diazocines cores of these compounds and their substitution patterns (4,4'-stilbenes vs 3,3'-diazocines) should account for the lower modulation registered for **Glu_brAzo4-5** under irradiation.

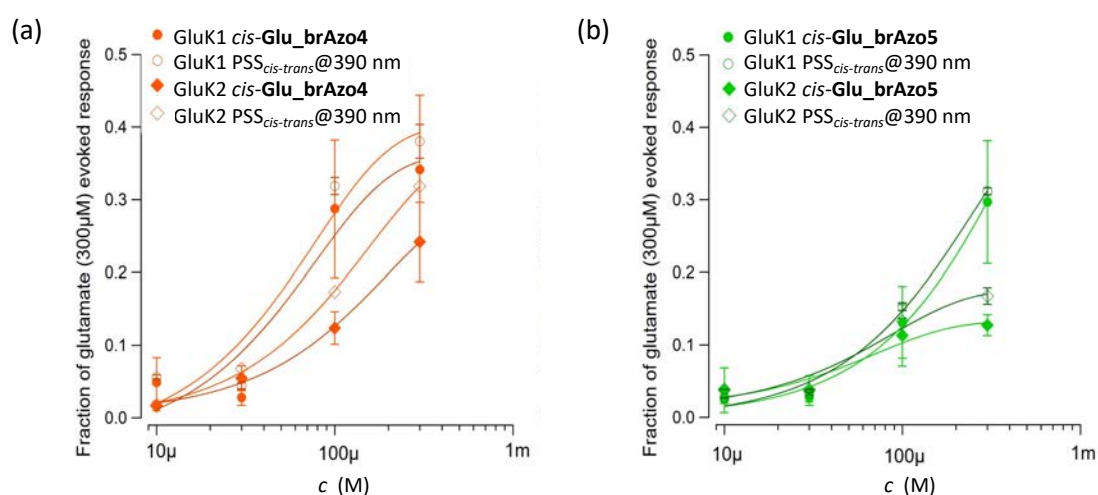
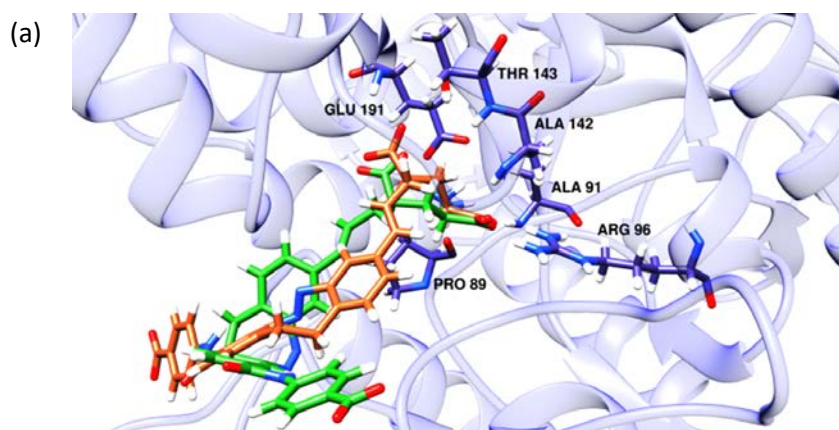


Figure V-17. (a) Dose-response curves of (a) **Glu_brAzo4** and (b) **Glu_brAzo5** in HEK293 cells transfected with GluK1 and GluK2. Measurements were conducted from 10 to 300 μM for their *cis* isomer and the *trans-cis* mixture obtained at $\lambda_{\text{exc}} = 390 \text{ nm}$ (PSS_{*cis-trans*}@390 nm).

From the experiments conducted it could be determined that both **Glu_brAzo4** and **Glu_brAzo5** present higher light-induced selectivity for GluK2, even though lower inward currents were registered with this receptor. This selectivity could be ascribed to the narrower ligand-binding cavity of GluK2 with respect to GluK1,³⁸ which may interact less efficiently with the *cis* isomer of the ligand due to higher steric effects with the appended diazocine.

Moreover, the effect of a bulky group tethered to the diazocine photoswitch could be analysed. On one hand, the presence of this group was found to enhance the difference in response obtained when switching between *cis* and *trans* configurations of the ligand (at 300 μ M: 12% (GluK1) and 35% (GluK2) for **Glu_brAzo4** vs 6% (GluK1) and 26% (GluK2) for **Glu_brAzo5**), as expected from our design, though it is also affected by the more *trans*-enriched PSS_{*cis-trans*} generated for **Glu_brAzo4**. On the other hand, the presence of the bulky group surprisingly did not diminish the absolute value of the biological signals obtained, but the opposite, larger inward currents were recorded. In order to understand this counterintuitive result, molecular docking calculations were performed by Àngels González and Josep M. Lluch of the Chemistry Department of the *Universitat Autònoma de Barcelona* for the two isomers of **Glu_brAzo4-5** on GluK2. These studies were performed keeping the protein rigid and optimising the initial geometries of the PCLs at the B3LYP/6-31G(d) level. The results obtained showed that, for all the compounds, the best docking solutions placed the glutamate moiety of the ligands in a very similar position as with *trans*-**GluAzo**,³⁹ thus suggesting a similar interaction via hydrogen bonds. However, different binding arrangement was observed for **Glu_brAzo4** and **Glu_brAzo5** (Figure V-18). Larger affinity of the *trans* isomer of **Glu_brAzo4** and **Glu_brAzo5** was observed in these figures, which confirmed that our ligands displayed the *trans*-active behaviour expected from their design. In addition, higher binding efficiency was confirmed for **Glu_brAzo4**, which arises from the additional attractive hydrogen bonding and lipophilic interactions formed between its bulky group and the receptor (Figure V-18a).



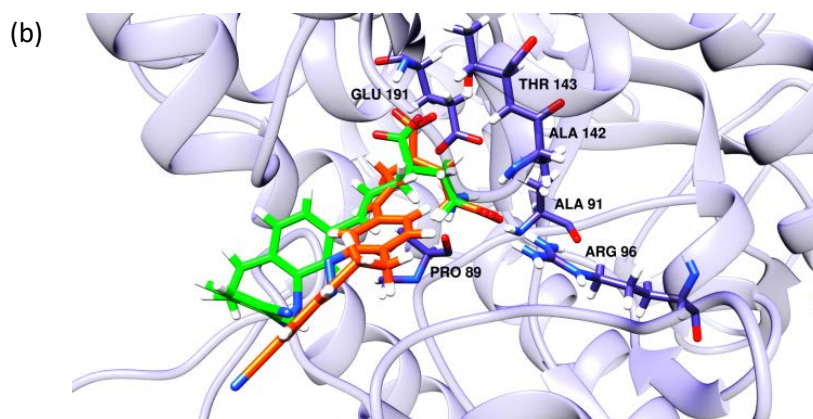


Figure V-18. The best docking solutions for (a) *trans*-**Glu_brAzo4** (orange) and *cis*-**Glu_brAzo4** (green); and (b) *trans*-**Glu_brAzo5** (orange) and *cis*-**Glu_brAzo5** (green) in GluK2. The protein residues interacting with the glutamate groups are also indicated. Oxygen, nitrogen and hydrogen atoms are depicted in red, blue and white, respectively.

V.4.2. EVALUATION OF THE OPTICAL ACTIVITY OF **Glu_brAzo4** and **Glu_brAzo5** ON HIPPOCAMPAL RAT ORGANOTYPIC SLICES

In view of the fairly good results obtained on cultured cells, we decided to test **Glu_brAzo4** and **Glu_brAzo5** activity as photoswitchable neurotransmitters in neuronal cells embedded in their physiological environment. Hence, we performed experiments in hippocampal rat organotypic slices containing neurons where GluK2 is highly expressed.⁴⁰ Importantly, the experiments were performed without the incubation of Concanavalin A to inhibit desensitisation, which implies that the measurements truly reported on intact neuronal gating and connectivity.

Initially, the physiological behaviour of the neurons was unaltered upon perfusion of either *cis*-**Glu_brAzo4** or *cis*-**Glu_brAzo5** in the dark (Figure V-19). This was due to their *trans*-active, *cis*-stable behaviour, which enables administration of the inactive isomer, thus providing a clear advantage over most PCLs reported for glutamate receptors to date (e.g. **GluAzo**).^{4-7,9-12} By contrast, clear changes in current through all membrane and neuronal firing were selectively induced upon *cis*→*trans* photoisomerisation of **Glu_brAzo4** at relatively low concentrations (30 μM) and weak light intensities (22.0 and 47.4 $\mu\text{W mm}^{-2}$ at $\lambda_{\text{exc}} = 390$ and 530 nm, respectively); (Figure V-19a). Actually, when monitoring the variation of membrane potential under irradiation, the generation of sequential and sustained trains of action potentials were observed with **Glu_brAzo4** after consecutively switching between violet and green light illumination, even at low irradiation powers and high excitation frequencies (up to 1 Hz, Figure V-20a-c).

Noticeably, the **Glu_brAzo4**-photoinduced behaviour could be inhibited by the addition of 6,7-dinitroquinoxaline-2,3-dione (DNQX),⁴¹ a well-known antagonist of kainate and AMPA GluRs (Figure V-20d), which confirmed that the efficient photomodulation of neuronal activity with **Glu_brAzo4** was triggered by its light-dependent interaction with GluK2.

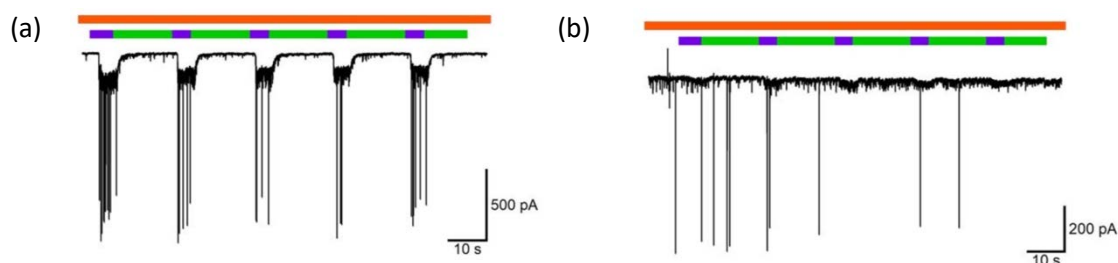


Figure V-19. Whole-cell voltage clamp recording of rat hippocampal neurons in culture. Perfusion of 30 μM of (a) *cis*-**Glu_brAzo4** and (b) *cis*-**Glu_brAzo5**. Light activation is induced by pulses at $\lambda_{\text{exc}} = 390$ and 530 nm (purple and green bars, respectively).

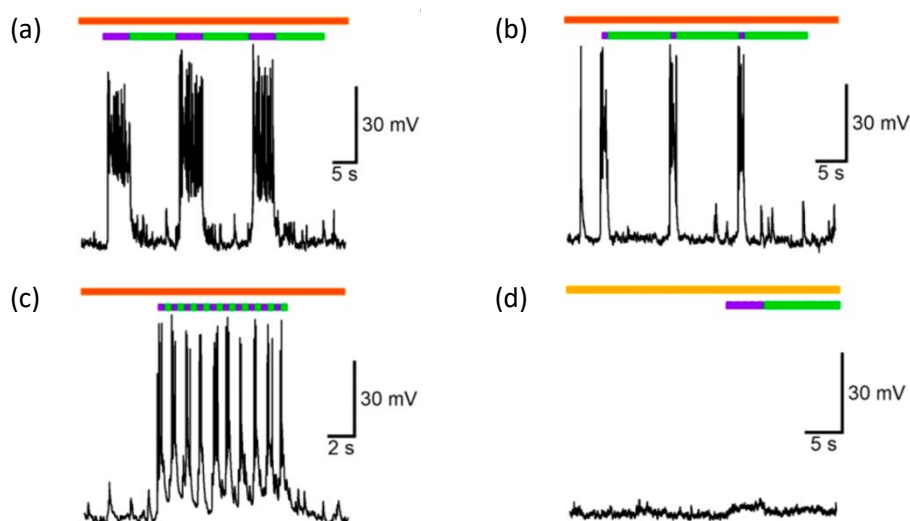


Figure V-20. Whole-cell current clamp recordings of rat hippocampal neurons in culture after perfusion of *cis*-**Glu_brAzo4** (30 μM) and irradiation at $\lambda_{\text{exc}} = 390$ (violet) and 530 (green) nm. Successful neuron activation was observed with 390 nm light pulses of (a) 5 s, (b) 1 s, and (c) 0.5 s (1 Hz stimulation), while it was inhibited upon perfusion of DNQX (10 μM). Neurons were current clamped at -60 mV.

Two rather surprising results were obtained in our electrophysiological measurements on rat hippocampal neurons. On one hand, no light-induced activity could be measured for **Glu_brAzo5** (Figure V-19b), though this PCL could induce photoresponses in cultured cells. On the other hand, a striking contrast was found between the clean physiological effect achieved with **Glu_brAzo4** in neurons and the limited modulation recorded in GluK2-expressing HEK293 cells for this compound (*ca.* 20% at 30 μM concentration). This can be accounted to the well-

known non-linear behaviour of neuronal signalling: only a minimum fraction of glutamate receptors needs to interact with the ligand to overcome the depolarisation threshold required to initiate an action potential.⁴ According to our results, this means that only *trans*-**Glu_brAzo4** could surpass such threshold at the current experimental conditions and thus trigger action potentials. This can be ascribed to its larger affinity for GluK2 with respect to *trans*-**Glu_brAzo5** and their *cis* isomers, as revealed by our measurements in cultured cells.

To sum up, the biological experiments conducted both in cultured cells and neurons demonstrate the potential of C₂-bridged azobenzene-based PCLs to optically-modulate the activity of iGluRs and light-control neural signalling. Importantly, this type of compounds preserve the larger activity typically observed for their *trans* state while ensuring higher stability for the inert *cis* isomer, thus enabling direct administration of the inactive isomer in contrast to common azobenzene-based PCLs.

V.5. CONCLUSIONS

In this chapter, the synthesis, characterisation and biological activity of new bridged azobenzene-based PCLs for the optical control of ionotropic glutamate receptors have been reported. Several, **Glu_brAzo** compounds were designed inspired by the molecular structure of **GluAzo**,⁴ by replacing its azobenzene photoswitch with a diazocine (either sulfur-bridged or ethylene-bridged, Figure V-21). The main idea behind these new compounds was to obtain *trans*-active PCLs whose thermodynamically stable state was its *cis* isomer, thus reverting the *trans*-active, *trans*-stable behaviour reported for most azobenzene-based ligands to date.

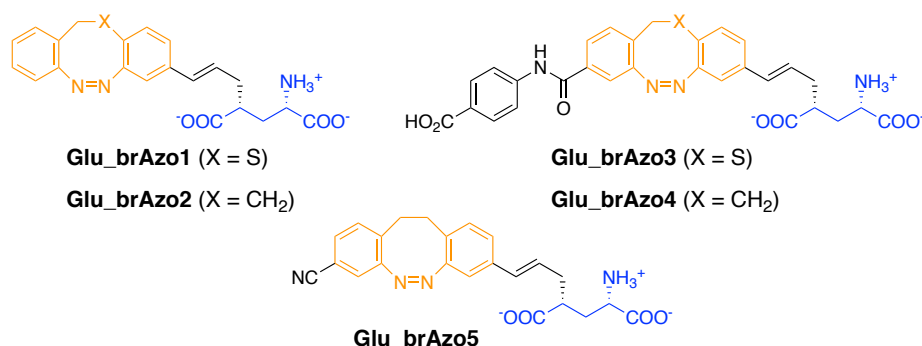


Figure V-21. Structure of the bridged azobenzene-based PCLs designed for the optical control of iGluRs with *trans*-active and *cis*-stable behaviour. Only **Glu_brAzo4** and **Glu_brAzo5** were finally successfully synthesised.

The main conclusions obtained from the studies conducted in **Glu_brAzo** are:

- Sulfur-bridged **Glu_brAzo1** and **Glu_brAzo3** could not be synthesised due to the low stability of the *S*-heterodiazocine core in the reaction conditions (i.e. acid or basic media and high temperatures). Moreover, the preparation of **Glu_brAzo2** was not possible for the difficulties encountered in the reduction of intermediate dinitrostilbene **73**. **Glu_brAzo5**, derived from the synthesis of **Glu_brAzo4**, finally emerged as an analogue to the monosubstituted **Glu_brAzo2**.
- The linear synthetic strategy designed to afford the **Glu_brAzo4** and **Glu_brAzo5** proved to be robust and reproducible, and provided these bridged azobenzene-based PCLs in 8 steps in 3% overall yield and 6 steps in 8% overall yield from commercially available 4-bromo-2-nitrotoluene, respectively. The novel oxidation-mediated methodology developed for the ring closing reaction of **87** enabled the obtention of diazocines in a better yield than those previously reported^{15-18,20-23} following a more robust and reproducible procedure.
- The photochemical studies in solution and biological measurements conducted in GluK1- and GluK2-expressing cells confirmed that **Glu_brAzo4-5** exhibit a *trans*-active, *cis*-stable behaviour. These compounds could be administered on cultured cells in their *cis* inactive form and be photoisomerised into the *trans* state, thus triggering an increase of the inward currents registered.
- Low-to-moderate photoinduced modulation of GluK1 and GluK2 activity was obtained with **Glu_brAzo4-5**. Moreover, the PCLs developed were found to be a partial agonist of GluK1 and GluK2 (i.e. the maximal inward currents registered were only about 20-40% of those triggered by free glutamate at 300 μ M).
- The introduction of a lateral bulky group was found to enhance the activity of the PCL by: (i) enabling better modulation upon photoisomerisation due to steric effects; and (ii) evoke larger inward currents, owing to additional attractive hydrogen bonding and lipophilic interactions formed between this bulky group and the receptor, which were demonstrated by molecular docking calculations.
- **Glu_brAzo4** has proved to efficiently trigger action potentials in hippocampal neurons upon stimulation with violet ($\lambda_{exc} = 390$ nm) light without background activity in the dark, despite the limited modulation recorded in GluK2-expressing HEK293 cells for this compound, which can be ascribed to the non-linear behaviour of neuronal systems.

To sum up, the results reported in this chapter demonstrate that bridged azobenzene-based PCLs are synthetically accessible and display convenient properties to arise as new photopharmacological tools for the optical control of iGluRs and other receptors, allowing direct administration of the inactive form in the dark, which can then be selectively activated upon irradiation, thus surpassing one of the main drawbacks of current azobenzene-based PCLs. Actually, during the publication of this work, two other reports of the potential of the application of diazocines in photopharmacology appeared: (i) Ellis-Davies and co-workers reported bridged azobenzene derivatives for the optical modulation of NMDA receptors and potassium ion channels activity (Figure V-22a),⁴² for which a low-yield 4-monosubstituted diazocine previously described was employed;²¹ and (ii) Trauner and co-workers reported two bridged azobenzene-based PCLs for the control of voltage-gated potassium channels and G-protein-coupled inwardly rectifying potassium (GIRK) channels (Figure V-22b).⁴³

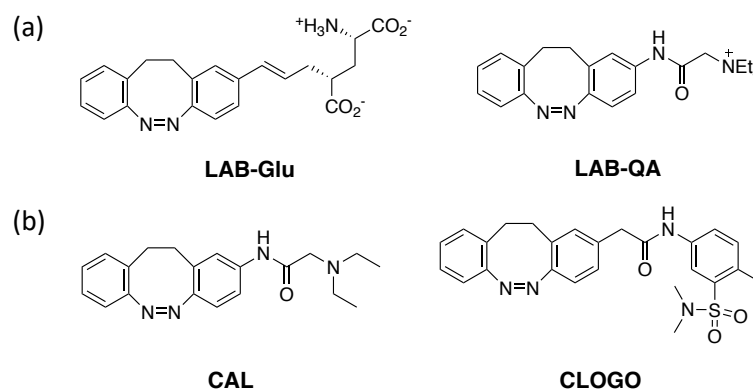


Figure V-22. (a) Bridged azobenzene based PCLs developed by Ellis-Davies and co-workers for the optical modulation of NMDA receptors (**LAB-Glu**) and potassium ion channels (**LAB-QA**) activity.⁴² (b) Bridged azobenzene based PCLs developed by Trauner and co-workers for the optical control of voltage-gated potassium channels (**CAL**) and GIRK channels (**CLOGO**).⁴³

V.6. REFERENCES

- (1) Hüll, K.; Morstein, J.; Trauner, D. *Chem. Rev.* **2018**, *118*, 10710-10747.
- (2) Broichhagen, J.; Frank, J. A.; Trauner, D. *Acc. Chem. Res.* **2015**, *48*, 1947-1960.

- (3) Szymansky, W.; Bierle, J. M.; Kistemarker, H. A. V.; Velema, W. A.; Feringa, B. L. *Chem. Rev.* **2013**, *113*, 6114-6178.
- (4) Volgraf, M.; Gorostiza, P.; Szobota, S.; Helix, M. R.; Isacoff, E. Y.; Trauner, D. *J. Am. Chem. Soc.* **2007**, *129*, 260-261.
- (5) Pittolo, S.; Gómez-Santacana, X.; Eckelt, K.; Rovira, X.; Dalton, J.; Goudet, C.; Pin, J-P.; Llobet, A.; Giraldo, J.; Llebaria, A.; Gorostiza, P. *Nat. Chem. Biol.* **2014**, *10*, 813-815.
- (6) Bandara, H. M. D.; Burdette, S. C. *Chem. Soc. Rev.* **2012**, *41*, 1809-1825.
- (7) Stawski, P.; Sumser, M.; Trauner, D. *Angew. Chem. Int. Ed.* **2012**, *51*, 5748-5751.
- (8) Laprell, L.; Repak, E.; Franckevicius, V.; Hartrampf, F.; Terhag, J.; Hollmann, M.; Sumser, M.; Rebola, N.; DiGregorio, D. A.; Trauner, D. *Nat. Commun.* **2015**, *6*, 8076.
- (9) Barber, D. M.; Liu, S-A.; Gottschling, K.; Sumser, M.; Hollmann, M.; Trauner, D. *Chem. Sci.* **2017**, *8*, 611-615.
- (10) Gómez-Santacana, X.; Pittolo, S.; Rovira, X.; Lopez, M.; Zussy, C.; Dalton, J. A. R.; Faucherre, A.; Jopling, C.; Pin, J-P.; Ciruela, F.; Goudet, C.; Giraldo, J.; Gorostiza, P.; Llebaria, A. *ACS Cent. Sci.* **2017**, *3*, 81-91.
- (11) Hartrampf, F. W. W.; Barber, D. M.; Gottschling, K.; Leippe, P.; Hollmann, M.; Trauner, D. *Tetrahedron* **2017**, *73*, 4905-4912.
- (12) Rovira, X.; Trapero, A.; Pittolo, S.; Zussy, C.; Faucherre, A.; Jopling, C.; Giraldo, J.; Pin, J-P.; Gorostiza, P.; Goudet, C.; Llebaria, A. *Cell Chem. Biol.* **2018**, *23*, 929-934.
- (13) Nørager, N. G.; Poulsen, M. H.; Strømgaard, K. *J. Med. Chem.* **2018**, *61*, 8048-8053.
- (14) Siewertsen, R.; Neumann, H.; Buchheim-Stehn, B.; Herges, R.; Nather, C.; Renth, F.; Temps, F. *J. Am. Chem. Soc.* **2009**, *131*, 15594-15595.
- (15) Sell, H.; Nather, C.; Herges, R. *Beilstein J. Org. Chem.* **2013**, *9*, 1-7.
- (16) Tellkamp, T.; Shen, J.; Okamoto, Y.; Herges, R. *Eur. J. Org. Chem.* **2014**, *25*, 5456-5461.
- (17) Hammerich, M.; Schütt, C.; Stahler, C.; Lentjes, P.; Rohricht, F.; Höppner, R.; Herges, R. *J. Am. Chem. Soc.* **2016**, *138*, 13111-13114.
- (18) Moormann, W.; Langbehn, D.; Herges, R. *Synthesis* **2017**, *49*, 3471-3475.
- (19) Moormann, W.; Langbehn, D.; Herges, R. *Beilstein J. Org. Chem.* **2019**, *16*, 727-732.

- (20) Samanta, S.; Qin, C. G.; Lough, A. J.; Woolley, G. A. *Angew. Chem. Int. Ed.* **2012**, *51*, 6452-6455.
- (21) Joshi, D. K.; Mitchell, M. J.; Bruce, D.; Lough, A. J.; Yan, H. *Tetrahedron* **2012**, *68*, 8670-8676.
- (22) Eljabu, F.; Dhruval, J.; Yan, H. *Bioorg. Med. Chem. Lett.* **2015**, *25*, 5594-5596
- (23) Jun, M.; Joshi, D. K.; Yalagala, R. S.; Vanloon, J.; Simionescu, R.; Lough, A. J.; Gordon, H. L.; Yan, H. *ChemistrySelect* **2018**, *3*, 2697-2701.
- (24) Duval, H. *Bull. Soc. Chim. Fr.* **1910**, *7*, 727.
- (25) Paudler, W. W.; Zeiler, A. G. *J. Org. Chem.* **1969**, *34*, 3237.
- (26) Tauer, E.; Machinek, R. *Liebigs. Ann.* **1996**, 1213.
- (27) Schehr, M.; Hugensch, D.; Moje, T.; Näther, C.; Herges, R. *Beilstein J. Org. Chem.* **2018**, *14*, 2799-2804.
- (28) Baeyer, A. *Ber. Dtsch. Chem. Ges.* **1874**, *7*, 1638-1640.
- (29) Mills, C. *J. Chem. Soc. Trans.* **1895**, *67*, 925-933.
- (30) Bamberger, E. *Ber. Dtsch. Chem. Ges.* **1896**, *29*, 102-104.
- (31) Wittig, G.; Schöllkopf, U. *Chem. Ber.* **1954**, *87*, 1318-1330.
- (32) Conrad, W. E.; Rodriguez, K. X.; Nguyen, H. H.; Fettingner, J. C.; Haddadin, M. J.; Kurth, M. *J. Org. Lett.* **2012**, *14*, 3870-3873.
- (33) Chaudhuri, N. K.; Ball, T. J. *J. Label. Compd. Radiopharm.* **1980**, *18*, 1189-1196.
- (34) Merino, E. *Chem. Soc. Rev.* **2011**, *40*, 3835-3853.
- (35) Mourrot, A.; Kienzler, M. A.; Banghart, M. R.; Fehrentz, T.; Huber, F. M. E.; Stein, M.; Kramer, R. H.; Trauner, D. *ACS Chem. Neurosci.* **2011**, *2*, 536-543.
- (36) Venkatachalam, T. K.; Huang, H.; Yu, G.; Uckun, F. M. *Synth. Commun.* **2004**, *34*, 1489-1497.
- (37) Higashiguchi, K.; Matsuda, K.; Asano, Y.; Murakami, A.; Nakamura, S.; Irie, M. *Eur. J. Org. Chem.* **2005**, 91-97.
- (38) Mayer, M. L. *Neuron* **2005**, *45*, 539-552.

- (39) Guo, Y.; Wolter, T.; Kubar, T.; Sumser, M.; Trauner, D.; Elstner, M. *PLoS One* **2015**, *10*, No. e0135399.
- (40) Carta, M.; Fievre, S.; Gorlewicz, A.; Mulle, C. *Eur. J. Neurosci.* **2014**, *39*, 1835-1844.
- (41) Honore, T.; Davies, S. N.; Drejer, J.; Fletcher, E. J.; Jacobsen, P.; Lodge, D.; Nielsen, F. E. *Science* **1988**, *241*, 701-703.
- (42) Thapaliya, E. R.; Zhao, J.; Ellis-Davies, G. C. R. *ACS Chem. Neurosci.* **2019**, *10*, 2481-2488.
- (43) Trads, J. B.; Hüll, K.; Matsuura, B. S.; Laprell, L.; Fehrentz, T.; Görldt, N.; Kozek, K. A.; Weaver, D.; Klöcker, N.; Barber, D. M.; Trauner, D. *ChemRxiv* **2019**, 10.26434/chemrxiv.8014580.

CHAPTER VI

Summary and conclusions

Three different projects were developed along this PhD thesis, which involved the synthesis, characterisation and biological evaluation of new photopharmacological tools for the light-induced control of ionotropic glutamate receptors. The main conclusions obtained from the studies conducted in this work are summarised herein.

Many photopharmacological tools have been developed along the years for the optical manipulation of neuronal signalling. Although they have been successfully applied *in vitro* and *in vivo*, the compounds reported to date still suffer from several issues that limit their use. In this thesis, three novel strategies to overcome some of the remaining challenges in this field have been investigated and the activity of the compounds developed has been tested in kainate-type ionotropic glutamate receptors GluK1 and GluK2. These novel approaches are next summarised:

New azobenzene-based PTLs for efficient two-photon neuronal excitation (Figure VI-1). Novel photoswitchable tethered ligands based on push-pull-substituted azobenzene photoswitches that exhibit both high two-photon absorption cross section and slow thermal back-isomerisation have been developed. This was accomplished by wise selection of azobenzene substituents, which were chosen to be weak mesomeric EDGs and EWGs and strong inductive EWGs. These compounds have proved to enable efficient 2P stimulation with NIR light of light-gated ionotropic glutamate receptors. The photoresponses obtained are comparable in intensity to those triggered with 1P stimulation and noticeably surpass those achieved with other azobenzene-based PTLs previously reported. These novel PTLs permitted sustained 2P neuronal stimulation both in light-scattering brain tissue and in *C. elegans* nematodes.

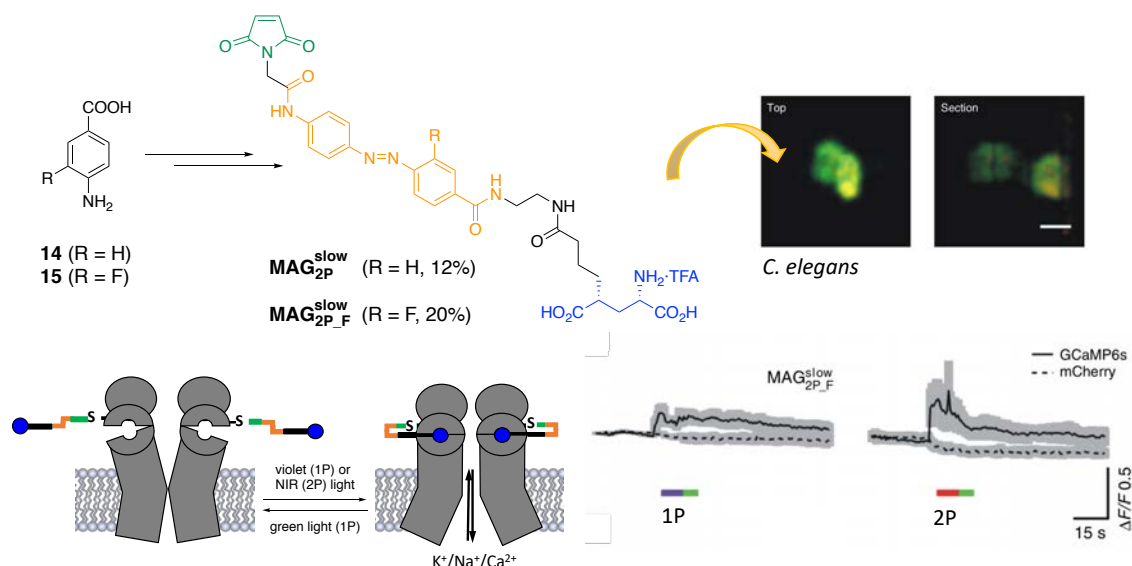


Figure VI-1. New azobenzene-based PTLs for efficient two-photon neuronal excitation.

Stilbene-based non-destructive caged ligands for the optical control of iGluRs (Figure VI-2). A new strategy has been developed for the optical control of iGluRs based on photochromic ligands that enable irreversible and quantitative photoisomerisation from the inactive to the active state, thus performing in a similar fashion as caged ligands but without by-product generation. To do so, stilbene functionalised with a phthalimide unit was chosen as a photoswitch, which enabled quantitative *cis*→*trans* transformation through isomerisation of the radical cation produced by photoinduced electron transfer. As a proof of concept, new glutamate photochromic ligands based on stilbene-phthalimide dyads have been prepared, which have proved to efficiently modulate GluK2 activity upon irradiation with UV light.

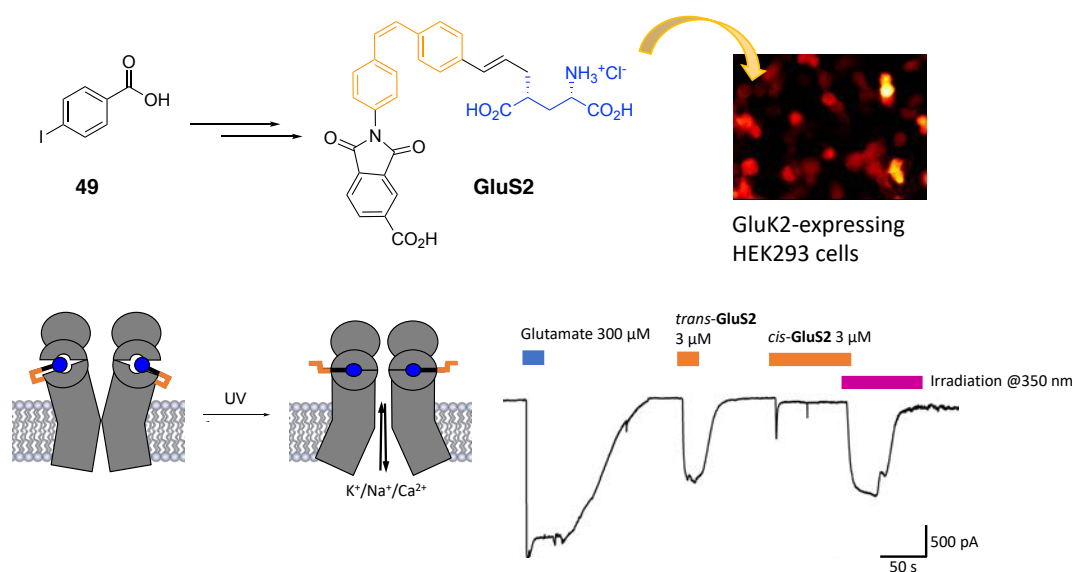


Figure VI-2. Stilbene-based non-destructive caged ligands for the optical control of iGluRs.

Synthetic photoswitchable neurotransmitters based on bridged azobenzenes (Figure VI-3). Novel photochromic ligands based on C₂-bridged azobenzenes (i.e. diazocines) have been prepared following a new methodology that furnishes these photoswitches in higher yields and reproducibility. The compounds developed exhibit singular properties which make them preserve the larger activity towards neural receptors typically observed for the *trans* isomer of azo-based PCLs, while ensuring larger thermal stability for the inert *cis* isomer. The performance of these compounds has been successfully tested on GluK1- and GluK2-expressing cultured cells and rat hippocampal neurons. With these novel PCLs, selective neuronal firing was triggered upon irradiation with visible light and no background activity was observed in the absence of illumination.

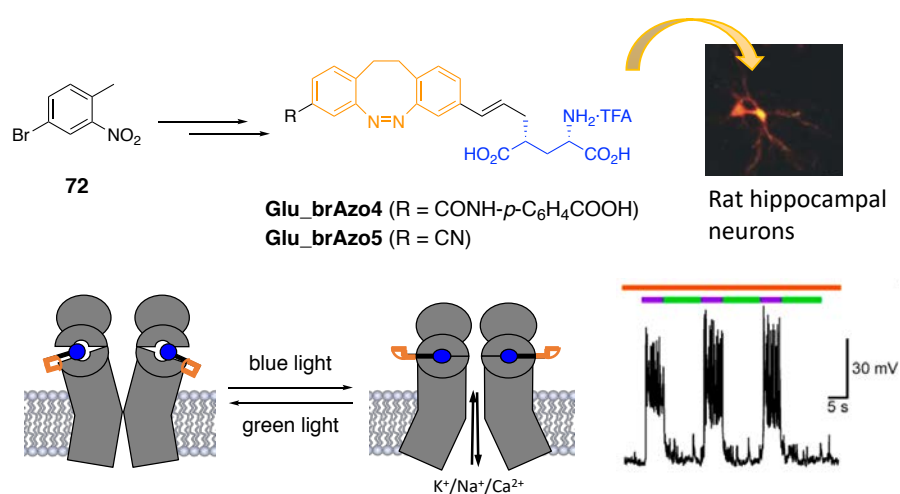


Figure VI-3. Synthetic photoswitchable neurotransmitters based on bridged azobenzenes.

CHAPTER VII

Experimental section

VII.1. GENERAL PROCEDURES

All commercially available reagents were used as received. Solvents were dried by distillation over the appropriate drying agents: CH₂Cl₂ (CaH₂), CH₃CN (CaH₂) and THF (Na⁰). When needed, reactions were performed avoiding moisture by standard procedures and under N₂ or Ar atmosphere.

VII.1.1. SPECTROSCOPY

Nuclear magnetic resonance spectra (NMR) were registered at the *Servei de Ressonància Magnètica Nuclear* of the Universitat Autònoma de Barcelona. ¹H NMR and ¹³C NMR spectra were recorded at 250, 360, 400, 500 or 600 MHz and 90.5, 100.6, 125.8 or 150 MHz, respectively. Proton chemical shifts are reported in ppm (δ) (CDCl₃, 7.26 ppm; MeOH-*d*₄, 3.31 ppm; DMSO-*d*₆, 2.50 ppm; and acetone-*d*₆, 2.06 ppm). Carbon chemical shifts are reported in ppm (CDCl₃, 77.2 ppm; MeOH-*d*₄, 49.0 ppm; DMSO-*d*₆, 39.5 ppm; and acetone-*d*₆, 206.7 ppm and 29.9 ppm). NMR signals were assigned with the help of COSY, DEPT135, HSQC and HMBC experiments. All spectra were measured at 298 K unless stated.

The abbreviations used to describe signal multiplicities are: s (singlet), br s (broad singlet), d (doublet), t (triplet), br t (broad triplet), dd (double doublet), dt (double triplet), dq (double quartet), ddt (double double triplet), td (triple doublet), m (multiplet) and *J* (coupling constant).

Infrared spectra (IR) were recorded on a Bruker Tensor 27 Spectrophotometer equipped with a Golden Gate Single Refraction Diamond ATR (Attenuated Total Reflectance) accessory at *Servei d'Anàlisi Química* of the Universitat Autònoma de Barcelona. Peaks are reported in cm^{-1} .

Electronic absorption spectra (UV-vis) were recorded on a HP 8453 Spectrophotometer. HPLC or spectroscopy quality solvents were used.

VII.1.2. MASS SPECTROMETRY

High resolution mass spectra (HRMS) were recorded at the *Centro de I+D+I* of the *Parque Científico Tecnológico* of the Burgos University in an Argilent 6454 Q-TP spectrometer with an Argilent Jetstream Technology (AJT) source.

VII.1.3. CHROMATOGRAPHY

All reactions were monitored by analytical thin-layer chromatography (TLC) using silica gel 60 F254 pre-coated aluminium plates (0.25 mm thickness). Development was made using an UV lamp at 254 nm and/or using a KMnO_4/KOH aqueous solution. Flash column chromatography was performed using silica gel (230-400 mesh).

VII.1.4. OPTICAL ROTATORY POWER

Specific optical rotations were measured on a Rudolph Autopol I polarimeter at 20 ± 0.3 °C using a 0.5 dm long cuvette.

VII.1.5. MELTING POINT

Melting points (Mp) were determined on a REICHERT Koffler hot stage melting point apparatus and are uncorrected.

VII.1.6. EXCITATION SOURCES

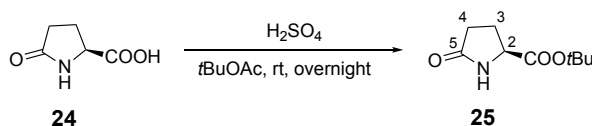
Different excitation sources were used in the photochemical experiments depending on the spectral requirements: (i) a Vilber Lourmat UV lamp equipped with two 4W tubes emitting light at 254 and 365 nm; (ii) a Vilber Lourmat UV lamp equipped with a 6W tube of 312 nm light; (iii) a Nd:YAG (Brilliant, Quantel) pulsed laser emitting at 355 and 532 nm; (iv) diode cw lasers at $\lambda_{\text{exc}} = 405$ nm (SciTec), $\lambda_{\text{exc}} = 473$ nm (SciTech) and $\lambda_{\text{exc}} = 532$ nm (Z-Laser); and (v) a Xe lamp emitting at 300-600 nm coupled to a spectrograph (Applied Physics).

VII.1.7. SINGLE-CELL CALCIUM IMAGING

Calcium imaging with 1P stimulation: Cells were imaged on an inverted fully motorized digital microscope (iMic 2000, Till Photonics) controlled with the Live Acquisition 2.1 software (Till Photonics). Images were acquired at room temperature with a UV Apochromat 40× oil objective lens (Olympus) with an imaging interval of 2 s. GCaMP6s was excited during 10 ms at 490 nm by using a Polychrome V light source (Till Photonics) equipped with a Xenon Short Arc lamp (Ushio) and a 505 nm dichroic beam splitter (Chroma Technology). Emission was filtered by a D535/40nm emission filter (Chroma Technology) and finally collected by a cooled CCD camera (Interline Transfer IMAGO QE, Till Photonics).

Calcium imaging with 2P stimulation: All two-photon experiments were performed in the Advanced Digital Microscopy Core Facility of IRB Barcelona with a SP5 spectral confocal multiphoton microscope (Leica) equipped with: a 405 nm cw diode laser, an Ar laser (514nm), and a pulsed broadband Ti:Sapphire laser (Mai Tai, Spectra-Physics, Santa-Clara, CA-USA) which can be tuned from 710-990 nm (80 MHz repetition rate, 80 fs pulse). We used a 40x/1.25-0.75-NA Oil objective (HCX PL APO, Leica). In HEK293 cell experiments, R-GECO1 was used as a Ca^{2+} fluorescent indicator instead of GCaMP6 because it does not absorb at 405 nm, the excitation wavelength used to test the 1P activity in the confocal multiphoton microscope employed. Imaging of R-GECO1 was done at 514 nm (3 μW) with a frame rate of 4 s, a minimal exposition time of 343 ms, and using bidirectional laser scanning at 400 Hz. Images were recorded with a HyD detector with a detection range from 569 to 648 nm, at 512x512 pixel resolution. Pinhole aperture was set at maximum (600 μm).

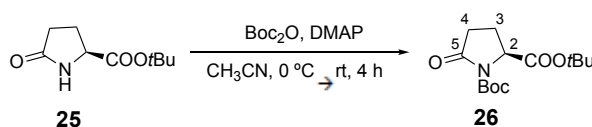
VII.2. EXPERIMENTAL DESCRIPTION

VII.2.1. SYNTHESIS OF GLUTAMATE DERIVATIVES¹Synthesis of *tert*-butyl (2*S*)-5-oxotetrahydro-1*H*-pyrrolicarboxylate, **25**

To a solution of L-pyrroglutamic acid **24** (10.0 g, 77.7 mmol) in *tert*-butyl acetate (125 mL), 96% H₂SO₄ (6 mL, 108 mmol) was added dropwise. The resulting solution was stirred overnight at rt. Then, a saturated aqueous solution of NaHCO₃ (174 mL) was slowly poured into the reaction mixture. The solution was basified to pH 5.5 with an aqueous solution of NaOH 30%. The product was extracted with EtOAc (4 x 175 mL). The combined organic extracts were washed with a saturated aqueous solution of NaHCO₃ (125 mL) and a saturated aqueous solution of NaCl (125 mL), dried over anhydrous Na₂SO₄ and the solvent was removed under vacuum. As there were still remains of acetic acid, CH₂Cl₂ was added to the product (100 mL) and the solution was washed again with a saturated aqueous solution of NaHCO₃ (100 mL) and a saturated aqueous solution of NaCl (100 mL), dried over anhydrous Na₂SO₄ and the solvent was removed under vacuum to furnish **25** (6.36 g, 34.4 mmol, 44% yield) as a white solid.

Spectroscopic data of **25**

¹H NMR (250 MHz, CDCl₃): δ 6.33 (br s, 1H, NH), 4.12 (m, 1H, H-2), 2.38 (m, 3H, H-3, H-4), 2.17 (m, 1H, H-3), 1.45 (s, 9H, C(CH₃)₃).

Synthesis of di(*tert*-butyl) (2*S*)-5-oxotetrahydro-1*H*-1,2-pyrroledicarboxylate, **26**

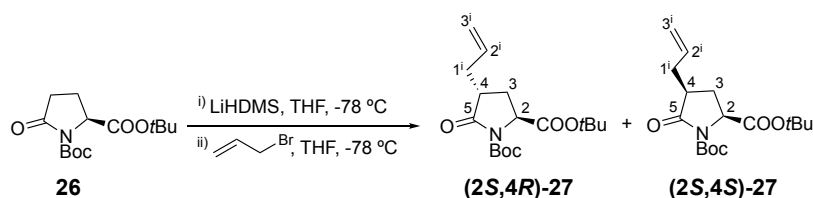
To an ice-cooled solution of *tert*-butyl ester **25** (5.51 g, 29.8 mmol) in anhydrous CH₃CN (138 mL), DMAP (1.13 g, 9.22 mmol) and Boc₂O (15.1 g, 69.3 mmol) were added. The solution was stirred at 0 °C for 30 minutes and then warmed up to rt and let stir for 4 h. The solvent

was removed under vacuum and the resulting residue was purified by column chromatography (hexane/EtOAc, 2:1) to provide **26** (8.40 g, 29.4 mmol, 98% yield) as a yellow solid.

Spectroscopic data of **26**

$^1\text{H NMR}$ (250 MHz, CDCl_3): δ 4.34 (dd, $J_{2,3} = 9.3$ Hz, $J_{2,3} = 2.6$ Hz, 1H, H-2), 2.32 (m, 3H, H-3, H-4), 1.85 (m, 1H, H-3), 1.36 (s, 9H, $\text{C}(\text{CH}_3)_3$), 1.34 (s, 9H, $\text{C}(\text{CH}_3)_3$).

Synthesis of di(*tert*-butyl) (2*S*,4*R*)-4-allyl-5-oxotetrahydro-1*H*-1,2-pyrroledicarboxylate, (**2*S*,4*R***)-**27**, and di(*tert*-butyl) (2*S*,4*R*)-4-allyl-5-oxotetrahydro-1*H*-1,2-pyrroledicarboxylate, (**2*S*,4*S***)-**27**



To a solution of carbamate **26** (4.05 g, 14.2 mmol) in anhydrous THF (107 mL) at -78 °C, LiHMDS 1.0 M in THF (15.5 mL, 15.5 mmol) was added dropwise under N_2 atmosphere. The reaction mixture was stirred at this temperature for 1 h and a solution of allyl bromide (5.02 mL, 56.8 mmol) in anhydrous THF (66 mL), previously stirred at -78 °C for 1 h, was added dropwise. After stirring for 4 h the reaction was quenched by adding silica and stirring 5 minutes. The residue was purified by column chromatography (hexane/EtOAc, 10:1) to afford a tan solid identified as (**2*S*,4*R***)-**27** (1.51 g, 4.64 mmol, 33% yield) and a tan solid identified as (**2*S*,4*S***)-**27** (0.92 g, 2.83 mmol, 20% yield).

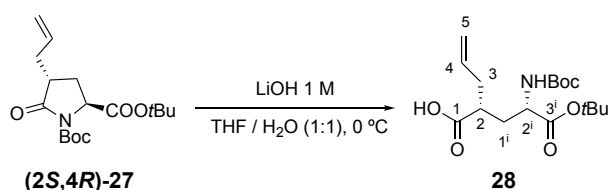
Spectroscopic data of (**2*S*,4*R***)-**27**

$^1\text{H NMR}$ (250 MHz, CDCl_3): δ 5.68 (ddt, $J_{2,3\text{trans}^i} = 17.1$ Hz, $J_{2,3\text{cis}^i} = 10.2$ Hz, $J_{2,1} = 7.0$ Hz, 1H, H-2ⁱ), 5.04 (m, 2H, H-3ⁱ), 4.36 (dd, $J_{2,3} = 9.4$ Hz, $J_{2,3} = 1.8$ Hz, 1H, H-2), 2.59 (m, 2H, H-4, H-1ⁱ), 2.03 (m, 3H, H-3, H-1ⁱ), 1.44 (s, 9H, $\text{C}(\text{CH}_3)_3$), 1.41 (s, 9H, $\text{C}(\text{CH}_3)_3$).

Spectroscopic data of (**2*S*,4*S***)-**27**

$^1\text{H NMR}$ (250 MHz, CDCl_3): δ 5.71 (m, 1H, H-2ⁱ), 5.04 (m, 2H, H-3ⁱ), 4.37 (dd, $J_{2,3} = 9.3$ Hz, $J_{2,3} = 5.7$ Hz, 1H, H-2), 2.60 (m, 2H, H-1ⁱ, H-4), 2.41 (dt, $J_{\text{gem}} = 13.4$ Hz, $J_{3,4} = J_{3,2} = 9.3$ Hz, 1H, H-3), 2.19 (m, 1H, H-1ⁱ), 1.69 (m, 1H, H-3), 1.48 (s, 9H, $\text{C}(\text{CH}_3)_3$), 1.46 (s, 9H, $\text{C}(\text{CH}_3)_3$).

Synthesis of (2*R*)-2-[(2*S*)-3-(*tert*-butoxy)-2-[(*tert*-butoxycarbonyl)amino]-3-oxopropyl]-4-pentenoic acid, **28**

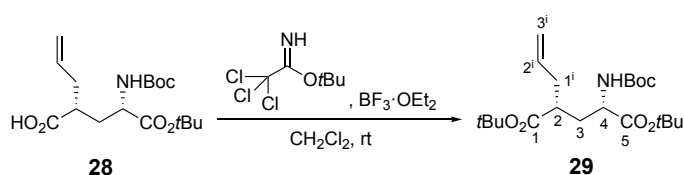


To an ice-cooled solution of (**2*S*,4*R*)-27** (2.57 g, 7.98 mmol) in a mixture 1:1 of THF (60 mL) and water (48 mL), 1 M LiOH (12 mL, 12.0 mmol) was slowly added. After stirring for 2 h at this temperature, the reaction mixture was acidified to pH 2 with 5% HCl and extracted with EtOAc (3 x 107 mL). The combined organic extracts were dried over anhydrous Na₂SO₄ and the solvent was removed under vacuum. The residue was purified by column chromatography (hexane/EtOAc, 1:1) to furnish a tan dense oil identified as **28** (2.71 g, 7.89 mmol, 83% yield).

Spectroscopic data of **28**

¹H NMR (250 MHz, CDCl₃): δ 10.79 (br s, COOH), 5.72 (m, 1H, H-4), 5.24 (d, *J*_{NH,2ⁱ} = 8.2 Hz, 1H, NH), 5.05 (m, 2H, H-5), 4.19 (m, 1H, H-2ⁱ), 2.46 (m, 2H, H-2, H-3), 2.20 (m, 2H, H-3, H-1ⁱ), 1.71 (m, 1H, H-1ⁱ), 1.44 (s, 9H, C(CH₃)₃), 1.41 (s, 9H, C(CH₃)₃).

Synthesis of di(*tert*-butyl) (2*R*,4*S*)-2-allyl-4-[(*tert*-butoxycarbonyl)amino] pentanedioate, **29**

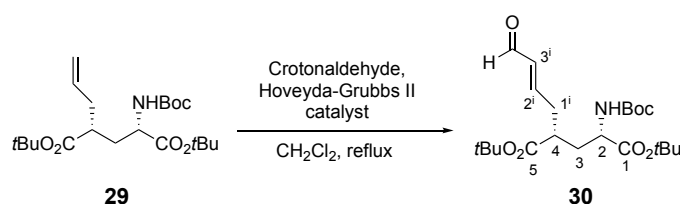


To a solution of compound **28** (1.33 g, 3.87 mmol) in anhydrous CH₂Cl₂ (34.5 mL), *tert*-butyl 2,2,2-trichloroacetimidate (1.38 mL, 7.74 mmol) and BF₃·OEt₂ (195 μL, 1.55 mmol) were added. The reaction mixture was let stir for 3 h at rt until TLC analysis (hexane/EtOAc, 3:1) indicated the complete consumption of the starting material. Afterwards, a mixture of saturated solution of NaHCO₃/H₂O (1:1) (8 mL) was added and the product was extracted with CH₂Cl₂ (3 x 18 mL). The combined organic extracts were dried over anhydrous Na₂SO₄ and the solvent was removed under vacuum. The residue was purified by column chromatography (hexane/EtOAc, 3:1) to give a tan solid identified as **29** (1.04 g, 2.60 mmol, 67% yield).

Spectroscopic data of **29**

$^1\text{H NMR}$ (250 MHz, CDCl_3): δ 5.64 (ddt, $J_{2^i,3^i\text{trans}^i} = 16.8$ Hz, $J_{2^i,3^i\text{cis}^i} = 10.1$ Hz, $J_{2^i,1^i} = 6.8$ Hz, 1H, H-2ⁱ), 4.97 (m, 3H, H-3ⁱ, NH), 4.16 (m, 1H, H-4), 2.29 (m, 2H, H-1ⁱ, H-2), 2.09 (m, 2H, H-1ⁱ, H-3), 1.60 (m, 1H, H-3), 1.39 (s, 9H, $\text{C}(\text{CH}_3)_3$), 1.38 (s, 9H, $\text{C}(\text{CH}_3)_3$), 1.36 (s, 9H, $\text{C}(\text{CH}_3)_3$).

Synthesis of di(*tert*-butyl) (2*S*,4*R*)-2-[(*tert*-butoxycarbonyl)amino]-4-[(2*E*)-4-oxo-2-butenyl] pentanedioate, **30**

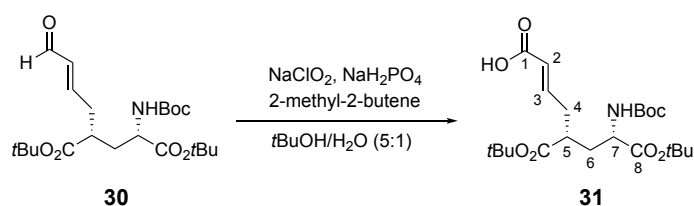


To a solution of allyl **29** (1.58 g, 3.94 mmol) in anhydrous CH_2Cl_2 (18 mL), crotonaldehyde (1.8 mL, 21.7 mmol) was added. The mixture was heated to reflux and a solution of Hoveyda-Grubbs II catalyst (61 mg, 0.07 mmol) in anhydrous CH_2Cl_2 (7 mL) was added in 3 portions. The reaction was stirred at these conditions for 3 h until TLC analysis (hexane/EtOAc, 3:1) showed no more evolution. The solvent was removed under vacuum and the resulting residue was purified by column chromatography (hexane/EtOAc, 3:1) to obtain a yellow dense oil identified as **30** (1.28 g, 2.99 mmol, 76 % yield). The unreacted **29** could be recovered.

Spectroscopic data of **30**

$^1\text{H NMR}$ (250 MHz, CDCl_3): δ 9.51 (d, $J_{\text{CHO},3^i} = 7.8$ Hz, 1H, CHO), 6.77 (dt, $J_{2^i,3^i} = 15.7$ Hz, $J_{2^i,1^i} = 6.9$ Hz, 1H, H-2ⁱ), 6.14 (dd, $J_{3^i,2^i} = 15.7$ Hz, $J_{3^i,\text{CHO}} = 7.8$ Hz, 1H, H-3ⁱ), 4.24 (m, 1H, H-2), 2.61 (m, 3H, H-1ⁱ, H-4), 2.19 (m, 1H, H-3), 1.68 (m, 1H, H-3), 1.45 (s, 9H, $\text{C}(\text{CH}_3)_3$), 1.42 (s, 9H, $\text{C}(\text{CH}_3)_3$), 1.41 (s, 9H, $\text{C}(\text{CH}_3)_3$).

Synthesis of (2*E*,5*R*,7*S*)-8-*tert*-butoxy-5-(*tert*-butoxycarbonyl)-7-[(*tert*-butoxycarbonyl) amino]-8-oxo-2-octenoic acid, **31**

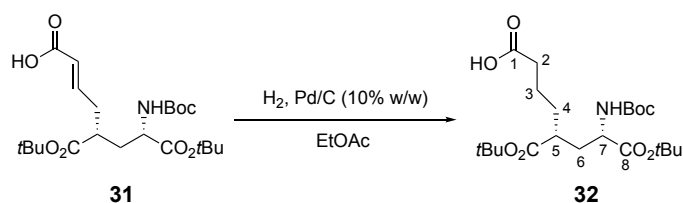


To an ice-cooled solution of **30** (1.27 g, 2.97 mmol) in a 5:1 mixture of *t*BuOH (101.6 mL) and H₂O (20.4 mL), 2-methyl-2-butene (3.15 mL, 29.7 mmol), NaH₂PO₄·2H₂O (2.34 g, 15.0 mmol) and NaCl₂O (1.61 g, 17.8 mmol) were successively added. The reaction mixture was let stir at 0 °C for 1 h, and then was warmed up to rt and stirred overnight. Then, H₂O (15.5 mL) was added and the solution was basified to pH 8 with a saturated aqueous solution of Na₂CO₃. The mixture was extracted with EtOAc (3 x 26 mL) and the combined organic extracts were dried over anhydrous Na₂SO₄ and concentrated under vacuum. The resulting residue was purified by column chromatography (hexane/EtOAc/CH₃COOH, 4:1:0.1) to furnish **31** (1.04 g, 2.34 mmol, 79% yield) as a colourless oil.

Spectroscopic data of **31**

¹H NMR (250 MHz, MeOH-*d*₄): δ 6.87 (d, *J*_{NH,7} = 8.6 Hz, 1H, NH), 6.76 (dt, *J*_{3,2} = 15.6 Hz, *J*_{3,4} = 7.2 Hz, 1H, H-3), 5.86 (d, *J*_{2,3} = 15.6 Hz, 1H, H-2), 4.07 (m, 1H, H-7), 2.56 (m, 1H, H-5), 2.40 (m, 2H, H-4), 2.08 (m, 1H, H-6), 1.66 (m, 1H, H-6), 1.46 (m, 27H, 3x(CH₃)₃).

Synthesis of (5*R*,7*S*)-8-*tert*-butoxy-5-(*tert*-butoxycarbonyl)-7-[(*tert*-butoxycarbonyl)amino]-8-oxooctanoic acid, **32**



To a solution of compound **31** (1.54 g, 3.47 mmol) in EtOAc (62 mL), 10 % Pd/C (154 mg) was added. The resulting suspension was stirred under H₂ atmosphere overnight.

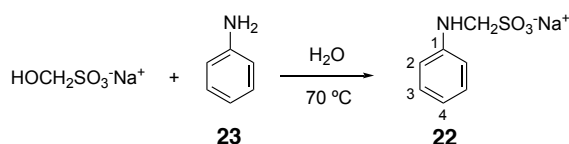
Afterwards, it was filtered through Celite® and the solvent was evaporated under vacuum to furnish **32** (1.55 g, 3.47 mmol, quantitative yield) as a colourless dense oil.

Spectroscopic data of **32**

¹H NMR (250 MHz, MeOH-*d*₄): δ 6.76 (d, *J*_{NH,7} = 8.4 Hz, 1H, NH), 3.94 (m, 1H, H-7), 2.38 (m, 1H, H-5), 2.25 (m, 2H, H-2), 1.99 (m, 1H, H-6), 1.57 (m, 5H, 2xH-3, 2xH-4, H-6), 1.44 (s, 9H, C(CH₃)₃), 1.43 (s, 9H, C(CH₃)₃), 1.41 (s, 9H, C(CH₃)₃).

VII.2.2. SYNTHESIS OF MAG_{2P}^{slow} AND MAG_{2P_F}^{slow}

Synthesis of sodium anilinomethylenesulfonate, **22**

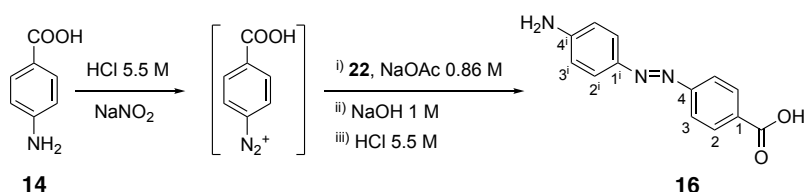


To a stirring solution of sodium hydroxymethylenesulfonate (10.0 g, 74.5 mmol) in H₂O (30 mL), aniline **23** (6.2 mL, 68.0 mmol) was added dropwise. The resulting solution was heated to 70 °C for 25 minutes. Afterwards, it was allowed to cool down until the appearance of a white precipitate. The precipitate was filtered and washed with Et₂O to furnish a white solid identified as **22** (11.7 g, 55.9 mmol, 82% yield).

Spectroscopic data of **22**

¹H NMR (250 MHz, DMSO-*d*₆): δ 7.02 (dd, *J*_{3,2} = 8.6 Hz, *J*_{3,4} = 7.2 Hz, 2H, H-3), 6.70 (dd, *J*_{2,3} = 8.6 Hz, *J*_{2,4} = 1.2 Hz, 2H, H-2), 6.50 (tt, *J*_{4,3} = 7.2 Hz, *J*_{4,2} = 1.2 Hz, 1H, H-4), 5.96 (t, *J*_{NH,CH₂} = 6.8 Hz, 1H, NH), 3.92 (d, *J*_{CH₂,NH} = 6.4 Hz, 2H, CH₂).

Synthesis of 4-[(4-aminophenyl)azo]benzoic acid, **16**²

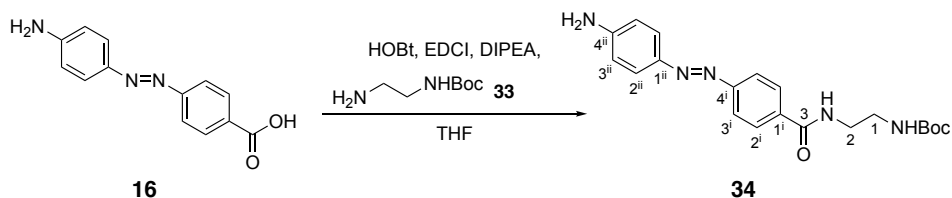


To an ice-cooled suspension of 4-aminobenzoic acid, **14**, (1.25 g, 9.11 mmol) in HCl 5.5 M (5.4 mL), a solution of NaNO₂ (0.71 g, 10.3 mmol) in H₂O (2 mL) was slowly poured. The resulting mixture was added dropwise to an ice-cooled solution of **22** (2.43 g, 11.6 mmol) in NaOAc 0.86 M (33 mL) and was let stir at 4 °C overnight. The brown paste formed was filtered, washed with H₂O and the solid obtained was dissolved in NaOH 1 M (40 mL). The resulting solution was heated to 90 °C for 2 h and, when cooled down, an orange precipitate appeared. It was filtered and recrystallised in NaOH 1 M. Afterwards, it was dissolved in the minimum quantity of H₂O and the solution was acidified to pH 2-3 with HCl 5.5 M. The orange precipitate obtained was filtered and washed with H₂O and Et₂O to **16** (826 mg, 3.42 mmol, 38% yield) as a dark orange solid.

Spectroscopic data of **16**

¹H NMR (250 MHz, DMSO-*d*₆): δ 8.07 (d, *J*_{2,3} = 8.6 Hz, 2H, H-2), 7.80 (d, *J*_{3,2} = 8.6 Hz, 2H, H-3), 7.71 (d, *J*_{2,3ⁱ} = 8.8 Hz, 2H, H-2ⁱ), 6.69 (d, *J*_{3,2ⁱ} = 8.8 Hz, 2H, H-3ⁱ).

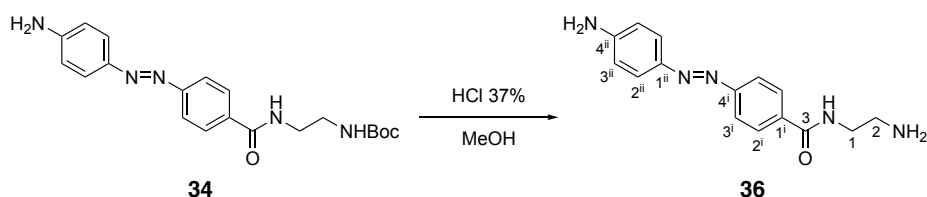
Synthesis of *tert*-butyl [2-({4-[(*E*-4-aminophenyl)diazenyl]benzoyl}amino)ethyl] carbamate, **34**



To a solution of acid **16** (553 mg, 2.29 mmol) in anhydrous THF (110 mL), a solution of HOBT (493 mg, 3.54 mmol), EDCI (0.58 mL, 3.22 mmol), DIPEA (1.73 mL, 9.88 mmol) and **33** (0.48 mL, 2.98 mmol) in anhydrous THF (55 mL) was added. The reaction mixture was stirred overnight at rt. The solution was washed with H₂O (2 x 80 mL) and the resulting aqueous extracts were extracted with CH₂Cl₂ (3 x 80 mL). The combined organic extracts were dried over anhydrous Na₂SO₄ and concentrated under vacuum. The resulting residue was purified by column chromatography (CH₂Cl₂/THF, 4:1) to obtain **34** as an orange solid (861 mg, 2.25 mmol, 98% yield).

Physical and spectroscopic data of 34

Mp = 203-205 °C (from THF); **¹H NMR** (250 MHz, DMSO-*d*₆): δ 8.56 (br t, $J_{\text{CONH},2} = 5.4$ Hz, 1H, CONH), 7.98 (d, $J_{2^i,3^i} = 8.5$ Hz, 2H, H-2ⁱ), 7.78 (d, $J_{3^i,2^i} = 8.5$ Hz, 2H, H-3ⁱ), 7.70 (d, $J_{2^{\text{ii}},3^{\text{ii}}} = 8.8$ Hz, 2H, H-2ⁱⁱ), 6.94 (br t, $J_{\text{NHoc},1} = 5.4$ Hz, 1H, NHoc), 6.69 (d, $J_{3^{\text{ii}},2^{\text{ii}}} = 8.8$ Hz, 2H, H-3ⁱⁱ), 6.35 (s, 2H, NH₂), 3.31 (m, 2H, H-2), 3.14 (m, 2H, H-1), 1.38 (s, 9H, C(CH₃)₃); **¹³C NMR** (100.6 MHz, DMSO-*d*₆): δ 165.8 (C-3), 155.7 (C, carbamate), 154.0 (C-4ⁱ), 153.4 (C-4ⁱⁱ), 142.9 (C-1ⁱⁱ), 134.6 (C-1ⁱ), 128.3 (C-2ⁱ), 125.6 (C-2ⁱⁱ), 121.3 (C-3ⁱ), 113.4 (C-3ⁱⁱ), 77.7 (C(CH₃)₃), 39.6 (C-1), 39.6 (C-2), 28.2 (C(CH₃)₃); **IR** (ATR): 3333, 2979, 2926, 1686, 1597, 1526, 1275, 1132 cm⁻¹; **HRMS** (HR-EI) calcd. for [C₂₀H₂₅N₅O₃]: 383.1957; found: 383.1949. **COSY**, **DEPT 135** and **¹H/¹³C** correlation were recorded.

Synthesis of (*E*)-*N*-(2-aminoethyl)-4-((4-aminophenyl)diazenyl)benzamide, **36**

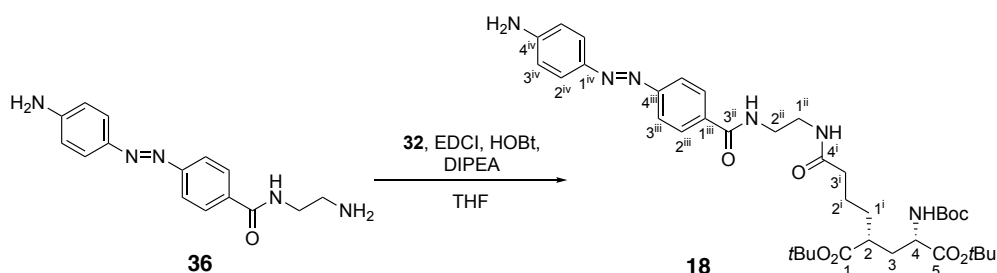
To a solution of carbamate **34** (257 mg, 0.67 mmol) in MeOH (26 mL), HCl 37% (7.5 mL, 90.6 mmol) was added dropwise. The mixture was stirred at rt for 90 min until the complete consumption of the starting material. Afterwards, the mixture was neutralised with a saturated aqueous solution of NaHCO₃, extracted with CH₂Cl₂ (3 x 40 mL) and the combined organic extracts were dried over anhydrous Na₂SO₄. The solvent was evaporated under vacuum and the resulting residue was washed with Et₂O and filtered to furnish amine **36** (100 mg, 0.35 mmol, 53% yield) as a dark orange solid.

Physical and spectroscopic data of 36

Mp = 150-156 °C (from Et₂O); **¹H NMR** (250 MHz, DMSO-*d*₆): δ 8.49 (br t, $J_{\text{CONH},1} = 5.3$ Hz, 1H, CONH), 7.98 (d, $J_{2^i,3^i} = 8.3$ Hz, 2H, H-2ⁱ), 7.78 (d, $J_{3^i,2^i} = 8.3$ Hz, 2H, H-3ⁱ), 7.69 (d, $J_{2^{\text{ii}},3^{\text{ii}}} = 8.5$ Hz, 2H, H-2ⁱⁱ), 6.68 (d, $J_{3^{\text{ii}},2^{\text{ii}}} = 8.5$ Hz, 2H, H-3ⁱⁱ), 6.23 (br s, 2H, NH₂), 3.30 (m, 2H, H-1), 2.69 (t, $J_{2,1} = 6.4$ Hz, 2H, H-2); **¹³C NMR** (100.6 MHz, DMSO-*d*₆): δ 165.8 (C-3), 153.9 (C-4ⁱ), 153.4 (C-4ⁱⁱ), 142.9 (C-1ⁱⁱ), 134.8 (C-1ⁱ), 128.3 (C-2ⁱ), 125.6 (C-2ⁱⁱ), 121.3 (C-3ⁱ), 113.4 (C-3ⁱⁱ), 42.9 (C-1), 41.2 (C-2); **IR**

(ATR): 3295, 2930, 1631, 1597, 1532, 1296, 1135 cm^{-1} ; **HRMS** (HR-EI) calcd. for $[\text{C}_{15}\text{H}_{17}\text{N}_5\text{O}]$: 283.1433; found: 283.1445. **COSY**, **DEPT 135** and $^1\text{H}/^{13}\text{C}$ correlation were recorded.

Synthesis of di-*tert*-butyl (2*R*,4*S*)-2-(4-([2-({4-[(*E*)-(4-aminophenyl)diazenyl]benzoyl)amino ethyl]amino)-4-oxobutyl)-4-[(*tert*-butoxycarbonyl)amino]pentanedioate, **18**



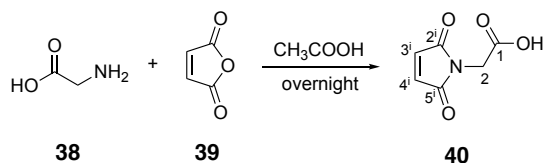
To a solution of amine **36** (85 mg, 0.30 mmol) in anhydrous THF (16 mL), a solution of **32** (149 mg, 0.33 mmol), HOBt (64 mg, 0.46 mmol), EDCI (72 μL , 0.40 mmol) and DIPEA (216 μL , 1.23 mmol) in anhydrous THF (11 mL) was added. The reaction mixture was stirred overnight at rt. The orange solution was washed with H_2O (2 x 25 mL) and the resulting aqueous extracts were extracted with CH_2Cl_2 (2 x 25 mL). The combined organic extracts were dried over anhydrous Na_2SO_4 and concentrated under vacuum. The resulting residue was purified by column chromatography (EtOAc, 100%) to give **18** (192 mg, 0.27 mmol, 90% yield) as an orange solid.

Physical and spectroscopic data of **18**

Mp = 75-78 $^{\circ}\text{C}$ (from EtOAc); $[\alpha]_{\text{D}}^{20}$ = 2.2 (c 0.50, CHCl_3); $^1\text{H NMR}$ (400 MHz, CDCl_3): δ 7.92 (d, $J_{2^{\text{iii}},3^{\text{iii}}} = 8.6$ Hz, 2H, H-2ⁱⁱⁱ), 7.84 (d, $J_{3^{\text{iii}},2^{\text{iii}}} = 8.6$ Hz, 2H, H-3ⁱⁱⁱ), 7.80 (d, $J_{2^{\text{iv}},3^{\text{iv}}} = 8.7$ Hz, 2H, H-2^{iv}), 7.58 (br t, $J_{\text{NH},2^{\text{ii}}} = 4.4$ Hz, 1H, CONH-3ⁱⁱ), 6.73 (d, $J_{3^{\text{iv}},2^{\text{iv}}} = 8.7$ Hz, 2H, H-3^{iv}), 6.65 (t, $J_{\text{NH},1^{\text{ii}}} = 5.0$ Hz, 1H, CONH-4ⁱ), 5.12 (d, $J_{\text{NHoc},4} = 8.6$ Hz, 1H, NHoc), 4.15 (m, 1H, H-4), 3.58 (m, 2H, H-2ⁱⁱ), 3.52 (m, 2H, H-1ⁱⁱ), 2.34 (m, 1H, H-2), 2.21 (m, 2H, H-3ⁱ), 2.05 (m, 1H, H-3), 1.62 (m, 5H, H-3, H-1ⁱ, H-2ⁱ), 1.43 (s, 18H, $2 \times \text{C}(\text{CH}_3)_3$), 1.41 (s, 9H, $\text{C}(\text{CH}_3)_3$); $^{13}\text{C NMR}$ (100.6 MHz, CDCl_3): δ 174.6 (C-1, C-4ⁱ), 171.7 (C-5), 167.8 (C-3ⁱⁱ), 155.5 (C, carbamate), 154.9 (C-4ⁱⁱⁱ), 150.4 (C-4^{iv}), 145.6 (C-1^{iv}), 134.6 (C-1ⁱⁱⁱ), 128.1 (C-2ⁱⁱⁱ), 125.7 (C-2^{iv}), 122.5 (C-3ⁱⁱⁱ), 114.7 (C-3^{iv}), 82.1 ($\text{C}(\text{CH}_3)_3$), 81.1 ($\text{C}(\text{CH}_3)_3$), 79.8 ($\text{C}(\text{CH}_3)_3$), 52.8 (C-4), 42.4 (C-2), 41.8 (C-2ⁱⁱ), 39.8 (C-1ⁱⁱ), 36.2 (C-3ⁱ), 34.8 (C-3), 32.0 (C-1ⁱ), 28.4 ($\text{C}(\text{CH}_3)_3$), 28.2 ($\text{C}(\text{CH}_3)_3$), 28.1 ($\text{C}(\text{CH}_3)_3$), 23.2 (C-2ⁱ); **IR** (ATR): 3345, 2976, 1706, 1637, 1599 cm^{-1}

¹; **HRMS** (HR-ESI) calcd. for [C₃₇H₅₄N₆O₈+H]⁺: 711.4076; found: 711.4073. **COSY**, **DEPT 135** and **¹H/¹³C** correlation were recorded.

Synthesis of 2-(2,5-dioxotetrahydro-1*H*-1-pyrrolyl)acetic acid, **40**³

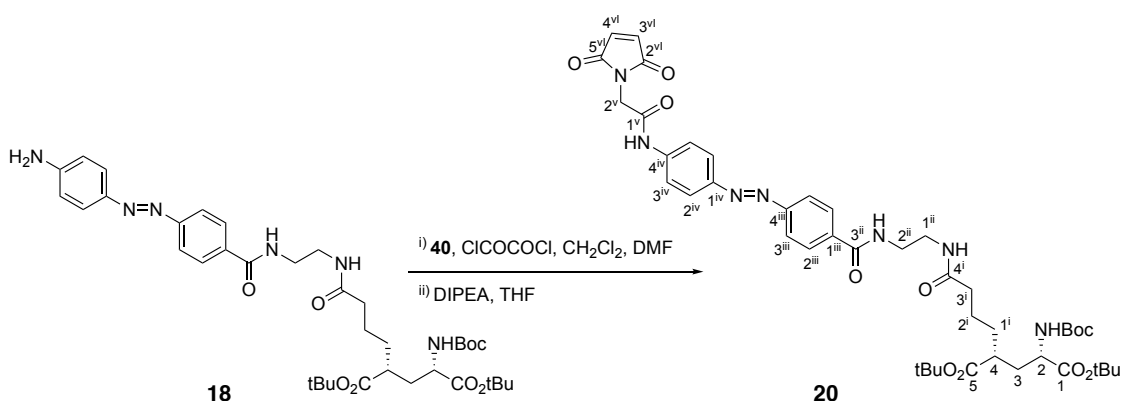


Glycine **38** (2.50 g, 33.3 mmol) and maleic anhydride **39** (3.27 g, 3.33 mmol) were dissolved in acetic acid (95 mL). The reaction mixture was stirred at rt overnight, under N₂ atmosphere. The resulting suspension was then warmed up to reflux for further 4 h to give a clear solution. The solvent was removed under vacuum and the residue was purified by column chromatography (CH₂Cl₂/CH₃COOH, 95:5) to afford a white solid identified as **40** (2.22 g, 14.3 mmol, 43% yield)

Spectroscopic data of **40**

¹H NMR (250 MHz, CDCl₃): δ 6.80 (s, 2H, H-3ⁱ, H-4ⁱ), 4.33 (s, 2H, H-2).

Synthesis di-*tert*-butyl (2*S*,4*R*)-2-[(*tert*-butoxycarbonyl)amino]-4-(4-[[2-({4-[(*E*)-(4-[[2,5-dioxo-2,5-dihydro-1*H*-pyrrol-1-yl)acetyl]amino}phenyl)diazanyl]benzoyl]amino)ethyl]amino)-4-oxobutyl]pentanedioate, **20**

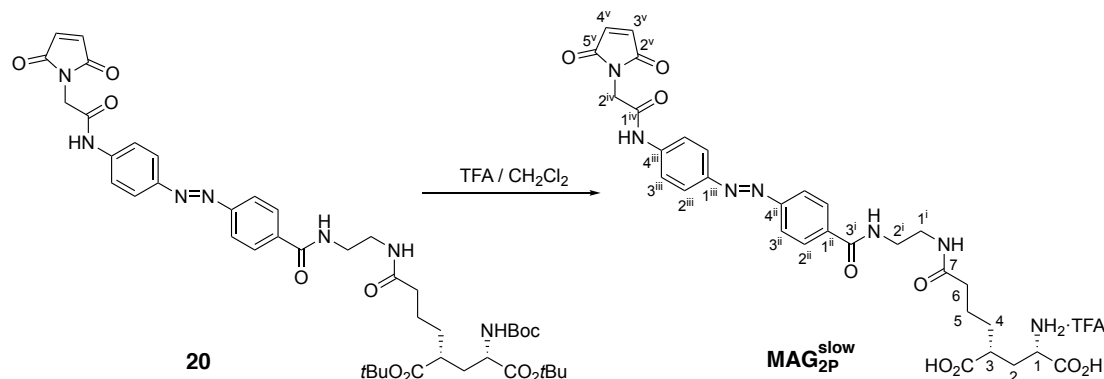


To a stirred solution of **40** (84 mg, 0.54 mmol) and oxalyl chloride 98% (49 μ L, 0.56 mmol) in dry CH_2Cl_2 (8.4 mL) was added one drop of DMF. After stirring for 2 h at rt, the mixture was concentrated. The resulting acid chloride was taken up in dry THF (3.5 mL) and slowly added to an ice-cooled solution of **18** (100 mg, 0.14 mmol), DIPEA (145 μ L, 1.19 mmol) in dry THF (17.5 mL). After stirring for 10 min at this temperature, the mixture was warmed up to rt and stirred for further 4 h. Then, it was diluted with EtOAc (21 mL) and the resulting solution was washed with water (3 x 7 mL). The organic extract was dried over anhydrous Na_2SO_4 , concentrated under vacuum and purified by column chromatography (EtOAc/MeOH, 9:1) to provide **20** (102 mg, 0.12 mmol, 86% yield) as an orange solid.

Physical and spectroscopic data of **20**

Mp = 230 °C (decomp. from EtOAc); $[\alpha]_{\text{D}}^{20}$ = -42.2 (*c* 1.02, CHCl_3); **$^1\text{H NMR}$** (400 MHz, CDCl_3 , 320 K): δ 8.36 (br s, 1H, CONH-1^v), 7.89 (d, $J_{2^{\text{iii}},3^{\text{iii}}}$ = 9.1 Hz, 2H, H-2ⁱⁱⁱ), 7.84 (m, 4H, H-3ⁱⁱⁱ, H-2^{iv}), 7.62 (d, $J_{3^{\text{iv}},2^{\text{iv}}}$ = 9.4 Hz, 2H, H-3^{iv}), 7.46 (t, $J_{\text{NH},2^{\text{ii}}}$ = 4.7 Hz, 1H, CONH-3ⁱⁱ), 6.82 (s, 2H, H-3^{vi}, H-4^{vi}), 6.49 (t, $J_{\text{NH},1^{\text{ii}}}$ = 4.9 Hz, 1H, CONH-4ⁱ), 5.07 (d, $J_{\text{NH},2^{\text{ii}}}$ = 8.4 Hz, 1H, NHBoc), 4.40 (s, 2H, H-2^v), 4.14 (m, 1H, H-2), 3.60 (m, 2H, H-2ⁱⁱ), 3.55 (m, 2H, H-1ⁱⁱ), 2.37 (m, 1H, H-4), 2.23 (m, 2H, H-3ⁱ), 2.08 (m, 1H, H-3), 1.64 (m, 5H, H-3, 2xH-1ⁱ, 2xH-2ⁱ), 1.45 (s, 9H, $\text{C}(\text{CH}_3)_3$), 1.44 (s, 9H, $\text{C}(\text{CH}_3)_3$), 1.42 (s, 9H, $\text{C}(\text{CH}_3)_3$); **$^{13}\text{C NMR}$** (100.6 MHz, CDCl_3 , 320 K): δ 174.6 (C-5, C-4ⁱ), 171.7 (C-1), 170.3 (C-2^{vi}, C-5^{vi}), 167.7 (C-3ⁱⁱ), 164.7 (C-1^v), 155.6 (C, carbamate), 154.5 (C-4ⁱⁱⁱ), 149.4 (C-4^{iv}), 140.5 (C-1^{iv}), 135.8 (C-1ⁱⁱⁱ), 134.8 (C-4^{vi}, C-3^{vi}), 128.2 (C-2ⁱⁱⁱ), 124.4 (C-2^{iv}), 123.0 (C-3ⁱⁱⁱ), 120.3 (C-3^{iv}), 82.1 ($\text{C}(\text{CH}_3)_3$), 81.1 ($\text{C}(\text{CH}_3)_3$), 79.8 ($\text{C}(\text{CH}_3)_3$), 53.1 (C-2), 42.5 (C-2), 41.8/41.5 (C-2ⁱⁱ/C-2^v), 40.0 (C-1ⁱⁱ), 36.4 (C-3ⁱ), 34.9 (C-3), 32.0 (C-1ⁱ), 28.5 ($\text{C}(\text{CH}_3)_3$), 28.3 ($\text{C}(\text{CH}_3)_3$), 28.2 ($\text{C}(\text{CH}_3)_3$), 23.2 (C-2ⁱ); **IR** (ATR): 3277, 3081, 2926, 1714, 1543, 1147 cm^{-1} ; **HRMS** (HR-ESI) calcd. for $[\text{C}_{43}\text{H}_{57}\text{N}_7\text{O}_{11}+\text{H}]^+$: 848.4189; found: 848.4184. **DEPT 135** and **$^1\text{H}/^{13}\text{C}$** correlation were recorded.

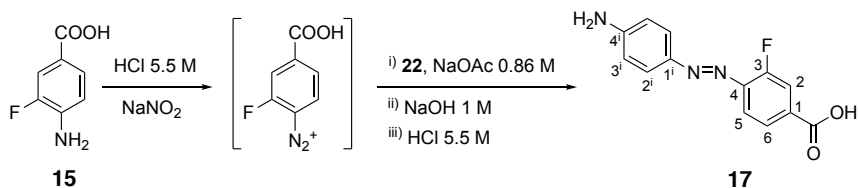
Synthesis of (1*S*,3*R*)-1,3-dicarboxy-7-[[2-({4-[(*E*)-(4-{{[(2,5-dioxo-2,5-dihydro-1*H*-pyrrol-1-yl)acetyl]amino}phenyl)diazenyl]benzoyl]amino)ethyl]amino)-7-oxo-1-heptanaminiumtrifluoroacetate, **MAG_{2P}^{slow}**



To a stirred solution of compound **20** (85 mg, 0.10 mmol) in CH₂Cl₂ (15 mL), trifluoroacetic acid (7.5 mL, 97.9 mmol) was added. The mixture was stirred at rt until the starting material was consumed. Then, the solution was concentrated under vacuum and the resulting purple solid was washed with Et₂O to furnish **MAG_{2P}^{slow}** (60 mg, 0.08 mmol, 80% yield) as a lilac solid.

Physical and spectroscopic data of **MAG_{2P}^{slow}**

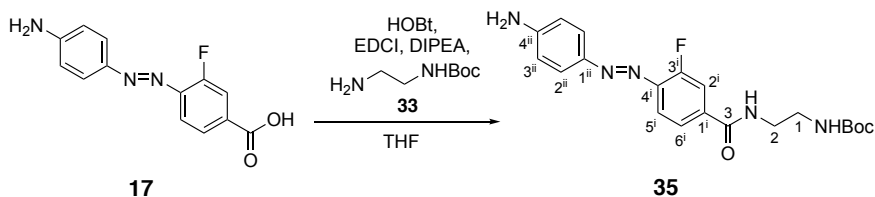
Mp > 230 °C (from Et₂O); $[\alpha]_D^{20} = -2.9$ (*c* 0.51, DMSO); **¹H NMR** (400 MHz, DMSO-*d*₆, 310 K): δ 10.68 (s, 1H, CONH-1^{iv}), 8.69 (br t, $J_{\text{NH},2^i} = 5.6$ Hz, 1H, CONH-3ⁱⁱ), 8.04 (m, 2H, H-2ⁱⁱ), 7.93 (m, 5H, H-2ⁱⁱⁱ, H-3ⁱⁱⁱ, CONH-7), 7.80 (m, 2H, H-3ⁱⁱⁱ), 7.15 (s, 2H, H-3^v, H-4^v), 4.34 (s, 2H, H-2^{iv}), 3.54 (m, 1H, H-1), 3.35 (m, 2H, H-2ⁱ), 3.25 (m, 2H, H-1ⁱ), 2.58 (m, 1H, H-3), 2.09 (m, 3H, H-2, 2xH-6), 1.69 (m, 1H, H-2), 1.51 (m, 4H, H-4, H-5); **¹³C NMR** (100.6 MHz, DMSO-*d*₆, 310 K): δ 175.7/172.2/172.1 (2xCOOH/C-7), 170.5 (C-2^v, C-5^v), 165.6 (C-1^{iv}), 165.4 (C-3ⁱ), 153.3 (C-4ⁱⁱ), 147.8 (C-4ⁱⁱⁱ), 141.8 (C-1ⁱⁱⁱ), 136.2 (C-1ⁱⁱ), 134.9 (C-3^v, C-4^v), 128.4 (C-2ⁱⁱ), 123.9 (C-2ⁱⁱⁱ), 122.0 (C-3ⁱⁱ), 119.4 (C-3ⁱⁱⁱ), 51.5 (C-1), 40.7 (C-3), 40.4 (C-2^{iv}), 38.2 (C-2ⁱ), 38.1 (C-1ⁱ), 35.3 (C-6), 32.2 (C-2), 31.1 (C-4), 22.5 (C-5); **IR** (ATR): 3280, 3089, 2922, 1711, 1545, 1431, 1143 cm⁻¹; **HRMS** (HR-ESI) calcd. for [C₃₀H₃₄N₇O₉]⁺: 636.2413; found: 636.2400. **COSY**, **DEPT 135** and **¹H/¹³C** correlation were recorded.

Synthesis of 4-[(*E*)-(4-aminophenyl)diazenyl]-3-fluorobenzoic acid, **17**

To an ice-cooled suspension of acid **15** (1.50 g, 9.67 mmol) in HCl 5.5 M (6.0 mL), a solution of NaNO₂ (753 mg, 10.9 mmol) in H₂O (6 mL) was slowly poured. The resulting mixture was added dropwise to an ice-cooled solution of aniline **22** (2.43 g, 11.6 mmol) in NaOAc 0.86 M (36 mL) and was stirred at 4 °C overnight. The dark brown paste formed was filtered, washed with H₂O and the solid obtained was dissolved in NaOH 1 M (300 mL). The resulting solution was heated to 90 °C for 2 h and, when cooled down, an orange precipitate appeared. It was filtered and recrystallised in NaOH 1 M. Afterwards, it was dissolved in the minimum quantity of H₂O and the solution was acidified to pH 2-3 with HCl 5.5 M. The orange precipitate obtained was filtered and washed with H₂O and Et₂O to afford **17** (1.19 g, 4.59 mmol, 47% yield) as an orange solid.

Physical and spectroscopic data of **17**

Mp > 265 °C (decomp. from H₂O); **¹H NMR** (250 MHz, DMSO-*d*₆): δ 7.83 (m, 2H, H-2, H-6), 7.72 (m, 3H, 2xH-2ⁱ, H-5), 6.69 (d, $_{3i,2i} = 8.6$ Hz, 2H, H-3ⁱ), 6.45 (s, 2H, NH₂); **¹³C NMR** (100.6 MHz, DMSO-*d*₆): δ 166.0 (d, $^4J_{C,F} = 2.3$ Hz, COOH), 157.8 (d, $^1J_{C,F} = 253.5$ Hz, C-3), 154.2 (C-4ⁱ), 143.6 (C-1ⁱ), 143.3 (d, $^2J_{C,F} = 7.2$ Hz, C-4), 132.2 (d, $^3J_{C,F} = 7.2$ Hz, C-1), 126.3 (C-2ⁱ), 125.8 (d, $^4J_{C,F} = 3.3$ Hz, C-6), 117.6 (C-5), 117.5 (d, $^2J_{C,F} = 21.1$ Hz, C-2), 113.6 (C-3ⁱ); **¹⁹F{¹H} NMR** (400 MHz, DMSO-*d*₆): δ -125.3 (s, F); **IR** (ATR): 3391, 1678, 1595, 1387, 1295, 1141 cm⁻¹; **HRMS** (HR-ESI) calcd. for [C₁₃H₁₀FN₃O₂+H]⁺: 258.0673; found: 258.0675. **¹H/¹³C** correlation were recorded.

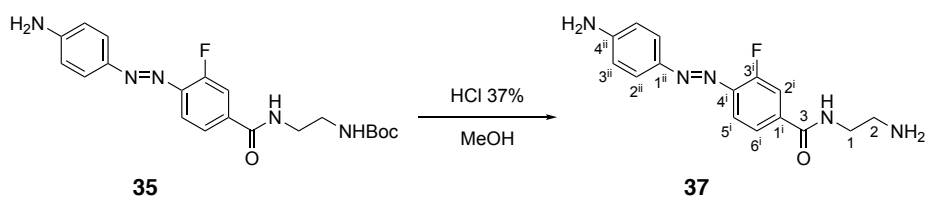
Synthesis of *tert*-butyl 2-({4-[(*E*)-(4-aminophenyl)diazenyl]-3-fluorobenzoyl}amino)ethylcarbamate, **35**

To a solution of acid **17** (200 mg, 0.77 mmol) in anhydrous THF (37 mL), a solution of HOBt (166 mg, 1.19 mmol), EDCI (0.20 mL, 1.11 mmol), DIPEA (0.58 mL, 3.31 mmol) and **33** (0.16 mL, 0.99 mmol) in anhydrous THF (20 mL) was added. The reaction mixture was stirred overnight at rt. The solution was washed with H₂O (2 x 50 mL) and the resulting aqueous extracts were extracted with CH₂Cl₂ (2 x 30 mL). The combined organic extracts were dried over anhydrous Na₂SO₄ and concentrated under vacuum. The resulting residue was purified by column chromatography (CH₂Cl₂/THF, 4:1) to obtain **35** (290 mg, 0.72 mmol, 94% yield) as an orange solid.

Physical and spectroscopic data of **35**

Mp = 170-175 °C (from THF); **¹H NMR** (400 MHz, DMSO-*d*₆): δ 8.62 (t, $J_{\text{CONH},2} = 5.6$ Hz, 1H, CONH), 7.83 (d, $J_{2^i,F} = 12.5$ Hz, 1H, H-2ⁱ), 7.72 (m, 4H, H-5ⁱ, H-6ⁱ, 2xH-2ⁱⁱ), 6.94 (br t, $J_{\text{NHBOC},1} = 5.8$ Hz, 1H, NHBoc), 6.70 (d, $J_{3^{\text{ii}},2^{\text{ii}}} = 8.9$ Hz, 2H, H-3ⁱⁱ), 6.39 (s, 2H, NH₂), 3.31 (m, 2H, H-2), 3.13 (m, 2H, H-1), 1.37 (s, 9H, C(CH₃)₃); **¹³C NMR** (100.6 MHz, DMSO-*d*₆): δ 164.7 (C-3), 157.8 (d, $^1J_{\text{C},F} = 253.0$ Hz, C-3ⁱ), 155.8 (C, carbamate), 154.0 (C-4ⁱⁱ), 143.4 (C-1ⁱⁱ), 142.0 (d, $^2J_{\text{C},F} = 7.3$ Hz, C-4ⁱ), 136.1 (d, $^3J_{\text{C},F} = 6.7$ Hz, C-1ⁱ), 126.1 (C-2ⁱⁱ), 123.8 (d, $^4J_{\text{C},F} = 3.3$ Hz, C-6ⁱ), 117.2 (C-5ⁱ), 115.8 (d, $^2J_{\text{C},F} = 21.4$ Hz, C-2ⁱ), 113.5 (C-3ⁱⁱ), 77.7 (C(CH₃)₃), 39.8 (C-1), 39.5 (C-2), 28.3 (C(CH₃)₃); **IR** (ATR): 3425, 3342, 3307, 3214, 2938, 1686, 1527, 1279, 1143 cm⁻¹; **HRMS** (HR-ESI) calcd. for [C₂₀H₂₄FN₅O₃+H]⁺: 402.1936; found: 402.1937. **COSY**, **DEPT 135** and **¹H/¹³C** correlation were recorded.

Synthesis of *N*-(2-aminoethyl)-4-[(*E*)-(4-aminophenyl)diazenyl]-3-fluorobenzamide, **37**

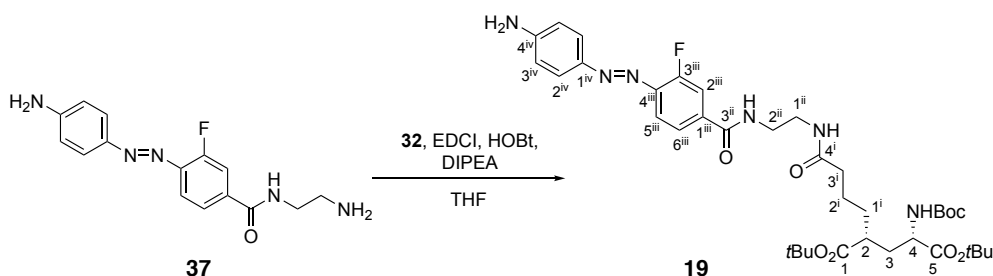


To a solution of carbamate **35** (1.09 g, 2.72 mmol) in MeOH (109 mL), HCl 37% (31 mL, 374 mmol) was added dropwise. The mixture was stirred at rt for 90 min until the complete consumption of the starting material. Afterwards, the mixture was neutralised with a saturated aqueous solution of NaHCO₃ and an orange precipitate appeared. The suspension was cooled to 0 °C, filtered and washed with Et₂O to furnish **37** (770 mg, 2.56 mmol, 94% yield) as an orange solid.

Physical and spectroscopic data of 37

Mp = 230 °C (decomp. From Et₂O); **¹H NMR** (400 MHz, DMSO-*d*₆): δ 8.99 (t, $J_{\text{CONH},2} = 5.5$ Hz, 1H, CONH), 7.96 (dd, $J_{2^{\text{i}},\text{F}} = 11.8$ Hz, $J_{2^{\text{i}},6^{\text{i}}} = 1.8$ Hz, 1H, H-2ⁱ), 7.84 (dd, $J_{6^{\text{i}},5^{\text{i}}} = 8.4$ Hz, $J_{6^{\text{i}},2^{\text{i}}} = 1.8$ Hz, 2H, H-6ⁱ), 7.69 (m, 3H, H-5ⁱ, 2xH-2ⁱⁱ), 6.69 (d, $J_{3^{\text{ii}},2^{\text{ii}}} = 8.9$ Hz, 2H, H-3ⁱⁱ), 6.45 (s, 2H, NH₂), 3.54 (m, 2H, H-1), 2.99 (t, $J_{2,1} = 5.9$ Hz, 2H, H-2); **¹³C NMR** (100.6 MHz, DMSO-*d*₆): δ 165.0 (C-3), 157.8 (d, $^1J_{\text{C},\text{F}} = 253.0$ Hz, C-3ⁱ), 154.1 (C-4ⁱⁱ), 143.3 (C-1ⁱⁱ), 142.1 (d, $^2J_{\text{C},\text{F}} = 7.3$ Hz, C-4ⁱ), 135.5 (d, $^3J_{\text{C},\text{F}} = 6.8$ Hz, C-1ⁱ), 126.1 (C-2ⁱⁱ), 124.0 (d, $^4J_{\text{C},\text{F}} = 3.1$ Hz, C-6ⁱ), 117.2 (C-5ⁱ), 116.0 (d, $^2J_{\text{C},\text{F}} = 21.7$ Hz, C-2ⁱ), 113.5 (C-3ⁱⁱ), 38.6 (C-2), 37.5 (C-1); **IR** (ATR): 3394, 3321, 3052, 2860, 2748, 2083, 1641, 1561, 1168 cm⁻¹; **HRMS** (HR-ESI) calcd. for [C₁₅H₁₆FN₅O+H]⁺: 302.1412; found: 302.1410. **¹H/¹³C** correlation was recorded.

Synthesis of di-*tert*-butyl (2*R*,4*S*)-2-(4-[[2-({4-[(*E*)-(4-aminophenyl)diazenyl]-3-fluorobenzoyl}amino)ethyl]amino]-4-oxobutyl)-4-[(*tert*-butoxycarbonyl)amino]pentanedioate, **19**



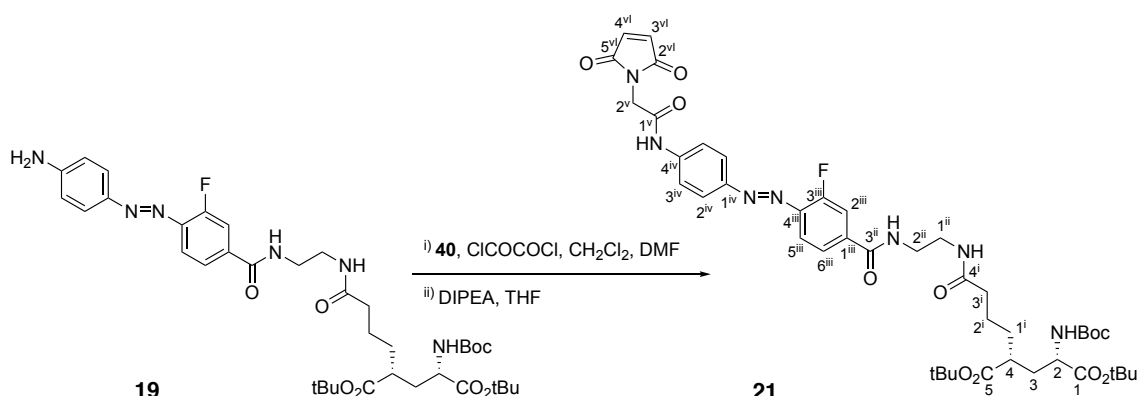
To a solution of amine **37** (200 mg, 0.66 mmol) in anhydrous THF (35 mL), a solution of **32** (324 mg, 0.72 mmol), HOBT (141 mg, 1.02 mmol), EDCI (0.16 mL, 0.89 mmol) and DIPEA (0.48 mL, 2.74 mmol) in anhydrous THF (24 mL) was added. The reaction mixture was stirred overnight at rt. The orange solution was washed with H₂O (2 x 50 mL) and the resulting aqueous extracts were extracted with CH₂Cl₂ (2 x 30 mL). The combined organic extracts were dried over anhydrous Na₂SO₄ and concentrated under vacuum. The resulting residue was purified by column chromatography (EtOAc, 100%) to give **19** (270 mg, 0.37 mmol, 53% yield) as an orange solid.

Physical and spectroscopic data of 19

Mp = 85-90 °C (from EtOAc); **[α]_D²⁰** = 2.2 (c 0.99, CHCl₃); **¹H NMR** (400 MHz, CDCl₃): δ 7.86 (d, $J_{2^{\text{iv}},3^{\text{iv}}} = 8.7$ Hz, 2H, H-2^{iv}), 7.76 (m, 2H, H-2ⁱⁱⁱ, H-5ⁱⁱⁱ), 7.71 (br t, $J_{\text{NH},2^{\text{ii}}} = 4.2$ Hz, 1H, CONH-3ⁱⁱ), 7.65

(dd, $J_{6\text{iii},5\text{iii}} = 8.5$ Hz, $J_{6\text{iii},2\text{iii}} = 1.8$ Hz, 1H, H-6ⁱⁱⁱ), 6.75 (d, $J_{3\text{iv},2\text{iv}} = 8.7$ Hz, 2H, H-3^{iv}), 6.54 (br t, $J_{\text{NH},1\text{ii}} = 5.0$ Hz, 1H, CONH-4ⁱ), 5.12 (d, $J_{\text{NHoc},4} = 8.6$ Hz, 1H, NHoc), 4.25 (s, 2H, NH₂), 4.17 (m, 1H, H-4), 3.60-3.50 (m, 4H, H-1ⁱⁱ, H-2ⁱⁱ), 2.37 (m, 1H, H-2), 2.25 (m, 2H, H-3ⁱ), 2.11 (m, 1H, H-3), 1.66 (m, 5H, H-3, 2xH-1ⁱ, 2xH-2ⁱ), 1.46 (s, 18H, 2xC(CH₃)₃), 1.43 (s, 9H, C(CH₃)₃); ¹³C NMR (100.6 MHz, CDCl₃): δ 174.7/174.6 (C-1/C-4ⁱ), 171.7 (C-5), 166.4 (d, $^4J_{\text{C},\text{F}} = 1.9$ Hz, C-3ⁱⁱ), 159.2 (d, $^1J_{\text{C},\text{F}} = 256.6$ Hz, C-3ⁱⁱⁱ), 155.5 (C, carbamate), 150.8 (C-4^{iv}), 146.0 (C-1^{iv}), 142.9 (d, $^2J_{\text{C},\text{F}} = 7.2$ Hz, C-4ⁱⁱⁱ), 136.2 (d, $^3J_{\text{C},\text{F}} = 6.8$ Hz, C-1ⁱⁱⁱ), 126.1 (C-2^{iv}), 122.9 (d, $^4J_{\text{C},\text{F}} = 3.2$ Hz, C-6ⁱⁱⁱ), 118.2 (C-5ⁱⁱⁱ), 116.2 (d, $^2J_{\text{C},\text{F}} = 21.7$ Hz, C-2ⁱⁱⁱ), 114.6 (C-3^{iv}), 82.2 (C(CH₃)₃), 81.2 (C(CH₃)₃), 79.9 (C(CH₃)₃), 52.8 (C-4), 42.3 (C-2), 42.2 (C-2ⁱⁱ), 39.7 (C-1ⁱⁱ), 36.2 (C-3ⁱ), 34.9 (C-3), 31.8 (C-1ⁱ), 28.4 (C(CH₃)₃), 28.2 (C(CH₃)₃), 28.1 (C(CH₃)₃), 23.1 (C-2ⁱ); IR (ATR): 3340, 2978, 1707, 1638, 1600, 1534, 1366, 1142 cm⁻¹; HRMS (HR-ESI) calcd. for [C₃₇H₅₃FN₆O₈+H]⁺: 729.3982; found: 729.3976. COSY, DEPT 135 and ¹H/¹³C correlation were recorded.

Synthesis of di-*tert*-butyl (2*S*,4*R*)-2-[(*tert*-butoxycarbonyl)amino]-4-(4-[[2-[[4-[(*E*)-(4-[[2,5-dioxo-2,5-dihydro-1*H*-pyrrol-1-yl)acetyl]amino]phenyl]diazenyl]-3-fluorobenzoyl] amino)ethyl], **21**

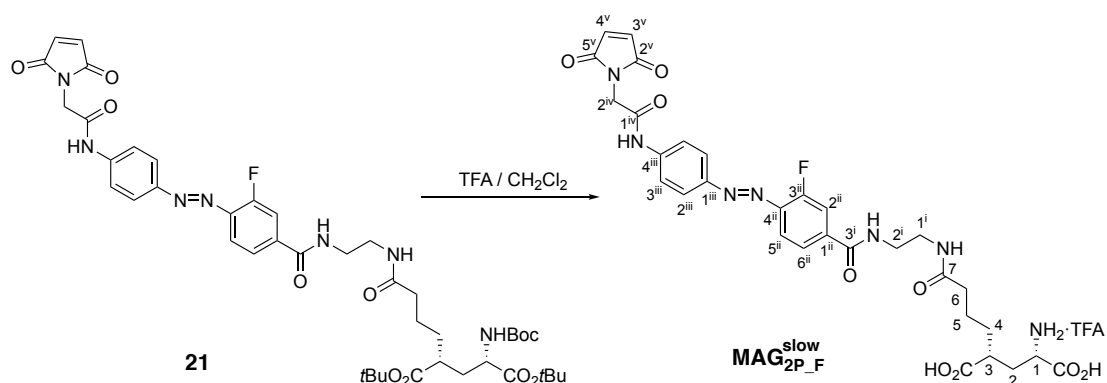


To a stirred solution of **40** (73 mg, 0.47 mmol) and oxalyl chloride 98% (43 μL, 0.50 mmol) in dry CH₂Cl₂ (7.0 mL) was added one drop of DMF. After stirring for 2 h at rt, the mixture was concentrated. The resulting acid chloride was taken up in dry THF (3.2 mL) and slowly added to an ice-cooled solution of **19** (90 mg, 0.12 mmol), DIPEA (0.13 mL, 0.74 mmol) in dry THF (15.5 mL). After stirring for 10 min at this temperature, the mixture was warmed up to rt and stirred overnight. Then, it was diluted with EtOAc (21 mL) and the resulting solution was washed with water (3 x 7 mL). The organic extract was dried over anhydrous Na₂SO₄, concentrated under vacuum and purified by column chromatography (EtOAc, 100%) to provide **21** (90 mg, 0.10 mmol, 84% yield) as an orange solid.

Physical and spectroscopic data of 21

Mp = 200-205 °C (from Et₂O); **[α]_D²⁰** = -3.1 (c 0.99, CHCl₃); **¹H NMR** (400 MHz, CDCl₃, 320 K): δ 7.94 (d, *J*_{2iv,3iv} = 8.2 Hz, 2H, H-2^{iv}), 7.92 (br s, 1H, CONH-1^v), 7.75 (m, 2H, H-2ⁱⁱⁱ, H-5ⁱⁱⁱ), 7.66 (m, 3H, 2xH-3^{iv}, H-6ⁱⁱⁱ), 7.58 (br s, 1H, CONH-3ⁱⁱ), 6.86 (s, 2H, H-3^{vi}, H-4^{vi}), 6.35 (br s, 1H, CONH-4ⁱ), 5.05 (br d, *J*_{NHBoc,2} = 6.8 Hz, 1H, NHBoc), 4.42 (s, 2H, H-2^v), 4.17 (m, 1H, H-2), 3.62 (m, 2H, H-2ⁱⁱⁱ), 3.58 (m, 2H, H-1ⁱⁱ), 2.40 (m, 1H, H-4), 2.26 (m, 2H, H-3ⁱ), 2.11 (m, 1H, H-3), 1.70 (m, 5H, H-3, 2xH-1ⁱ, 2xH-2ⁱ), 1.48 (s, 18H, 2x $C(CH_3)_3$), 1.45 (s, 9H, $C(CH_3)_3$); **¹³C NMR** (100.6 MHz, CDCl₃, 320 K): δ 174.8/174.5 (C-5/C-4ⁱ), 171.7 (C-1), 170.3 (C-2^{vi}, C-5^{vi}), 166.4 (C-3ⁱⁱ), 164.6 (C-1^v), 159.7 (d, ¹*J*_{C,F} = 259.9 Hz, C-3ⁱⁱⁱ), 155.6 (C, carbamate), 149.7 (C-1^{iv}), 142.5 (d, ²*J*_{C,F} = 7.2 Hz, C-4ⁱⁱⁱ), 140.8 (C-4^{iv}), 137.6 (d, ³*J*_{C,F} = 7.2 Hz, C-1ⁱⁱⁱ), 134.8 (C-3^{vi}, C-4^{vi}), 124.8 (C-2^{iv}), 123.0 (d, ⁴*J*_{C,F} = 3.7 Hz, C-6ⁱⁱⁱ), 120.2 (C-3^{iv}), 118.3 (C-5ⁱⁱⁱ), 116.5 (d, ²*J*_{C,F} = 21.5 Hz, C-2ⁱⁱⁱ), 82.2 ($C(CH_3)_3$), 81.2 ($C(CH_3)_3$), 80.0 ($C(CH_3)_3$), 53.1 (C-2), 42.5 (C-4), 42.1 (C-2ⁱⁱ), 41.6 (C-2^v), 39.8 (C-1ⁱⁱ), 36.3 (C-3ⁱ), 34.9 (C-3), 31.9 (C-1ⁱ), 28.5 ($C(CH_3)_3$), 28.3 ($C(CH_3)_3$), 28.2 ($C(CH_3)_3$), 23.1 (C-2ⁱ); **IR** (ATR): 3273, 3088, 2977, 2933, 1715, 1540, 1147 cm⁻¹; **HRMS** (HR-ESI) calcd. for [C₄₃H₅₆FN₇O₁₁+H]⁺: 866.4095; found: 866.4087. **COSY**, **DEPT 135** and **¹H/¹³C** correlation were recorded.

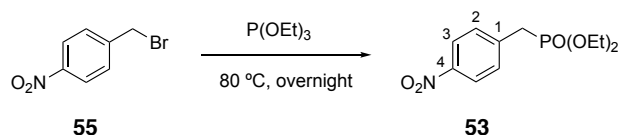
Synthesis of (1*S*,3*R*)-1,3-dicarboxy-7-[(2-((4-((*E*)-(4-((2,5-dioxo-2,5-dihydro-1*H*-pyrrol-1-yl)acetyl)amino)phenyl)diazenyl)-3-fluorobenzoyl)amino)ethyl)amino]-7-oxoheptan-1-aminium trifluoroacetate, **MAG_{2P_F}^{slow}**



To a stirred solution of compound **21** (90 mg, 0.10 mmol) in CH₂Cl₂ (20 mL), trifluoroacetic acid (7.5 mL, 97.9 mmol) was added. The mixture was stirred at rt until the starting material was consumed. Then, the solution was concentrated under vacuum and the resulting orange solid was washed with Et₂O to furnish **MAG_{2P_F}^{slow}** (77 mg, 0.10 mmol, quantitative yield).

Physical and spectroscopic data of **MAG_{2P-E}**^{slow}

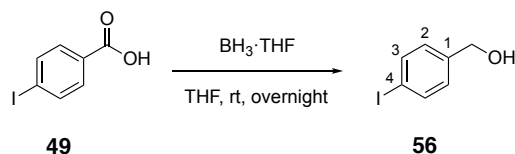
Mp > 230 °C (from Et₂O); **[α]_D²⁰** = 3.5 (*c* 0.50, DMSO); **¹H NMR** (360 MHz, DMSO-*d*₆): δ 10.77 (s, 1H, CONH-1^{iv}), 8.88 (t, *J*_{NH,2i} = 5.6 Hz, 1H, CONH-3ⁱⁱ), 8.03 (t, *J*_{NH,1i} = 5.7 Hz, 1H, CONH-7), 7.94 (m, 3H, H-2ⁱⁱ, 2xH-2ⁱⁱⁱ), 7.81 (m, 4H, 2xH-3ⁱⁱⁱ, H-5ⁱⁱ, H-6ⁱⁱ), 7.17 (s, 2H, H-3^v, H-4^v), 4.35 (s, 2H, H-2^{iv}), 3.56 (m, 1H, H-1), 3.33 (m, 2H, H-2ⁱ), 3.24 (m, 2H, H-1ⁱ), 2.57 (m, 1H, H-3), 2.08 (m, 3H, H-2, 2xH-6), 1.68 (m, 1H, H-2), 1.48 (m, 4H, H-4, H-5); **¹³C NMR** (90.5 MHz, DMSO-*d*₆): δ 175.9/172.1 (2xCOOH/C-7), 170.7 (C-2^v, C-5^v), 165.6 (C-1^{iv}), 164.4 (C-3ⁱ), 158.6 (d, ¹*J*_{C,F} = 255.3 Hz, C-3ⁱⁱ), 148.0 (C-4ⁱⁱⁱ), 142.4 (C-1ⁱⁱⁱ), 141.3 (d, ²*J*_{C,F} = 7.2 Hz, C-4ⁱⁱ), 138.1 (d, ³*J*_{C,F} = 6.5 Hz, C-1ⁱⁱⁱ), 135.0 (C-3^v, C-4^v), 124.4 (C-2ⁱⁱⁱ), 124.0 (d, ⁴*J*_{C,F} = 3.3 Hz, C-6ⁱⁱ), 119.5 (C-3ⁱⁱⁱ), 117.6 (C-5ⁱⁱⁱ), 116.1 (d, ²*J*_{C,F} = 21.7, C-2ⁱⁱ), 51.6 (C-1), 40.7 (C-3), 40.5 (C-2^{iv}), 38.7 (C-2ⁱ), 38.1 (C-1ⁱ), 35.2 (C-6), 32.3 (C-2), 31.1 (C-4), 22.5 (C-5); **IR** (ATR): 3271, 3081, 2929, 1712, 1542, 1429, 1147, 1105 cm⁻¹; **HRMS** (HR-ESI) calcd. for [C₃₀H₃₃FN₇O₉]⁺: 654.2318; found: 654.2311. **COSY**, **DEPT 135** and **¹H/¹³C** correlation were recorded.

VII.2.3. SYNTHESIS OF **Glus1** AND **Glus2**Synthesis of diethyl (4-nitrobenzyl)phosphonate, **53**

To 4-nitrobenzyl bromide **55** (3.22 g, 14.7 mmol), triethylphosphite (2.00 g, 11.8 mmol) was added at rt. The mixture was heated to 80 °C and stirred for 17 h. Afterwards, it was cooled down to rt and the leftover triethylphosphite was removed under vacuum. The resulting crude was purified by column chromatography (hexane/EtOAc, 1:1) to afford a yellow oil identified as **53** (2.93 g, 10.7 mmol, 91% yield).

Spectroscopic data of **53**

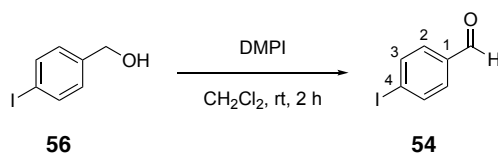
¹H NMR (250 MHz, CDCl₃): δ 8.13 (d, *J*_{3,2} = 8.9 Hz, 2H, H-3), 7.43 (d, *J*_{2,3} = 8.9 Hz, 2H, H-2), 4.01 (dq, *J*_{CH₂,CH₃} = 7.1 Hz, *J*_{CH₂,P} = 8.2 Hz, 4H, 2x-CH₂-), 3.21 (d, *J*_{CH₂P,P} = 22.1 Hz, 2H, 2x-CH₂P-), 1.22 (td, *J*_{CH₃,CH₂} = 7.1 Hz, *J*_{CH₃,P} = 0.5 Hz, 6H, 2xCH₃).

Synthesis of (4-iodophenyl)methanol, **56**

A 1.0 M solution of $\text{BH}_3\cdot\text{THF}$ complex (15 mL, 15.0 mmol) was added dropwise to a solution of 4-iodobenzoic acid **49** (2.15 g, 8.48 mmol) in dry THF (20 mL). The reaction mixture was stirred overnight at rt and then was quenched with a 2 M HCl solution (50 mL). The product was extracted with CH_2Cl_2 (3 x 70 mL), washed with a saturated solution of NaHCO_3 (2 x 80 mL) and brine (2 x 80 mL), dried over anhydrous Na_2SO_4 and concentrated under vacuum to afford **56** (1.98 g, 8.48 mmol, quantitative yield) as a beige solid.

Spectroscopic data of **56**

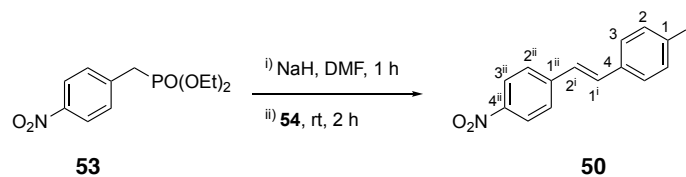
$^1\text{H NMR}$ (250 MHz, CDCl_3): δ 7.68 (d, $J_{3,2} = 8.8$ Hz, 2H, H-3), 7.12 (d, $J_{2,3} = 8.8$ Hz, 2H, H-2), 4.65 (s, 2H, $-\text{CH}_2\text{OH}$).

Synthesis of 4-iodobenzaldehyde, **54**

To alcohol **56** (640 mg, 2.73 mmol) under N_2 atmosphere, a solution of 8% DMPI in CH_2Cl_2 (15 mL, 3.86 mmol) was added. The reaction mixture was stirred at rt for 2 h and, then, was quenched with 7.5 mL of a solution prepared by the addition of $\text{Na}_2\text{S}_2\text{O}_3$ (1.7 g) to a saturated aqueous solution of Na_2HCO_3 (9 mL). Afterwards, the product was extracted with CH_2Cl_2 (3 x 40 mL) and the combined organic extracts were dried over anhydrous Na_2SO_4 and concentrated under vacuum. The resulting residue was purified by column chromatography (hexane/EtOAc, 2:1) to obtain **54** (595 mg, 2.56 mmol, 94% yield) as a beige solid.

Spectroscopic data of **54**

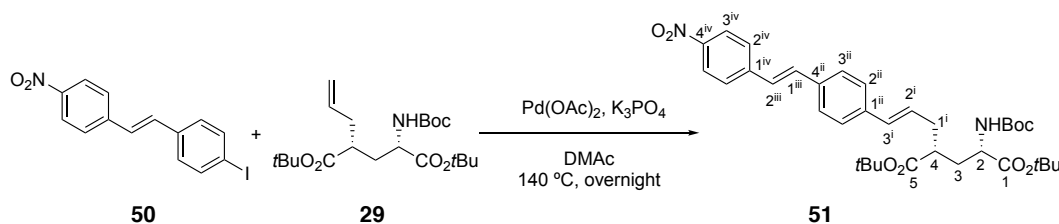
$^1\text{H NMR}$ (250 MHz, CDCl_3): δ 9.96 (s, 1H, $-\text{COH}$), 7.92 (d, $J_{3,2} = 8.4$ Hz, 2H, H-3), 7.59 (d, $J_{2,3} = 8.4$ Hz, 2H, H-2).

Synthesis of 1-iodo-4-[(*E*)-2-(4-nitrophenyl)vinyl]benzene, **50**⁴

To a solution of phosphonate **53** (1.87 g, 7.20 mmol) in dry DMF (30 mL), a 60% dispersion in mineral oil of NaH (330 mg, 13.9 mmol) was added. The resulting red suspension was stirred for 1 h, followed by the addition of aldehyde **54**. The suspension was stirred for another 2 h. Water (80 mL) was added and a green solid was collected by filtration. The obtained green solid was washed with cold water and identified as **50** (1.97 g, 5.61 mmol, 84% yield).

Spectroscopic data of **50**

¹H NMR (250 MHz, DMSO-*d*₆): δ 8.24 (d, $J_{3^{\text{ii}},2^{\text{ii}}} = 8.9$ Hz, 2H, H-3ⁱⁱ), 7.87 (d, $J_{2^{\text{ii}},3^{\text{ii}}} = 8.9$ Hz, 2H, H-2ⁱⁱ), 7.79 (d, $J_{2,3} = 8.4$ Hz, 2H, H-2), 7.48 (m, 4H, H-3, H-1ⁱ, H-2ⁱ).

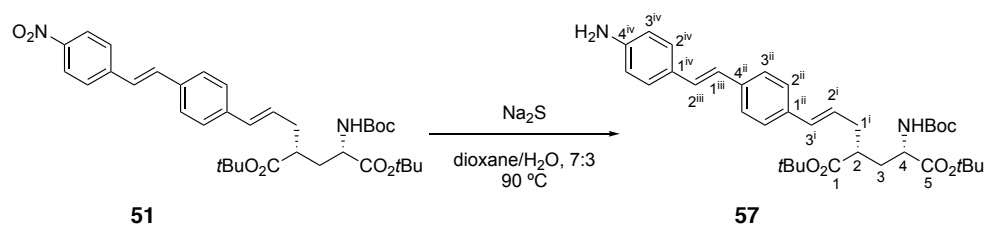
Synthesis of di-*tert*-butyl (2*S*,4*R*)-2-[(*tert*-butoxycarbonyl)amino]-4-((2*E*)-3-{4-[(*E*)-2-(4-nitrophenyl)vinyl]phenyl}prop-2-en-1-yl)pentanedioate, **51**

A mixture of stilbene **50** (73 mg, 0.21 mmol), glutamate derivative **29** (100 mg, 0.25 mmol), Pd(OAc)₂ (5 mg, 22 μmol) and K₃PO₄ (62 mg, 0.29 mmol) in DMAc (1 mL) was heated at 140 °C overnight. Then, the solvent was evaporated, and the resulting residue was purified by column chromatography (hexane/EtOAc, 8:1) to give **51** (100 mg, 0.16 mmol, 78% yield) as a yellow solid.

Physical and spectroscopic data of 51

Mp = 55-59 °C (from EtOAc); $[\alpha]_D^{20}$ = 22.9 (*c* 1.0, CHCl₃); **¹H NMR** (360 MHz, CDCl₃): δ 8.21 (d, $J_{3^{iv},2^{iv}}$ = 8.5 Hz, 2H, H-3^{iv}), 7.62 (d, $J_{2^{iv},3^{iv}}$ = 8.5 Hz, 2H, H-2^{iv}), 7.48 (d, $J_{3^{ii},2^{ii}}$ = 8.0 Hz, 2H, H-3ⁱⁱ), 7.35 (d, $J_{2^{ii},3^{ii}}$ = 8.0 Hz, 2H, H-2ⁱⁱ), 7.23 (d, $J_{2^{iii},1^{iii}}$ = 16.3 Hz, 1H, H-2ⁱⁱⁱ), 7.11 (d, $J_{1^{iii},2^{iii}}$ = 16.3 Hz, 1H, H-1ⁱⁱⁱ), 6.43 (d, $J_{3^i,2^i}$ = 15.8 Hz, 1H, H-3ⁱ), 6.15 (m, 1H, H-2ⁱ), 5.02 (d, $J_{\text{NH}Boc,2}$ = 7.8 Hz, 1H, NHBoc), 4.21 (m, 1H, H-2), 2.49 (m, 2H, H-1ⁱ, H-4), 2.41 (m, 1H, H-1ⁱ), 2.15 (m, 1H, H-3), 1.71 (m, 1H, H-3), 1.44 (s, 27H, 3xCH(CH₃)₃); **¹³C NMR** (90.5 MHz, CDCl₃): δ 174.0 (C-5), 171.8 (C-1), 155.3 (C, carbamate), 146.8 (C-4^{iv}), 144.0 (C-1^{iv}), 138.0 (C-1ⁱⁱ), 135.2 (C-4ⁱⁱ), 133.0 (C-2ⁱⁱⁱ), 131.9 (C-3ⁱ), 127.8 (C-2ⁱ), 127.4 (C-3ⁱⁱ), 126.9 (C-2^{iv}), 126.7 (C-2ⁱⁱ), 126.0 (C-1ⁱⁱⁱ), 124.3 (C-3^{iv}), 82.1 (C(CH₃)₃), 81.0 (C(CH₃)₃), 79.8 (C(CH₃)₃), 52.7 (C-2), 42.8 (C-4), 36.4 (C-1ⁱ), 34.4 (C-3), 28.4 (C(CH₃)₃), 28.2 (C(CH₃)₃), 28.1 (C(CH₃)₃); **IR** (ATR): 3367, 2976, 2930, 1713, 1337, 1148 cm⁻¹; **HRMS** (HR-ESI) calcd. for [C₃₅H₄₆N₂O₈+H]⁺: 623.3327; found: 623.3316 **COSY** and **¹H/¹³C** correlation were recorded.

Synthesis of di-*tert*-butyl (2*S*,4*R*)-2-((2*E*)-3-{4-[(*E*)-2-(4-nitrophenyl)vinyl]phenyl}prop-2-en-1-yl)-4-[(*tert*-butoxycarbonyl)amino]pentanedioate, **57**

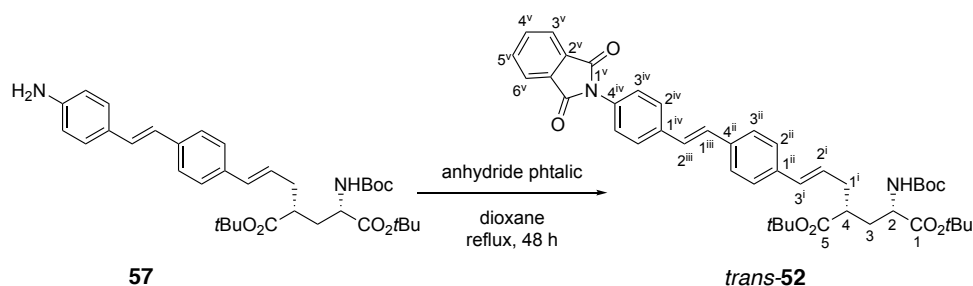


Compound **51** (200 mg, 0.32 mmol) was dissolved in a 7:3 degassed mixture of dioxane and water (4 ml) under N₂ atmosphere. The reaction mixture was heated to 90 °C and sodium sulphide (50 mg, 0.64 mmol) was added portion-wise over 1 h. After 2 h, TLC analysis (hexane/EtOAc, 1:1) of the reaction mixture revealed the absence of starting material. Then, the reaction was quenched with a saturated aqueous solution of NaHCO₃ (4.6 mL) and the crude product was extracted with CH₂Cl₂ (3 x 15 ml). The combined organic layers were dried over anhydrous Na₂SO₄ and the solvent was evaporated under vacuum to furnish an orange oil identified as **57** (190 mg, 0.32 μmol, 96% yield).

Physical and spectroscopic data of **57**

$[\alpha]_D^{20} = 40.1$ (*c* 0.98, CHCl₃); **¹H NMR** (400 MHz, CDCl₃): δ 7.39 (d, $J_{3^{ii},2^{ii}} = 8.1$ Hz, 2H, H-3ⁱⁱ), 7.32 (d, $J_{2^{iv},3^{iv}} = 8.3$ Hz, 2H, H-2^{iv}), 7.28 (d, $J_{2^{ii},3^{ii}} = 8.1$ Hz, 2H, H-2ⁱⁱ), 7.01 (d, $J_{2^{iii},1^{iii}} = 16.3$ Hz, 1H, H-2ⁱⁱⁱ), 6.88 (d, $J_{1^{iii},2^{iii}} = 16.3$ Hz, 1H, H-1ⁱⁱⁱ), 6.67 (d, $J_{3^{iv},2^{iv}} = 8.3$ Hz, 2H, H-3^{iv}), 6.40 (d, $J_{3^{i},2^{i}} = 15.7$ Hz, 1H, H-3ⁱ), 6.12 (m, 1H, H-2ⁱ), 5.02 (d, $J_{\text{NH}Boc,2} = 7.7$ Hz, 1H, NHBoc), 4.25 (m, 1H, H-4), 2.52 (m, 2H, H-1ⁱ, H-2), 2.36 (m, 1H, H-1ⁱ), 2.18 (m, 1H, H-3), 1.72 (m, 1H, H-3), 1.46/1.45 (s, 27H, 3x C(CH₃)₃); **¹³C NMR** (100.6 MHz, CDCl₃): δ 174.1 (C-5), 171.8 (C-1), 155.4 (C, carbamate), 146.3 (C-4^{iv}), 137.1 (C-1ⁱⁱ), 136.0 (C-4ⁱⁱ), 132.3 (C-3ⁱ), 128.5 (C-2ⁱⁱⁱ), 128.2 (C-1^{iv}), 127.8 (C-2^{iv}), 126.5/126.4 (C-2ⁱ/C-2ⁱⁱ/C-3ⁱⁱ), 124.8 (C-1ⁱⁱⁱ), 115.3 (C-3^{iv}), 82.0 (C(CH₃)₃), 81.0 (C(CH₃)₃), 79.7 (C(CH₃)₃), 52.8 (C-4), 42.9 (C-2), 36.4 (C-1ⁱ), 34.3 (C-3), 28.4 (C(CH₃)₃), 28.2 (C(CH₃)₃), 28.1 (C(CH₃)₃); **IR** (ATR): 3368, 2927, 2362, 1710, 1148 cm⁻¹; **HRMS** (HR-ESI) calcd. for [C₃₅H₄₈N₂O₆+H]⁺: 593.3585; found: 593.3588. **¹H/¹³C** correlation were recorded.

Synthesis of di-*tert*-butyl (2*S*,4*R*)-2-[(*tert*-butoxycarbonyl)amino]-4-[(*E*)-3-(4-[(*E*)-2-[4-(1,3-dioxo-1,3-dihydro-2*H*-isoindol-2-yl)phenyl]vinyl]phenyl)prop-2-en-1-yl] pentanedioate, *trans*-**52**



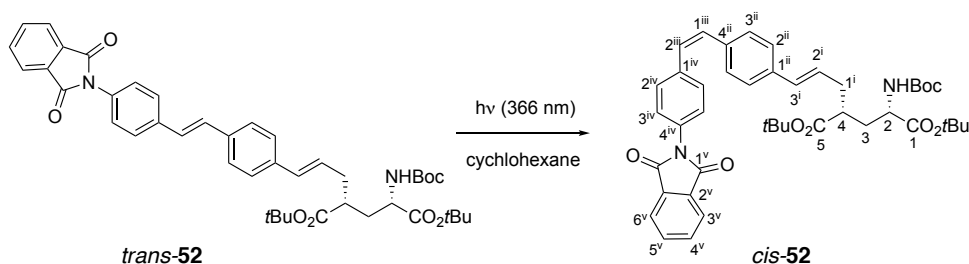
A solution of amine **57** (50 mg, 84 μ mol) and anhydride phthalic (12.5 mg, 84 μ mol) in dioxane (0.55 mL) was heated to reflux for 48 h. When TLC analysis (hexane/EtOAc, 3:1) showed no presence of the starting material, the solvent was evaporated and the resulting crude was purified by column chromatography (hexane/EtOAc, 3:1) to afford *trans*-**52** (47 mg, 65 μ mol, 77% yield) as a pale orange solid.

Physical and spectroscopic data of *trans*-**52**

Mp = 69–74 °C (from EtOAc); $[\alpha]_D^{20} = 16.1$ (*c* 1.0, CHCl₃); **¹H NMR** (360 MHz, CDCl₃): δ 7.96 (m, 2H, H-3^v, H-6^v), 7.79 (m, 2H, H-4^v, H-5^v), 7.63 (d, $J_{2^{iv},3^{iv}} = 8.5$ Hz, 2H, H-2^{iv}), 7.47 (d, $J_{3^{ii},2^{ii}} = 8.1$ Hz, 2H, H-3ⁱⁱ), 7.63 (d, $J_{3^{iv},2^{iv}} = 8.5$ Hz, 2H, H-3^{iv}), 7.33 (d, $J_{2^{ii},3^{ii}} = 8.1$ Hz, 2H, H-2ⁱⁱ), 7.12 (s, 2H, H-1ⁱⁱⁱ, H-

2ⁱⁱⁱ), 6.42 (d, $J_{3,2^i} = 15.7$ Hz, 1H, H-3ⁱ), 6.15 (m, 1H, H-2ⁱ), 5.03 (d, $J_{\text{NHoc},2} = 8.3$ Hz, 1H, NHoc), 4.21 (m, 1H, H-2), 2.51 (m, 2H, H-1ⁱ, H-4), 2.37 (m, 1H, H-1ⁱ), 2.18 (m, 1H, H-3), 1.68 (m, 1H, H-3), 1.46 (s, 9H, C(CH₃)₃), 1.45 (s, 9H, C(CH₃)₃), 1.44 (s, 9H, C(CH₃)₃); ¹³C NMR (90.5 MHz, CDCl₃): δ 174.0 (C-5), 171.8 (C-1), 167.4 (C-1^v), 155.4 (C, carbamate), 137.3 (C-1^{iv}), 137.0 (C-1ⁱⁱ), 136.1 (C-4ⁱⁱ), 134.6 (C-4^v, C-5^v), 132.1 (C-3ⁱ), 131.9 (C-2^v), 130.8 (C-4^{iv}), 129.5 (C-2ⁱⁱⁱ), 127.4 (C-1ⁱⁱⁱ), 127.1 (C-2^{iv}), 127.0 (C-2ⁱ, C-3^{iv}), 126.7 (C-3ⁱⁱ), 126.6 (C-2ⁱⁱ), 123.9 (C-3^v, C-6^v), 82.1 (C(CH₃)₃), 81.0 (C(CH₃)₃), 79.8 (C(CH₃)₃), 52.7 (C-2), 42.8 (C-4), 36.4 (C-1ⁱ), 34.4 (C-3), 28.4 (C(CH₃)₃), 28.2 (C(CH₃)₃), 28.1 (C(CH₃)₃); IR (ATR): 3367, 2974, 2926, 2954, 1709, 1515, 1366, 1148 cm⁻¹; HRMS (HR-ESI) calcd. for [C₄₃H₅₀N₂O₈+H]⁺: 723.3640; found: 723.3529. COSY, DEPT 135 and ¹H/¹³C correlation were recorded.

Synthesis of di-*tert*-butyl (2*S*,4*R*)-2-[(*tert*-butoxycarbonyl)amino]-4-[(*E*)-3-(4-[(*Z*)-2-[4-(1,3-dioxo-1,3-dihydro-2*H*-isindol-2-yl)phenyl]vinyl)phenyl]prop-2-en-1-yl] pentanedioate, *cis*-**52**



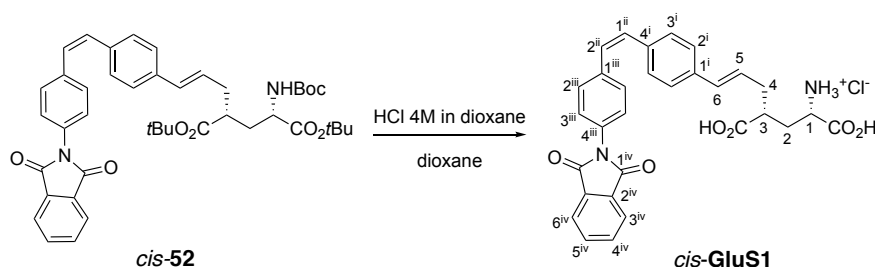
A solution of *trans*-**52** (130 mg, 0.18 mmol) in cyclohexane (122 mL) under N₂ atmosphere was irradiated at 366 nm overnight. When the mixture reached the PSS (*trans*/*cis*, 1:2), the solvent was evaporated and the two isomers were separated by column chromatography (hexane/EtOAc, from 7:1 to 5:1) to obtain *cis*-**52** as a pale yellow oil (74 mg, 0.10 mmol, 57% yield). The unreacted *trans*-**52** could be recovered and irradiated again.

Physical and spectroscopic data of *cis*-**52**

[α]_D²⁰ = 15.9 (c 1.0, CHCl₃); ¹H NMR (360 MHz, CDCl₃): δ 7.95 (m, 2H, H-3^v, H-6^v), 7.79 (m, 2H, H-4^v, H-5^v), 7.40 (d, $J_{2^{\text{iv}},3^{\text{iv}}} = 8.5$ Hz, 2H, H-2^{iv}), 7.31 (d, $J_{3^{\text{iv}},2^{\text{iv}}} = 8.5$ Hz, 2H, H-3^{iv}), 7.23 (m, 4H, H-2ⁱⁱ, H-3ⁱⁱ), 6.62 (d, $J_{2^{\text{iii}},1^{\text{iii}}} = 12.0$ Hz, 1H, H-2ⁱⁱⁱ), 6.57 (d, $J_{1^{\text{iii}},2^{\text{iii}}} = 12.0$ Hz, 1H, H-1ⁱⁱⁱ), 6.38 (d, $J_{3^{\text{i}},2^{\text{i}}} = 15.7$ Hz, 1H, H-3ⁱ), 6.09 (m, 1H, H-2ⁱ), 5.00 (d, $J_{\text{NHoc},2} = 8.0$ Hz, 1H, NHoc), 4.25 (m, 1H, H-2), 2.51 (m, 2H, H-1ⁱ, H-4), 2.34 (m, 1H, H-1ⁱ), 2.16 (m, 1H, H-3), 1.68 (m, 1H, H-3), 1.44 (s, 18H, 2x C(CH₃)₃), 1.43 (s, 9H, C(CH₃)₃); ¹³C NMR (90.5 MHz, CDCl₃): δ 174.1 (C-5), 171.8 (C-1), 167.4 (C-1^v), 155.3

(C, carbamate), 137.2 (C-1^{iv}), 136.4 (C-1ⁱⁱ), 135.9 (C-4ⁱⁱ), 134.6 (C-4^v, C-5^v), 132.1 (C-3ⁱ), 131.9 (C-2^v), 130.9 (C-4^{iv}), 130.5 (C-2ⁱⁱⁱ), 129.7 (C-2^{iv}), 129.2 (C-3ⁱⁱ), 127.0 (C-2ⁱ), 126.4 (C-3^{iv}), 126.2 (C-2ⁱⁱ, C-1ⁱⁱⁱ), 123.9 (C-3^v, C-6^v), 82.1 (C(CH₃)₃), 81.0 (C(CH₃)₃), 79.7 (C(CH₃)₃), 52.7 (C-2), 42.8 (C-4), 36.4 (C-1ⁱ), 34.3 (C-3), 28.4 (C(CH₃)₃), 28.2 (C(CH₃)₃), 28.1 (C(CH₃)₃); **IR** (ATR): 3379, 2976, 2931, 2361, 1714, 1367, 1149 cm⁻¹; **HRMS** (HR-ESI) calcd. for [C₄₃H₅₀N₂O₈+H]⁺: 723.3640; found: 723.3629. **COSY**, **DEPT 135** and ¹H/¹³C correlation were recorded.

Synthesis of (1*S*,3*R*,*E*)-1,3-dicarboxy-6-(4-((*Z*)-4-(1,3-dioxoisindolin-2-yl)styryl)phenyl) hex-5-en-1-aminium chloride, *cis*-**GluS1**

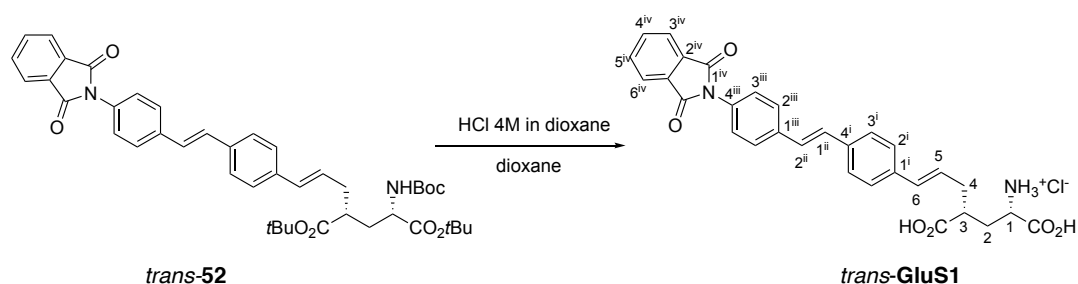


To a stirred solution of compound *cis*-**52** (74 mg, 0.10 mmol) in dioxane (4 mL), HCl 4 M in dioxane (8 mL, 32 mmol) was added dropwise. The mixture was stirred at rt for 24 h. Then, the solution was concentrated under vacuum and the resulting residue was purified by reversed phase chromatography (H₂O/MeOH, 1:2) to furnish *cis*-**GluS1** as a white-yellow solid (30 mg, 55 μmol, 55% yield).

Physical and spectroscopic data of *cis*-**GluS1**

Mp = 168-173 °C (from H₂O/MeOH); [α]_D²⁰ = -3.5 (c 0.69, DMSO); ¹H NMR (400 MHz, DMSO-*d*₆): δ 7.97 (m, 2H, H-3^{iv}, H-6^{iv}), 7.92 (m, 2H, H-4^{iv}, H-5^{iv}), 7.37 (m, 4H, H-2ⁱⁱⁱ, H-3ⁱⁱⁱ), 7.31 (m, 2H, H-2ⁱ), 7.23 (m, 2H, H-3ⁱ), 6.67 (m, 2H, H-1ⁱⁱ, H-2ⁱⁱ), 6.40 (d, *J*_{6,5} = 15.1 Hz, 1H, H-6), 6.24 (m, 1H, H-5), 3.27 (m, 1H, H-1), 2.71 (m, 1H, H-3), 2.39 (m, 1H, H-4), 2.20 (m, 1H, H-4), 2.04 (m, 1H, H-2), 1.65 (m, 1H, H-2); ¹³C NMR (150 MHz, DMSO-*d*₆, 320 K): δ 177.5/174.9 (2xCOOH), 166.7 (C-1^{iv}), 136.5 (C-1ⁱⁱⁱ), 136.1 (C-1ⁱ), 135.2 (C-4ⁱ), 134.5 (C-4^{iv}, C-5^{iv}), 131.4 (C-2^{iv}), 130.8 (C-6), 130.6 (C-4ⁱⁱⁱ), 130.4 (C-2ⁱⁱ), 128.9 (C-1ⁱⁱ), 128.7 (C-2ⁱⁱⁱ), 128.6 (C-3ⁱ), 128.0 (C-5), 126.9 (C-3ⁱⁱⁱ), 125.8 (C-2ⁱ), 123.2 (C-3^{iv}, C-6^{iv}), 53.1 (C-1), 39.3 (C-3), 33.6 (C-4), 30.5 (C-2); **IR** (ATR): 2928, 1719, 1599, 1510, 1381 cm⁻¹; **HRMS** (HR-ESI) calcd. for [C₃₀H₂₇N₂O₆]⁺: 511.1864; found: 511.1866. **COSY**, **DEPT 135** and ¹H/¹³C correlation were recorded.

Synthesis of (1*S*,3*R*,*E*)-1,3-dicarboxy-6-(4-((*E*)-4-(1,3-dioxoisindolin-2-yl)styryl)phenyl) hex-5-en-1-aminium chloride, *trans*-**GluS1**

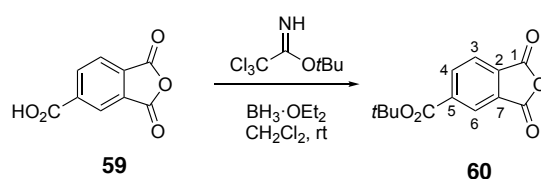


To a solution of compound *trans*-**52** (56 mg, 0.08 mmol) in dioxane (3 mL), HCl 4 M in dioxane (6 mL, 24 mmol) was added dropwise. The mixture was stirred at rt for 40 h. The resulting suspension was concentrated under vacuum and the solid obtained was washed with Et₂O, hexane and EtOAc. The cream solid was identified as *trans*-**GluS1** (35 mg, 64 μmol, 83% yield).

Physical and spectroscopic data of *trans*-**GluS1**

Mp = 213-218 °C (from EtOAc); $[\alpha]_D^{20} = 7.8$ (*c* 0.36, DMSO); **¹H NMR** (600 MHz, DMSO-*d*₆): δ 8.36 (br s, 3H, NH₃), 7.98 (m, 2H, H-3^{iv}, H-6^{iv}), 7.92 (m, 2H, H-4^{iv}, H-5^{iv}), 7.75 (d, $J_{2^{iii},3^{iii}} = 8.1$ Hz, 2H, H-2ⁱⁱⁱ), 7.59 (d, $J_{3^i,2^i} = 8.1$ Hz, 2H, H-3ⁱ), 7.46 (d, $J_{3^{iii},2^{iii}} = 8.1$ Hz, 2H, H-3ⁱⁱⁱ), 7.43 (d, $J_{2^i,3^i} = 8.1$ Hz, 2H, H-2ⁱ), 7.32 (s, 2H, H-1ⁱⁱ, H-2ⁱⁱ), 6.49 (d, $J_{6,5} = 15.7$ Hz, 1H, H-6), 6.25 (m, 1H, H-5), 3.87 (m, 1H, H-1), 2.80 (m, 1H, H-3), 2.50 (m, 2H, H-4), 2.20 (m, 1H, H-2), 1.88 (m, 1H, H-2); **¹³C NMR** (150 MHz, DMSO-*d*₆, 320 K): δ 174.7/170.5 (2xCOOH), 166.7 (C-1^{iv}), 136.7 (C-1ⁱⁱⁱ), 136.4 (C-1ⁱ), 135.8 (C-4ⁱ), 134.5 (C-4^{iv}, C-5^{iv}), 131.5 (C-6), 131.4 (C-2^{iv}), 130.9 (C-4ⁱⁱⁱ), 129.0 (C-2ⁱⁱ), 127.3 (C-1ⁱⁱ), 127.2 (C-3ⁱⁱⁱ), 126.7 (C-3ⁱ), 126.5 (C-2ⁱⁱⁱ), 126.2 (C-2ⁱ), 126.1 (C-5), 123.2 (C-3^{iv}, C-6^{iv}), 50.8 (C-1), 40.6 (C-3), 34.9 (C-4), 31.3 (C-2); **IR** (ATR): 2907, 1703, 1516, 1380 cm⁻¹; **HRMS** (HR-ESI) calcd. for [C₃₀H₂₇N₂O₆]⁺: 511.1864; found: 511.1871. **COSY**, **DEPT 135** and **¹H/¹³C** correlation were recorded.

Synthesis of *tert*-butyl 1,3-dioxo-1,3-dihydroisobenzofuran-5-carboxylate, **60**

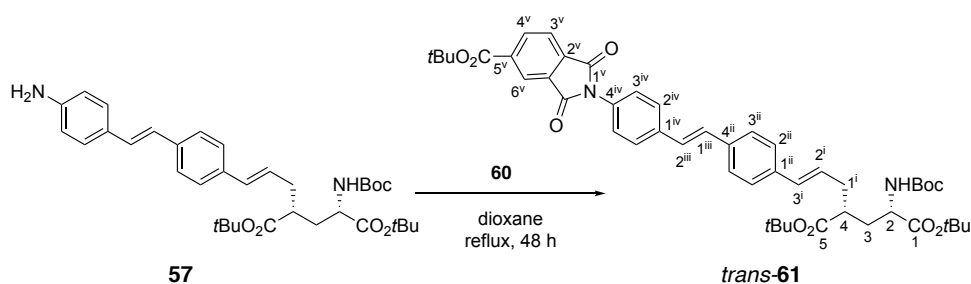


To a solution of 1,2,4-benzenetricarboxylic anhydride **59** (500 mg, 2.60 mmol) in anhydrous CH₂Cl₂ (23 mL), *tert*-butyl 2,2,2-trichloroacetimidate (1.00 mL, 5.60 mmol) and BF₃·OEt₂ (130 μL, 1.04 mmol) were added. The reaction mixture was let stir for 3 h at rt. Afterwards, a mixture of saturated solution of NaHCO₃/H₂O (1:1) (5.5 mL) was added and the product was extracted with CH₂Cl₂ (3 x 20 mL). The combined organic extracts were dried over anhydrous Na₂SO₄ and the solvent was removed under vacuum. The resulting white solid was recrystallised with hexane to give **60** (285 mg, 1.15 mmol, 44% yield) as a white solid.

Physical and spectroscopic data of **60**

Mp = 82-86 °C (from hexane); ¹H NMR (400 MHz, CDCl₃): δ 8.58 (dd, *J*_{6,4} = 1.4 Hz, *J*_{6,3} = 0.8 Hz, 1H, H-6), 8.52 (dd, *J*_{4,3} = 7.9 Hz, *J*_{4,6} = 1.4 Hz, 1H, H-4), 8.07 (dd, *J*_{3,4} = 7.9 Hz, *J*_{3,6} = 0.8 Hz, 1H, H-3), 1.64 (s, 9H, C(CH₃)₃); ¹³C NMR (100.6 MHz, CDCl₃): δ 163.0 (C-5ⁱ), 162.2 (C-1), 139.7 (C-5), 137.1 (C-4), 134.0 (C-2), 131.6 (C-7), 126.8 (C-6), 125.8 (C-3), 83.7 (C(CH₃)₃), 28.2 (C(CH₃)₃); IR (ATR): 2924, 2549, 1846, 1816, 1779, 1705, 1305, 1244 cm⁻¹; HRMS (HR-ESI) calcd. for [C₁₃H₁₂O₅+H]⁺: 249.0757; found: 249.0765. COSY and ¹H/¹³C correlation were recorded.

Synthesis of di-*tert*-butyl (2*R*,4*S*)-2-((*E*)-3-(4-((*E*)-4-(5-(*tert*-butoxycarbonyl)-1,3-dioxoisindolin-2-yl)styryl)phenyl)allyl)-4-((*tert*-butoxycarbonyl)amino)pentanedioate, *trans*-**61**



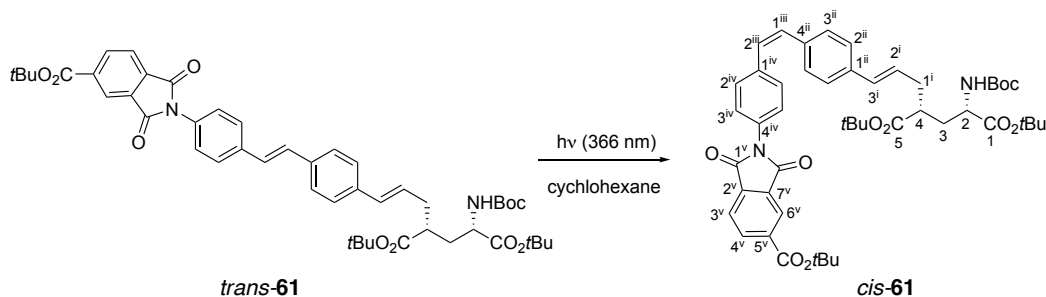
A solution of amine **57** (200 mg, 0.34 mmol) and anhydride **60** (84 mg, 0.34 mmol) in dioxane (2.3 mL) was heated to reflux for 48 h. Then, the solvent was evaporated and the resulting crude was purified by column chromatography (hexane/EtOAc, 3:1) to afford *trans*-**61** (170 mg, 0.21 mmol, 62% yield) as a yellow solid.

Physical and spectroscopic data of *trans*-**61**

Mp = 129-133 °C (from EtOAc); [α]_D²⁰ = 26.9 (c 0.9, CHCl₃); ¹H NMR (400 MHz, CDCl₃): δ 8.52 (dd, *J*_{6^v,4^v} = 1.4 Hz, *J*_{6^v,3^v} = 0.7 Hz, 1H, H-6^v), 8.43 (dd, *J*_{4^v,3^v} = 7.8 Hz, *J*_{4^v,6^v} = 1.4 Hz, 1H, H-4^v), 8.00

(dd, $J_{3v,4v} = 7.8$ Hz, $J_{3v,6v} = 0.7$ Hz, 1H, H-3^v), 7.64 (d, $J_{2iv,3iv} = 8.6$ Hz, 2H, H-2^{iv}), 7.46 (d, $J_{3ii,2ii} = 8.3$ Hz, 2H, H-3ⁱⁱ), 7.45 (d, $J_{3iv,2iv} = 8.6$ Hz, 2H, H-3^{iv}), 7.33 (d, $J_{2ii,3ii} = 8.3$ Hz, 2H, H-2ⁱⁱ), 7.12 (s, 2H, H-1ⁱⁱⁱ, H-2ⁱⁱⁱ), 6.42 (d, $J_{3i,2i} = 15.7$ Hz, 1H, H-3ⁱ), 6.15 (dt, $J_{2i,3i} = 15.7$ Hz, $J_{2i,1i} = 6.9$ Hz, 1H, H-2ⁱ), 5.03 (d, $J_{\text{NHBOC},2} = 8.6$ Hz, 1H, NHBoc), 4.27 (m, 1H, H-2), 2.52 (m, 2H, H-1ⁱ, H-4), 2.40 (m, 1H, H-1ⁱ), 2.18 (m, 1H, H-3), 1.73 (m, 1H, H-3), 1.64 (s, 9H, C(CH₃)₃), 1.46 (s, 9H, C(CH₃)₃), 1.45 (s, 9H, C(CH₃)₃), 1.44 (s, 9H, C(CH₃)₃); ¹³C NMR (100.6 MHz, CDCl₃): δ 174.0 (C-5), 171.8 (C-1), 166.7 (C-1^v), 163.8 (C-5^{vi}), 155.4 (C, carbamate), 138.2 (C-5^v), 137.6 (C-1^{iv}), 137.1 (C-1ⁱⁱ), 136.1 (C-4ⁱⁱ), 135.8 (C-4^v), 134.7 (C-2^v), 132.1 (C-3ⁱ), 131.9 (C-7^v), 130.6 (C-4^{iv}), 129.7 (C-2ⁱⁱⁱ), 127.3 (C-1ⁱⁱⁱ), 127.2 (C-2^{iv}), 127.0 (C-2ⁱ, C-3^{iv}), 126.7 (C-3ⁱⁱ), 126.6 (C-2ⁱⁱ), 124.9 (C-6^v), 123.8 (C-3^v), 83.0 (C(CH₃)₃), 82.1 (C(CH₃)₃), 81.0 (C(CH₃)₃), 79.8 (C(CH₃)₃), 52.8 (C-2), 42.9 (C-4), 36.4 (C-1ⁱ), 34.4 (C-3), 28.5 (C(CH₃)₃), 28.4 (C(CH₃)₃), 28.2 (C(CH₃)₃), 28.1 (C(CH₃)₃); IR (ATR): 3380, 2977, 2930, 1780, 1712, 1516, 1366, 1151 cm⁻¹; HRMS (HR-ESI) calcd. for [C₄₈H₅₈N₂O₁₀+H]⁺: 823.4164; found: 823.4149. COSY, DEPT 135 and ¹H/¹³C correlation were recorded.

Synthesis of di-*tert*-butyl (2*R*,4*S*)-2-((*E*)-3-(4-((*Z*)-4-(5-(*tert*-butoxycarbonyl)-1,3-dioxoisindolin-2-yl)styryl)phenyl)allyl)-4-((*tert*-butoxycarbonyl)amino)pentanedioate, *cis*-**61**



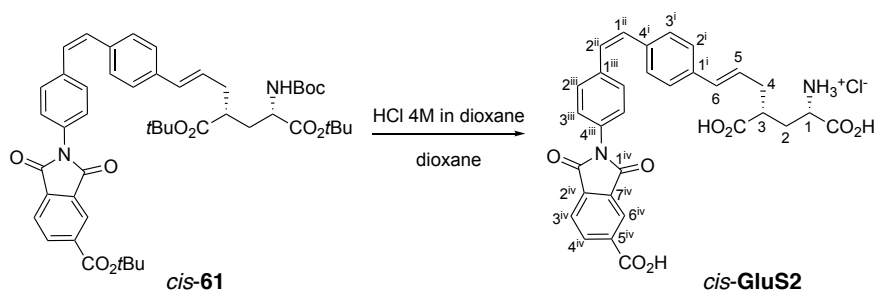
A solution of *trans*-**61** (170 mg, 0.21 mmol) in cyclohexane (160 mL) under N₂ atmosphere was irradiated at 366 nm overnight. When the mixture reached the PSS (*trans/cis*, 5:6), the solvent was evaporated and the two isomers were separated by column chromatography (hexane/EtOAc, 5:1) to obtain *cis*-**61** as a pale yellow oil (86 mg, 0.10 mmol, 50% yield). The unreacted *trans*-**61** could be fully recovered and irradiated again.

Physical and spectroscopic data of *cis*-**61**

[α]_D²⁰ = 12.4 (c 1.0, CHCl₃); ¹H NMR (360 MHz, CDCl₃): δ 8.51 (d, $J_{6v,4v} = 1.4$ Hz, 1H, H-6^v), 8.42 (dd, $J_{4v,3v} = 7.8$ Hz, $J_{4v,6v} = 1.4$ Hz, 1H, H-4^v), 7.99 (d, $J_{3v,4v} = 7.8$ Hz, 1H, H-3^v), 7.41 (d, $J_{2iv,3iv} = 8.4$ Hz, 2H, H-2^{iv}), 7.32 (d, $J_{3iv,2iv} = 8.4$ Hz, 2H, H-3^{iv}), 7.24 (m, 4H, H-2ⁱⁱ, H-3ⁱⁱ), 6.63 (d, $J_{2iii,1iii} = 12.3$ Hz, 1H,

H-2ⁱⁱⁱ), 6.57 (d, $J_{1^{iii},2^{iii}} = 12.3$ Hz, 1H, H-1ⁱⁱⁱ), 6.38 (d, $J_{3^i,2^i} = 15.7$ Hz, 1H, H-3ⁱ), 6.09 (m, 1H, H-2ⁱ), 5.00 (d, $J_{\text{NH}Boc,2} = 8.7$ Hz, 1H, NHBoc), 4.26 (m, 1H, H-2), 2.50 (m, 2H, H-1ⁱ, H-4), 2.35 (m, 1H, H-1ⁱ), 2.16 (m, 1H, H-3), 1.71 (m, 1H, H-3), 1.64 (s, 9H, C(CH₃)₃), 1.44 (s, 9H, C(CH₃)₃), 1.44 (s, 9H, C(CH₃)₃), 1.43 (s, 9H, C(CH₃)₃); ¹³C NMR (90.5 MHz, CDCl₃): δ 174.1 (C-5), 171.8 (C-1), 166.7 (C-1^v), 163.8 (C-5^{vi}), 155.5 (C, carbamate), 138.1 (C-5^v), 137.4 (C-1^{iv}), 136.4 (C-1ⁱⁱ), 135.9 (C-4ⁱⁱ), 135.8 (C-4^v), 134.7 (C-2^v), 132.1 (C-3ⁱ), 131.9 (C-7^v), 131.1 (C-2ⁱⁱⁱ), 130.2 (C-4^{iv}), 129.7 (C-2^{iv}), 129.2 (C-3ⁱⁱ), 129.1 (C-1ⁱⁱⁱ), 127.0 (C-2ⁱ), 126.3 (C-3^{iv}), 126.2 (C-2ⁱⁱ), 124.8 (C-6^v), 123.8 (C-3^v), 83.0 (C(CH₃)₃), 82.1 (C(CH₃)₃), 81.0 (C(CH₃)₃), 79.8 (C(CH₃)₃), 52.7 (C-2), 42.8 (C-4), 36.4 (C-1ⁱ), 34.3 (C-3), 28.5 (C(CH₃)₃), 28.3 (C(CH₃)₃), 28.2 (C(CH₃)₃), 28.1 (C(CH₃)₃); IR (ATR): 2923, 2853, 1782, 1714, 1366, 1152 cm⁻¹; HRMS (HR-ESI) calcd. for [C₄₈H₅₈N₂O₁₀+H]⁺: 823.4164; found: 823.4149. COSY, DEPT 135 and ¹H/¹³C correlation were recorded.

Synthesis of (1*S*,3*R*,*E*)-1,3-dicarboxy-6-(4-((*Z*)-4-(5-carboxy-1,3-dioxoisindolin-2-yl)styryl)phenyl)hex-5-en-1-aminium chloride, *cis*-GluS2



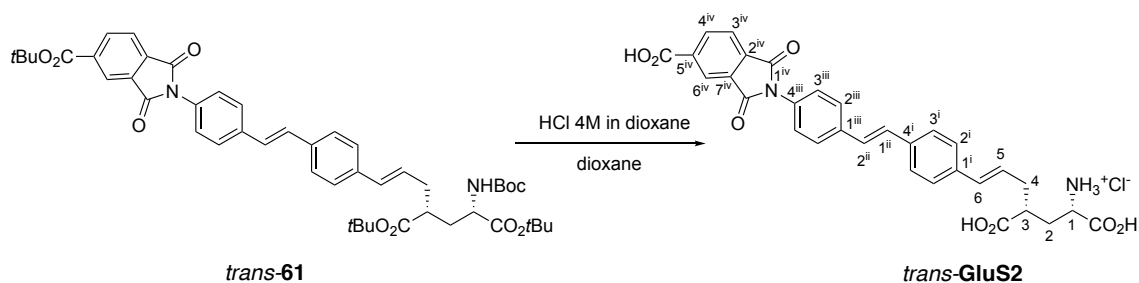
To a stirred solution of compound *cis*-61 (90 mg, 0.11 mmol) in dioxane (4.4 mL), HCl 4 M in dioxane (12 mL, 48 mmol) was added dropwise. The mixture was stirred at rt under N₂ atmosphere for 48 h. Then, the solution was concentrated under vacuum and the resulting solid was washed with Et₂O, hexane and EtOAc to furnish *cis*-GluS2 as a yellow solid (53 mg, 90 μ mol, 82% yield).

Physical and spectroscopic data of *cis*-GluS2

Mp = 172-175 °C (from EtOAc); [α]_D²⁰ = 10.3 (*c* 0.39, DMSO); ¹H NMR (360 MHz, MeOH-*d*₄): δ 8.48 (m, 2H, H-4^{iv}, H-6^{iv}), 8.03 (d, $J_{4^{iv},3^{iv}} = 7.6$ Hz, 1H, H-3^{iv}), 7.38 (d, $J_{2^{iii},3^{iii}} = 8.6$ Hz, 2H, H-2ⁱⁱⁱ), 7.33 (d, $J_{3^{iii},2^{iii}} = 8.6$ Hz, 2H, H-3ⁱⁱⁱ), 7.27 (d, $J_{2^i,3^i} = 8.1$ Hz, 2H, H-2ⁱ), 7.21 (d, $J_{3^i,2^i} = 8.1$ Hz, 2H, H-3ⁱ), 6.66 (m, 2H, H-1ⁱⁱ, H-2ⁱⁱ), 6.48 (d, $J_{6,5} = 15.8$ Hz, 1H, H-6), 6.21 (m, 1H, H-5), 4.03 (m, 1H, H-1), 2.81 (m, 1H, H-3), 2.59 (m, 2H, H-4), 2.37 (m, 1H, H-2), 2.00 (m, 1H, H-2); ¹³C NMR (100.6 MHz,

MeOH- d_4): δ 177.3/171.5 (2xCOOH), 167.9 (C-1^{iv}), 167.5 (C-5^v), 138.7 (C-1ⁱⁱⁱ), 138.1 (C-5^{iv}), 137.7 (C-1ⁱ), 137.5 (C-4ⁱ), 136.9 (C-4^{iv}), 136.4 (C-2^{iv}), 134.0 (C-6), 133.5 (C-7^{iv}), 132.0 (C-2ⁱⁱ, C-4ⁱⁱⁱ), 130.4 (C-2ⁱⁱⁱ), 130.2 (C-3ⁱ, C-1ⁱⁱ), 127.8 (C-3ⁱⁱⁱ), 127.2 (C-5, C-2ⁱ), 125.3 (C-6^{iv}), 124.7 (C-3^{iv}), 52.5 (C-1), 42.5 (C-3), 36.8 (C-4), 32.6 (C-2); **IR** (ATR): 3479, 2919, 1777, 1714, 1511, 1370, 1211 cm^{-1} ; **HRMS** (HR-ESI) calcd. for $[\text{C}_{31}\text{H}_{27}\text{ClN}_2\text{O}_8]^+$: 555.1762; found: 555.1774. **COSY**, **DEPT 135** and $^1\text{H}/^{13}\text{C}$ correlation were recorded.

Synthesis of (1*S*,3*R*,*E*)-1,3-dicarboxy-6-(4-((*E*)-4-(5-carboxy-1,3-dioxoisindolin-2-yl)styryl)phenyl)hex-5-en-1-aminium chloride, *trans*-**GluS2**



To a stirred solution of compound *trans*-**61** (40 mg, 0.05 mmol) in dioxane (2 mL), HCl 4 M in dioxane (5.5 mL, 22 mmol) was added dropwise. The mixture was stirred at rt under N_2 atmosphere for 48 h. The resulting suspension was concentrated under vacuum and the solid obtained was washed with Et_2O , hexane and EtOAc to furnish *trans*-**GluS2** as a yellow solid (29 mg, 0.05 mmol, quantitative yield).

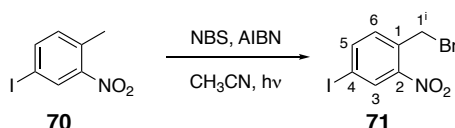
Physical and spectroscopic data of *trans*-**GluS2**

Mp = 230 °C (decomp. from EtOAc); $[\alpha]_{\text{D}}^{20}$ = 9.9 (c 0.37, DMSO); $^1\text{H NMR}$ (400 MHz, DMSO- d_6): δ 8.43 (d, $J_{4^{\text{iv}},3^{\text{iv}}} = 7.6$ Hz, 1H, H-4^{iv}), 8.36 (br s, 3H, NH₃), 8.32 (s, 1H, H-6^{iv}), 8.09 (d, $J_{3^{\text{iv}},4^{\text{iv}}} = 7.6$ Hz, 1H, H-3^{iv}), 7.76 (d, $J_{2^{\text{iii}},3^{\text{iii}}} = 8.1$ Hz, 2H, H-2ⁱⁱⁱ), 7.60 (d, $J_{3^{\text{i}},2^{\text{i}}} = 8.1$ Hz, 2H, H-3ⁱ), 7.47 (d, $J_{3^{\text{iii}},2^{\text{iii}}} = 8.1$ Hz, 2H, H-3ⁱⁱⁱ), 7.43 (d, $J_{2^{\text{i}},3^{\text{i}}} = 8.1$ Hz, 2H, H-2ⁱ), 7.32 (s, 2H, H-1ⁱⁱ, H-2ⁱⁱ), 6.49 (d, $J_{6,5} = 15.6$ Hz, 1H, H-6), 6.25 (m, 1H, H-5), 3.89 (m, 1H, H-1), 2.80 (m, 1H, H-3), 2.50 (m, 2H, H-4), 2.18 (m, 1H, H-2), 1.87 (m, 1H, H-2); $^{13}\text{C NMR}$ (100.6 MHz, DMSO- d_6): δ 175.0/170.9 (2xCOOH), 166.3 (C-1^{iv}), 165.8 (C-5^v), 137.0 (C-1ⁱⁱⁱ), 136.4 (C-1ⁱ, C-5^{iv}), 135.9 (C-4ⁱ), 135.5 (C-4^{iv}), 134.9 (C-2^{iv}), 132.1 (C-7^{iv}), 131.7 (C-6), 130.8 (C-4ⁱⁱⁱ), 129.1 (C-2ⁱⁱ), 127.4 (C-3ⁱⁱⁱ), 127.2 (C-1ⁱⁱ), 126.9 (C-3ⁱ), 126.7 (C-2ⁱⁱⁱ), 126.4 (C-2ⁱ, C-5), 123.8 (C-6^{iv}), 123.4 (C-3^{iv}), 50.8 (C-1), 40.5 (C-3), 35.1 (C-4), 31.2 (C-2); **IR**

(ATR): 3477, 2932, 1712, 1516, 1374 cm^{-1} ; **HRMS** (HR-ESI) calcd. for $[\text{C}_{31}\text{H}_{27}\text{ClN}_2\text{O}_8]^+$: 555.1762; found: 555.1774. **COSY** and $^1\text{H}/^{13}\text{C}$ correlation were recorded.

VII.2.4. SYNTHESIS OF **Glu_brAzo**

Synthesis of 1-(bromomethyl)-4-iodo-2-nitrobenzene, **71**⁵

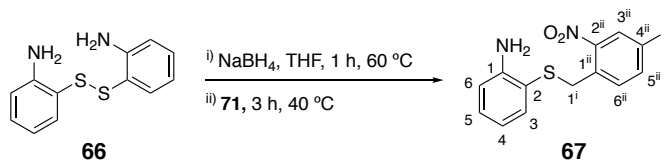


To a solution of 4-iodo-2-nitrotoluene **70** (5.00 g, 19.0 mmol) in anhydrous CH_3CN (54 mL), NBS (10.0 g, 56.2 mmol) and AIBN (312 mg, 1.90 mmol) were added. The reaction mixture was stirred overnight under reflux conditions and irradiated with white light (40 W tungsten bulb). The resulting solution was purified by column chromatography (CH_2Cl_2 100%) and the solid obtained was recrystallized with petroleum ether. Compound **71** was obtained as a cream colour solid (3.15 g, 9.21 mmol, 49% yield).

Spectroscopic data of **71**

$^1\text{H NMR}$ (250 MHz, CDCl_3): δ 8.35 (d, $J_{3,6} = 1.8$ Hz, 1H, H-3), 7.93 (dd, $J_{5,6} = 8.2$ Hz, $J_{5,3} = 1.8$ Hz, 1H, H-5), 7.30 (d, $J_{6,5} = 8.2$ Hz, 1H, H-6), 4.76 (s, 2H, H-1ⁱ).

Synthesis of 2-((4-iodo-2-nitrobenzyl)thio)aniline, **675**



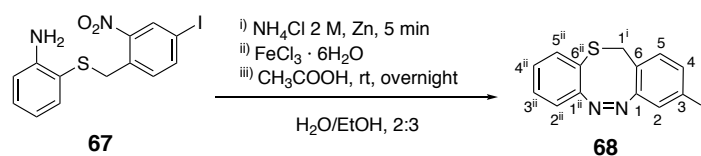
To a solution of 2,2'-disulfaneyldianiline **66** (1.20 g, 4.83 mmol) in anhydrous THF (30 mL), NaBH_4 (238 mg, 6.29 mmol) was added and the mixture was stirred at 60 °C for 1 h until the reaction had a milky appearance. Then, a solution of **71** (3.10 g, 9.07 mmol) in anhydrous THF (10 mL) was added and the resulting orange solution was heated at 40 °C for 3 h. Afterwards, the reaction mixture was poured into 200 mL of ice-water and extracted with

EtOAc (3 x 100 mL). The combined organic extracts were dried over anhydrous MgSO₄ and the solvent was removed under vacuum. The residue was purified by column chromatography (cyclohexane/EtOAc, 5:1) to give an orange oil identified as **67** (2.60 g, 6.73 mmol, 74% yield).

Spectroscopic data of **67**

¹H NMR (600 MHz, acetone-*d*₆): δ 8.29 (d, *J*_{3ⁱⁱ,5ⁱⁱ} = 1.9 Hz, 1H, H-3ⁱⁱ), 7.84 (dd, *J*_{5ⁱⁱ,6ⁱⁱ} = 8.1 Hz, *J*_{5ⁱⁱ,3ⁱⁱ} = 1.9 Hz, 1H, H-5ⁱⁱ), 7.06 (m, 1H, H-5), 6.97 (dd, *J*_{3,4} = 7.7 Hz, *J*_{3,5} = 1.5 Hz, 1H, H-3), 6.90 (d, *J*_{6ⁱⁱ,5ⁱⁱ} = 8.1 Hz, 1H, H-6ⁱⁱ), 6.76 (dd, *J*_{6,5} = 8.1 Hz, *J*_{6,4} = 1.3 Hz, 1H, H-6), 6.76 (dd, *J*_{4,5} = 7.5 Hz, *J*_{4,6} = 1.3 Hz, 1H, H-4), 5.05 (br s, 2H, -NH₂), 4.22 (s, 2H, H-1ⁱ).

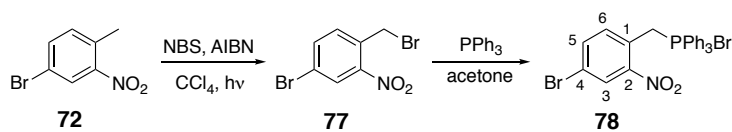
Synthesis of (*Z*)-3-iodo-12*H*-dibenzo[*b,f*][1,4,5]thiadiazocine, **68**⁵



To a solution of **67** (2.30 g, 5.96 mmol) in H₂O (55 mL) and EtOH (83 mL) at 70 °C, a 2 M solution of NH₄Cl in H₂O (27.6 mL, 55.2 mmol) was added. After that, Zn powder (1.46 g, 22.3 mmol) was added and the reaction mixture was stirred for 5 min at 70 °C. The resulting suspension was hot filtrated and then allowed to cool to 40-45 °C. The solution was added dropwise to an ice cooled solution of FeCl₃·6H₂O (3.17 g, 11.7 mmol) in 5 mL of H₂O and 4 g of ice. The ice bath was removed, and the mixture was stirred for further 15 min. Acetic acid (173 mL) was added and the reaction mixture was stirred at rt overnight. Afterwards, the solution was neutralized with NaHCO₃ and then extracted CH₂Cl₂ (2 x 100 mL). The combined organic layers were dried over MgSO₄ and the solvent was removed under vacuum. The resulting residue was purified by column chromatography (cyclohexane/EtOAc, 5:1) to furnish **68** (400 mg, 1.14 mmol, 19% yield) as a yellow solid.

Spectroscopic data of **68**

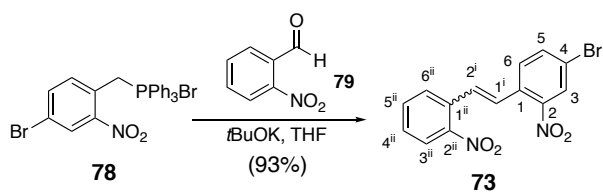
¹H NMR (600 MHz, acetone-*d*₆): δ 7.52 (dd, *J*_{4,5} = 8.1 Hz, *J*_{4,2} = 1.7 Hz, 1H, H-4), 7.28 (m, 1H, H-4ⁱⁱ), 7.21 (dd, *J*_{2,4} = 1.7 Hz, 1H, H-2), 7.14 (dd, *J*_{2ⁱⁱ,3ⁱⁱ} = 7.9 Hz, *J*_{2ⁱⁱ,4ⁱⁱ} = 1.0 Hz, 1H, H-2ⁱⁱ), 7.09 (d, *J*_{5,4} = 8.1 Hz, 1H, H-5), 7.64 (m, 1H, H-3ⁱⁱ), 6.83 (dd, *J*_{5ⁱⁱ,4ⁱⁱ} = 8.0 Hz, *J*_{5ⁱⁱ,3ⁱⁱ} = 1.3 Hz, 1H, H-5ⁱⁱ), 3.95 (d, *J*_{gem} = 11.8 Hz, 1H), 3.86 (d, *J*_{gem} = 11.8 Hz, 1H).

Synthesis of [(4-bromo-2-nitrophenyl)methyl]triphenylphosphonium bromide, **78**

To a solution of 4-bromo-2-nitrotoluene **72** (2.00 g, 9.25 mmol) in distilled CCl_4 (6.4 mL), NBS (1.90 g, 10.7 mmol) and AIBN (158 mg, 0.96 mmol) were added. The reaction mixture was stirred overnight under reflux conditions while irradiated with white light (40 W tungsten bulb). The solution was cooled down to rt, filtered and washed with CH_2Cl_2 (6 mL). The resulting red solution was washed with a saturated solution of NaHCO_3 (6 mL) and H_2O (6 mL), dried over anhydrous MgSO_4 , filtered and concentrated under vacuum. The residue was dissolved in acetone (50 mL) and PPh_3 was added (2.40 g, 9.15 mmol). The mixture was stirred under reflux conditions for 3 h and a solid precipitated. The suspension was cooled down to rt and the cream solid was filtrated and washed with acetone to give **78** (2.54 g, 4.55 mmol, 50% yield).

Spectroscopic data of **78**

$^1\text{H NMR}$ (400 MHz, $\text{DMSO}-d_6$): δ 8.24 (d, $J_{3,6} = 2.0$ Hz, 1H, H-3), 7.93 (m, 4H, H-5, Ph-3), 7.75 (m, 6H, Ph-2), 7.63 (m, 6H, Ph-1), 7.31 (dd, $J_{6,5} = 8.0$ Hz, $J_{6,P} = 2.4$ Hz, 1H, H-5), 5.42 (d, $J_{\text{CH}_2,P} = 15.2$ Hz, 2H, CH_2).

Synthesis of 4-bromo-2-nitro-1-(2-nitrostyryl)benzene, **73**

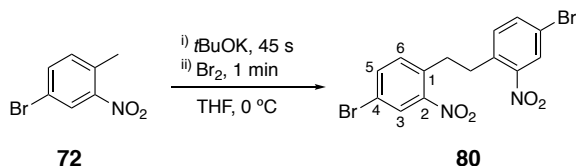
To a solution of **78** (2.54 g, 4.55 mmol) in anhydrous THF (300 mL), *t*BuOK (561 mg, 5.00 mmol) was added. The suspension was heated under reflux conditions for 10 min. Then, it was cooled down to 50 °C and 2-nitrobenzaldehyde **79** (756 mg, 5.00 mmol) was added. After stirring at this temperature for 1 h, H_2O (100 mL) was added and the product was extracted with EtOAc (100 mL). The organic layer was dried over anhydrous MgSO_4 , filtered and concentrated under vacuum. The resulting residue was purified by column chromatography

(cyclohexane/EtOAc, 1:1) affording **73** (1.47 g, 4.21 mmol, 93% yield) as a yellow solid. The product is a mixture *cis:trans* (3:1) isomers.

Physical and spectroscopic data of **73**

Mp = 90.6 °C (from EtOAc); **¹H NMR** (500 MHz, CDCl₃): δ 8.21 (d, $J_{3,5} = 2.0$ Hz, 1H, *cis*-H-3), 8.19 (d, $J_{3,5} = 2.0$ Hz, 1H, *trans*-H-3), 8.09 (dd, $J_{3ii,4ii} = 8.0$ Hz, $J_{3ii,5ii} = 1.5$ Hz, 1H, *cis*-H-3ⁱⁱ), 8.05 (dd, $J_{3ii,4ii} = 8.0$ Hz, $J_{3ii,5ii} = 1.0$ Hz, 1H, *trans*-H-3ⁱⁱ), 7.79 (m, 2H, *trans*-5, *trans*-6ⁱⁱ), 7.69 (d, $J_{6,5} = 8.4$ Hz, 1H, *trans*-H-6), 7.68 (dt, $J_{5ii,4ii} = J_{5ii,6ii} = 7.6$ Hz, $J_{5ii,3ii} = 1.0$ Hz, 1H, *trans*-H-5ⁱⁱ), 7.59 (d, $J_{2i,1i} = 16.0$ Hz, 1H, *trans*-H-2ⁱ), 7.50 (dt, $J_{4ii,3ii} = 8.0$ Hz, $J_{4ii,5ii} = 7.6$ Hz, $J_{4ii,6ii} = 1.4$ Hz, 1H, *trans*-H-4ⁱⁱ), 7.48 (d, $J_{1i,2i} = 16.0$ Hz, 1H, *trans*-H-1ⁱ), 7.42 (dd, $J_{5,6} = 8.3$ Hz, $J_{5,3} = 2.0$ Hz, 1H, *cis*-H-5), 7.37 (m, 2H, *cis*-H-4ⁱⁱ, *cis*-H-5ⁱⁱ), 7.13 (d, $J_{2i,1i} = 11.8$ Hz, 1H, *cis*-H-2ⁱ), 7.00 (d, $J_{1i,2i} = 11.8$ Hz, 1H, *cis*-H-1ⁱ), 7.00 (m, 1H, *cis*-H-6ⁱⁱ), 6.89 (d, $J_{6,5} = 8.3$ Hz, 1H, *cis*-H-6); **¹³C NMR** (125.8 MHz, CDCl₃): δ 136.8 (*trans*-C-5), 136.3 (*cis*-C-5), 133.9 (*cis*-C-6, *trans*-C-5ⁱⁱ), 133.6 (*cis*-C-5ⁱⁱ), 132.5 (*cis*-C-6ⁱⁱ, *trans*-C-1ⁱⁱ), 132.3 (*cis*-C-1ⁱⁱ), 131.6 (*trans*-C-1), 131.5 (*cis*-C-1), 130.4 (*trans*-C-6), 129.9 (*trans*-C-1ⁱ), 129.8 (*cis*-C-2ⁱ), 129.3 (*trans*-C-4ⁱⁱ), 129.2 (*trans*-C-6ⁱⁱ), 128.9 (*cis*-C-4ⁱⁱ), 128.0 (*trans*-C-3), 127.9 (*trans*-C-2ⁱ, *cis*-C-3), 127.8 (*cis*-C-1ⁱ), 125.1 (*trans*-C-3ⁱⁱ), 125.0 (*cis*-C-3ⁱⁱ), 122.2 (*trans*-C-4), 121.8 (*cis*-C-4); **IR** (ATR): 1982, 1517, 1338 cm⁻¹; **COSY** and **¹H/¹³C** correlation were recorded.

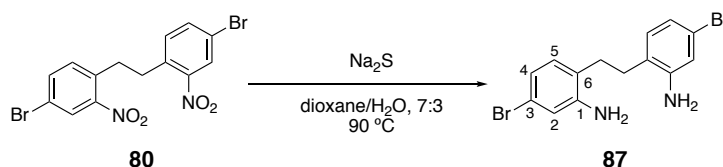
Synthesis of 1,2-bis(4-bromo-2-nitrophenyl)ethane, **80**⁶



To an ice-cooled solution of 4-bromo-2-nitrotoluene **72** (4.00 g, 18.5 mmol) in anhydrous THF (130 mL), *t*BuOK (3.10 g, 27.7 mmol) was added and the solution was stirred for 45 s. Then, Br₂ (1.4 mL, 27.3 mmol) was added and the mixture was stirred for 1 min. The reaction mixture was let warm up to rt and then was poured into ice. The resulting suspension was filtrated and the solid was washed with acetone to furnish **80** (2.84 g, 6.60 mmol, 71%) as an orange solid.

Physical and spectroscopic data of **80**

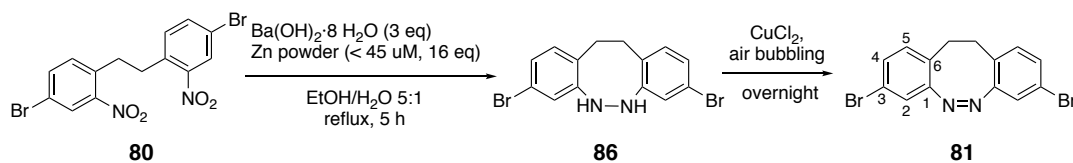
Mp = 219 °C (from acetone); **¹H NMR** (500 MHz, CDCl₃): δ 8.16 (d, $J_{3,5}$ = 2.1 Hz, 2H, H-3), 7.87 (dd, $J_{5,6}$ = 8.3 Hz, $J_{5,3}$ = 2.1 Hz, 2H, H-5), 7.41 (d, $J_{6,5}$ = 8.3 Hz, 2H, H-6), 3.10 (s, 4H, 2xCH₂); **¹³C NMR** (125.8 MHz, CDCl₃): δ 149.3 (C-2), 134.0 (C-5), 133.9 (C-6), 133.7 (C-1), 126.8 (C-3), 119.6 (C-4), 31.9 (CH₂); **IR** (ATR): 3088, 1557, 1519, 1473, 1390, 1335 cm⁻¹; **MS** (EI, 70 eV): *m/z* (%) = 213.97 (100) [M²⁺], 155.97 (66) [M-C₈H₇BrN₂O₄]; **Elemental Analysis** calcd. for [C₁₄H₁₀Br₂N₂O₄]: C, 39.10; H, 2.35; N, 6.51; found: C, 39.17; H, 2.33; N, 6.29. **COSY** and **¹H/¹³C** correlation were recorded.

Synthesis of 6,6'-(ethane-1,2-diyl)bis(3-bromoaniline), **87**

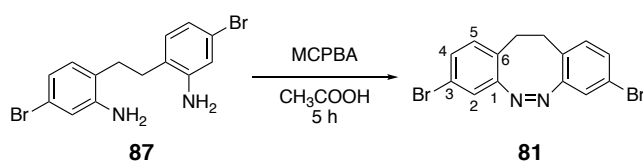
Compound **80** (100 mg, 0.23 mmol) was dissolved in a 7:3 degassed mixture of dioxane and water (2.6 ml) under N₂ atmosphere. The reaction mixture was heated to 90 °C and sodium sulfide (168 mg, 2.15 mmol) was added portion-wise over 2 h. The mixture was stirred overnight. Then, the reaction was quenched with a saturated aqueous solution of NaHCO₃ (4 mL) and the crude product was extracted with CH₂Cl₂ (3 x 5 ml). The combined organic layers were washed with H₂O, dried over anhydrous MgSO₄ and the solvent was evaporated under vacuum to furnish a crude solid identified as **87** (77 mg, 0.21 mmol, 90% yield).

Physical and spectroscopic data of **87**

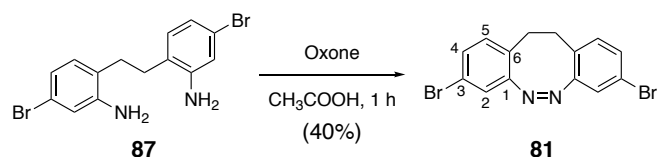
Mp = 158.8 °C (from CH₂Cl₂); **¹H NMR** (500 MHz, CDCl₃): δ 6.84 (m, 4H, H-4, H-5), 6.81 (m, 2H, H-2), 3.63 (br s, 4H, 2x-NH₂), 2.71 (s, 4H, 2xCH₂); **¹³C NMR** (125.8 MHz, CDCl₃): δ 145.8 (C-1), 131.1 (C-5), 124.7 (C-6), 121.9 (C-4), 120.7 (C-3), 118.5 (C-2), 30.4 (CH₂); **IR** (ATR): 3430, 3354, 1619, 1491, 1409, 1179 cm⁻¹; **HRMS** (HR-EI) calcd. for [C₁₄H₁₄⁷⁹Br₂N₂]: 367.9524; found: 367.9525. **COSY** and **¹H/¹³C** correlation were recorded.

Synthesis of (Z)-3,8-dibromo-11,12-dihydrodibenzo[*c,g*][1,2]diazocine, **81**

To a solution of **80** (1.50 g, 3.49 mmol) in EtOH (750 mL), a solution of Ba(OH)₂·8H₂O (3.30 g, 10.5 mmol) in H₂O (150 mL) was added. After the following addition of Zn powder (3.65 g, 55.8 mmol), the suspension was stirred for 5 h under reflux conditions. Then, the mixture was cooled down to rt and filtered through Celite[®]. A catalytic amount of CuCl₂ was added to the solution and O₂ was bubbled into it overnight. The resulting solution was neutralised with HCl 1 M. After the addition of NaHCO₃ (100 mL) a green precipitate was formed. The suspension was filtered off and the solution was concentrated under vacuum and extracted with CH₂Cl₂ (3 x 100 mL). The combined organic extracts were dried over anhydrous MgSO₄ and the solvent was removed under vacuum. The resulting residue was purified by column chromatography (cyclohexane/EtOAc, 1:1) to give a yellow solid identified as **81** (177 mg, 0.48 mmol, 14% yield).



To a solution of **87** (100 mg, 0.27 mmol) in acetic acid (200 mL), MCPBA (94 mg, 0.54 mmol) was added portion-wise for 5 h. Then, the solution was neutralised with NaOH and the product was extracted with CH₂Cl₂ (2 x 100 mL). The combined organic layers were dried over anhydrous MgSO₄, filtered and concentrated under vacuum. The resulting residue was purified by column chromatography (cyclohexane/EtOAc, 5:1) to give **81** (51 mg, 0.14 mmol, 52% yield).



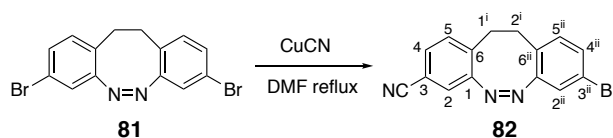
To a solution of **87** (204 mg, 0.55 mmol) in acetic acid (150 mL), Oxone[®] (126 mg, 0.83 mmol) was added in portions. The mixture was stirred at room temperature for 1 h. Then, the solvent was evaporated under vacuum and the residue was dissolved in CH₂Cl₂ (25 mL) and

washed with saturated NaHCO₃ solution (30 mL) and saturated NaCl solution (30 mL). The organic layer was dried over anhydrous MgSO₄ and the solvent was removed under vacuum. The resulting residue was purified by column chromatography (from cyclohexane/ethyl acetate 10% to ethyl acetate 100%) to give **81** as a yellow solid (80 mg, 0.22 mmol, 40% yield).

Physical and spectroscopic data of **81**

Mp = 179 °C (from EtOAc); **¹H NMR** (500 MHz, CDCl₃): δ 7.16 (dd, $J_{4,5} = 8.2$ Hz, $J_{4,2} = 2.0$ Hz, 2H, H-4), 7.00 (d, $J_{2,4} = 2.0$ Hz, 2H, H-2), 6.86 (d, $J_{5,4} = 8.2$ Hz, 2H, H-5), 2.82 (m, 4H, 2xCH₂); **¹³C NMR** (125.8 MHz, CDCl₃): δ 155.9 (C-1), 131.2 (C-5), 130.4 (C-4), 126.8 (C-6), 121.3 (C-2), 120.3 (C-3), 31.0 (CH₂); **IR** (ATR): 3042, 2162, 2046, 1743, 1585, 1559, 1465, 1382 cm⁻¹; **MS** (EI, 70 eV): m/z (%) = 365.92 (6) [M⁺], 257.99 (14) [M-BrN₂], 205.08 (3) [M-Br₂], 178.03 (100) [M-Br₂N₂]; **HRMS** (EI) calcd. for [C₁₄H₁₀⁷⁹Br₂N₂]⁺: 363.9211; found: 363.9201; **Elemental Analysis** calcd. for [C₁₄H₁₀Br₂N₂]: C, 45.94; H, 2.75; N, 7.65; found: C, 45.83; H, 2.80; N, 7.50. **COSY** and **¹H/¹³C** correlation were recorded.

Synthesis of (*Z*)-8-bromo-11,12-dihydrodibenzo[*c,g*][1,2]diazocine-3-carbonitrile, **82**



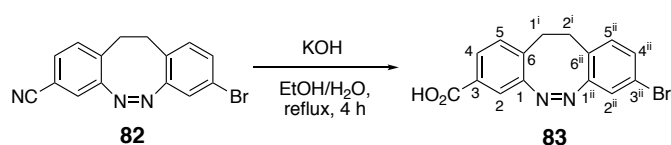
To a solution of **81** (600 mg, 1.64 mmol) in dry DMF (4 mL), CuCN (147 mg, 1.64 mmol) was added. The reaction mixture was stirred for 2 h under reflux conditions. Then, it was let to cool down to rt and a 10% aqueous solution of ethylenediamine (45 mL) was added. The product was extracted with CH₂Cl₂ (3 x 50 mL). The combined organic extracts were washed with H₂O (2 x 50 mL), dried over anhydrous MgSO₄ and concentrated under vacuum. The resulting residue was purified by column chromatography (cyclohexane/EtOAc, 3:1) to furnish unreacted **81** (210 mg, 0.57 mmol, 35%) and compound **82** (260 mg, 0.83 mmol, 51% yield; 78% yield considering recovered **81**) as a yellow solid.

Physical and spectroscopic data of **82**

Mp = 179.3 °C (from EtOAc); **¹H NMR** (500 MHz, CDCl₃): δ 7.34 (dd, $J_{4,5} = 7.9$ Hz, $J_{4,2} = 1.6$ Hz, 1H, H-4), 7.18 (dd, $J_{4^{ii},5^{ii}} = 8.2$ Hz, $J_{4^{ii},2^{ii}} = 2.0$ Hz, 1H, H-4ⁱⁱ), 7.14 (d, $J_{2,4} = 1.6$ Hz, 1H, H-2), 7.12 (d,

$J_{5,4} = 7.9$ Hz, 1H, H-5), 7.02 (d, $J_{2^{\text{ii}},4^{\text{ii}}} = 2.0$ Hz, 1H, H-2ⁱⁱ), 6.87 (d, $J_{5^{\text{ii}},4^{\text{ii}}} = 8.2$ Hz, 1H, H-5ⁱⁱ), 2.90 (m, 4H, H-1ⁱ, H-2ⁱ); **¹³C NMR** (125.8 MHz, CDCl₃): δ 155.8 (C-1ⁱⁱ), 155.1 (C-1), 133.6 (C-6), 131.3 (C-5ⁱⁱ), 130.9 (C-4), 130.7 (C-5), 130.7 (C-4ⁱⁱ), 126.2 (C-6ⁱⁱ), 122.5 (C-2), 121.7 (C-2ⁱⁱ), 120.6 (C-3ⁱⁱ), 117.9 (CN), 111.2 (C-3), 31.7 (C-1ⁱ), 30.8 (C-2ⁱ); **IR** (ATR): 3045, 2922, 2231, 1587, 1471 cm⁻¹; **HRMS** (HR-EI) calcd. for [C₁₅H₁₀⁷⁹BrN₃]: 311.0058; found: 311.0055; calcd. for [C₁₅H₁₀⁸¹BrN₃]: 313.0036; found: 313.0036. **COSY** and **¹H/¹³C** correlation were recorded.

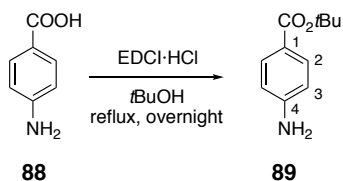
Synthesis of (Z)-8-bromo-11,12-dihydrodibenzo[*c,g*][1,2]diazocine-3-carboxylic acid, **83**



To a solution of nitrile **82** (260 mg, 0.84 mmol) in EtOH (36 mL), a solution of KOH (5.20 g, 92.7 mmol) in H₂O (11 mL) was added dropwise. The mixture was heated at reflux temperature for 4 h. Then, the EtOH was removed under vacuum and the resulting aqueous solution was acidified to pH 4. The product was extracted with EtOAc (3 x 50 mL) and the combined organic extracts were dried over anhydrous Na₂SO₄ and concentrated under vacuum to give **83** (265 mg, 0.80 mmol, 95% yield) as a black solid.

Physical and spectroscopic data of **83**

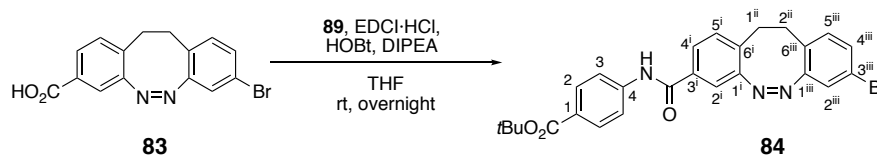
Mp > 230 °C (from EtOAc); **¹H NMR** (400 MHz, acetone-d₆): δ 7.72 (dd, $J_{4,5} = 7.9$ Hz, $J_{4,2} = 1.7$ Hz, 1H, H-4), 7.48 (d, $J_{2,4} = 1.7$ Hz, 1H, H-2), 7.24 (d, $J_{5,4} = 7.9$ Hz, 1H, H-5), 7.22 (dd, $J_{4^{\text{ii}},5^{\text{ii}}} = 8.2$ Hz, $J_{4^{\text{ii}},2^{\text{ii}}} = 2.0$ Hz, 1H, H-4ⁱⁱ), 7.11 (d, $J_{2^{\text{ii}},4^{\text{ii}}} = 2.0$ Hz, 1H, H-2ⁱⁱ), 7.06 (d, $J_{5^{\text{ii}},4^{\text{ii}}} = 8.2$ Hz, 1H, H-5ⁱⁱ), 2.94 (m, 4H, H-1ⁱ, H-2ⁱ); **¹³C NMR** (100.6 MHz, acetone-d₆): δ 166.5 (-COOH), 157.5 (C-1ⁱⁱ), 156.2 (C-1), 134.4 (C-6), 132.7 (C-5ⁱⁱ), 131.3 (C-4ⁱⁱ), 130.9 (C-5), 130.3 (C-3), 129.2 (C-4), 128.4 (C-6ⁱⁱ), 122.1 (C-2ⁱⁱ), 120.5 (C-2), 120.5 (C-3ⁱⁱ), 31.9 (C-1ⁱ), 31.3 (C-2ⁱ); **IR** (ATR): 2922, 2852, 2538, 1683, 1430, 1296, 1226 cm⁻¹; **HRMS** (HR-ESI) calcd. for [C₁₅H₁₀BrN₂O₂+H]⁺: 331.0077; found: 331.0082. **COSY** and **¹H/¹³C** correlation were recorded.

Synthesis of *tert*-butyl aminobenzoate, **89**⁷

To a solution of 4-aminobenzoic acid **88** (500 mg, 3.64 mmol) in *tert*-butyl alcohol (12 mL, dried over anhydrous Na₂SO₄), a solution of EDCI-HCl (764 mg, 3.99 mmol) in *tert*-butyl alcohol (12 mL) was added. The reaction mixture was heated to reflux temperature overnight. Then, it was cooled down to 0 °C and H₂O (20 mL) was added. The resultant mixture was extracted with EtOAc (4 x 20 mL) and the combined organic extracts were dried over anhydrous Na₂SO₄, filtered and concentrated under vacuum. A cream colour solid was obtained which was identified as **89** (690 mg, 3.57 mmol, 98% yield).

Spectroscopic data of **89**

¹H NMR (250 MHz, CDCl₃): δ 7.80 (d, *J*_{2,3} = 8.7 Hz, 2H, H-2), 6.62 (d, *J*_{3,2} = 8.7 Hz, 2H, H-3), 4.00 (br s, 2H, NH₂), 1.56 (s, 9H, C(CH₃)₃).

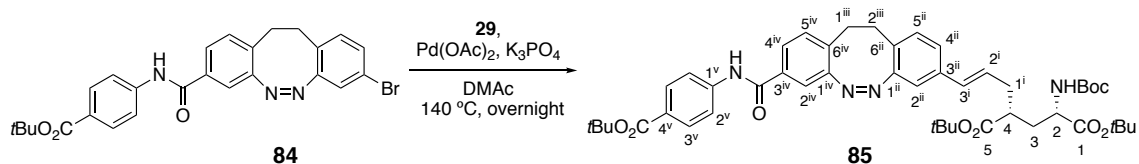
Synthesis of *tert*-butyl (*Z*)-4-(8-bromo-11,12-dihydrodibenzo[*c,g*][1,2]diazocine-3-carboxamido) benzoate, **84**

To a solution of acid **83** (50 mg, 0.15 mmol) in dry THF (7 mL), a solution of amine **89** (35 mg, 0.18 mmol), EDCI-HCl (40 mg, 0.21 mmol), HOBT (32 mg, 0.24 mmol) and DIPEA (0.11 mL, 0.63 mmol) in dry THF (3.6 mL) were added. The reaction mixture was stirred at rt overnight. Then, H₂O (20 mL) was added and the resulting mixture was extracted with CH₂Cl₂ (3 x 20 mL). The combined organic extracts were dried over anhydrous Na₂SO₄, filtered and concentrated under vacuum. The resulting residue was purified by column chromatography (hexane/EtOAc, 3:1) to furnish **84** (60 mg, 0.12 mmol, 78% yield) as a pale yellow solid.

Physical and spectroscopic data of **84**

Mp = 226-230 °C (from EtOAc); **¹H NMR** (400 MHz, CDCl₃): δ 7.98 (d, $J_{2,3} = 8.7$ Hz, 2H, H-2), 7.90 (br s, 1H, CONH), 7.67 (d, $J_{3,2} = 8.7$ Hz, 2H, H-3), 7.57 (dd, $J_{4i,5i} = 8.0$ Hz, $J_{4i,2i} = 1.9$ Hz, 1H, H-4ⁱ), 7.37 (d, $J_{2i,4i} = 1.9$ Hz, 1H, H-2ⁱ), 7.16 (dd, $J_{4iii,5iii} = 8.2$ Hz, $J_{4ii,2ii} = 2.0$ Hz, 1H, H-4ⁱⁱⁱ), 7.13 (d, $J_{5i,4i} = 8.0$ Hz, 1H, H-5ⁱ), 7.01 (d, $J_{2iii,4iii} = 2.0$ Hz, 1H, H-2ⁱⁱⁱ), 6.88 (d, $J_{5ii,4ii} = 8.2$ Hz, 1H, H-5ⁱⁱⁱ), 2.90 (m, 4H, H-1ⁱⁱ, H-2ⁱⁱ), 1.59 (s, 9H, C(CH₃)₃); **¹³C NMR** (100.6 MHz, CDCl₃): δ 165.3 (C, ester), 164.5 (C, amide), 156.1 (C-1ⁱⁱⁱ), 155.4 (C-1ⁱ), 141.5 (C-4), 133.6 (C-3ⁱ), 132.5 (C-6ⁱ), 131.4 (C-5ⁱⁱⁱ), 130.8 (C-2, C-4ⁱⁱⁱ), 130.6 (C-5ⁱ), 128.2 (C-1), 126.8 (C-6ⁱⁱⁱ), 126.2 (C-4ⁱ), 122.0 (C-2ⁱⁱⁱ), 120.6 (C-3ⁱⁱⁱ), 119.3 (C-3), 118.0 (C-2ⁱ), 81.1 (C(CH₃)₃), 31.7 (C-1ⁱⁱ), 31.1 (C-2ⁱⁱ), 28.4 (C(CH₃)₃); **IR** (ATR): 3415, 2965, 1705, 1673, 1521, 1290, 1161, 1103 cm⁻¹; **HRMS** (HR-ESI) calcd. for [C₂₆H₂₄BrN₃O₃+H]⁺: 506.1074; found: 506.1085. **COSY** and **¹H/¹³C** correlation were recorded.

Synthesis of di-tert-butyl (2*S*,4*R*)-2-((*tert*-butoxycarbonyl)amino)-4-((*E*)-3-((*Z*)-8-((4-((*tert*-butoxy carbonyl)phenyl)carbamoyl)-11,12-dihydrodibenzo[*c,g*][1,2]diazocin-3-yl)allyl) pentanedioate, **85**



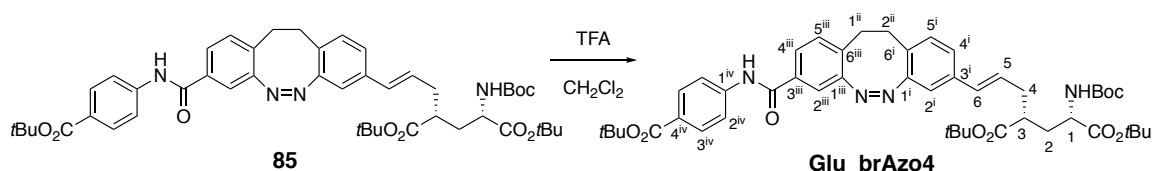
A mixture of diazocine **84** (60 mg, 0.12 mmol), glutamate derivative **29** (57 mg, 0.14 mmol), Pd(OAc)₂ (3 mg, 13 μmol) and K₃PO₄ (35 mg, 0.16 mmol) in DMAc (1.0 mL) under Ar atmosphere was heated at 140 °C overnight. Then, the solvent was evaporated and the resulting residue was purified by column chromatography (hexane/EtOAc, 5:1) to give **85** (50 mg, 60 μmol, 51% yield) as a yellow foam.

Spectroscopic data of **85**

¹H NMR (360 MHz, CDCl₃): δ 8.10 (s, 1H, -NHCO), 7.95 (d, $J_{3v,2v} = 8.2$ Hz, 2H, H-3^v), 7.66 (d, $J_{2v,3v} = 8.2$ Hz, 2H, H-2^v), 7.55 (d, $J_{4iv,5iv} = 8.0$ Hz, 1H, H-4^{iv}), 7.36 (s, 1H, H-2^{iv}), 7.11 (d, $J_{5iv,4iv} = 8.0$ Hz, 1H, H-5^{iv}), 6.98 (d, $J_{4ii,5ii} = 8.0$ Hz, 1H, H-4ⁱⁱ), 6.90 (d, $J_{5ii,4ii} = 8.0$ Hz, 1H, H-5ⁱⁱ), 6.79 (s, 1H, H-2ⁱⁱ), 6.26 (d, $J_{3i,2i} = 15.7$ Hz, 1H, H-3ⁱ), 6.02 (m, 1H, H-2ⁱ), 4.99 (d, $J_{\text{NH}Boc,2} = 8.5$ Hz, 1H, NHBoc), 4.21 (m, 1H, H-2), 2.97 (m, 2H, H-1ⁱⁱⁱ, H-2ⁱⁱⁱ), 2.79 (m, 2H, H-1ⁱⁱⁱ, H-2ⁱⁱⁱ), 2.43 (m, 2H, H-1ⁱ, H-4), 2.31 (m, 1H, H-

1ⁱ), 2.13 (m, 1H, H-3), 1.68 (m, 1H, H-3), 1.58 (s, 9H, C(CH₃)₃), 1.40 (s, 18H, C(CH₃)₃), 1.37 (s, 9H, C(CH₃)₃); ¹³C NMR (90.6 MHz, CDCl₃): δ 173.9 (C-5), 171.7 (C-1), 165.4 (C, ester), 164.7 (C, amide), 155.4 (C, carbamate, C-1ⁱⁱ, C-1^{iv}), 141.7 (C-1^v), 133.5 (C-3ⁱⁱ), 133.3 (C-3^{iv}), 132.9 (C-6^{iv}), 131.1 (C-3ⁱ), 130.7 (C-3^v), 130.5 (C-5^{iv}), 130.1 (C-5ⁱⁱ), 127.9 (C-2ⁱ, C-4^v), 126.4 (C-6ⁱⁱ), 126.0 (C-4^{iv}), 125.3 (C-4ⁱⁱ), 119.2 (C-2^v), 118.0 (C-2^{iv}), 116.5 (C-2ⁱⁱ), 82.1 (C(CH₃)₃), 81.0 (C(CH₃)₃), 79.8 (C(CH₃)₃), 52.7 (C-2), 42.7 (C-4), 36.2 (C-1ⁱ), 34.4 (C-3), 31.8 (C-1ⁱⁱⁱ), 31.4 (C-2ⁱⁱⁱ), 28.4 (C(CH₃)₃), 28.3 (C(CH₃)₃), 28.1 (2xC(CH₃)₃); IR (ATR): 3343, 2983, 2931, 1710, 1528, 1148 cm⁻¹; HRMS (HR-ESI) calcd. for [C₄₇H₆₀N₄O₉+H]⁺: 825.4433; found: 825.4418. COSY and ¹H/¹³C correlation were recorded.

Synthesis of (1*S*,3*R*,*E*)-1,3-dicarboxy-6-((*Z*)-8-((4-carboxyphenyl)carbamoyl)-11,12-dihydrodibenzo[*c,g*][1,2]diazocin-3-yl)hex-5-en-1-aminium trifluoroacetate, **Glu_brAzo4**



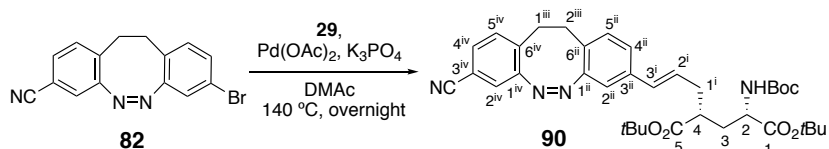
To a solution of **85** (50 mg, 61 μmol) in CH₂Cl₂ (9 mL), trifluoroacetic acid (4.5 mL, 59 mmol) was added. The mixture was stirred for 2 h and the solvent was evaporated under vacuum. The resulting solid was washed with Et₂O, hexane and EtOAc to give **Glu_brAzo4** (20 mg, 30 μmol, 50% yield) as a pale orange solid.

Physical and spectroscopic data of **Glu_brAzo4**

Mp > 230 °C (from EtOAc); [α]_D²⁰ = -6.0 (c 0.25, DMSO); ¹H NMR (400 MHz, DMSO-*d*₆): δ 10.50 (s, 1H, -NHCO), 7.92 (d, *J*_{3^{iv},2^{iv}} = 8.7 Hz, 2H, H-3^{iv}), 7.85 (d, *J*_{2^{iv},3^{iv}} = 8.7 Hz, 2H, H-2^{iv}), 7.68 (d, *J*_{4ⁱⁱⁱ,5ⁱⁱⁱ} = 7.9 Hz, 1H, H-4ⁱⁱⁱ), 7.46 (s, 1H, H-2ⁱⁱⁱ), 7.29 (d, *J*_{5ⁱⁱⁱ,4ⁱⁱⁱ} = 7.9 Hz, 1H, H-5ⁱⁱⁱ), 7.11 (d, *J*_{4ⁱ,5ⁱ} = 8.0 Hz, 1H, H-4ⁱ), 7.06 (d, *J*_{5ⁱ,4ⁱ} = 8.0 Hz, 1H, H-5ⁱ), 6.90 (s, 1H, H-2ⁱ), 6.34 (d, *J*_{6,5} = 15.5 Hz, 1H, H-6), 6.15 (m, 1H, H-5), 3.29 (m, 1H, H-1), 2.86 (m, 4H, H-1ⁱⁱ, H-2ⁱⁱ), 2.68 (m, 1H, H-3), 2.50 (m, 2H, H-4), 2.04 (m, 1H, H-2), 1.65 (m, 1H, H-2); ¹³C NMR (90.6 MHz, DMSO-*d*₆): δ 172.8/171.8 (2xCOOH), 166.9 (COOH), 164.7 (C, amide), 155.1 (C-1ⁱⁱⁱ), 154.6 (C-1ⁱ), 143.0 (C-1^{iv}), 135.9 (C-3ⁱ), 133.0 (C-3ⁱⁱⁱ), 132.3 (C-6ⁱⁱⁱ), 130.2 (C-3^{iv}, C-5ⁱ, C-5ⁱⁱⁱ), 128.2 (C-6), 126.6 (C-5, C-6ⁱ), 125.6 (C-4ⁱⁱⁱ, C-4^{iv}), 124.7 (C-4ⁱ), 119.5 (C-2^{iv}), 118.0 (C-2ⁱⁱⁱ), 116.0 (C-2ⁱ), 50.7 (C-1), 40.1 (C-3), 35.5 (C-4), 31.1 (C-2), 30.9 (C-

1ⁱⁱ), 31.4 (C-2ⁱⁱ); **IR** (ATR): 2923, 1676, 1599, 1521, 1247, 1176 cm⁻¹; **HRMS** (HR-ESI) calcd. for [C₃₀H₂₉N₄O₇]⁺: 557.2031; found: 557.2040. **COSY** and ¹H/¹³C correlation were recorded.

Synthesis of di-*tert*-butyl (2*S*,4*R*)-2-((*tert*-butoxycarbonyl)amino)-4-((*E*)-3-((*Z*)-8-cyano-11,12-dihydrodibenzo[*c,g*][1,2]diazocin-3-yl)allyl)pentanedioate, **90**

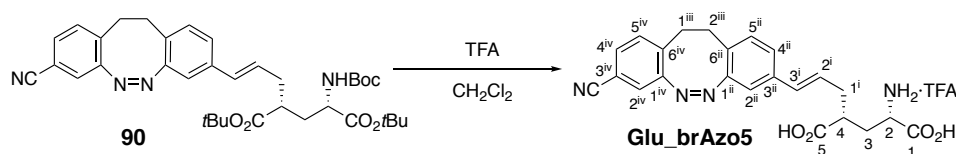


A mixture of diazocine **82** (30 mg, 96 μmol), glutamate derivative **29** (46 mg, 0.12 mmol), Pd(OAc)₂ (3 mg, 10 μmol) and K₃PO₄ (30 mg, 0.14 mmol) in DMAc (0.5 mL) under Ar atmosphere was heated at 140 °C overnight. Then, the solvent was evaporated and the resulting residue was purified by column chromatography (hexane/EtOAc, 3:1) to give **90** (37 mg, 59 μmol, 61% yield) as a yellow solid.

Physical and spectroscopic data of **90**

Mp = 66.5 °C (from EtOAc); [α]_D²⁰ = 14.4 (c 1.0, CHCl₃); ¹H NMR (500 MHz, CDCl₃): δ 7.30 (dd, *J*_{4^{iv},5^{iv}} = 7.9 Hz, *J*_{4^{iv},2^{iv}} = 1.7 Hz, 1H, H-4^{iv}), 7.11 (d, *J*_{5^{iv},4^{iv}} = 7.9 Hz, 1H, H-5^{iv}), 7.09 (d, *J*_{2^{iv},4^{iv}} = 1.7 Hz, 1H, H-2^{iv}), 7.00 (d, *J*_{4ⁱⁱ,5ⁱⁱ} = 8.0 Hz, 1H, H-4ⁱⁱ), 6.89 (d, *J*_{5ⁱⁱ,4ⁱⁱ} = 8.0 Hz, 1H, H-5ⁱⁱ), 6.87 (s, 1H, H-2ⁱⁱ), 6.29 (d, *J*_{3ⁱ,2ⁱ} = 15.8 Hz, 1H, H-3ⁱ), 6.07 (m, 1H, H-2ⁱ), 4.99 (d, *J*_{NHBoc,2} = 8.5 Hz, 1H, NHBoc), 4.23 (m, 1H, H-2), 2.90 (m, 4H, H-1ⁱⁱⁱ, H-2ⁱⁱⁱ), 2.44 (m, 2H, H-1ⁱ, H-4), 2.35 (m, 1H, H-1ⁱ), 2.15 (m, 1H, H-3), 1.68 (m, 1H, H-3), 1.44 (s, 9H, C(CH₃)₃), 1.43 (s, 9H, C(CH₃)₃), 1.40 (s, 9H, C(CH₃)₃); ¹³C NMR (125.8 MHz, CDCl₃): δ 173.9 (C-5), 171.7 (C-1), 155.6 (C carbamate, C-1ⁱⁱ), 155.1 (C-1^{iv}), 136.7 (C-3ⁱⁱ), 134.3 (C-6^{iv}), 130.8 (C-3ⁱ, C-5^{iv}), 130.7 (C-4^{iv}), 130.2 (C-5ⁱⁱ), 128.2 (C-2ⁱ), 126.0 (C-6ⁱⁱ), 125.4 (C-4ⁱⁱ), 122.5 (C-2^{iv}), 118.1 (CN), 116.3 (C-2ⁱⁱ), 111.0 (C-3^{iv}), 82.1 (C(CH₃)₃), 81.1 (C(CH₃)₃), 79.8 (C(CH₃)₃), 52.7 (C-2), 42.7 (C-4), 36.2 (C-1ⁱ), 34.4 (C-3), 32.0 (C-1ⁱⁱⁱ), 31.2 (C-2ⁱⁱⁱ), 28.4 (C(CH₃)₃), 28.1 (2xC(CH₃)₃); **IR** (ATR): 2978, 2932, 2232, 1714, 1367, 1148 cm⁻¹; **HRMS** (HR-ESI) calcd. for [C₃₆H₄₆N₄O₆+Na]⁺: 653.3310; found: 653.3296. **COSY** and ¹H/¹³C correlation were recorded.

Synthesis of (1*S*,3*R*,*E*)-1,3-dicarboxy-6-((*Z*)-8-cyano-11,12-dihydrodibenzo[*c,g*][1,2] diazocin-3-yl)hex-5-en-1-aminium chloride, **Glu_brAzo5**



To a solution of **90** (45 mg, 0.07 mmol) in CH_2Cl_2 (11 mL), trifluoroacetic acid (4 mL, 52.2 mmol) was added. After stirring 2 h at rt, the solution was concentrated under vacuum. The resulting solid was washed with Et_2O , hexane and EtOAc to furnish **Glu_brAzo5** (30 mg, 0.06 mmol, 81% yield) as a brown solid.

Physical and spectroscopic data of **Glu_brAzo5**

Mp = 134-139°C (from EtOAc); $[\alpha]_D^{20}$ = 20.8 (*c* 0.18, DMSO- d_6); **$^1\text{H NMR}$** (360 MHz, DMSO- d_6): δ 7.55 (d, $J_{4^{iii},5^{iv}}$ = 7.8 Hz, 1H, H-4ⁱⁱⁱ), 7.44 (s, 1H, H-2ⁱⁱⁱ), 7.34 (d, $J_{5^{iii},4^{iii}}$ = 7.8 Hz, 1H, H-5ⁱⁱⁱ), 7.12 (d, $J_{4^i,5^i}$ = 7.9 Hz, 1H, H-4ⁱ), 7.04 (d, $J_{5^i,4^i}$ = 7.9 Hz, 1H, H-5ⁱ), 6.88 (s, 1H, H-2ⁱ), 6.37 (d, $J_{6,5}$ = 15.6 Hz, 1H, H-6), 6.15 (m, 1H, H-5), 3.80 (m, 1H, H-1), 2.87 (m, 4H, H-1ⁱⁱ, H-2ⁱⁱ), 2.71 (m, 1H, H-3), 2.50 (m, 2H, H-4), 2.13 (m, 1H, H-2), 1.77 (m, 1H, H-2); **$^{13}\text{C NMR}$** (90.5 MHz, DMSO- d_6): δ 175.0/170.9 (2xCOOH), 155.1 (C-1ⁱⁱⁱ), 155.0 (C-1ⁱ), 135.9 (C-3ⁱ), 134.6 (C-6ⁱⁱⁱ), 131.2 (C-5ⁱⁱⁱ), 131.0 (C-4ⁱⁱⁱ), 130.8 (C-6), 130.4 (C-5ⁱ), 127.7 (C-5), 126.3 (C-6ⁱ), 125.0 (C-4ⁱ), 122.2 (C-2ⁱⁱⁱ), 118.1 (CN), 115.8 (C-2ⁱ), 109.6 (C-3ⁱⁱⁱ), 50.9 (C-1), 40.4 (C-3), 35.0 (C-4), 31.3 (C-2), 30.9 (C-1ⁱⁱ), 30.3 (C-2ⁱⁱ); **IR** (ATR): 2934, 2231, 1675, 1606, 1243, 1200, 1134 cm^{-1} ; **HRMS** (HR-ESI) calcd. for $[\text{C}_{23}\text{H}_{23}\text{N}_4\text{O}_4]^+$: 419.1714; found: 419.1718. **COSY** and **$^1\text{H}/^{13}\text{C}$** correlation were recorded.

VII.3. PHOTOCHEMICAL CHARACTERISATION

VII.3.1. PHOTOINDUCED ISOMERISATION

10^{-5} M solutions of the compounds of interest in the corresponding solvent mixtures (**MAG_{2P}^{slow}** and **MAG_{2P-F}^{slow}** in PBS:DMSO 99:1, **GluS1-2** in MeOH or PBS:MeOH 2:1, **Glu_brAzo4-5** in PBS:DMSO 1:1) were irradiated close to the maxima of their absorption bands with monochromatic light (**MAG_{2P}^{slow}** and **MAG_{2P-F}^{slow}**, λ_{exc} = 355, 366, 473 nm; **GluS1-2**, λ_{exc} = 355 nm;

Glu_brAzo4-5, $\lambda_{\text{exc}} = 405, 532 \text{ nm}$). Photoinduced changes arising from *trans*→*cis* or *cis*→*trans* isomerisation were monitored by UV-Vis absorption spectroscopy.

VII.3.2. COMPOSITION OF THE PHOTOSTATIONARY STATES BY NMR

Solutions of 5-10 mg of the compounds of interest in 0.5 mL of DMSO-*d*₆ were irradiated close to the maxima of their absorption bands with monochromatic light (**MAG**_{2P}^{slow}, **MAG**_{2P}^{slow}_F and **GluS2**, $\lambda_{\text{exc}} = 366 \text{ nm}$; **Glu_brAzo4-5**, $\lambda_{\text{exc}} = 405 \text{ nm}$). Then ¹H-NMR and UV-vis spectra of the mixtures were registered to determine: (i) the composition of the PSS states; and (ii) the absorption spectrum of the *cis* isomer of **MAG**_{2P}^{slow} and **MAG**_{2P}^{slow}_F and the *trans* isomer of **Glu_brAzo4-5**.

VII.3.3. ISOMERISATION QUANTUM YIELDS

Photoisomerisation quantum yields were determined by comparison with reported reference compounds. Equation VII-1 was employed to determine *trans*→*cis* and *cis*→*trans* photoisomerisation quantum yield values ($\Phi_{\text{trans} \rightarrow \text{cis}}$ and $\Phi_{\text{cis} \rightarrow \text{trans}}$) of **GluS2** in PBS:MeOH 2:1 and **Glu_brAzo4-5** in PBS:DMSO 1:1 from UV-vis absorption measurements of the sample and reference of interest:⁸

$$\ln \left(\frac{C_R}{C_R^0} \right) = \alpha \int_{t_0}^t \frac{1 - 10^{-\text{Abs}^{\text{tot}}}}{\text{Abs}^{\text{tot}}} dt \quad (\text{VII-1})$$

where

$$\alpha = -\Phi \cdot I_0 \cdot \epsilon_R \cdot b \quad (\text{VII-2})$$

In this equation C_R is the concentration of the starting isomer at various illumination times t , I_0 is the incident light intensity, b is the cell path length, and Abs^{tot} and ϵ_R are the total absorbance and molar absorptivity of R at the irradiation wavelength. Azobenzene ($\Phi_{\text{trans} \rightarrow \text{cis}} = 0.15$ and $\Phi_{\text{cis} \rightarrow \text{trans}} = 0.35$ in acetonitrile)⁹ and 1,2-bis(5-chloro-2-methyl-3-thienyl)perfluoro cyclopentene ($\Phi_{\text{ring opening}} = 0.13$ in hexane)¹⁰ were used as references in the measurements of **GluS2** and **Glu_brAzo4-5**, respectively.

Equation VII-3 was employed to determine *trans*→*cis* and *cis*→*trans* photoisomerisation quantum yield values ($\Phi_{trans\rightarrow cis}$ and $\Phi_{cis\rightarrow trans}$) of **MAG**, **MAG_{2P}^{slow}** and **MAG_{2P-F}^{slow}** in PBS:DMSO 99:1 from UV-vis absorption measurements of the sample and reference of interest:¹¹

$$\frac{d[A]}{dt} = - \left[\left(\Phi_{A\rightarrow B} \varepsilon_A^{\lambda_{exc}} + \Phi_{B\rightarrow A} \varepsilon_B^{\lambda_{exc}} \right) I_0 \cdot l \cdot F + k_{B\rightarrow A}^{thermal} \right] [A] + \left(\Phi_{B\rightarrow A} \varepsilon_B^{\lambda_{exc}} \cdot I_0 \cdot l \cdot F + k_{B\rightarrow A}^{thermal} \right) [A_0] \quad \text{(VII-3)}$$

where

$$F = \frac{(1 - 10^{-Abs^{tot}})}{Abs^{tot}} \quad \text{(VII-4)}$$

In this equation [A] is the concentration of the starting isomer at various illumination times *t*, [A₀] is the initial concentration of the starting isomer, *I*₀ is the incident light intensity, *l* is the cell path length, Abs^{tot} is the total absorbance, ε_A and ε_B are the molar absorptivity of the starting isomer A and the short-lived isomer B at the irradiation wavelength. Azobenzene ($\Phi_{trans\rightarrow cis} = 0.15$ and $\Phi_{cis\rightarrow trans} = 0.35$ in acetonitrile)⁹ was used as reference in these measurements.

VII.3.4. THERMAL BACK-ISOMERISATION

10⁻⁵ M solutions of the compounds of interest were irradiated with monochromatic light (**MAG_{2P}^{slow}** and **MAG_{2P-F}^{slow}** in PBS:DMSO 99:1, $\lambda_{exc} = 366$ nm; **Glu_brAzo4-5** in PBS:DMSO 1:1, $\lambda_{exc} = 405$ nm) until no changes were observed by UV-vis absorption spectroscopy. The PSS mixtures absorption variation in the dark at 25 °C was recorded and the changes in the absorption at their maximum wavelength were plotted to determine thermal *cis*→*trans* (**MAG_{2P}^{slow}** and **MAG_{2P-F}^{slow}**) or *trans*→*cis* (**Glu_brAzo4-5**) back-isomerisation rate constants.

VII.4. BIOLOGICAL EXPERIMENTS

The experimental details reported in this section are only those directly conducted in this work (cell culture, transfection and incubation, and 1P and 2P single-cell calcium imaging measurements). Electrophysiological measurements, hippocampal slice experiments and 2P *in vivo* stimulation experiments, whose results are described in Chapters III, IV and V; were

carried out by Aida Garrido-Charles, Dr. Núria Camarero, Dr. Miquel Bosch, Dr. Montserrat Porta de la Riva and Dr. Michael Krieg and a detailed explanation of those experiments can be found elsewhere.^{12,13}

VII.4.I. CELL CULTURE AND TRANSIENT TRANSFECTION

HEK293 tsA201 cell line (SV40-transformed, Human Embryonic Kidney 293 cells) was maintained at 37 °C in a 5% CO₂ humid incubator with Dulbecco's Modified Eagle Medium/Nutrient Mixture F-12 media (DMEM) (1:1, Invitrogen) supplemented with 10% Fetal Bovine Serum (FBS) and 1% Penicillin/Streptomycin.

The expression plasmids for GluK2-L439C and GluK2-L439C-eGFP were kindly provided by Ehud Y. Isacoff (University of California) and subcloned as previously described.¹⁴ Cells were transfected with pcDNA3-GluK2-L439C-eGFP for electrophysiology, co-transfected with pcDNA3-GluK2-L439C:GCaMP6s (1:1) for 1P calcium imaging, and with pcDNA3-GluK2-L439C:RGECO1 (2:1) or pcDNA3-GluK2-L439C:RCaMP for 2P calcium imaging.

The expression plasmid for GluK2 was kindly provided by Ehud Y. Isacoff (University of California). GluK2 was subcloned into EcoRI site of the pcDNA3.1 expression vector. To obtain the GluK2-eGFP pcDNA3 construct, a fragment spanning the C-terminal domain of GluK2 and eGFP was amplified by PCR using Afel/XbaI flanked primers and subcloned into GluK2-pcDNA3 plasmid by replacing the former Afel/XbaI cassette.

GluK1(Q)-2b(GGAA) was kindly provided by G. Swanson (Northwestern University, Feinberg School of Medicine), with the endoplasmic reticulum retention motif of the carboxy-terminal mutated to increase surface expression.

DNA-X-tremGENE 9 Transfection Reagent (Roche) mix was used following manufacturer's instructions with a Reagent:DNA ratio of 3:1. GluK1(Q)- 2b-GGAA plasmid was co-transfected with peGFP with a Transfection Reagent:GluK1:eGFP ratio of 3:1:0.1.

The mix was incubated for 20 min at room temperature, meanwhile cells were detached and freshly plated into a 12-mulltiwell plate at a density of $3 \cdot 10^5$ cells before the DNA-Transfection Reagent mix was added dropwise into each well. Experiments were performed after 48–72 h,

and the day before the experiment cells were plated at low density on 16-mm coverslips (Fisher Scientific) treated with collagen (Sigma-Aldrich) to allow cell adhesion.

Electrophysiological experiments were performed 24-48 h after transfection, with cells plated at low density. One-photon calcium imaging experiments were performed 48-72 h after transfection with cells plated on PLL-coverslips at high density. Two-photon calcium imaging experiments were performed 48 h after transfection with cells plated at high density on 25 mm diameter glass coverslips (Fisher Scientific) pretreated with PLL into a 6-multiwell plate.

VII.4.2. CONJUGATION OF LiGluR WITH PHOTOSWITCHED TETHERED LIGANDS

All **MAG**-type compounds were stored at 10 mM in DMSO at -20 °C. Before each experiment cells were incubated with one of the compounds for 10 min in the absence of light in an extracellular solution (ES) composed of (in mM): 140 NaCl, 1 MgCl₂, 2.5 KCl, 10 HEPES, 0.5 CaCl₂ and 10-20 glucose to fix osmolarity to 300 mOsm·kg⁻¹, while pH 7.4 was adjusted with NaOH. For HEK cell line, **MAG**, **MAG**_{2P}, **MAG**_{2P_F}^{slow} or **MAG**_{2P_F}^{slow} were added at a concentration of 50 μM. After incubation, cells were washed three times with ES and incubated 10 min with 0.3 mg·mL⁻¹ Concanavalin A (Sigma) -to block GluK2 desensitization- on an ES based on NMDG⁺ (to avoid depolarization due to open LiGluRs, in mM): 110 NMDG⁺, 2.5 KCl, 1 MgCl₂, 10 HEPES, 10-20 glucose to fix osmolarity to 300 mOsm·kg⁻¹, while pH 7.4 was adjusted with HCl. Before placing the coverslip to the recording chamber, cells were washed again three times with ES.

VII.4.3. SINGLE-CELL CALCIUM IMAGING

Calcium imaging with 1P stimulation: Photoisomerisation was achieved by illuminating the focused sample with flashes of violet light ($\lambda_{\text{exc}} = 380$ nm, 0.5 s duration) for activation, and flashes of green light ($\lambda_{\text{exc}} = 500$ nm, 0.5 s duration) for deactivation, using the same light source as for the dye excitation. Calcium imaging activation spectra at one-photon ranged from 280 to 480 increasing 20 nm at a time. Light flashes were nested in between GCaMP6s fluorescence measures keeping the frame rate. Photostimulation intervals lasted a total of 3.2 min for activation and 2.4 min for deactivation. Addition of agonists was carried out by carefully pipetting 100 μL of a 300 μM glutamate stock solution directly into the accessory pool

of the recording chamber. Cells with no response to free glutamate were excluded from the analysis.

Calcium imaging with 2P stimulation: Photostimulation flashes were fit to keep imaging interval, and periods lasted in total 1 min. One-photon photostimulation was done at $\lambda_{exc} = 405$ nm ($0.37 \text{ mW } \mu\text{m}^{-2}$), and two-photon stimulation was done at $\lambda_{exc} = 780$ nm ($2.8 \text{ mW } \mu\text{m}^{-2}$). Back-photoisomerisation was achieved at $\lambda_{exc} = 514$ nm ($0.35 \text{ mW } \mu\text{m}^{-2}$). Inter-stimulus imaging periods lasted 1 min. Photostimulation was done at 256x256 resolution with bidirectional laser scan (400 Hz) by zooming in (x3) in the center of the image. To characterise the wavelength dependence of two-photon LiGluR activation, we measured photoresponses at different wavelengths: from 720 nm to 840 nm for **MAG_{2P}^{slow}**, and from 740 nm to 820 nm for **MAG** and **MAG_{2P}^{slow}**. Addition of agonists was carried out by carefully pipetting 100 μL of a 300 μM glutamate stock solution directly into the accessory pool of the recording chamber. Cells with no response to free glutamate were excluded from the analysis.

Imaging conditions were adjusted to obtain the best signal to noise ratio and minimal photobleaching of the sample during long temporal recordings. Wavelength, intensity and duration of the photostimulation intervals were adjusted to obtain optimal photoresponses with high reproducibility while keeping cell integrity.

VII.4.3. DATA ANALYSIS AND STATISTICS

Amplitude of LiGluR, Gluk1 and GluK2 photocurrents were analysed using IgorPro (Wavemetrics). Displayed whole-cell current traces have been filtered using the infinite impulse response digital filter from IgorPro (low-pass filter with cutoff of 50 Hz). The drift in current observed during light spectra recordings was corrected where appropriate with the IgorPro (WaveMetrics) software using a custom-made macro for drift correction.

1P and 2P calcium images were acquired with the Live Acquisition 2.1 software (Till Photonics) and stored by the Arivis Browser 2.5.5 (Arivis AG). These images were analysed with ImageJ and the mean fluorescence value for each cell profile was calculated using the same software. The fluorescence signals were treated to obtain $\Delta F/F$ values according to:

$$\frac{\Delta F}{F} = \frac{F - F_0}{F_0}$$

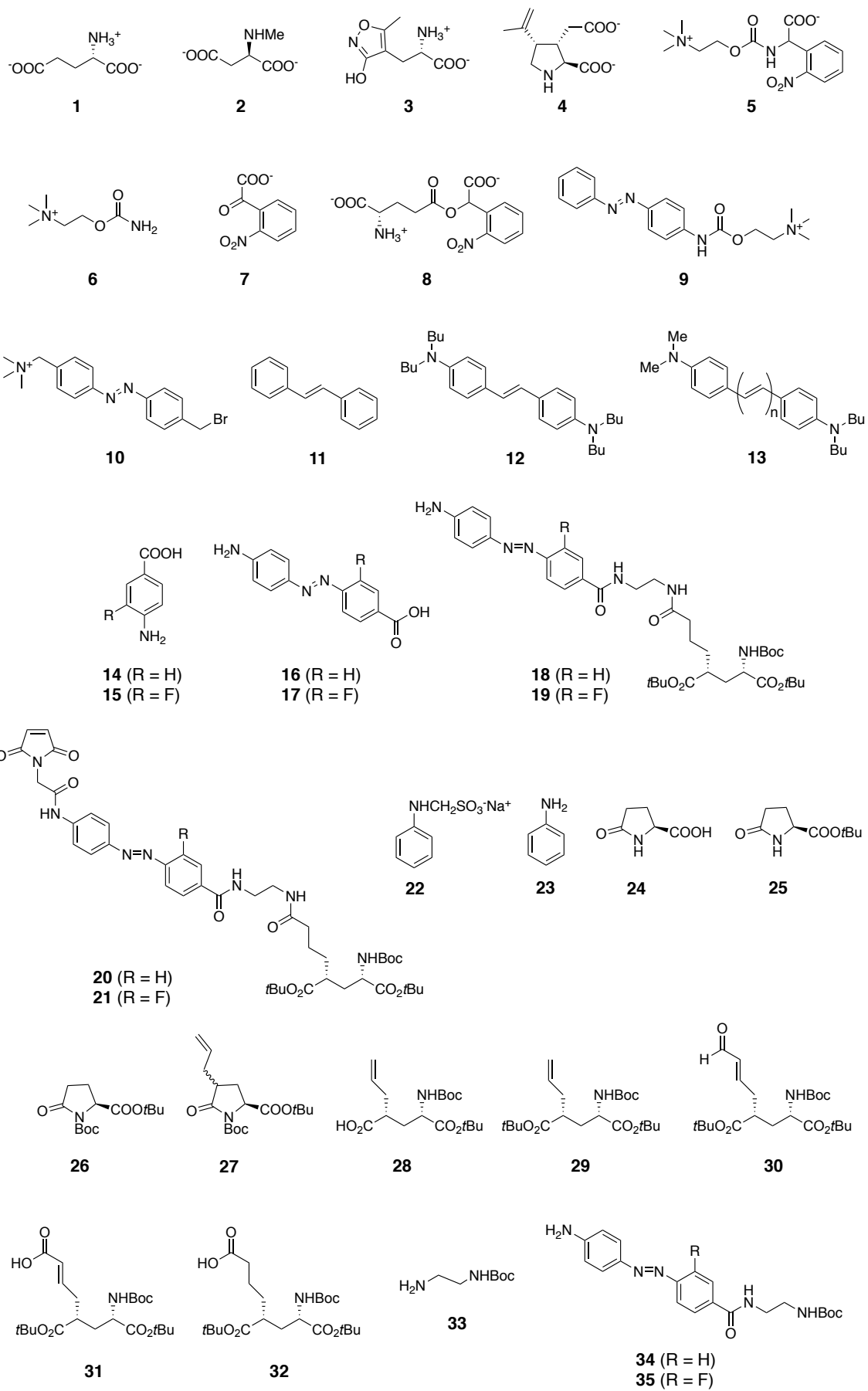
where F_0 is each cell's average signal for the experiment's baseline and F is the fluorescence signal upon stimulation. The resulting fluorescence ratios were analysed in OriginLab. To obtain cell-averaged 1P action spectra, $\Delta F/F$ values were first normalized with respect to the maximum photoresponse obtained for each cell after perfusion of free glutamate at the end of the experiment. To obtain cell-averaged 2P action spectra, 2P $\Delta F/F$ responses were first normalized with respect to the 1P $\Delta F/F$ response at 405 nm for the same cell.

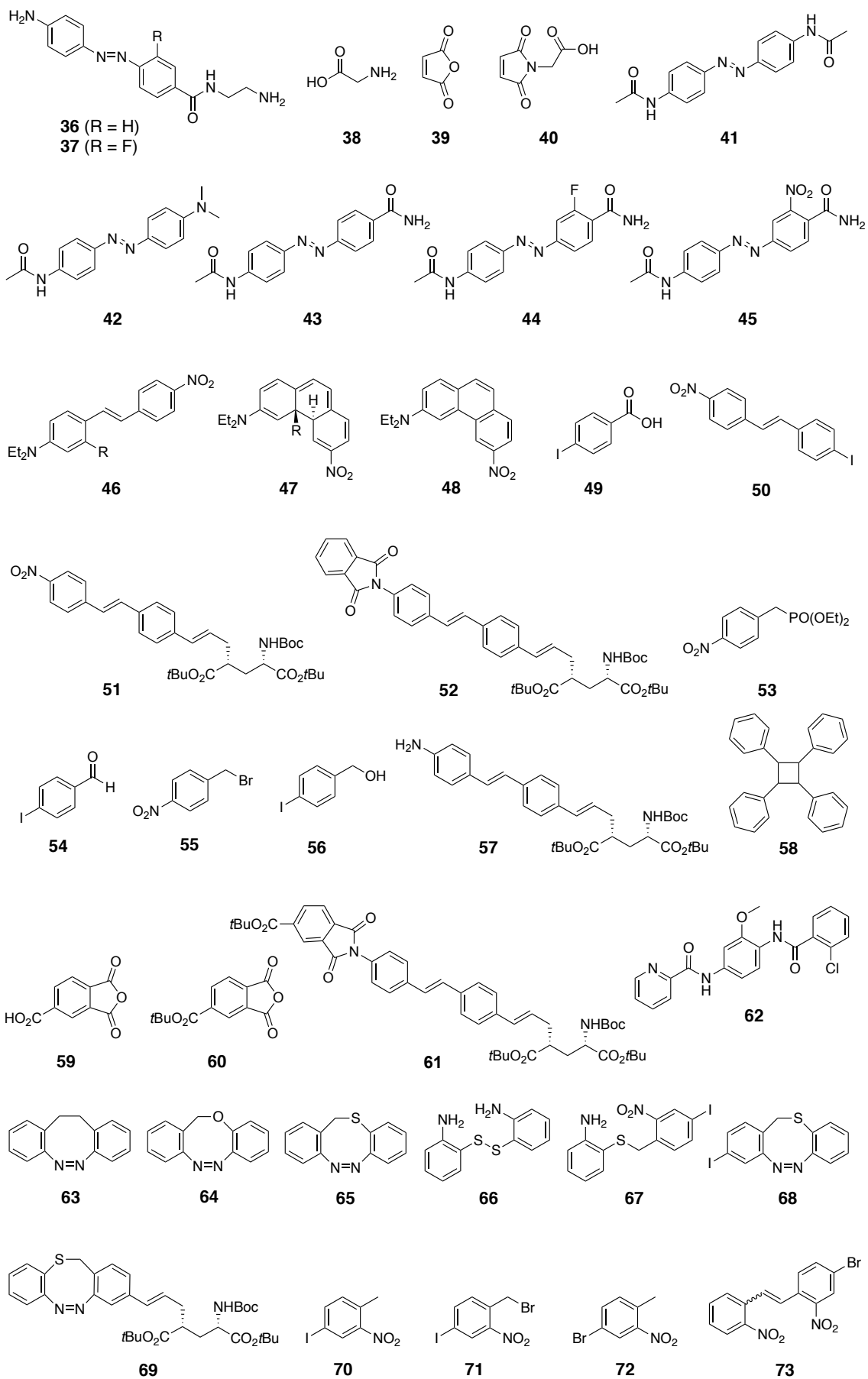
VII.5. REFERENCES

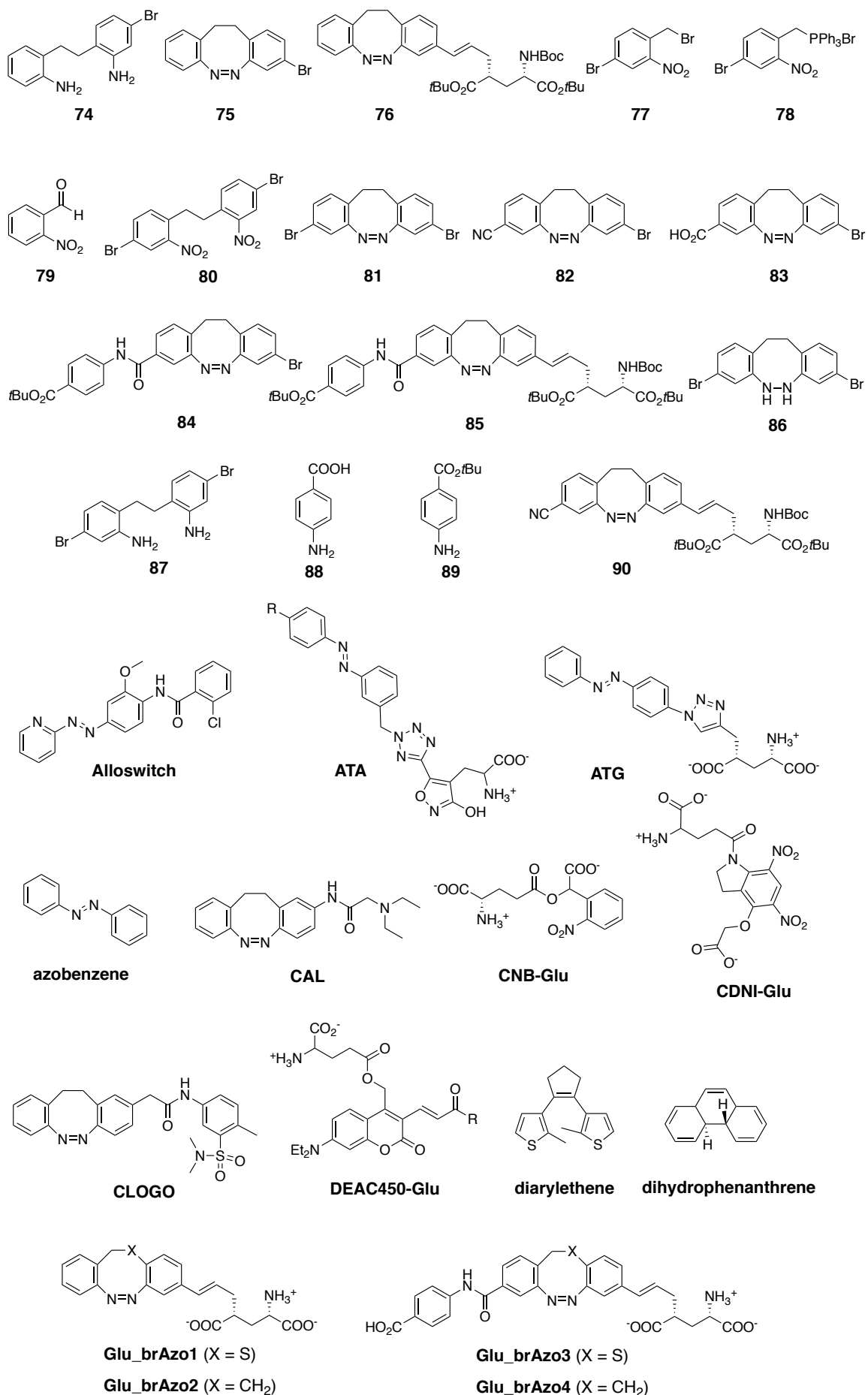
- (1) Gascón-Moya, M.; Pejoan, A.; Izquierdo-Serra, M.; Pittolo, S.; Cabré, G.; Hernando, J.; Alibés, R.; Gorostiza, P.; Busqué, F. *J. Org. Chem.* **2015**, *80*, 9915-9925.
- (2) Supuran, C.; Vullo, D.; Scozzafava, A.; Maresca, A.; Carta, F. *Bioorg. Med. Chem.* **2009**, *17*, 7093-7099.
- (3) Pearson, R. J.; Kassianidis, E.; Slawin, A. M. Z.; Philp, D. *Org. Biomol. Chem.* **2004**, *2*, 3434-3441.
- (4) Wu, C.; Wei, J.; Tian, D.; Feng, Y.; Miller, R. H.; Wang, Y. *J. Med. Chem.* **2008**, *51*, 6682-6688.
- (5) Schehr, M.; Huguenbusch, D.; Moje, T.; Näther, C.; Herges, R. *Beilstein J. Org. Chem.* **2018**, *14*, 2799-2804.
- (6) Moormann, W.; Langbehn, D.; Herges, R. *Synthesis* **2017**, *49*, 3471-3475.
- (7) Higashiguchi, K.; Matsuda, K.; Asano, Y.; Murakami, A.; Nakamura, S.; Irie, M. *Eur. J. Org. Chem.* **2005**, 91-97.
- (8) Lees, A. J. *Anal. Chem.* **1996**, *68*, 226-229.
- (9) Bandara, H. M. D.; Burdette, S. C. *Chem. Soc. Rev.* **2012**, *41*, 1809-1825.
- (10) Higashiguchi, K.; Matsuda, K.; Asano, Y.; Murakami, A.; Nakamura, S.; Irie, M. *Eur. J. Org. Chem.* **2005**, 91-97.
- (11) Pimienta, V.; Lavabre, D.; Levy, G.; Guglielmetti, R.; Micheau, J. C. *J. Phys. Chem.* **1996**, *100*, 4485-4490.

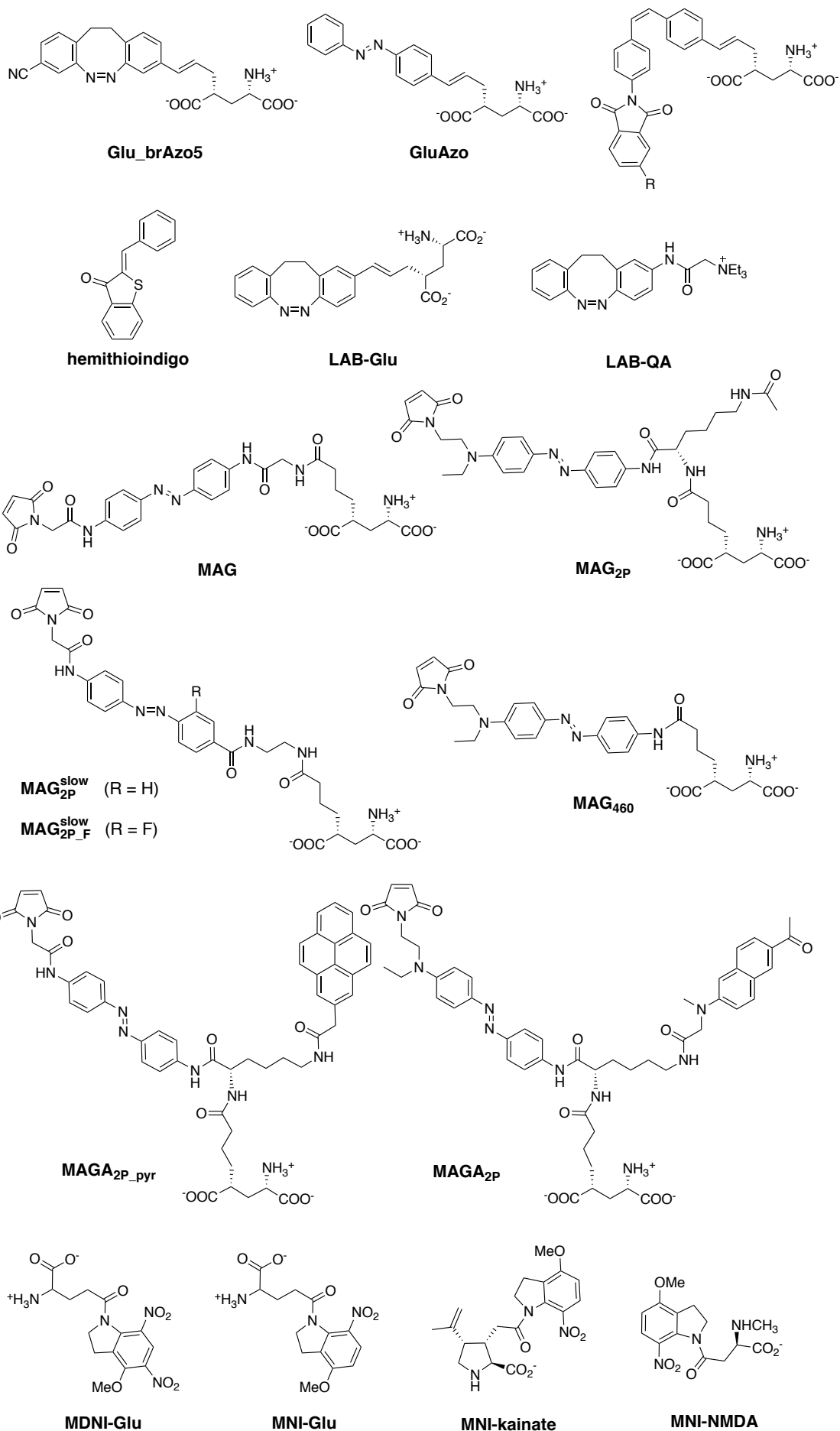
- (12) Cabré, G.; Garrido-Charles, A.; Moreno, M.; Bosch, M.; Porta de la Riva, M.; Krieg, M.; Gascón-Moya, M.; Camarero, N.; Gelabert, R.; Lluch, J. M.; Busqué, F.; Hernando, J.; Gorostiza, P.; Alibés, R. *Nat. Commun.* **2019**, *10*:907.
- (13) Cabré, G.; Garrido-Charles, A.; González-Lafont, A.; Moormann, W.; Langbehn, D.; Egea, D.; Lluch, J. M.; Herges, R.; Alibés, R.; Busqué, F.; Gorostiza, P.; Hernando, J. *Org. Lett.* **2019**, *21*, 3780-3784.
- (14) Izquierdo-Serra M.; Gascón-Moya, M.; Hirtz, J. J.; Pittolo, S.; Poskanzer, K. E.; Ferrer, E.; Alibés, R.; Busqué, F.; Yuste, R.; Hernando, J.; Gorostiza, P. *J. Am. Chem. Soc.* **2014**, *136*, 8693-8701.

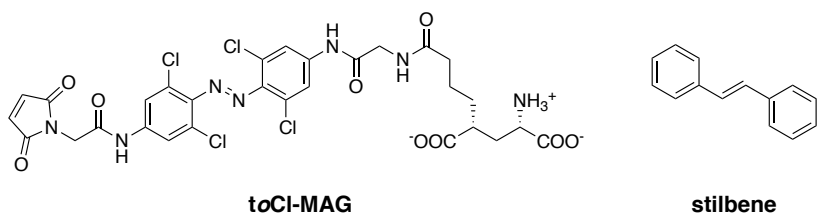
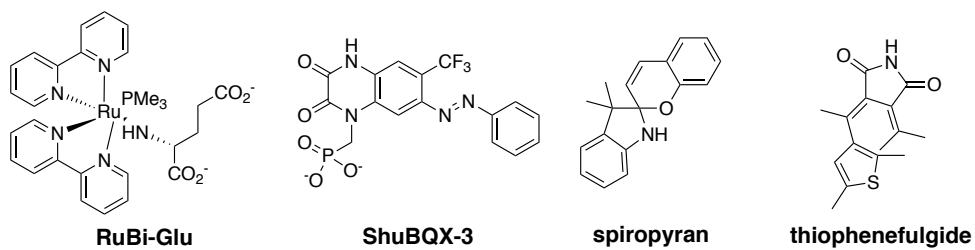
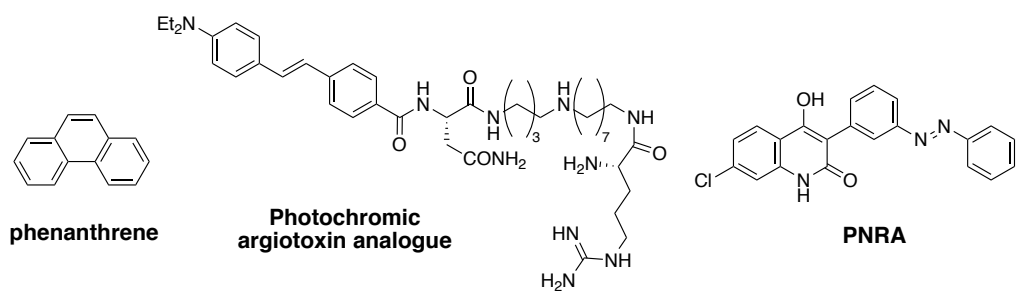
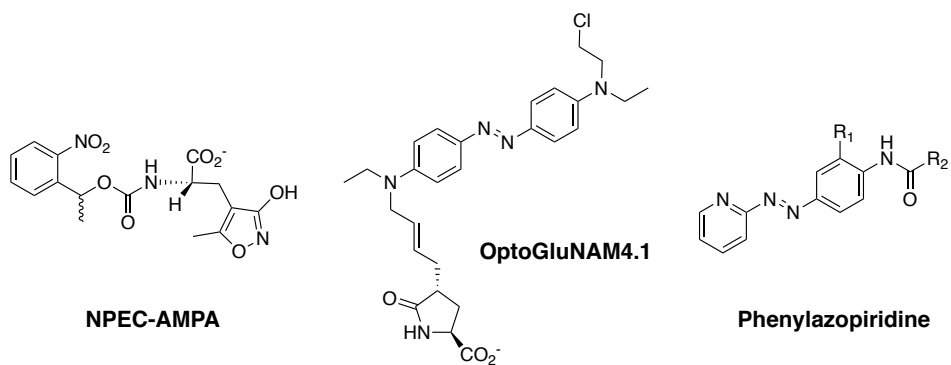
FORMULA INDEX





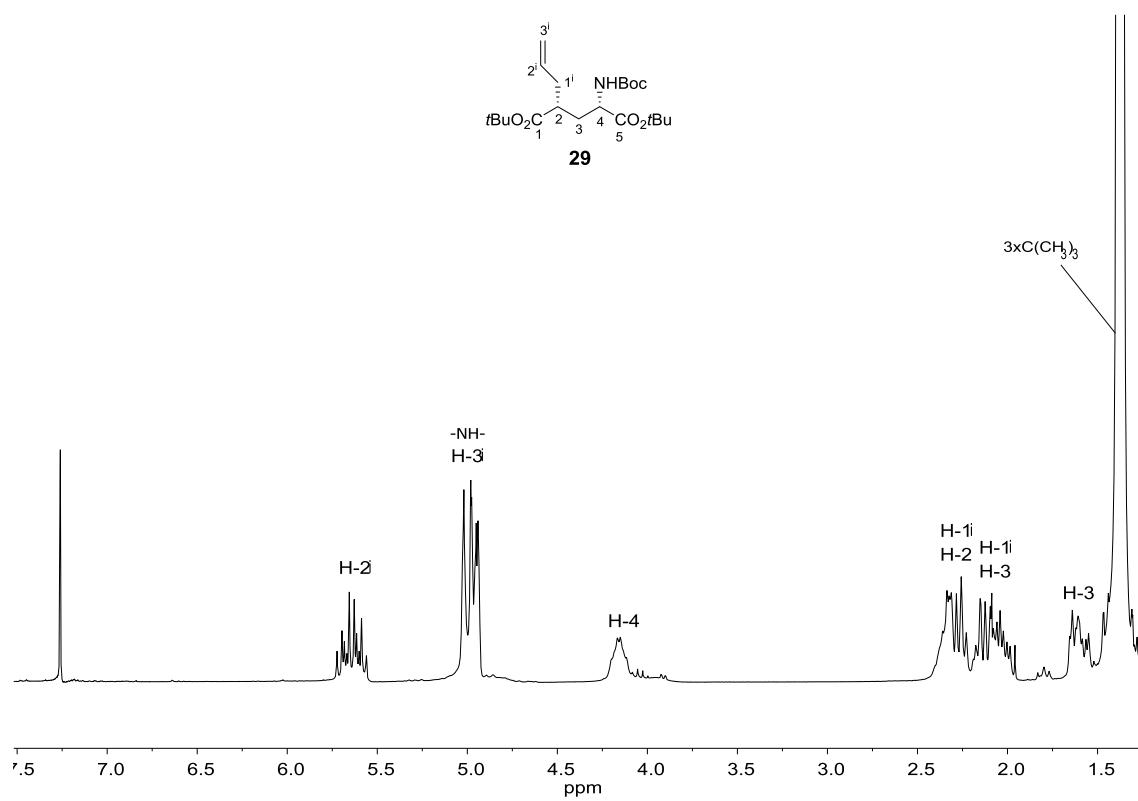
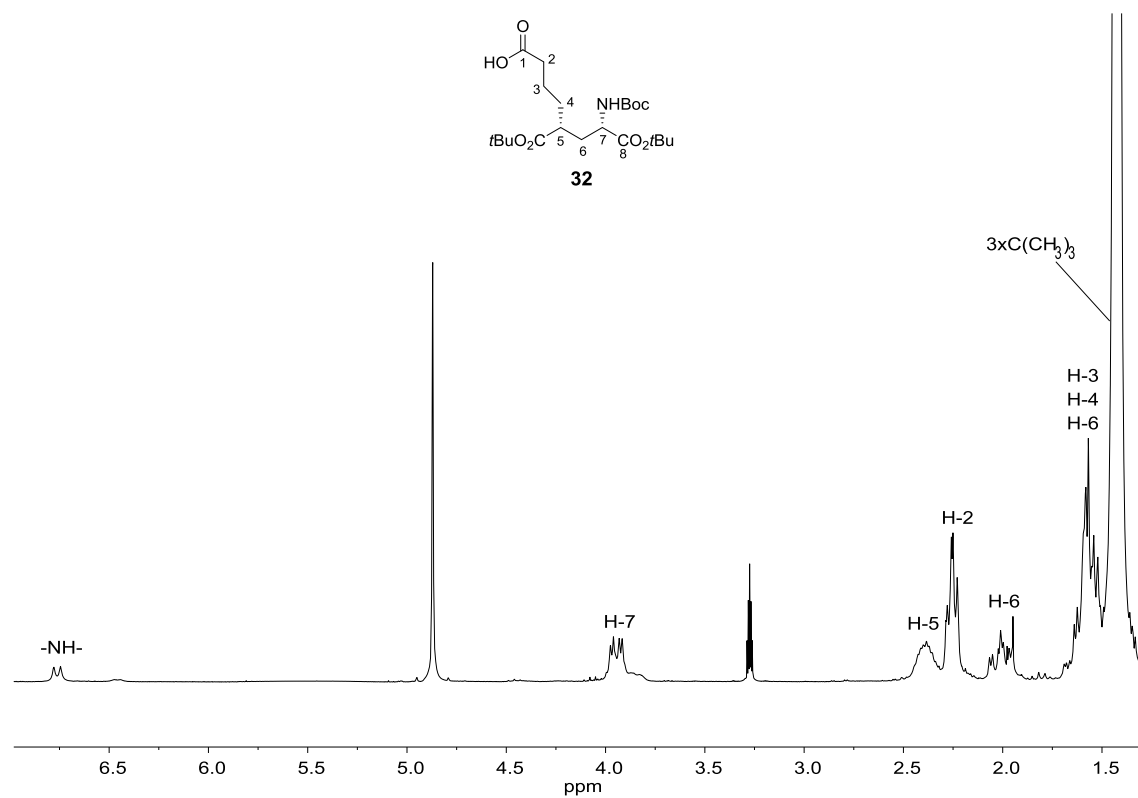




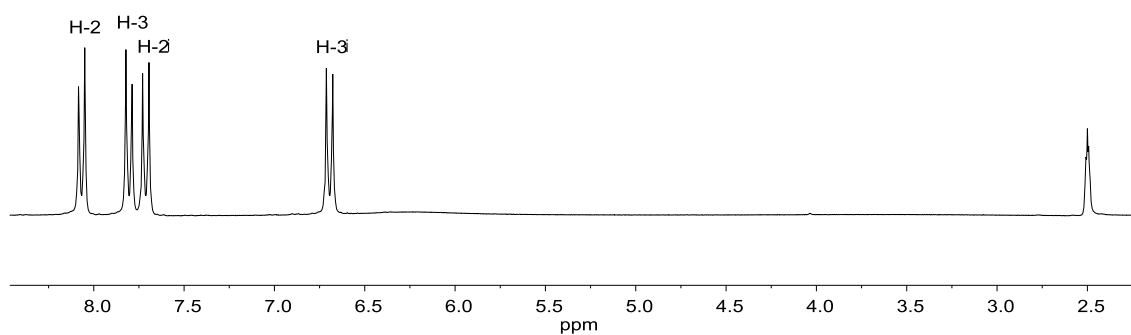
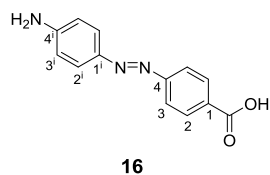


APPENDIX

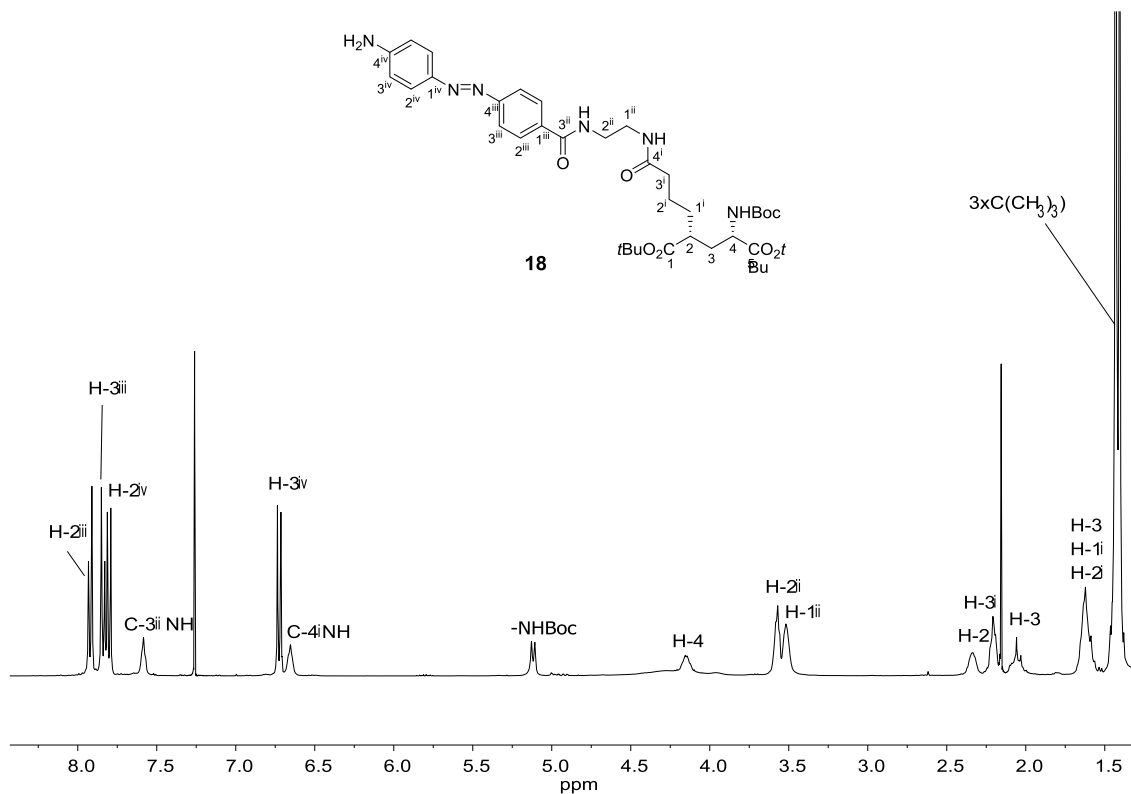
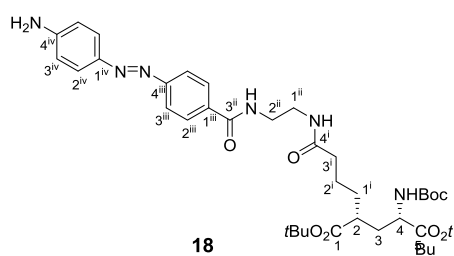
Spectra of selected compounds

¹H NMR (250 MHz, CDCl₃)¹H NMR (250 MHz, MeOH-d₄)

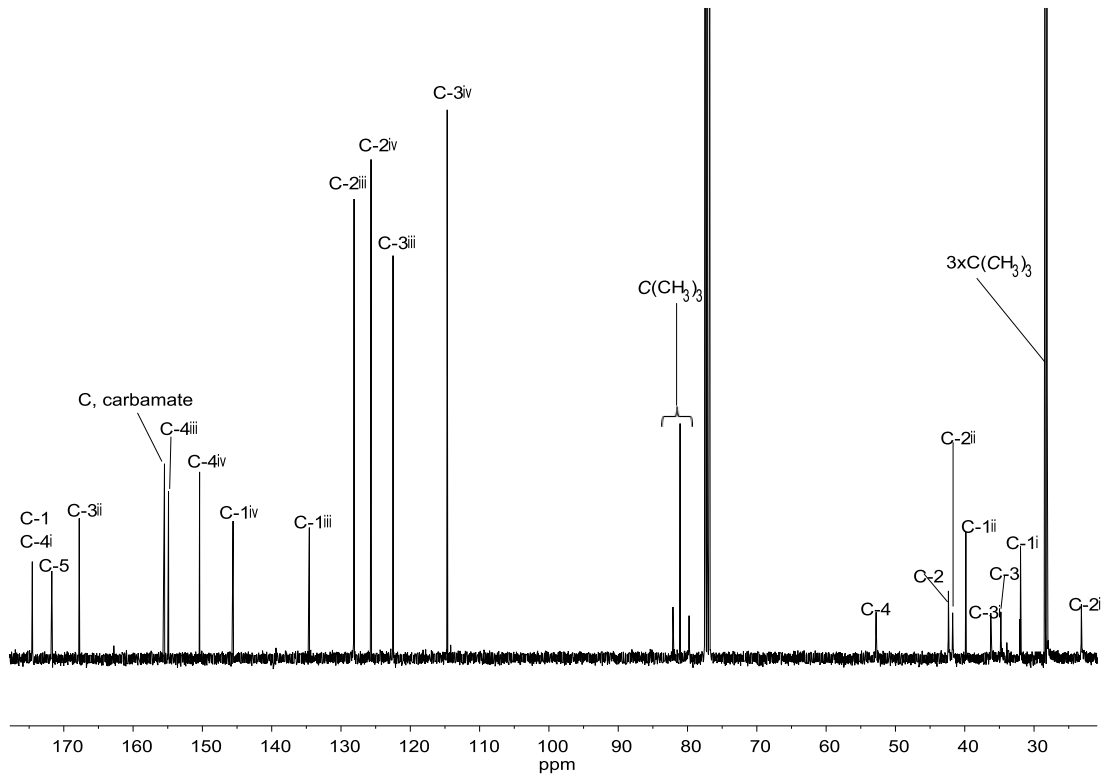
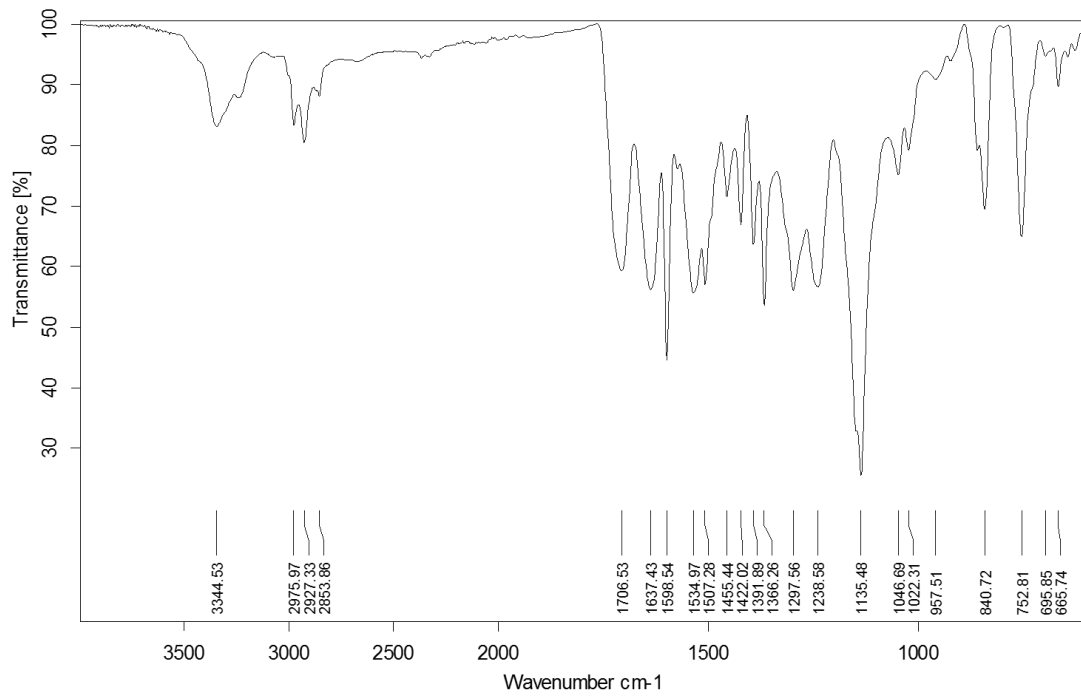
Spectra of selected compounds



$^1\text{H NMR}$ (250 MHz, $\text{DMSO-}d_6$)

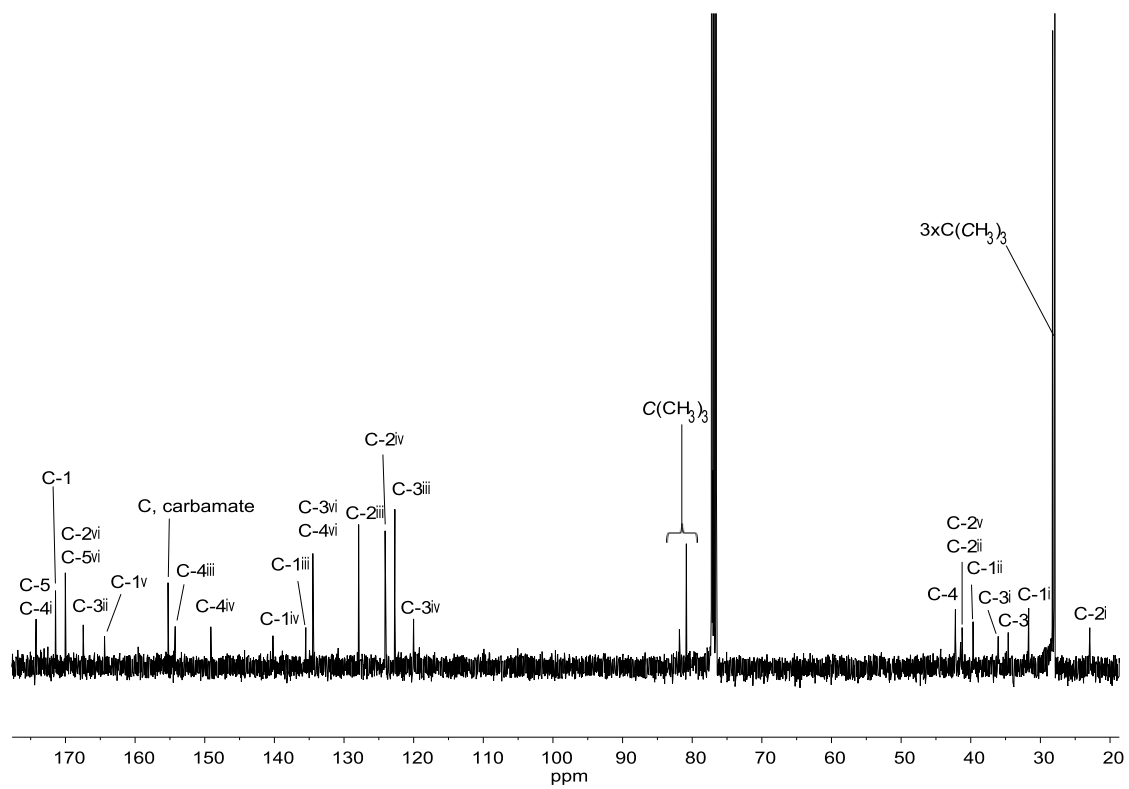
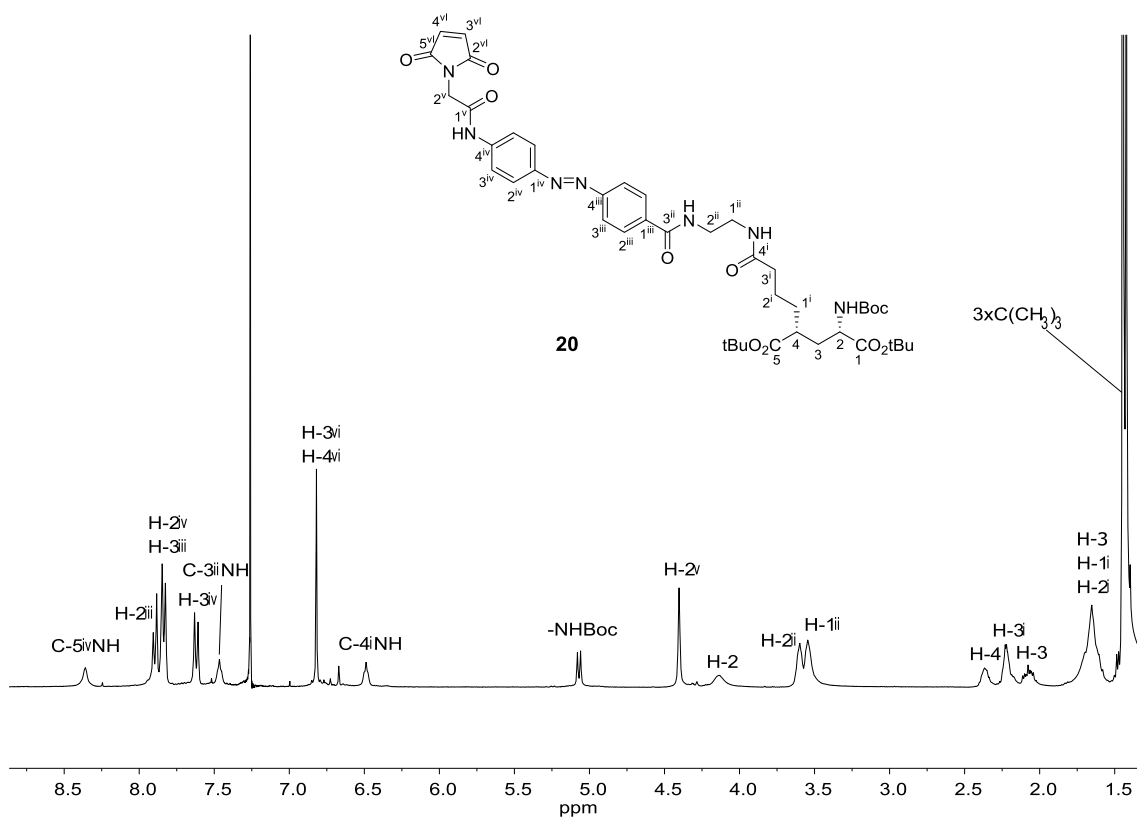


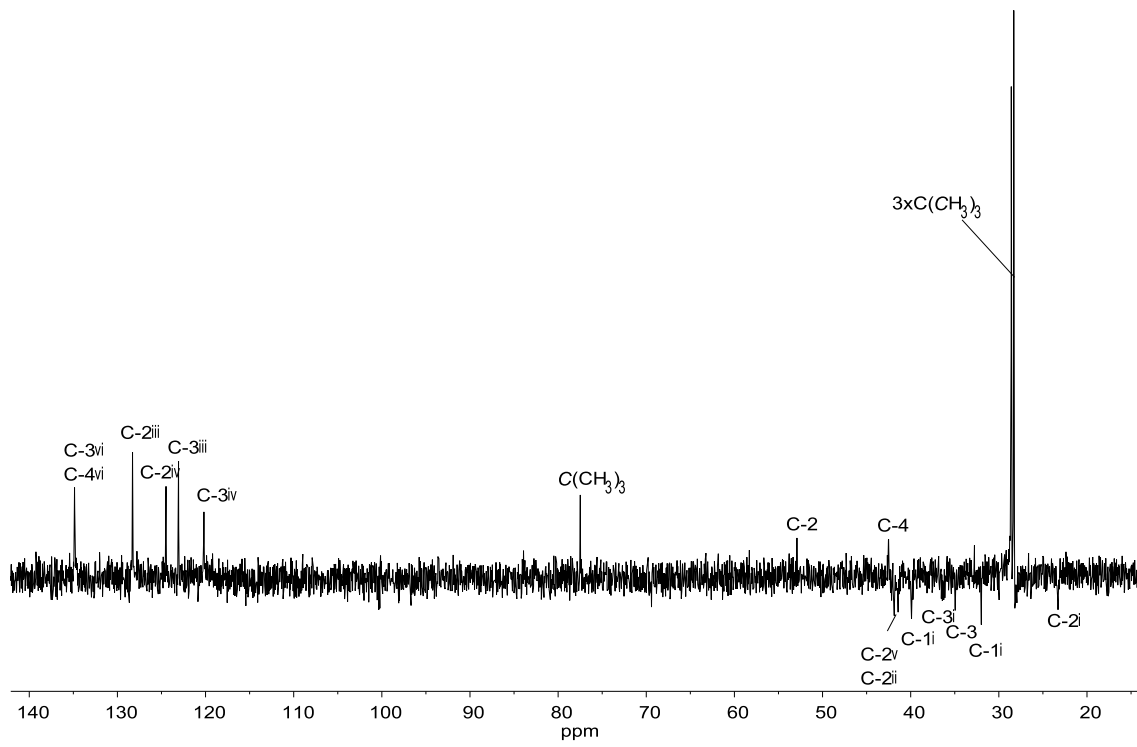
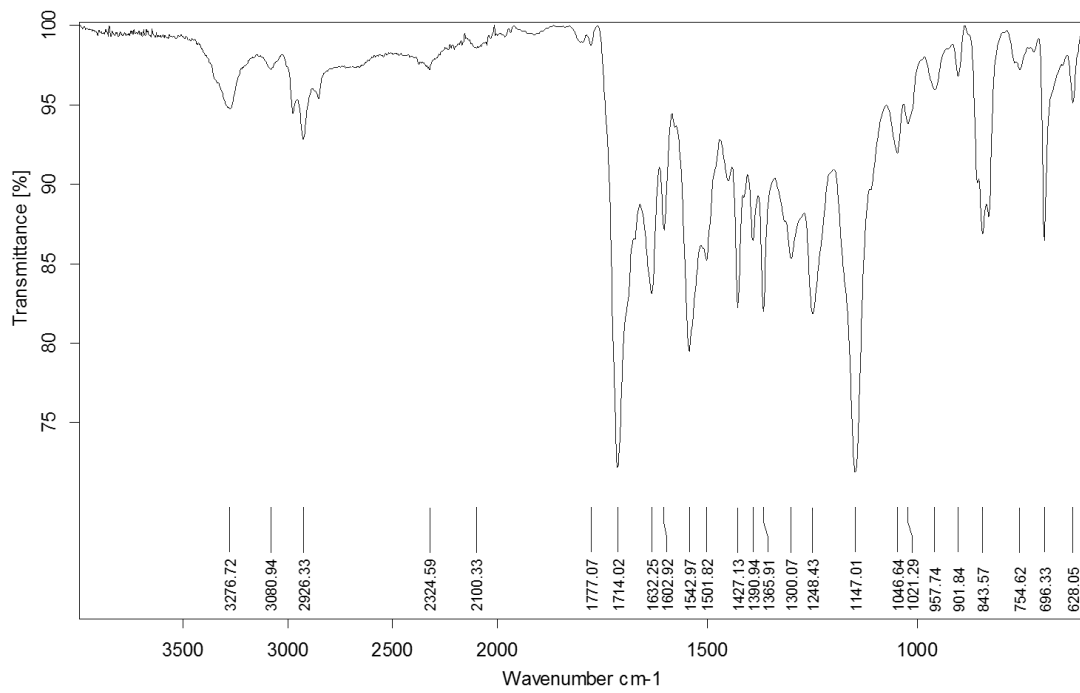
$^1\text{H NMR}$ (400 MHz, CDCl_3)

 ^{13}C NMR (100.6 MHz, CDCl₃)

IR (ATR)

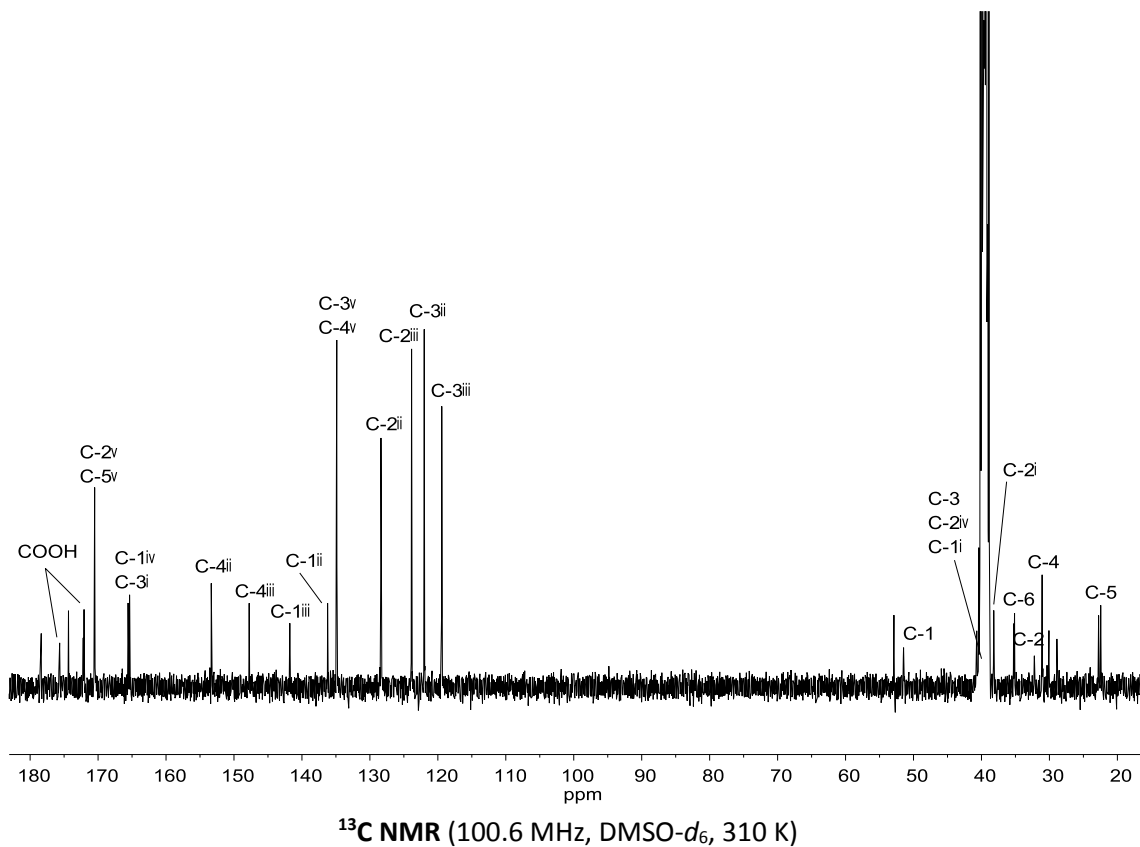
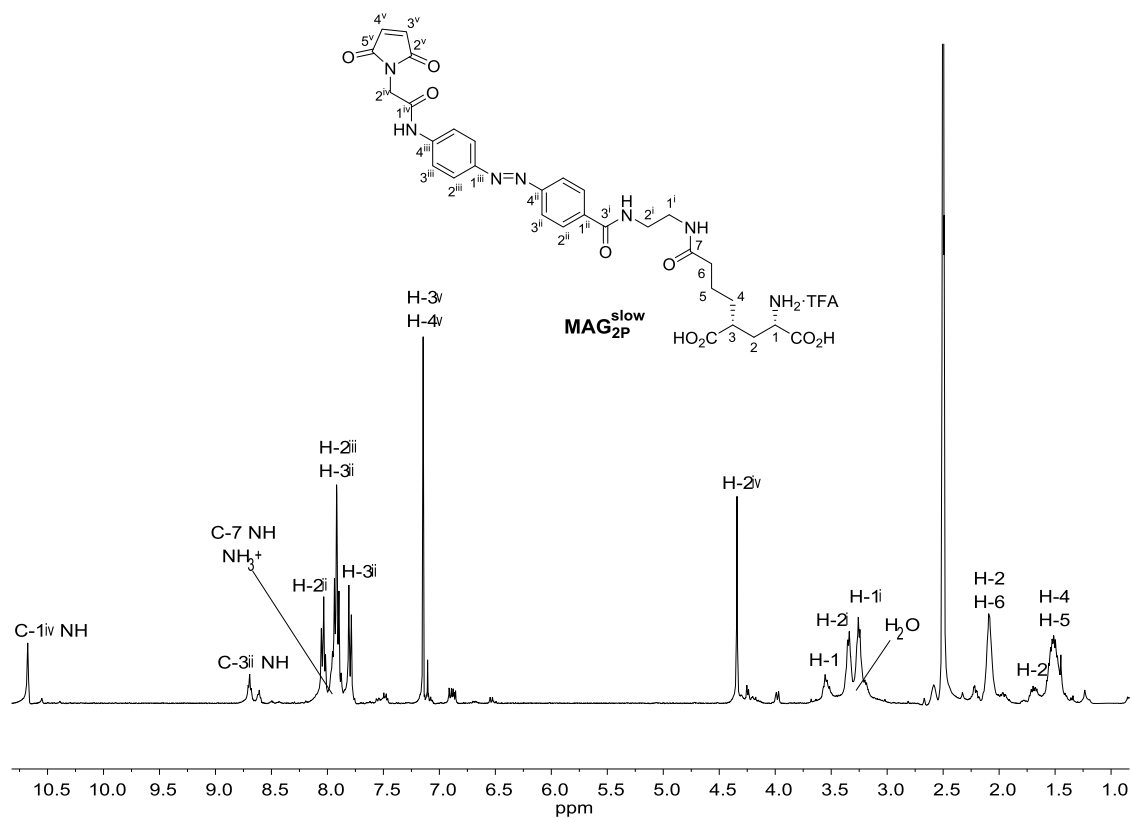
Spectra of selected compounds

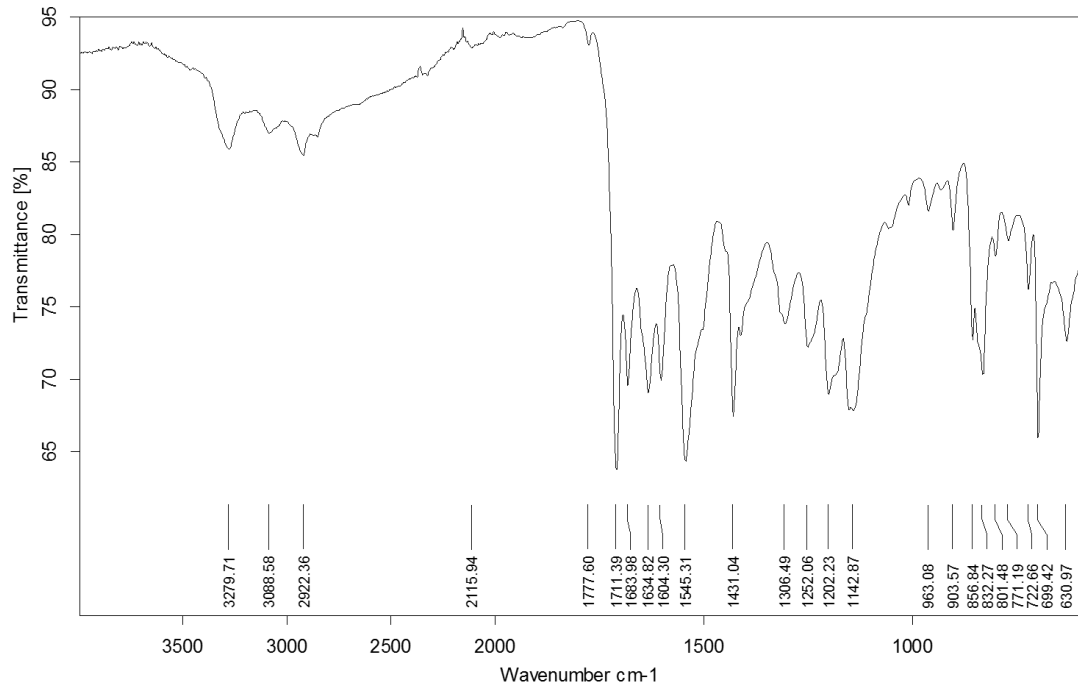


DEPT135 (90.5 MHz, CDCl₃, 320 K)

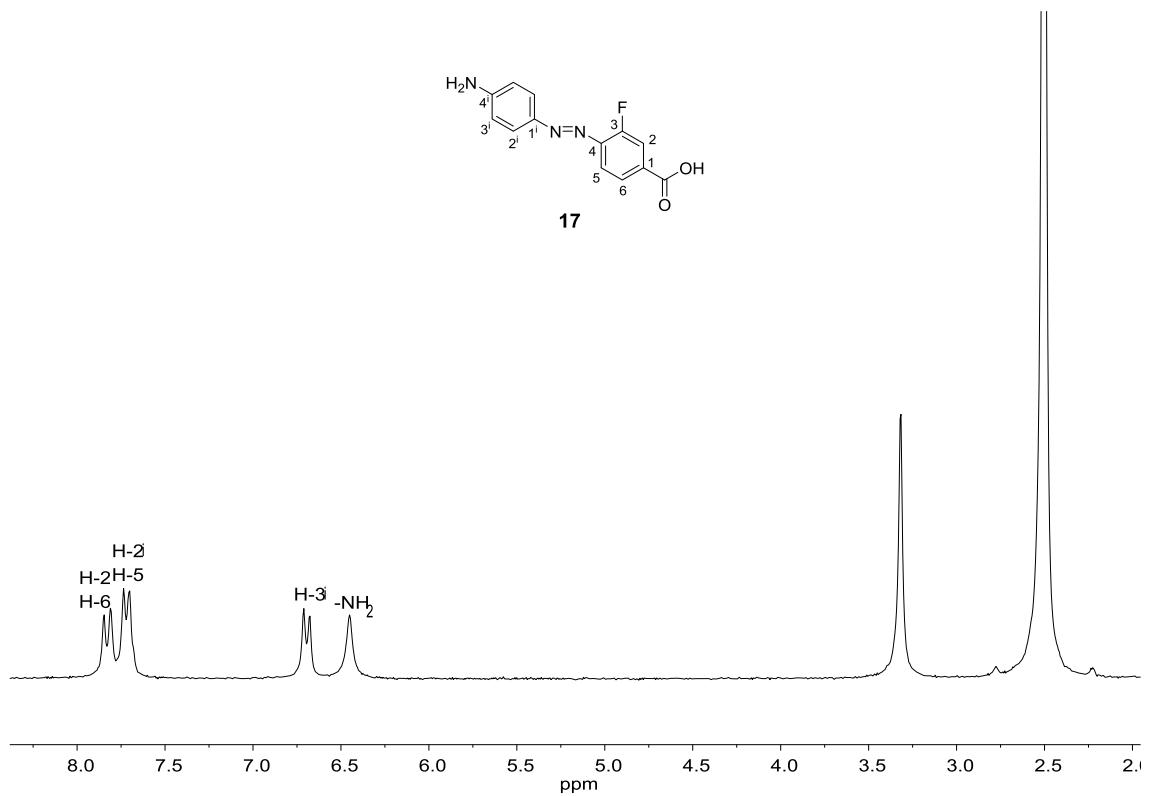
IR (ATR)

Spectra of selected compounds

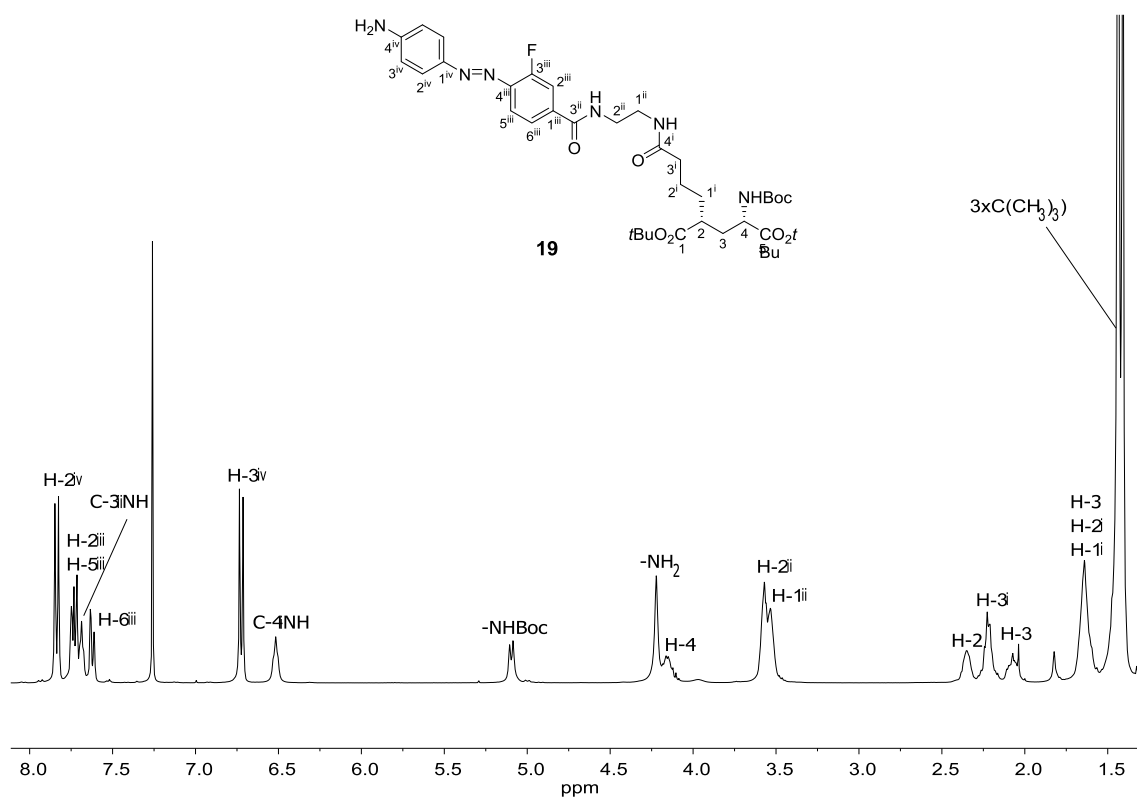




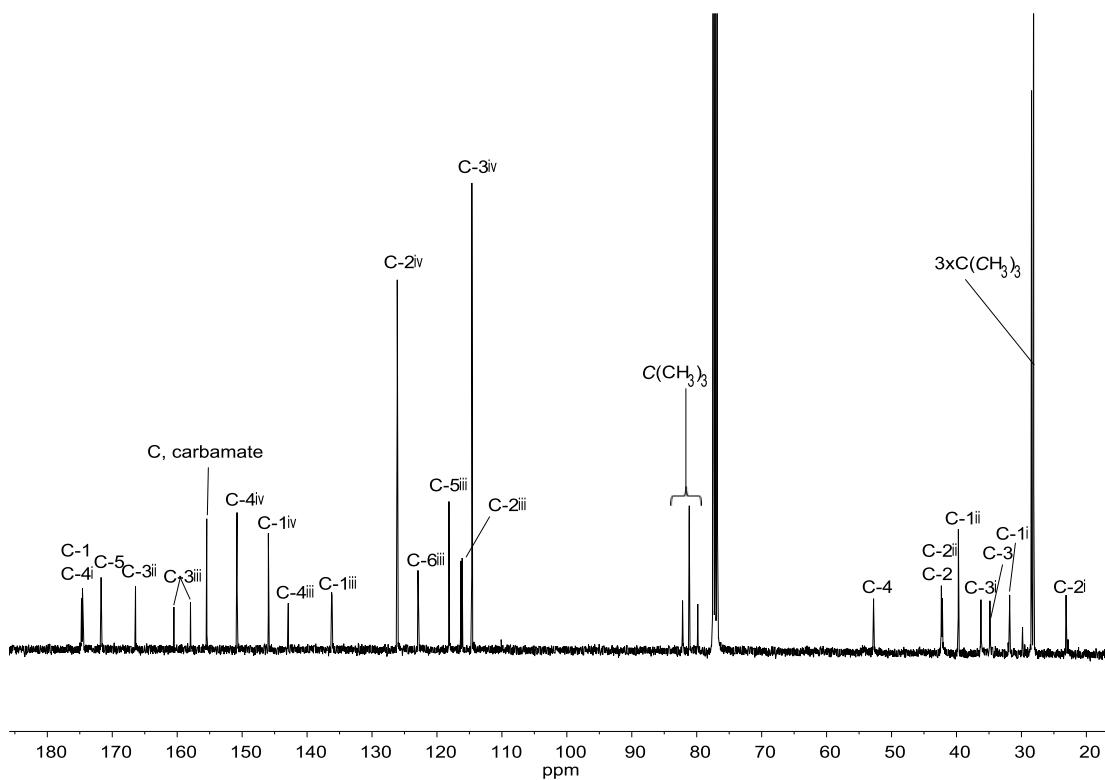
IR (ATR)

¹H NMR (250 MHz, DMSO-d₆)

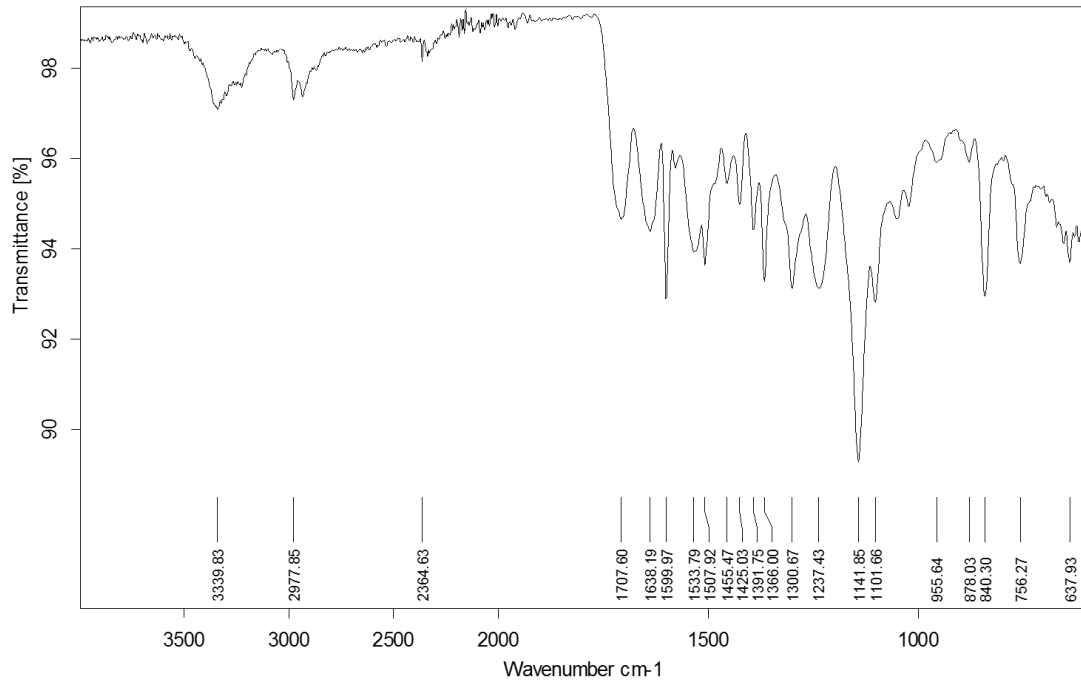
Spectra of selected compounds



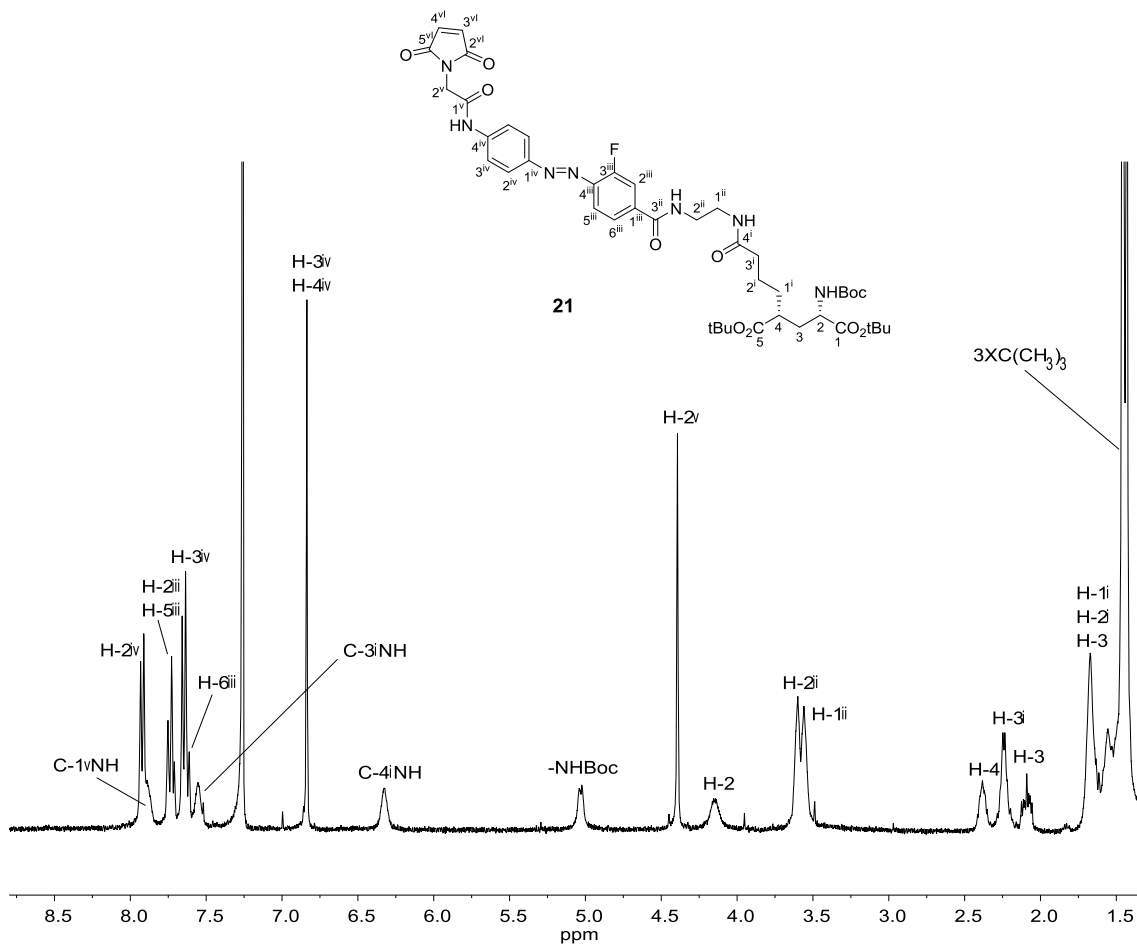
¹H NMR (400 MHz, CDCl₃)



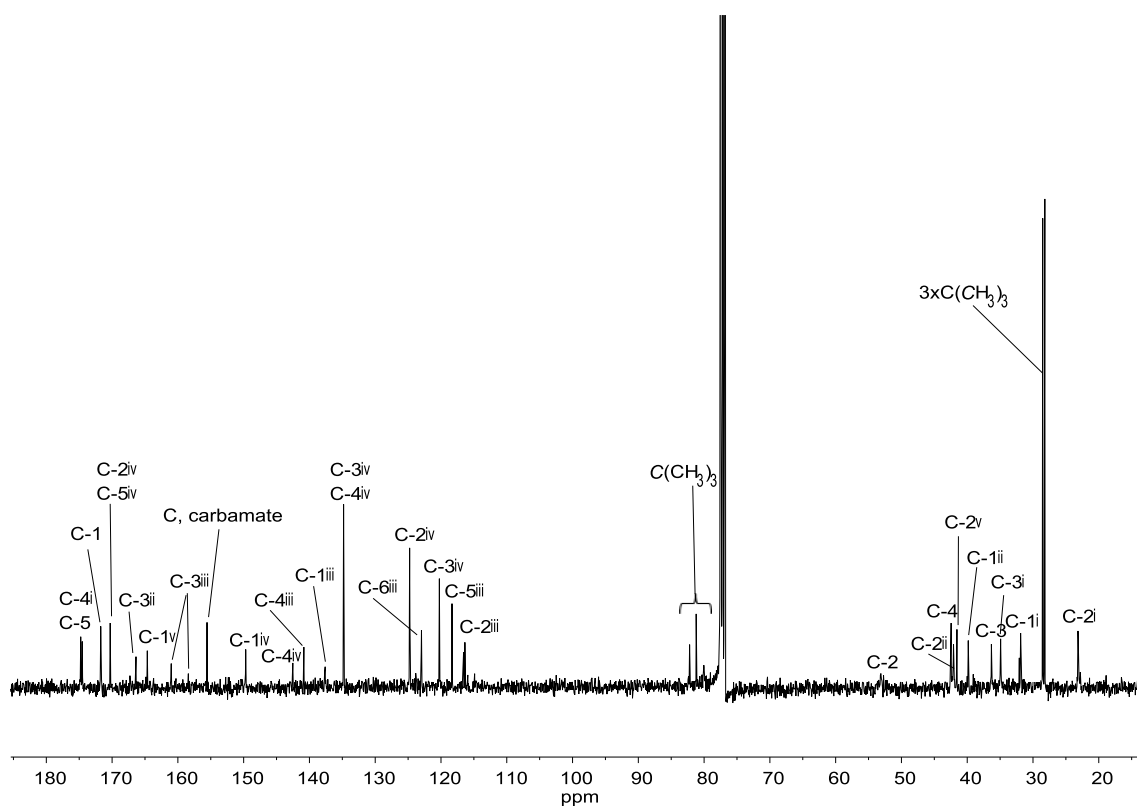
¹³C NMR (100.6 MHz, CDCl₃)



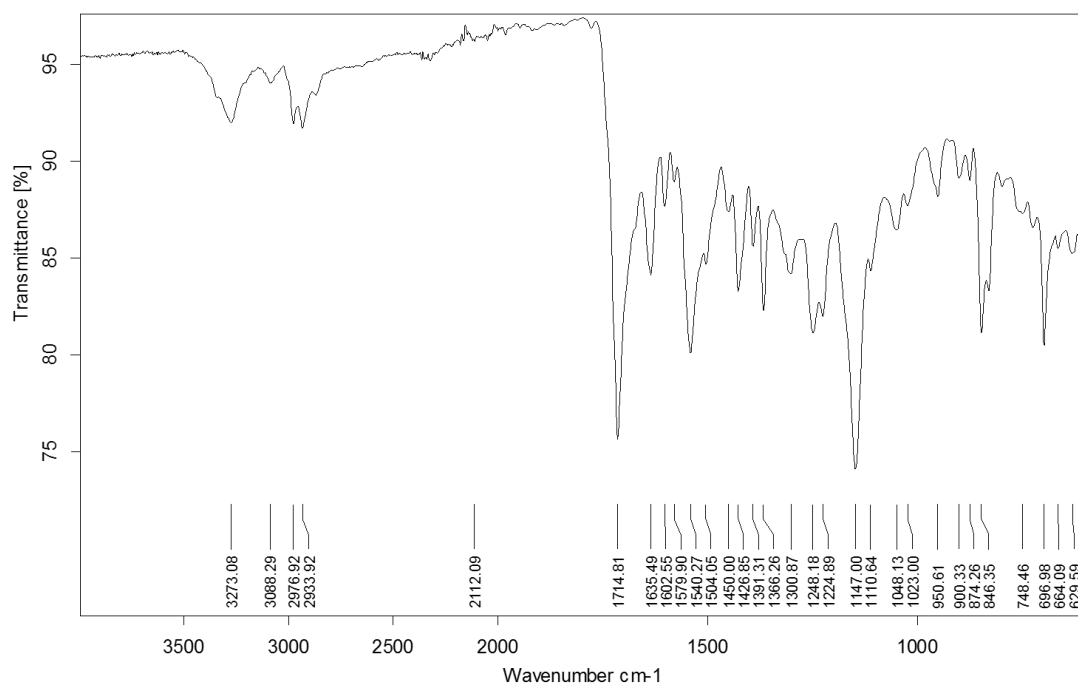
IR (ATR)

¹H NMR (400 MHz, CDCl₃)

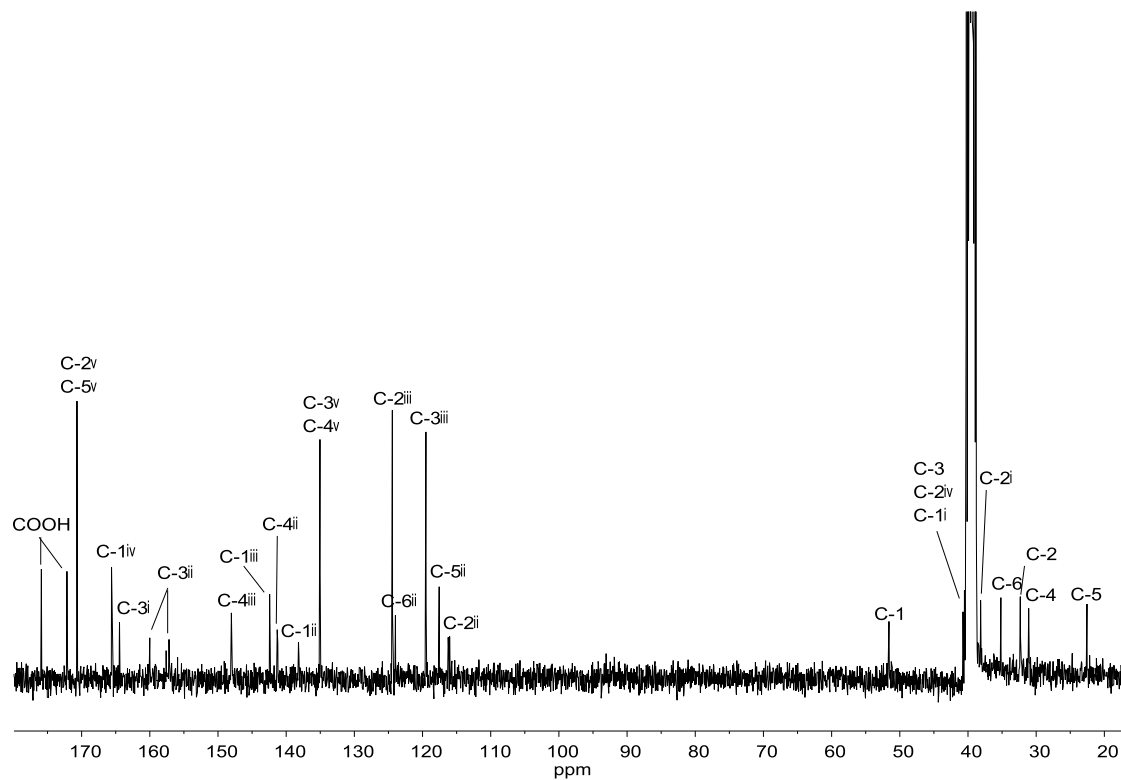
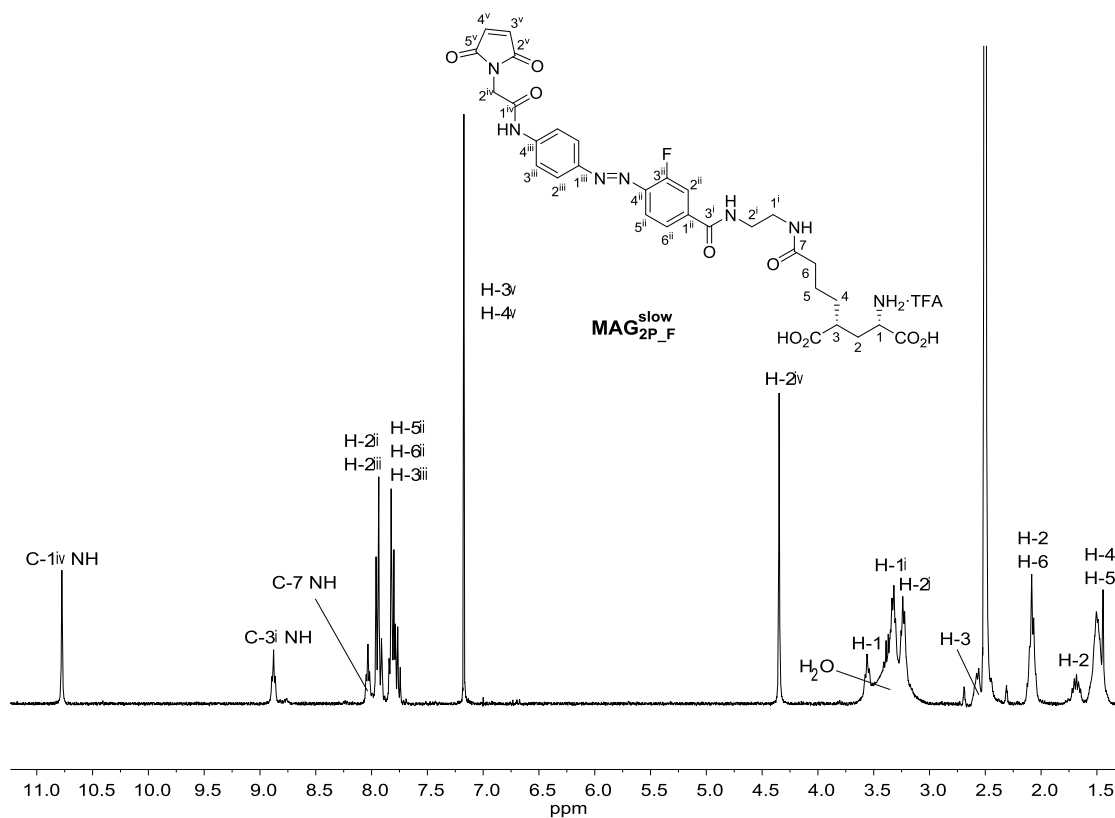
Spectra of selected compounds



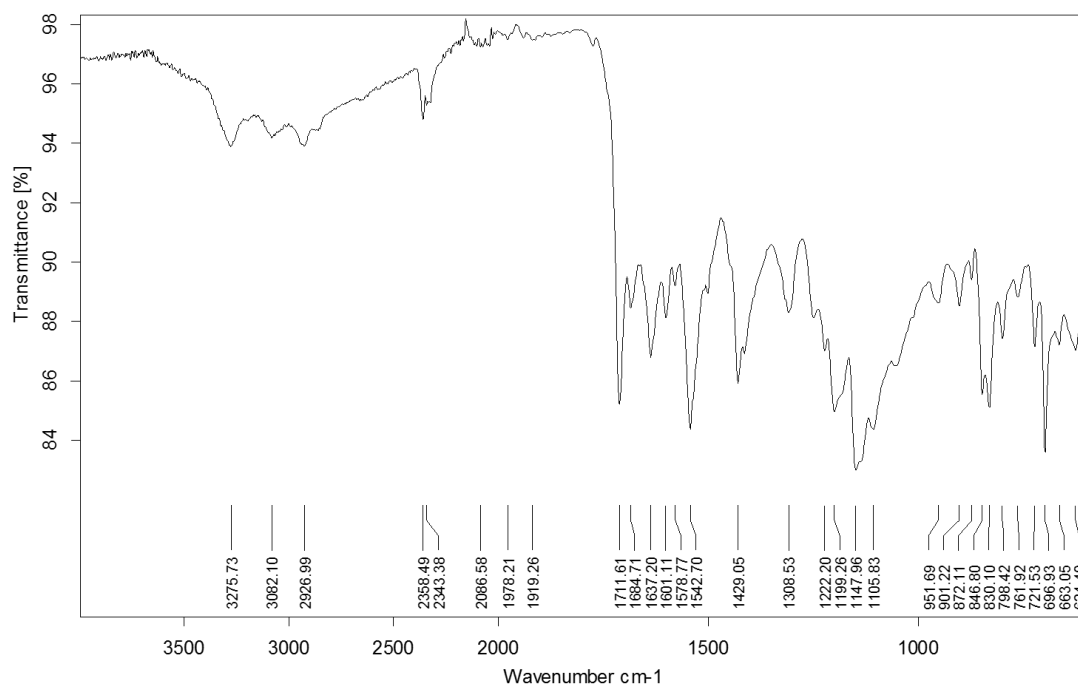
¹³C NMR (100.6 MHz, CDCl₃)



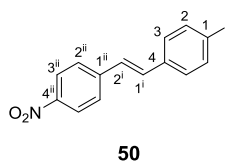
IR (ATR)



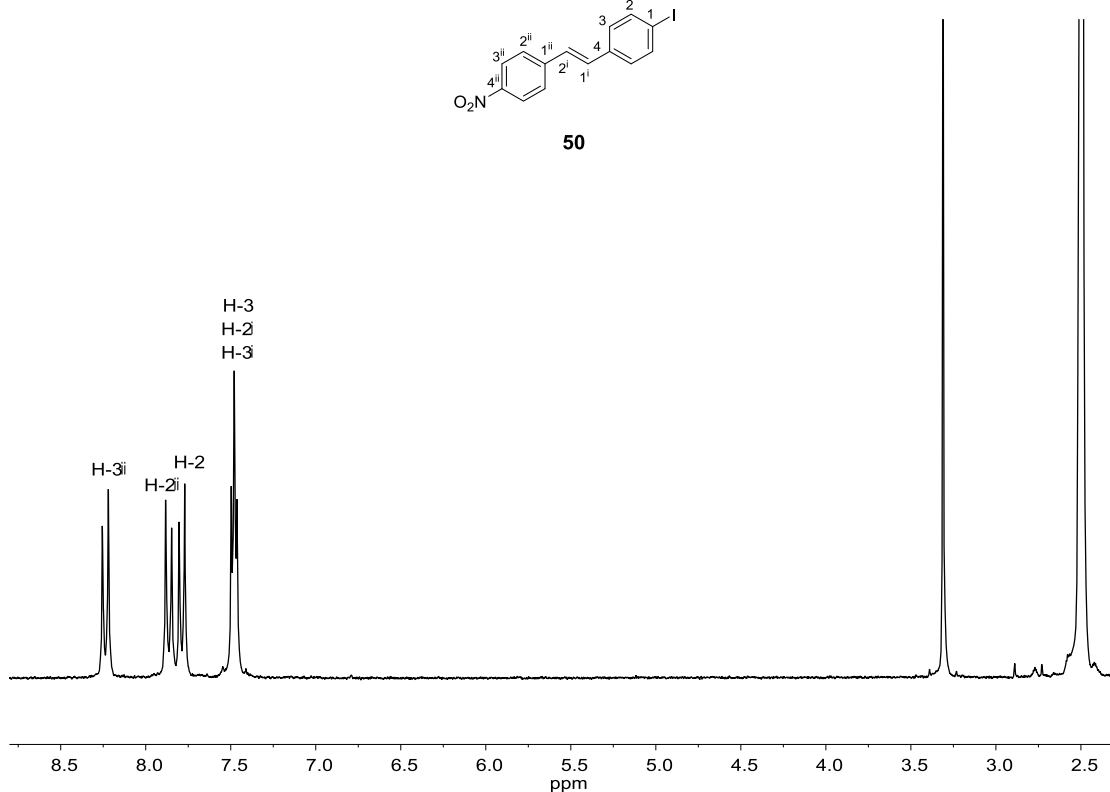
Spectra of selected compounds



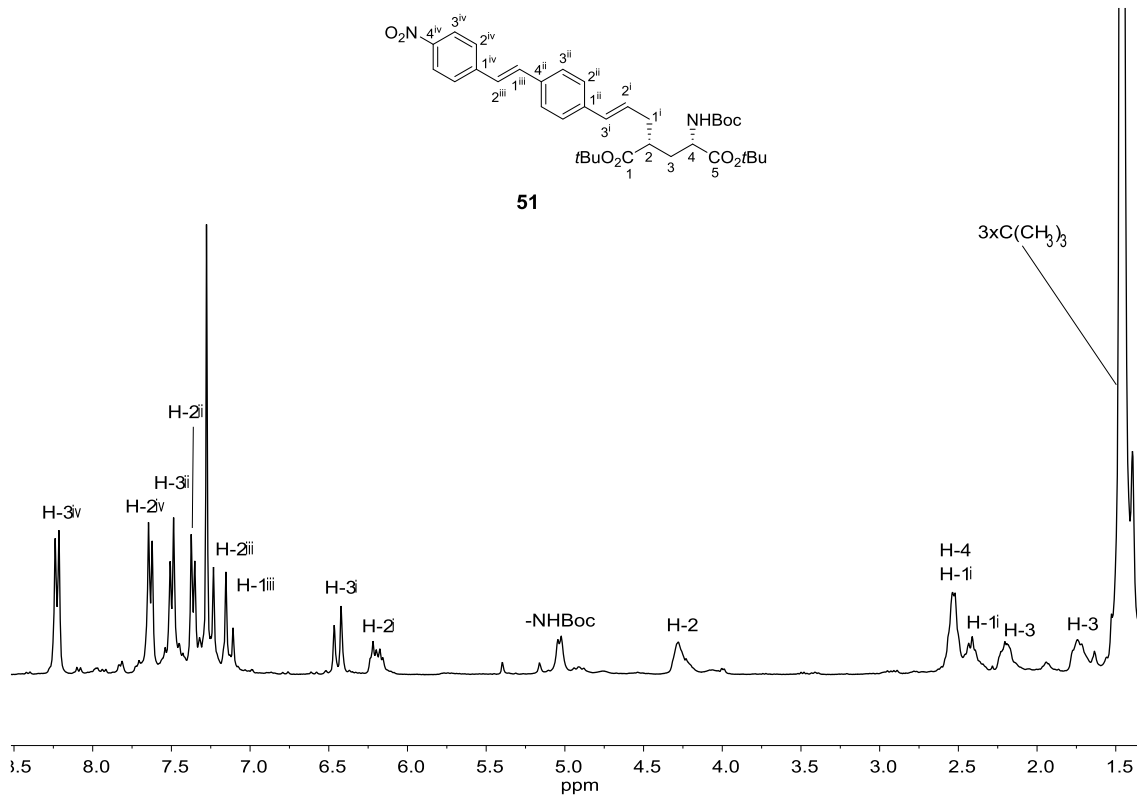
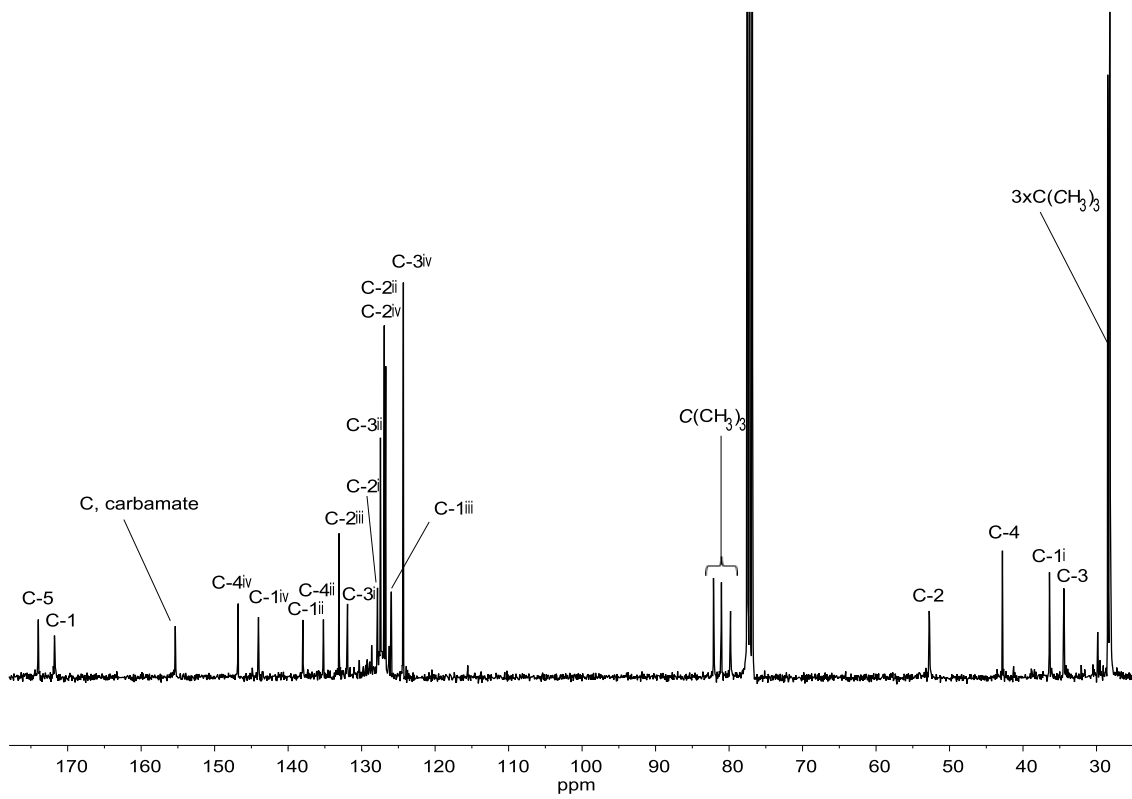
IR (ATR)



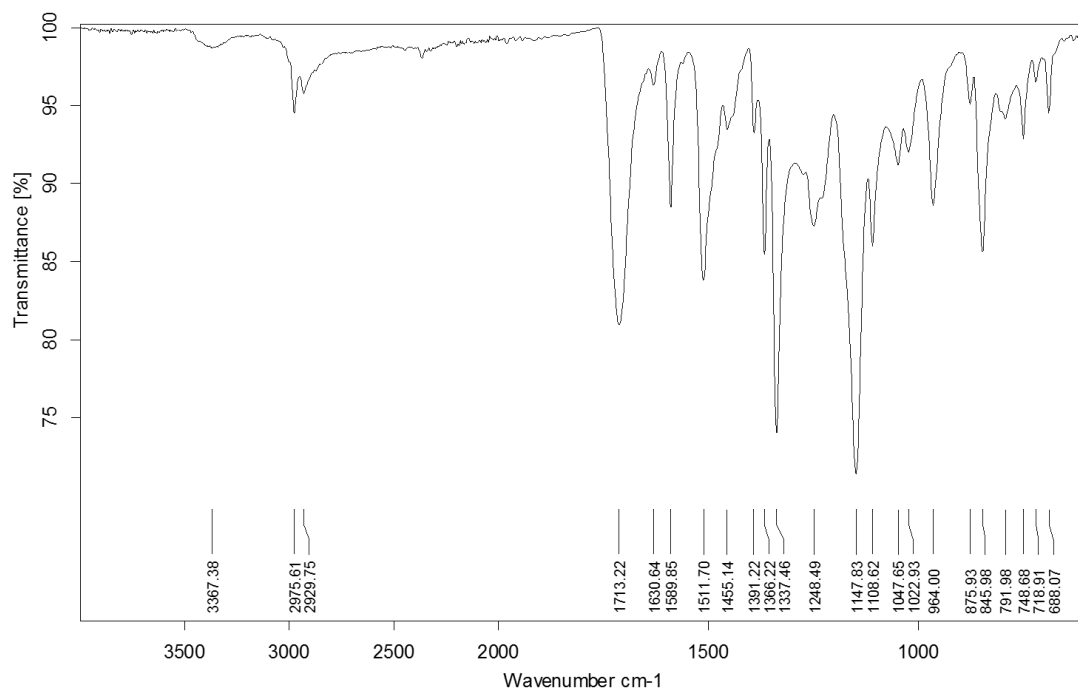
50



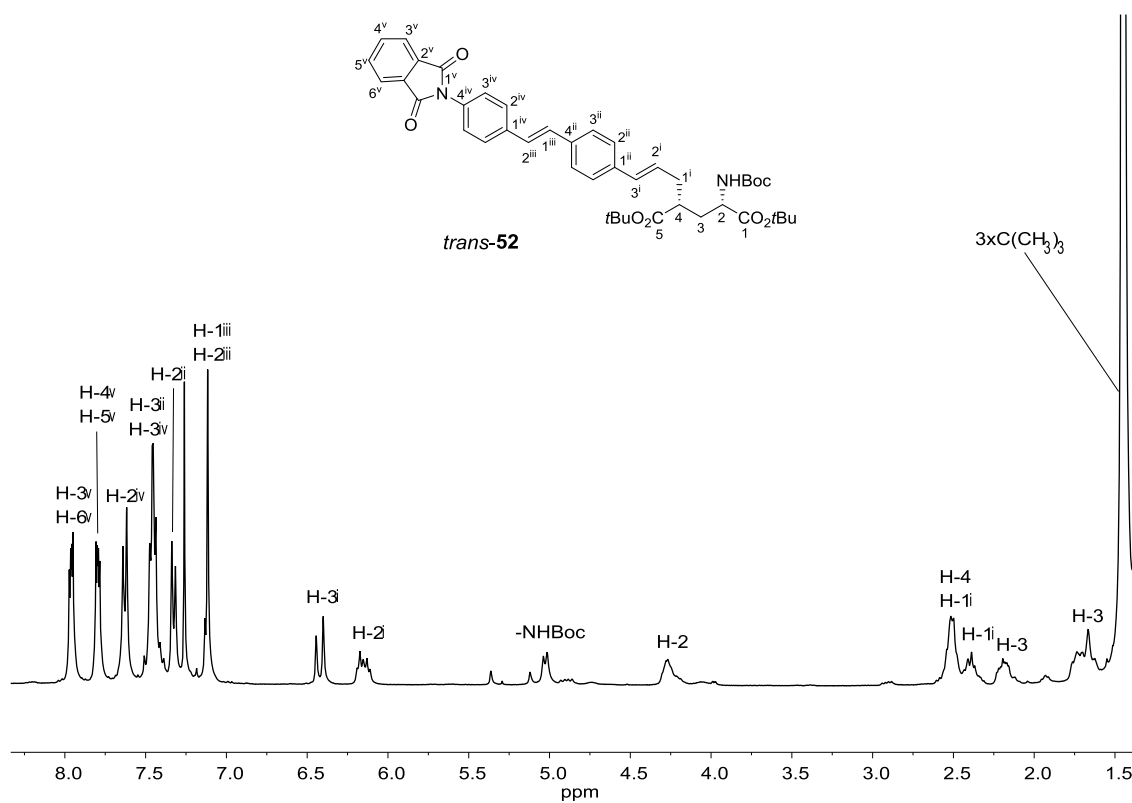
¹H NMR (250 MHz, DMSO-*d*₆)

 ^1H NMR (360 MHz, CDCl_3) ^{13}C NMR (90.5 MHz, CDCl_3)

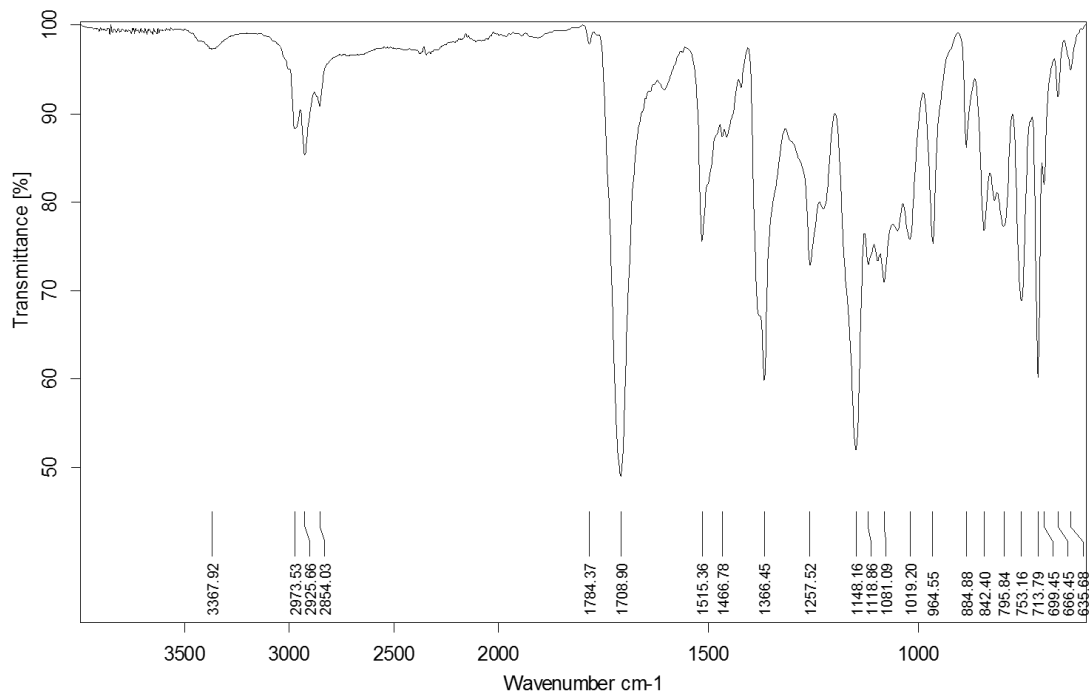
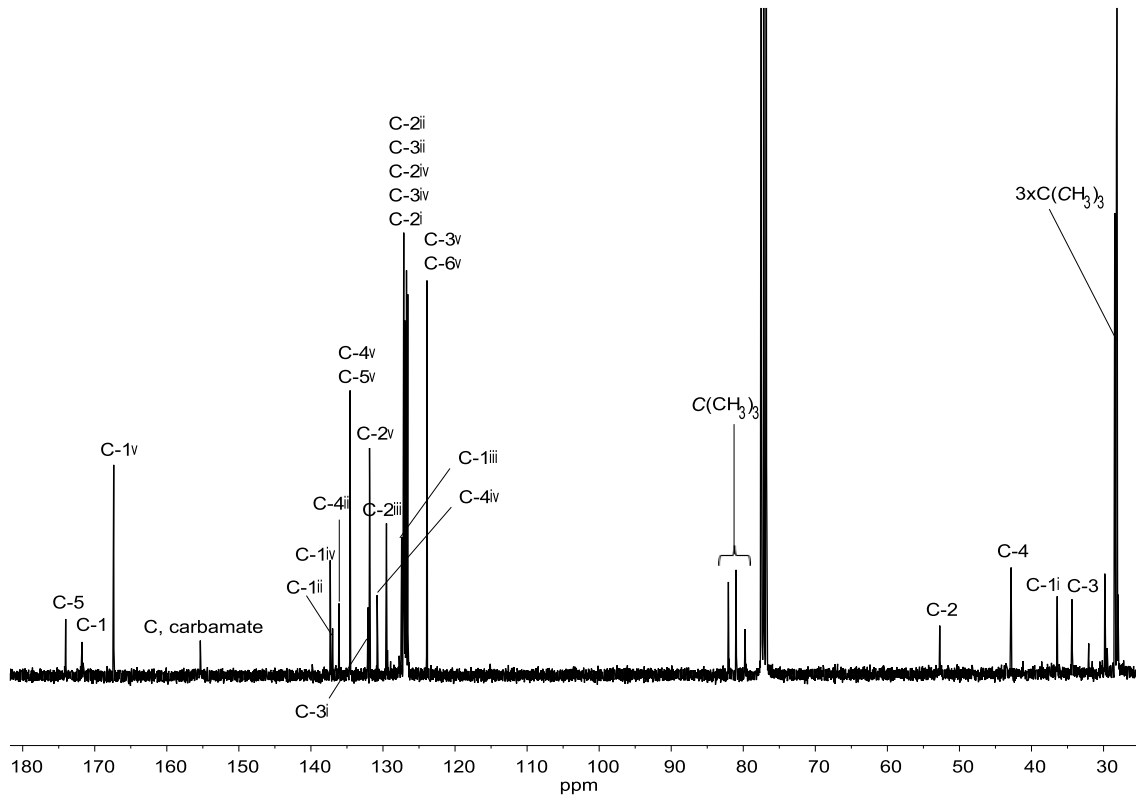
Spectra of selected compounds



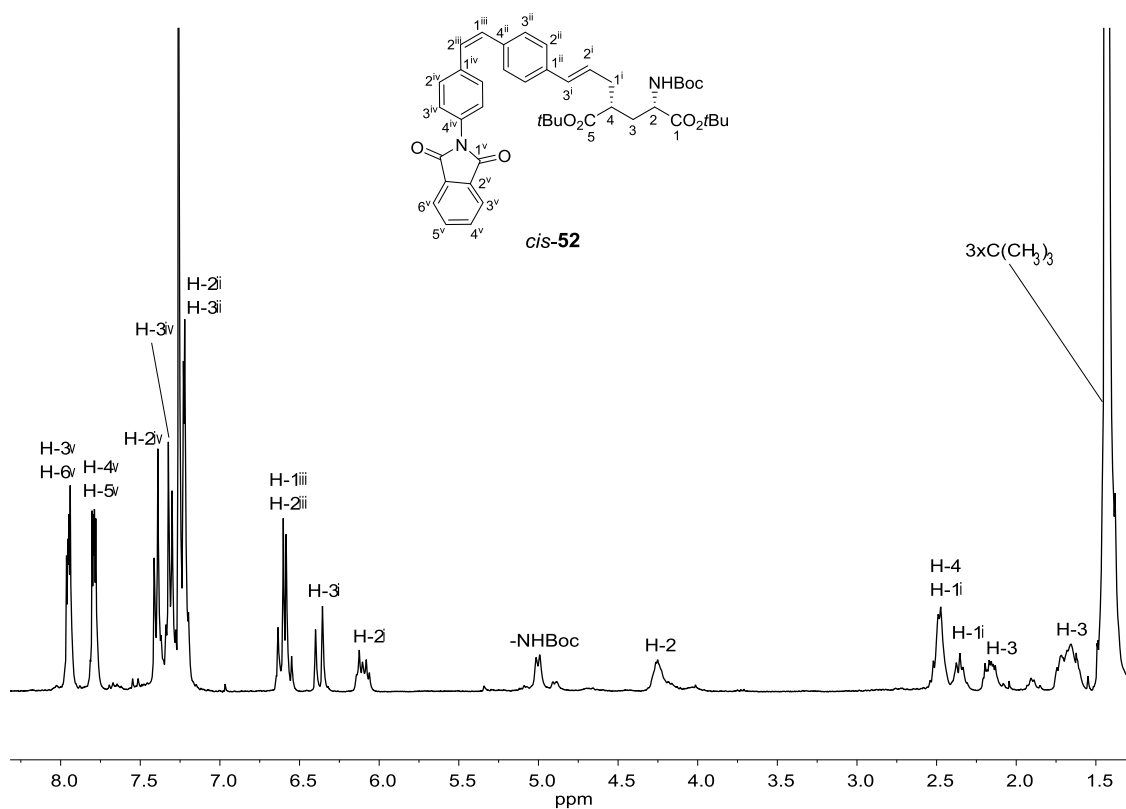
IR (ATR)



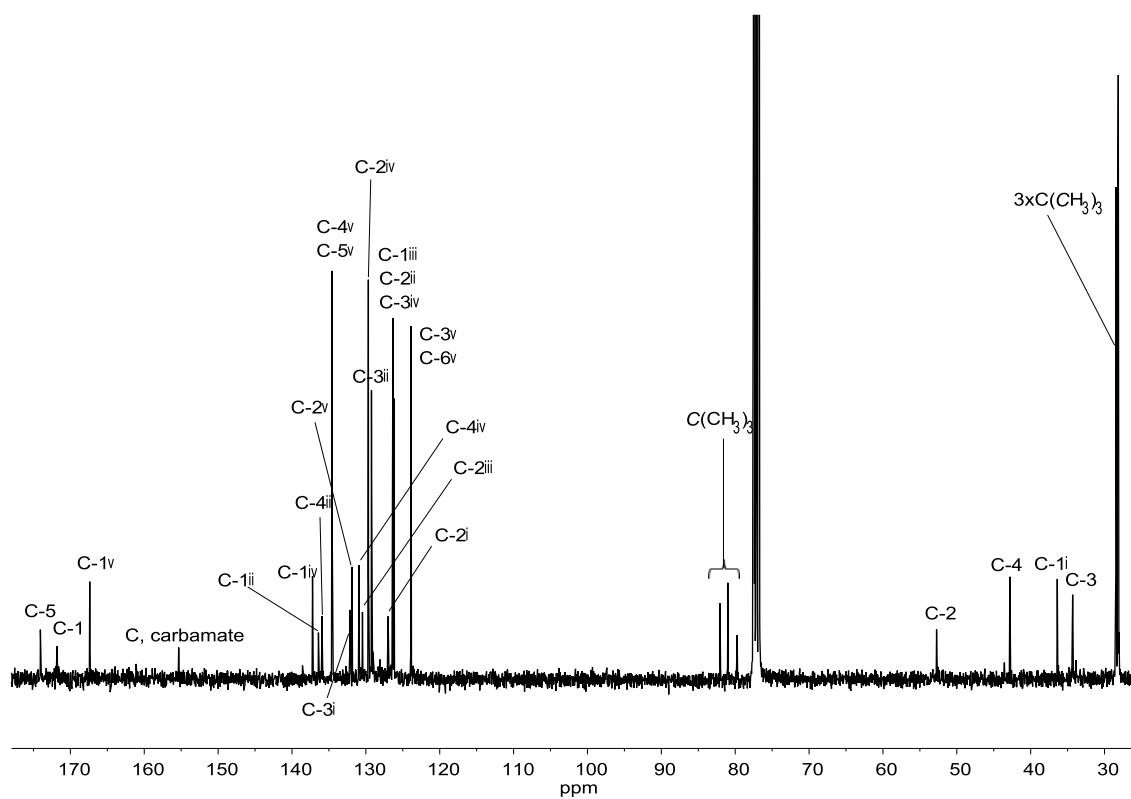
¹H NMR (360 MHz, CDCl₃)



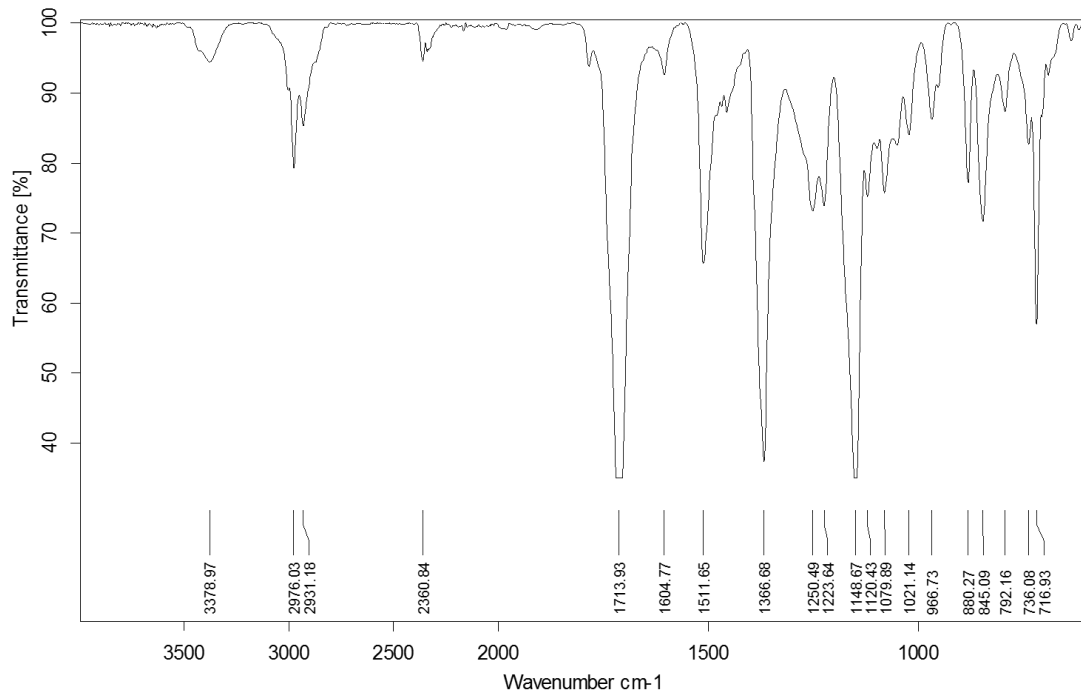
Spectra of selected compounds



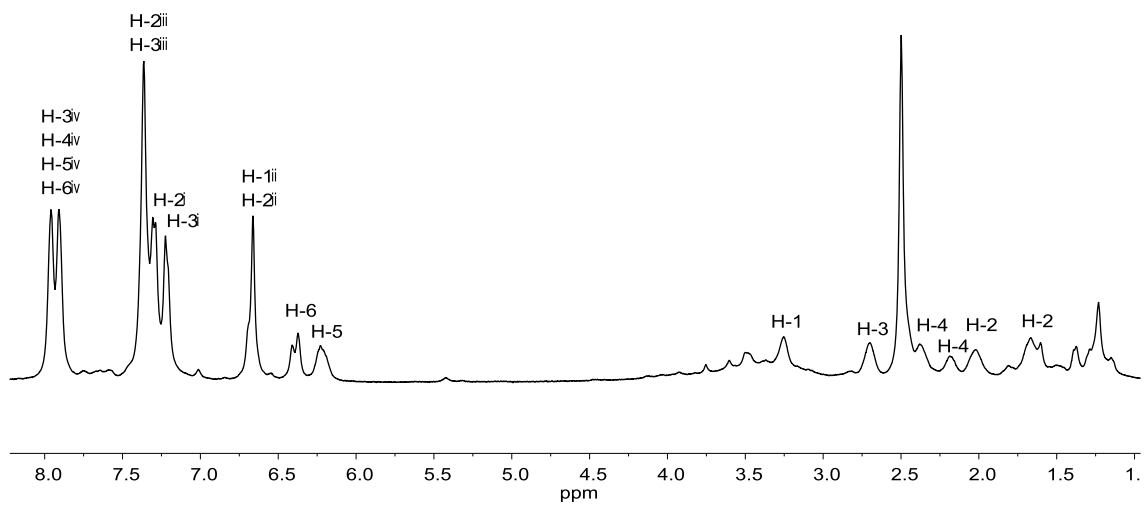
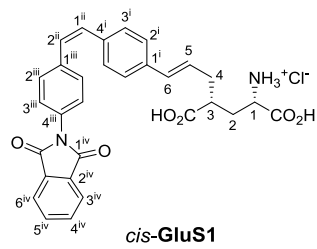
¹H NMR (360 MHz, CDCl₃)



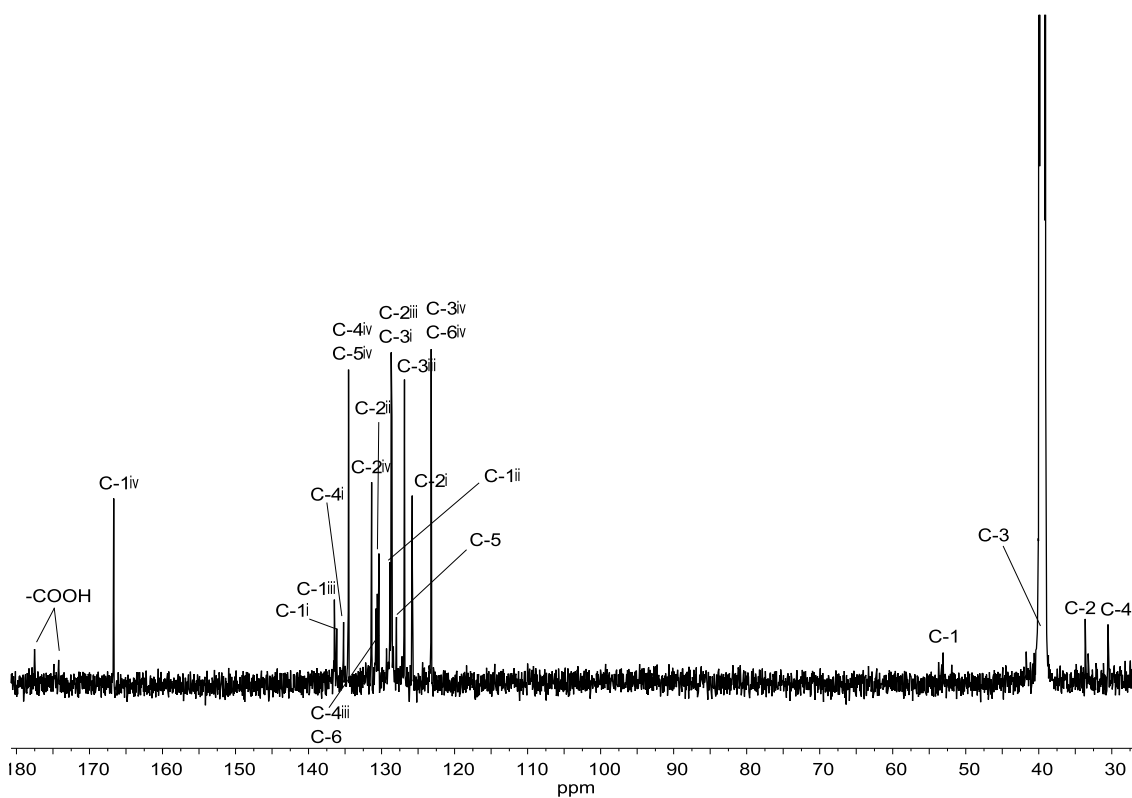
¹³C NMR (90.5 MHz, CDCl₃)



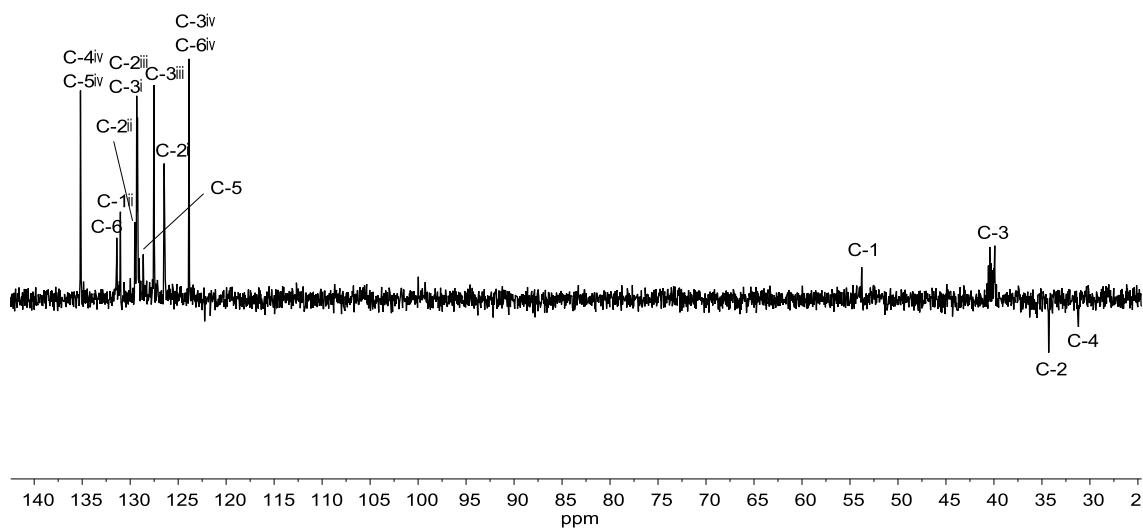
IR (ATR)

¹H NMR (400 MHz, DMSO-*d*₆)

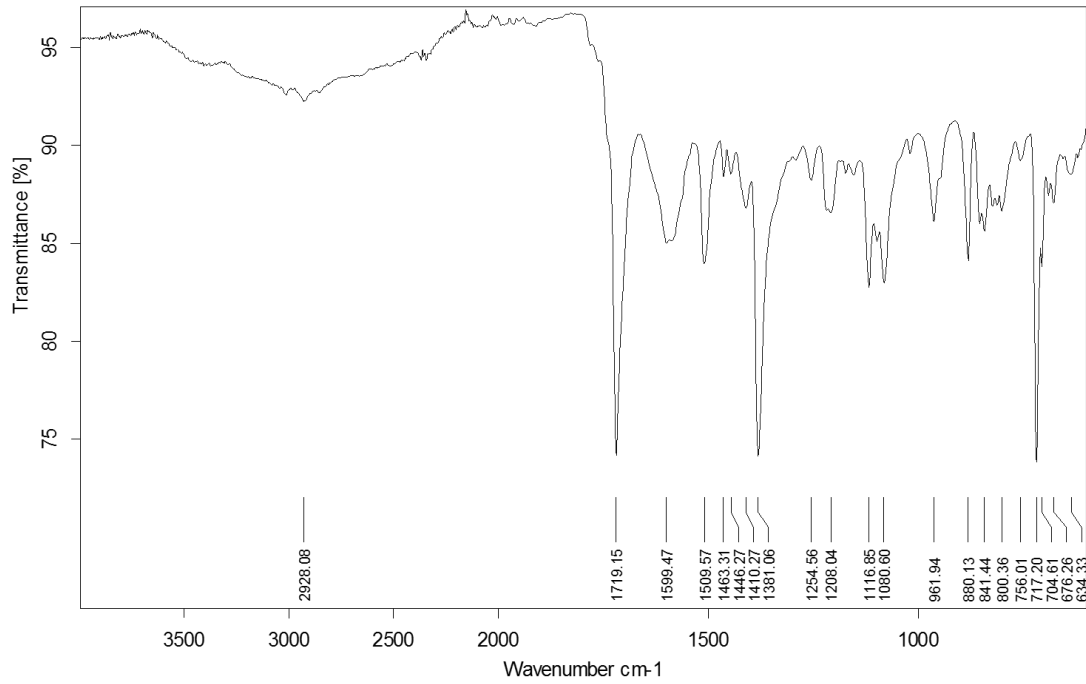
Spectra of selected compounds



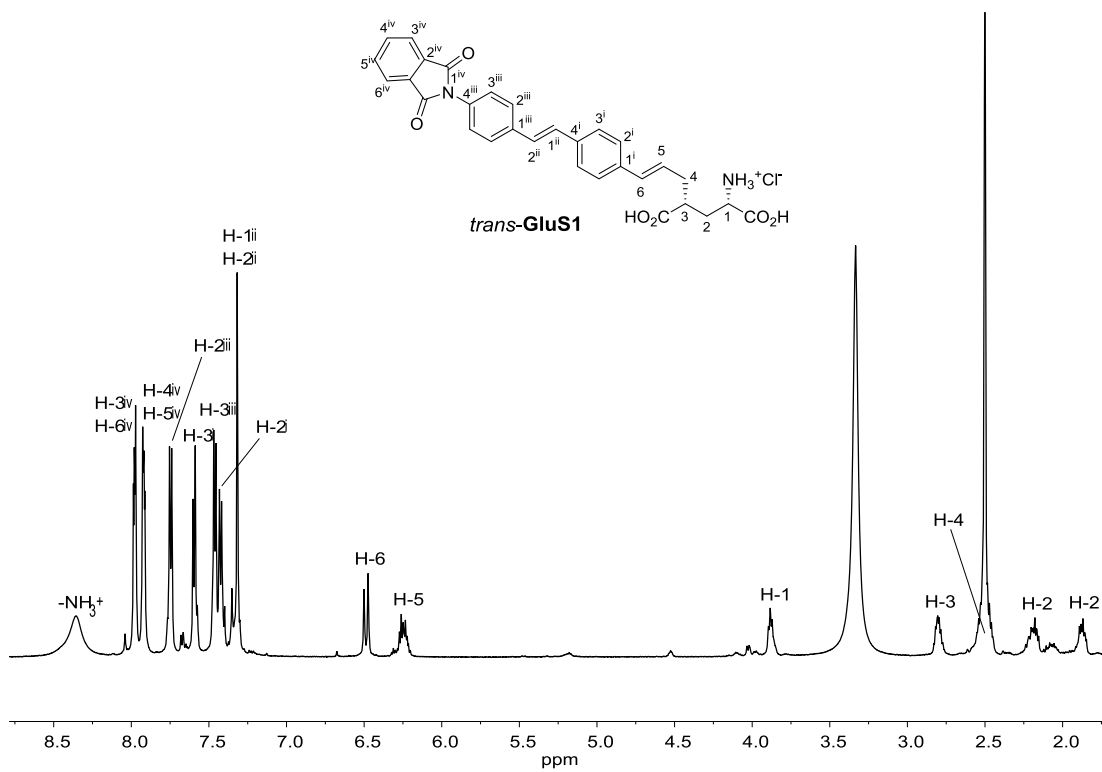
¹³C NMR (100.6 MHz, DMSO-*d*₆, 320 K)



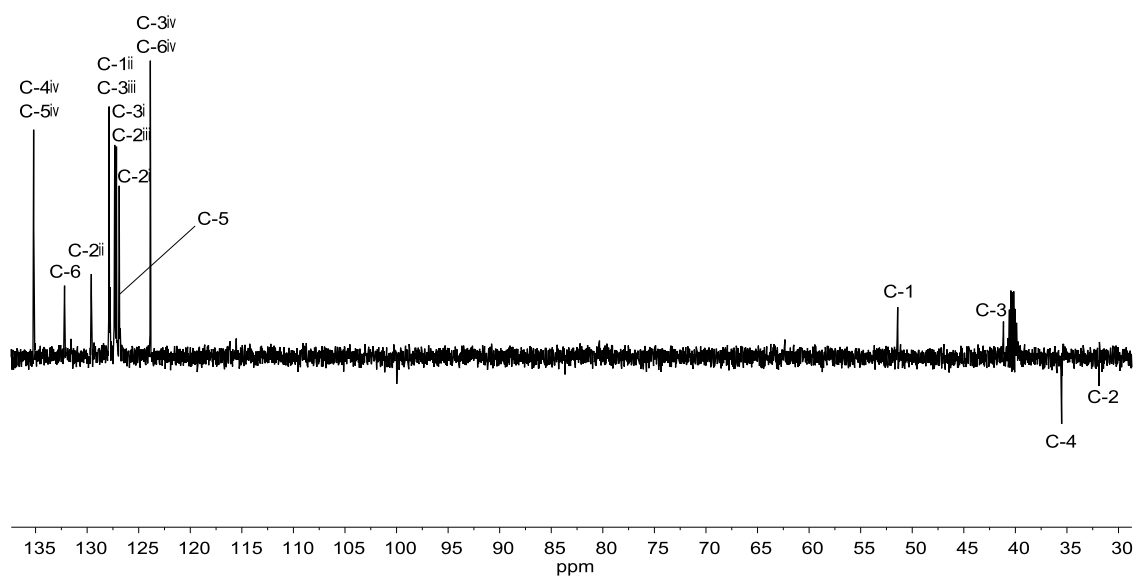
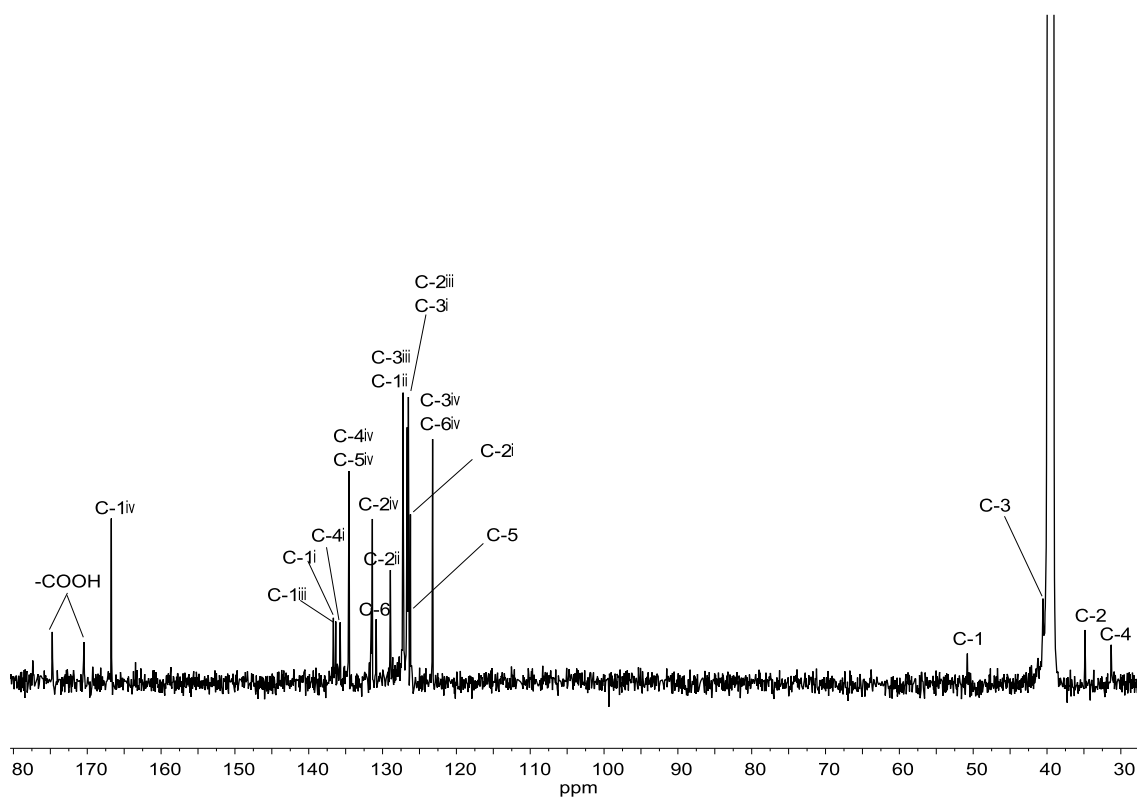
DEPT135 (90.5 MHz, DMSO-*d*₆, 320 K)

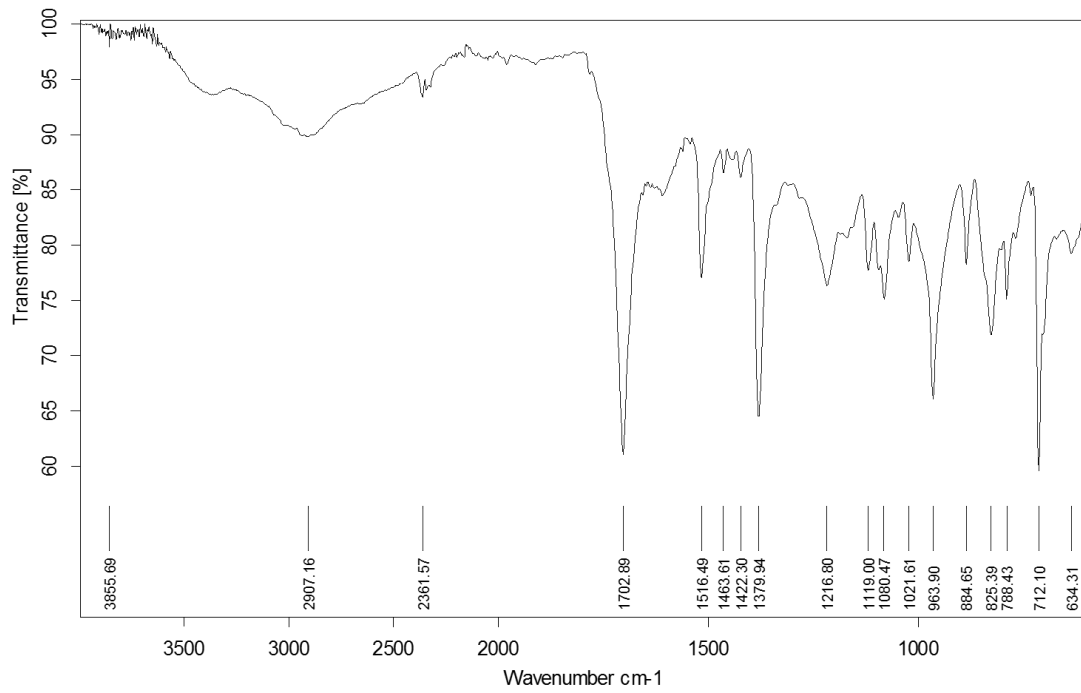


IR (ATR)

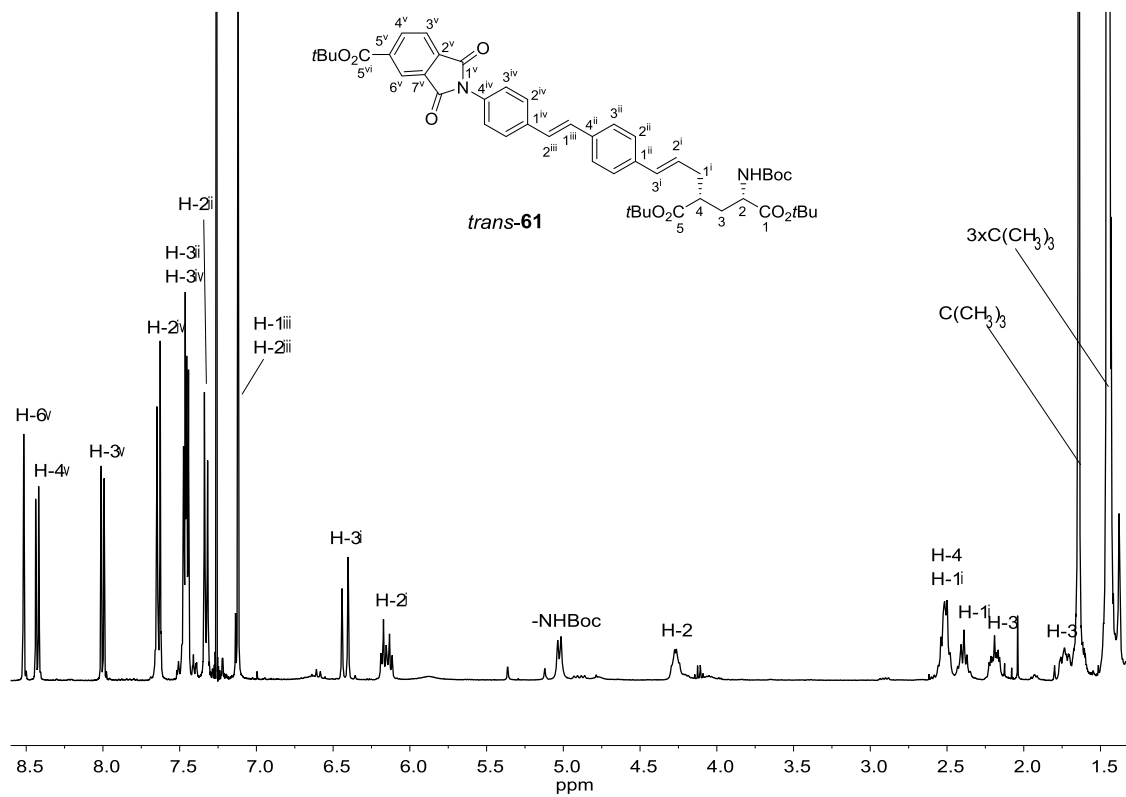
¹H NMR (400 MHz, DMSO-*d*₆, 320 K)

Spectra of selected compounds

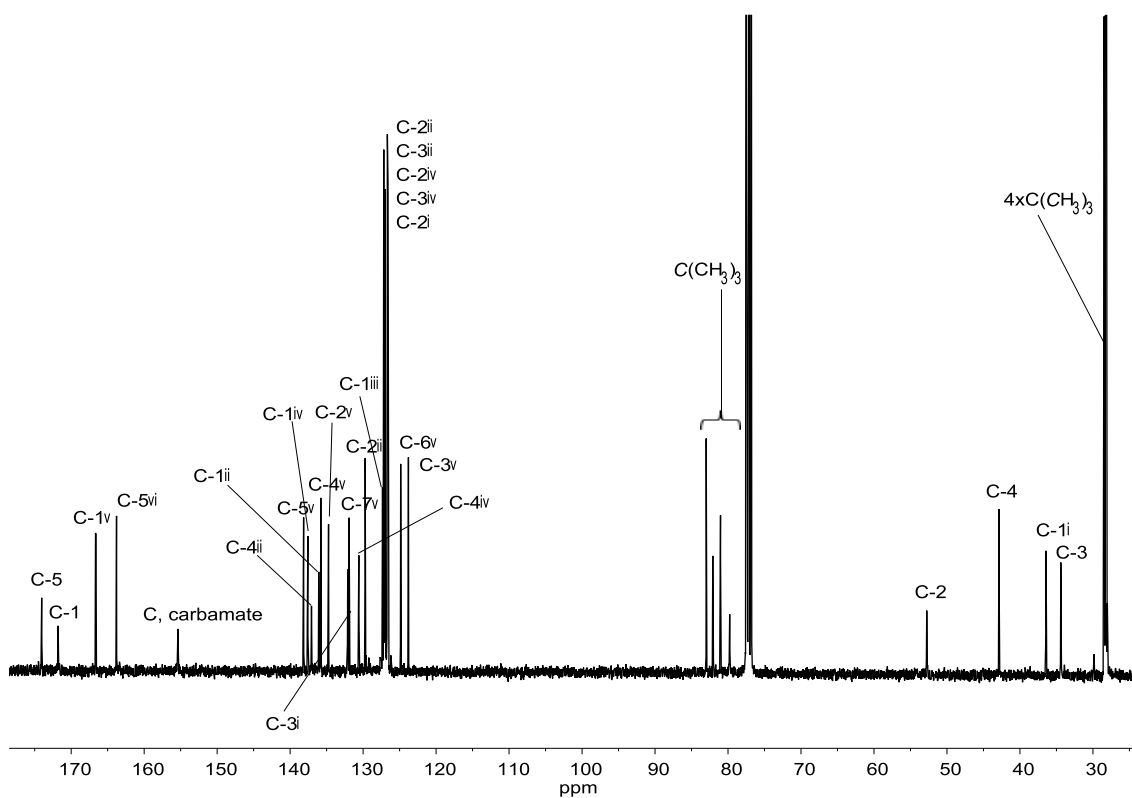




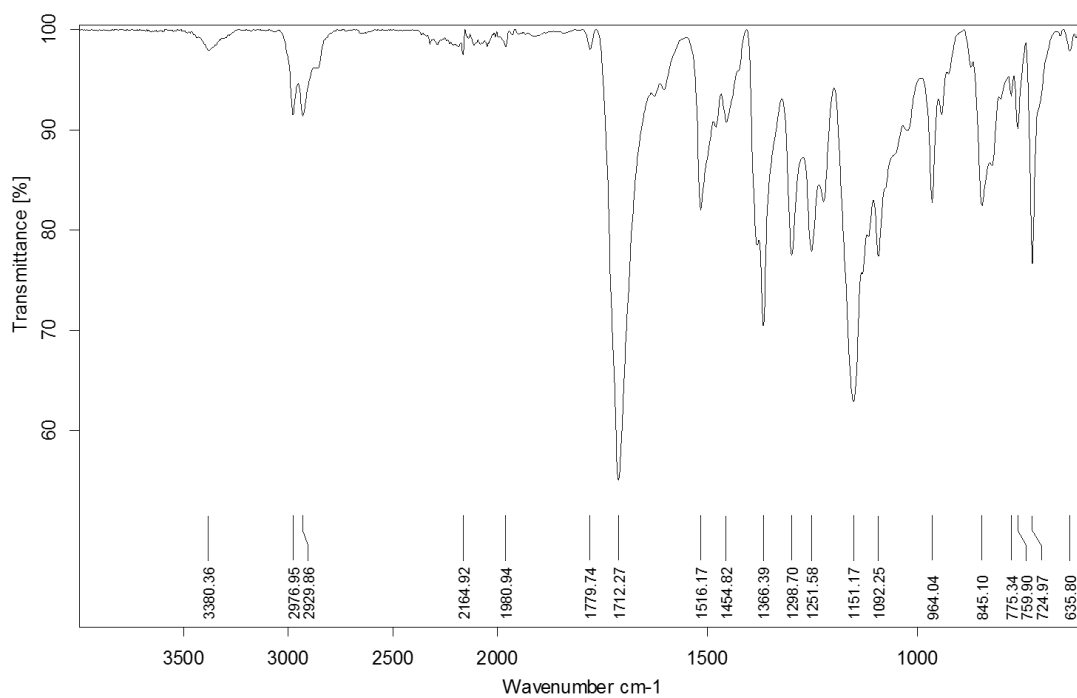
IR (ATR)

¹H NMR (400 MHz, CDCl₃)

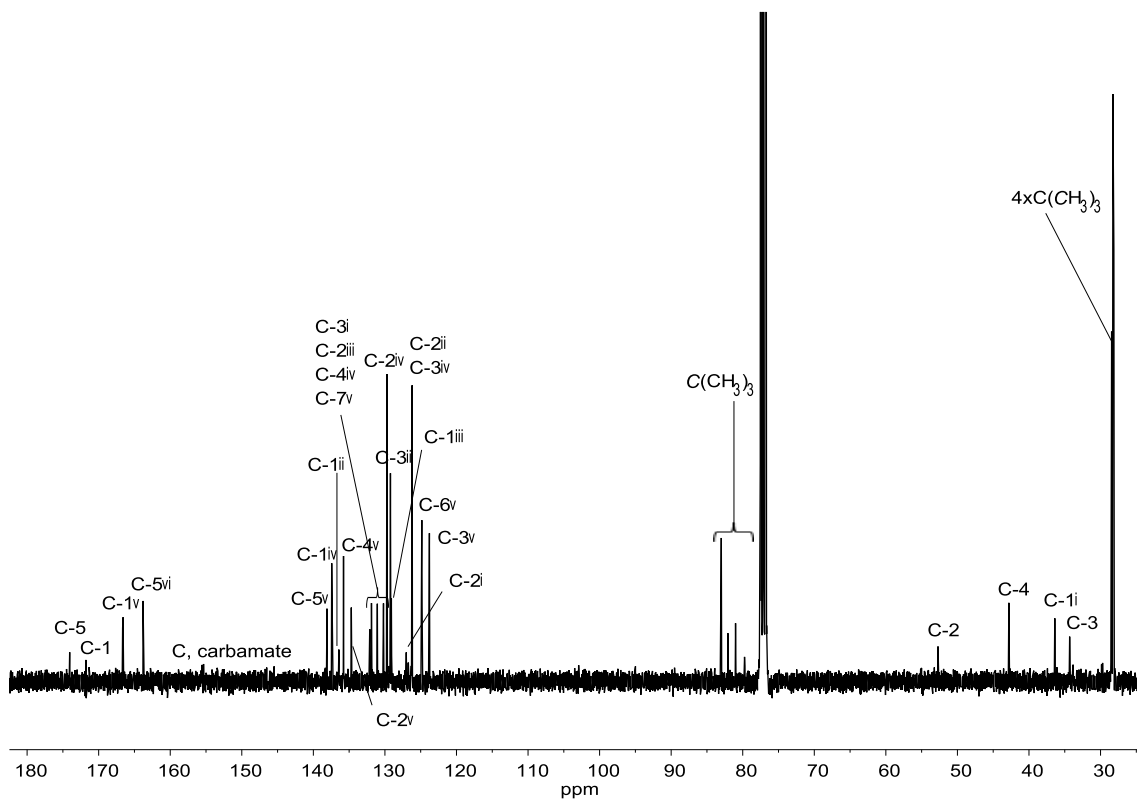
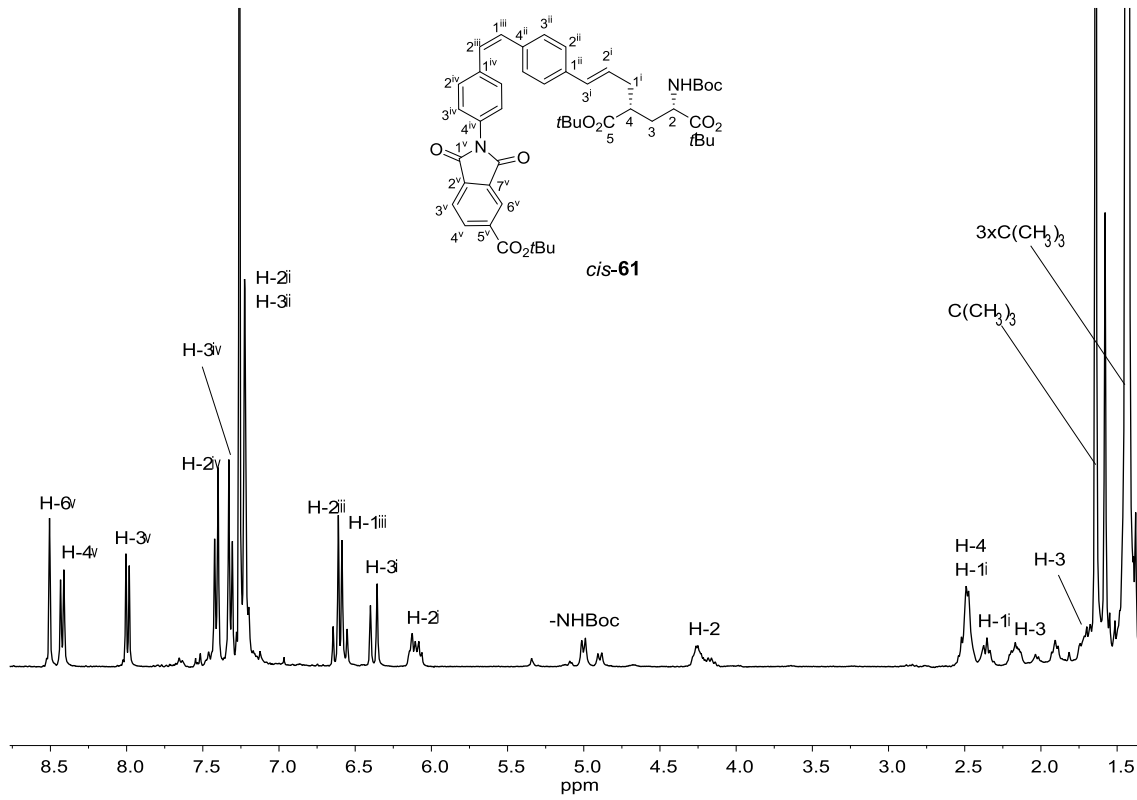
Spectra of selected compounds



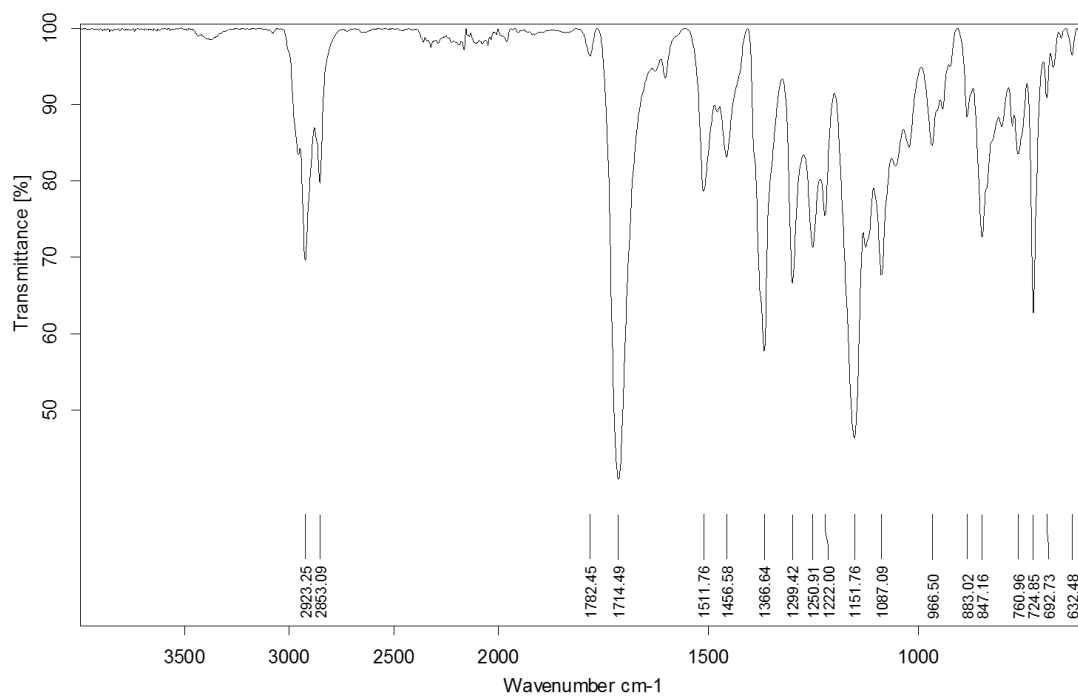
^{13}C NMR (100.6 MHz, CDCl₃)



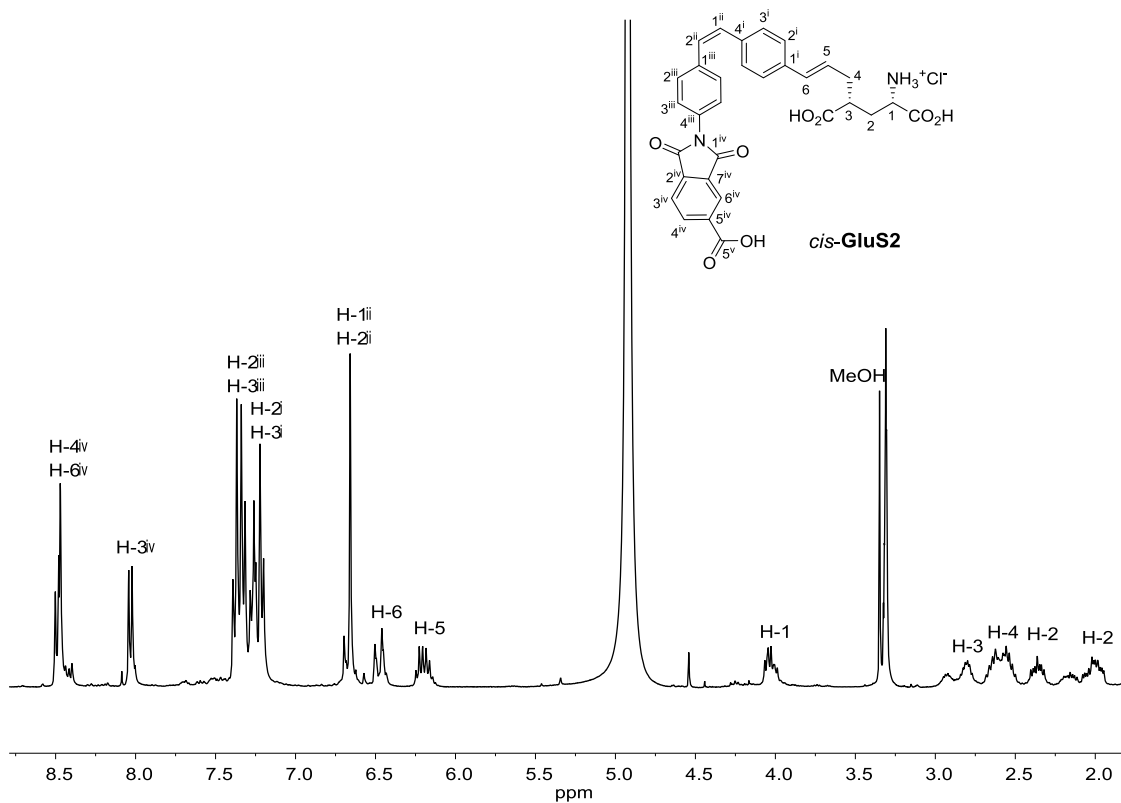
IR (ATR)



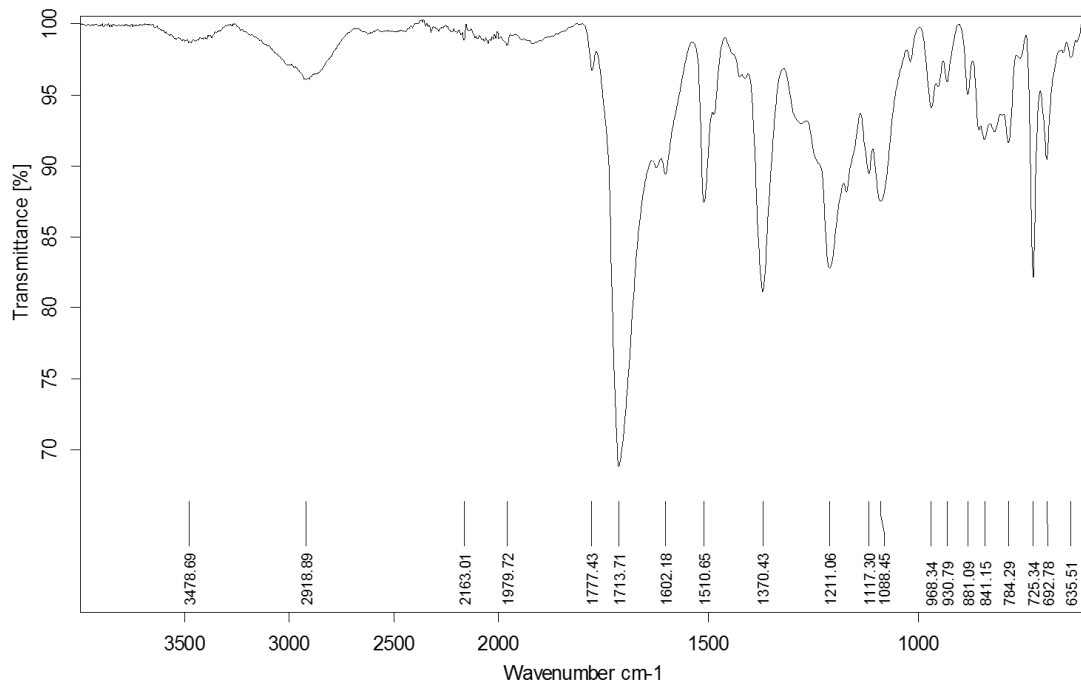
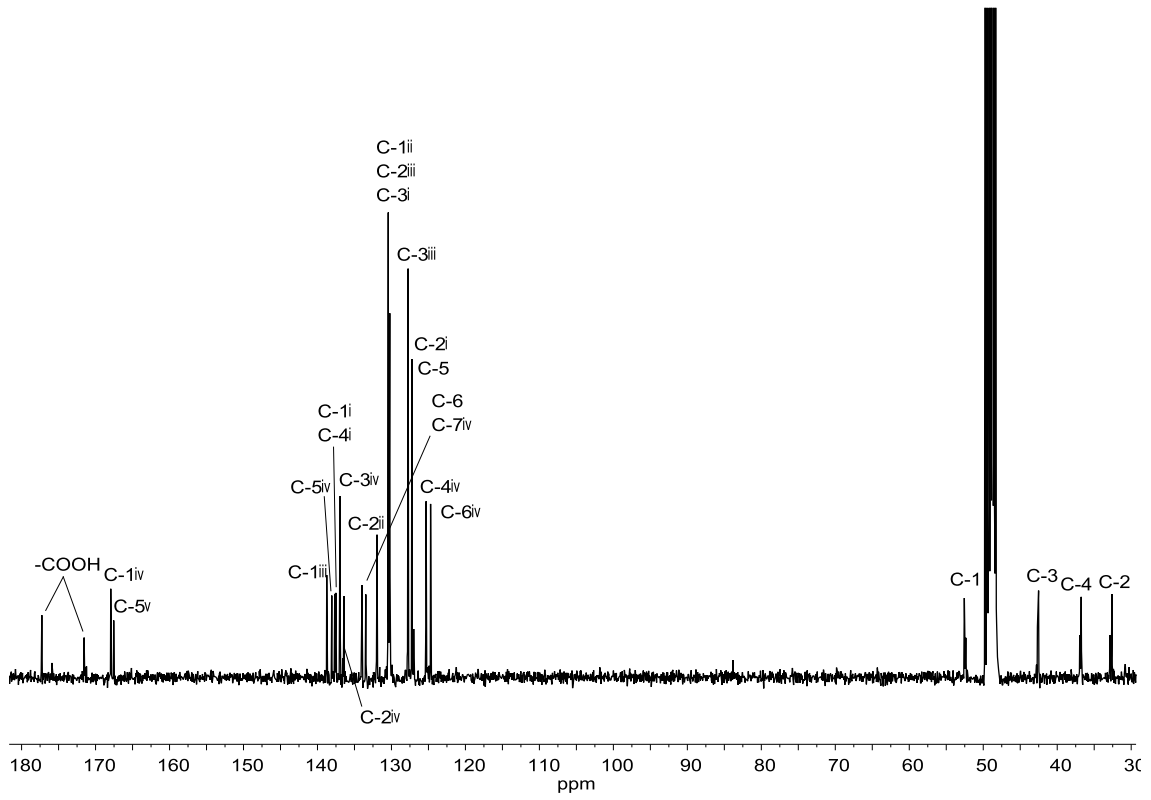
Spectra of selected compounds



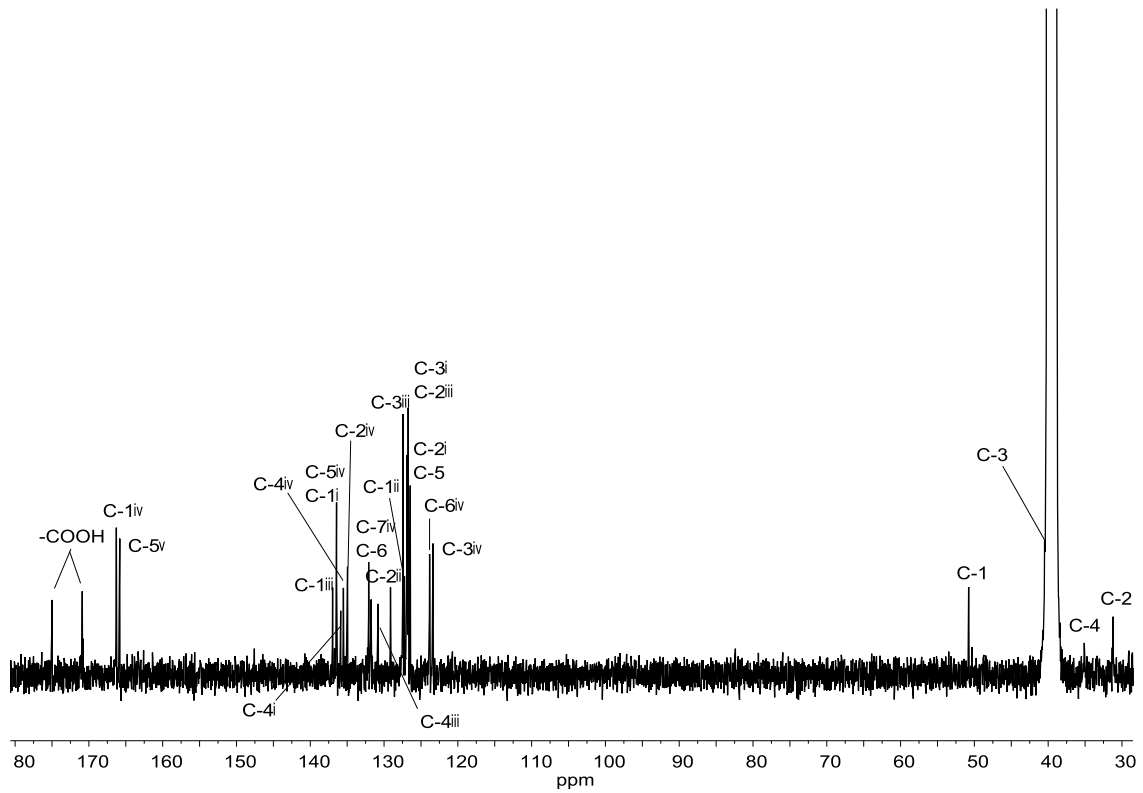
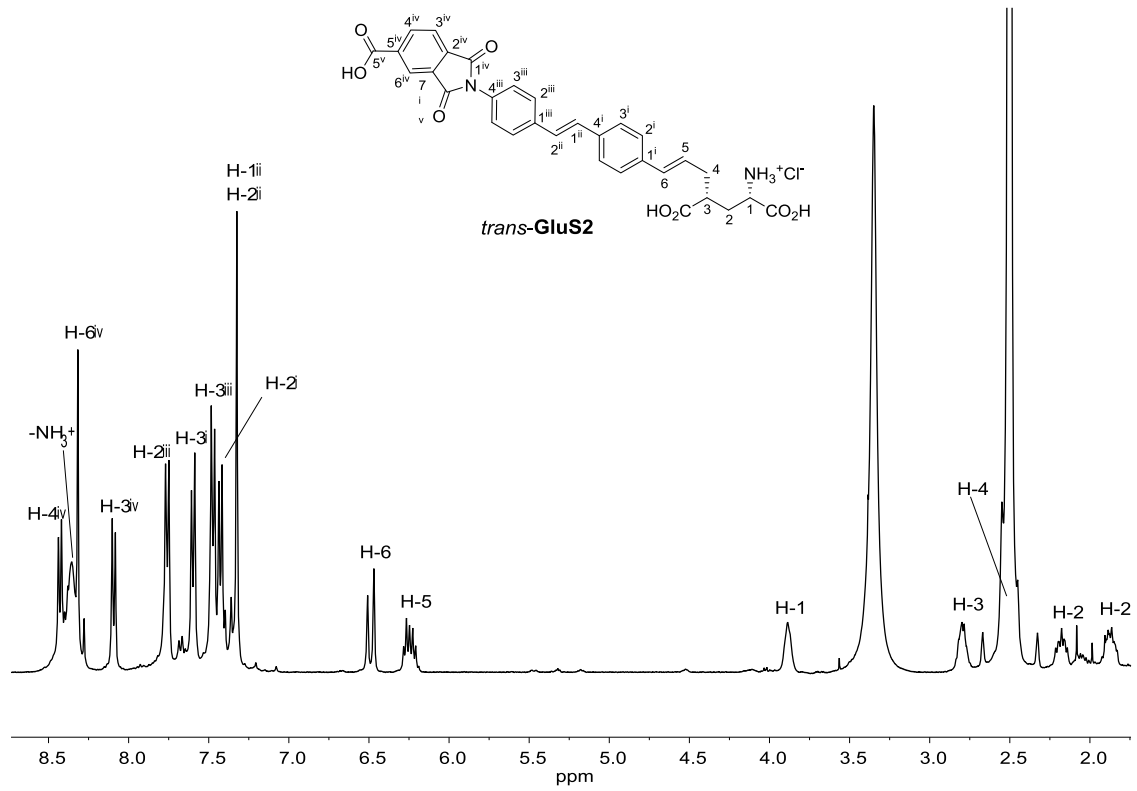
IR (ATR)



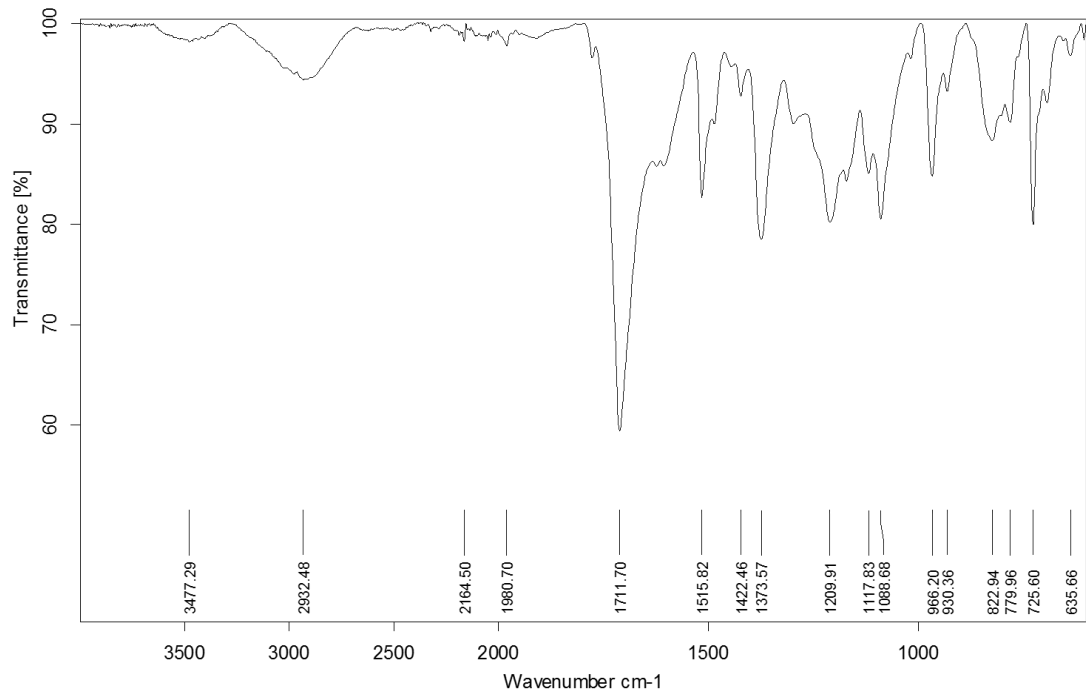
¹H NMR (360 MHz, MeOH-*d*₄)



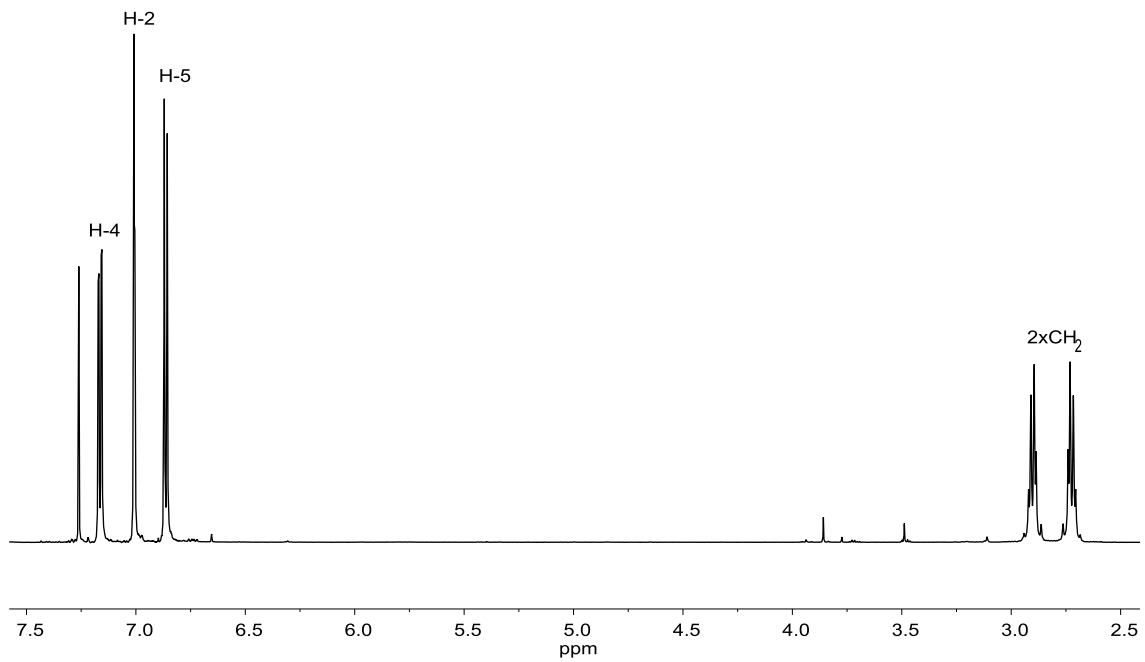
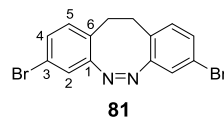
Spectra of selected compounds



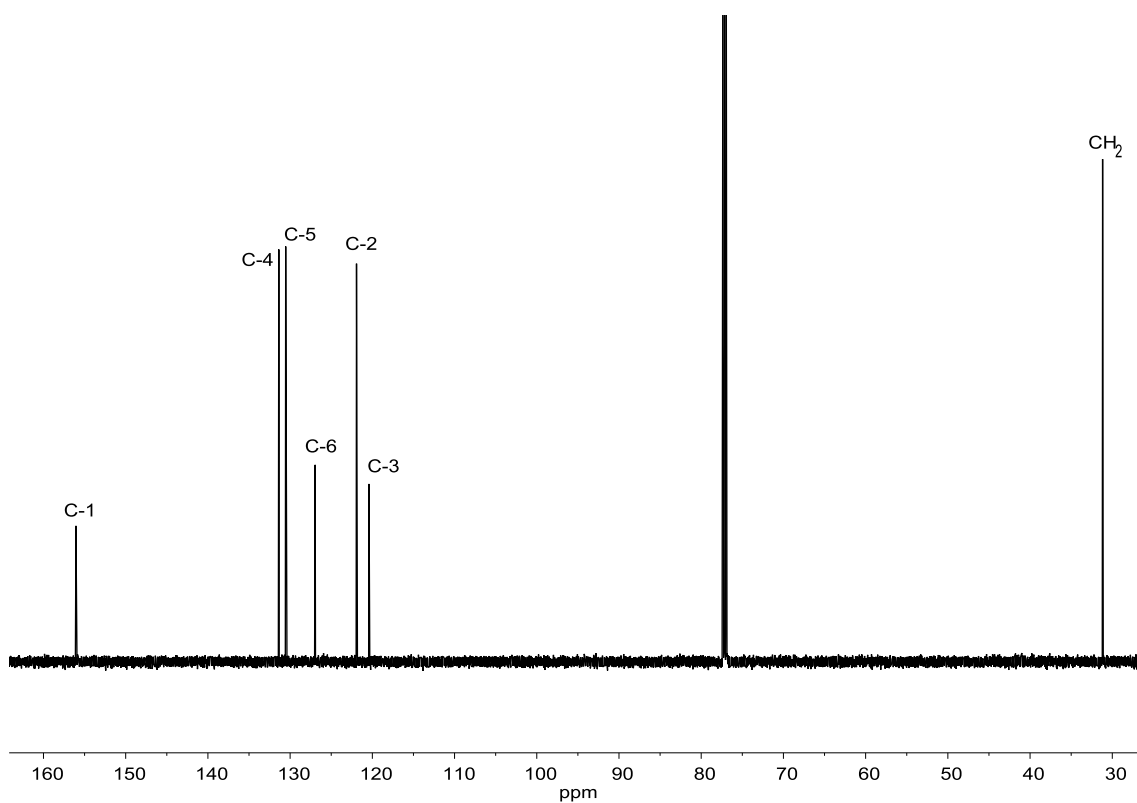
$^{13}\text{C NMR}$ (100.6 MHz, $\text{DMSO-}d_6$)



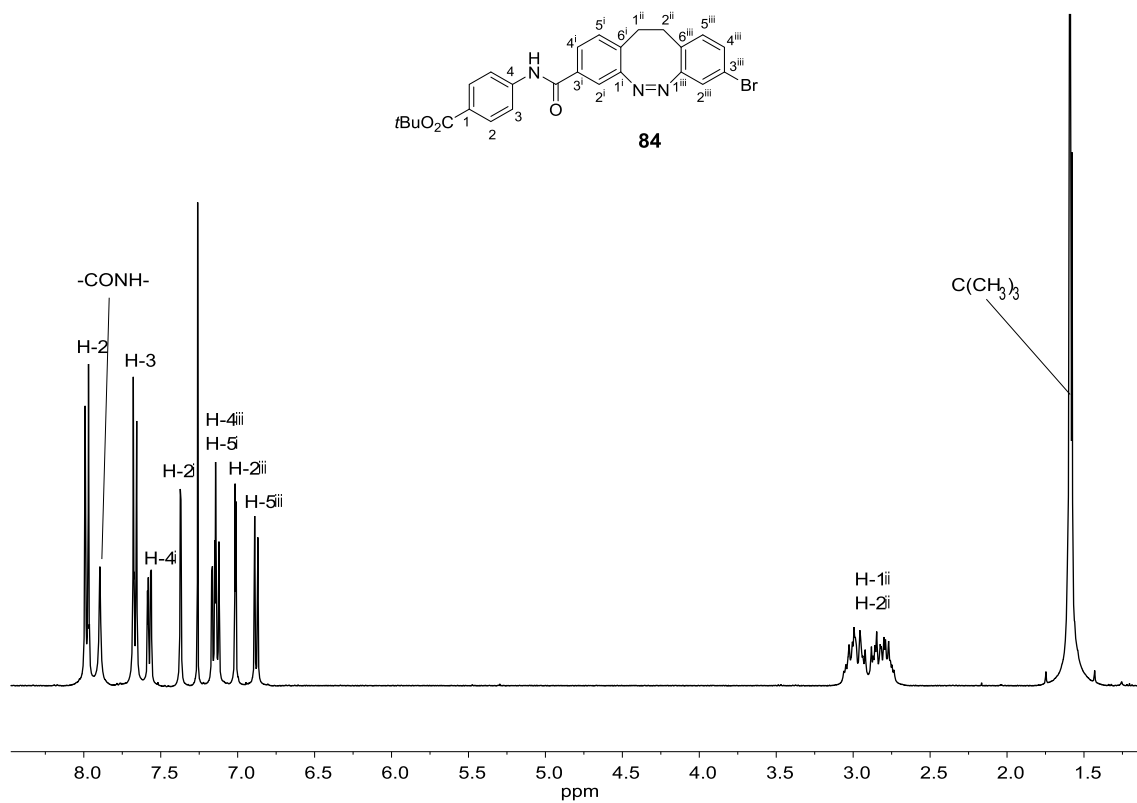
IR (ATR)

¹H NMR (500 MHz, CDCl₃)

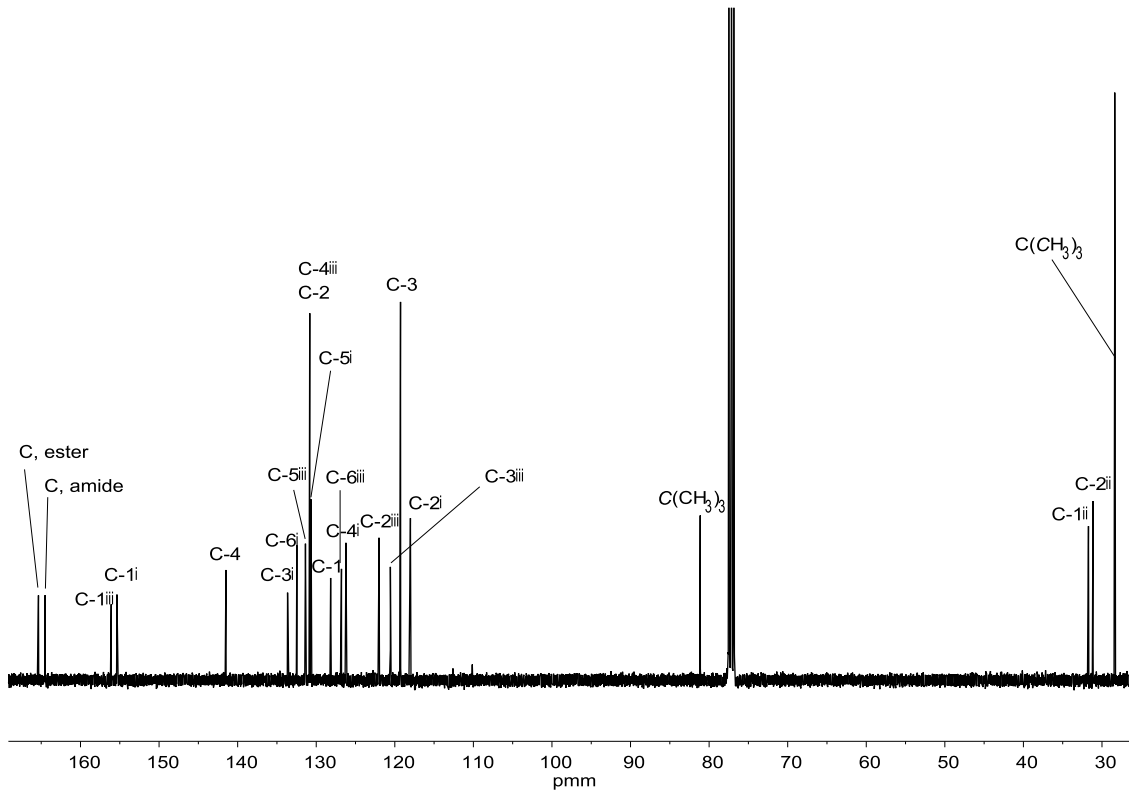
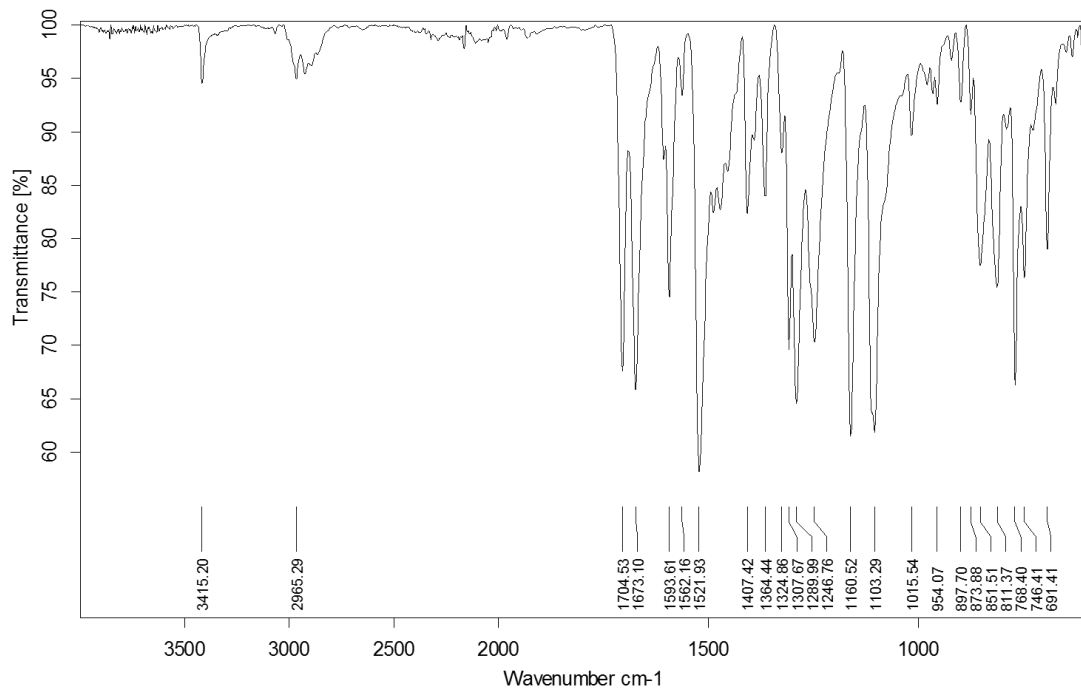
Spectra of selected compounds



^{13}C NMR (125.8 MHz, CDCl_3)

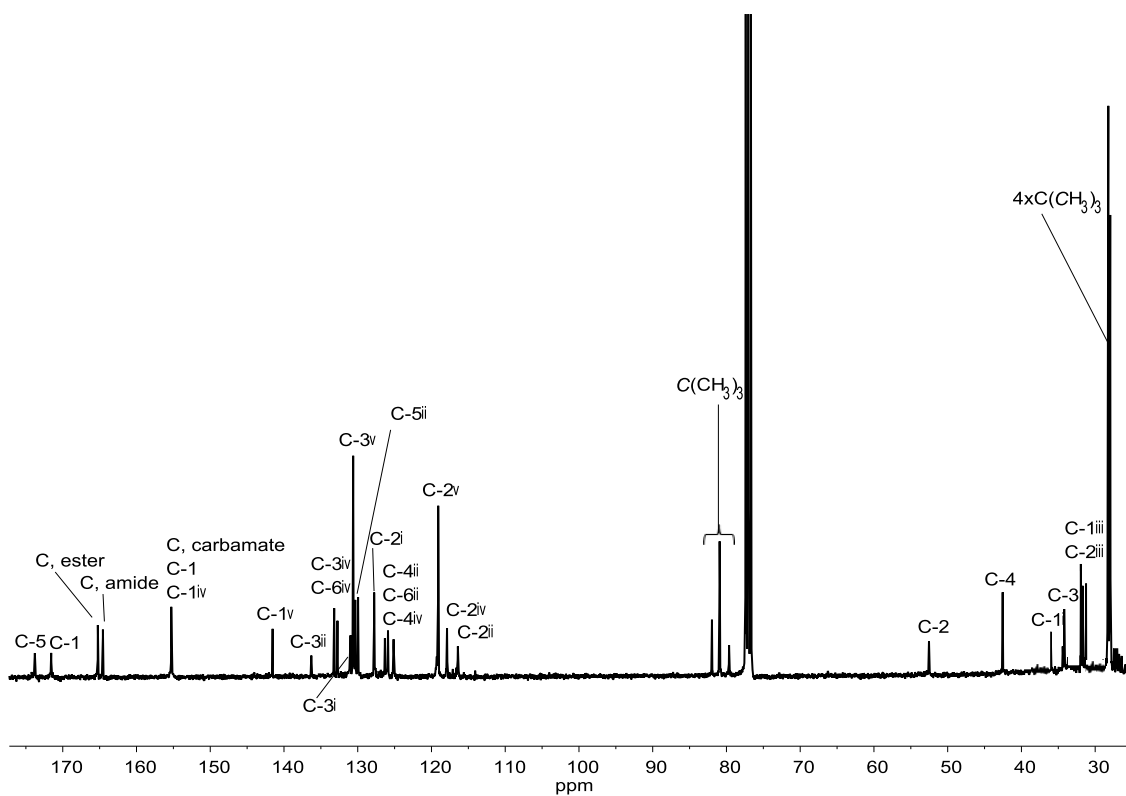
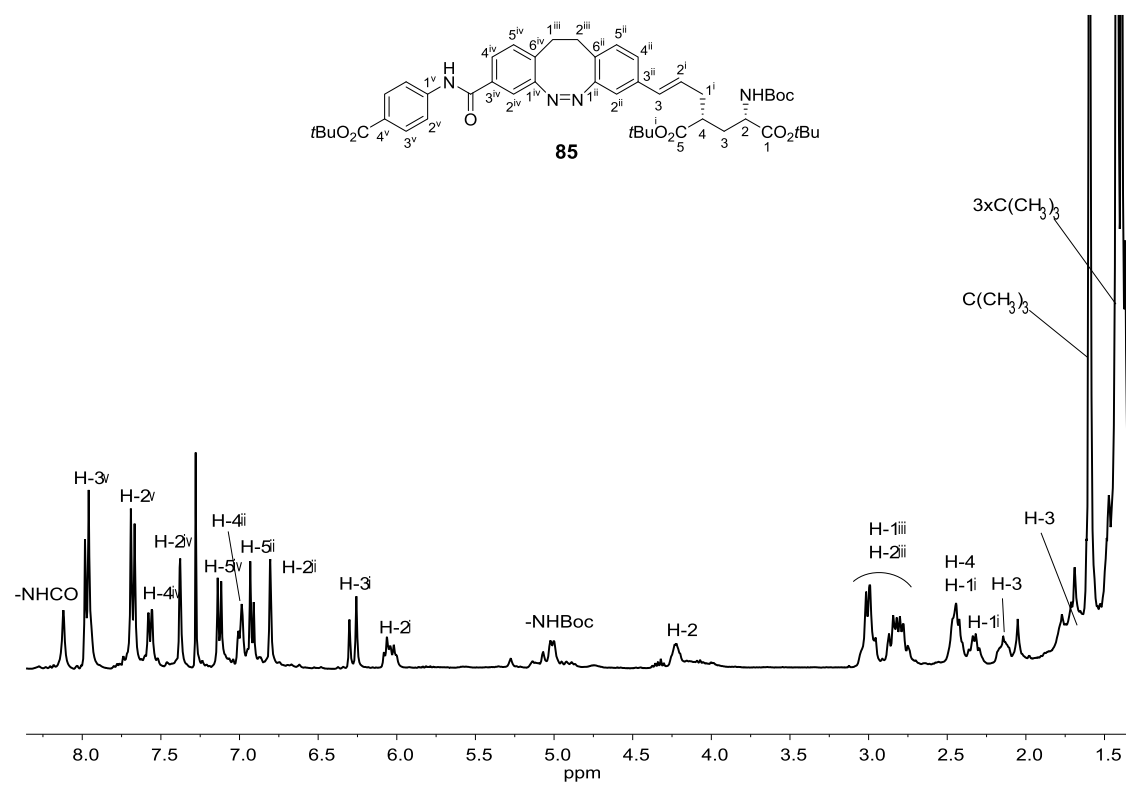


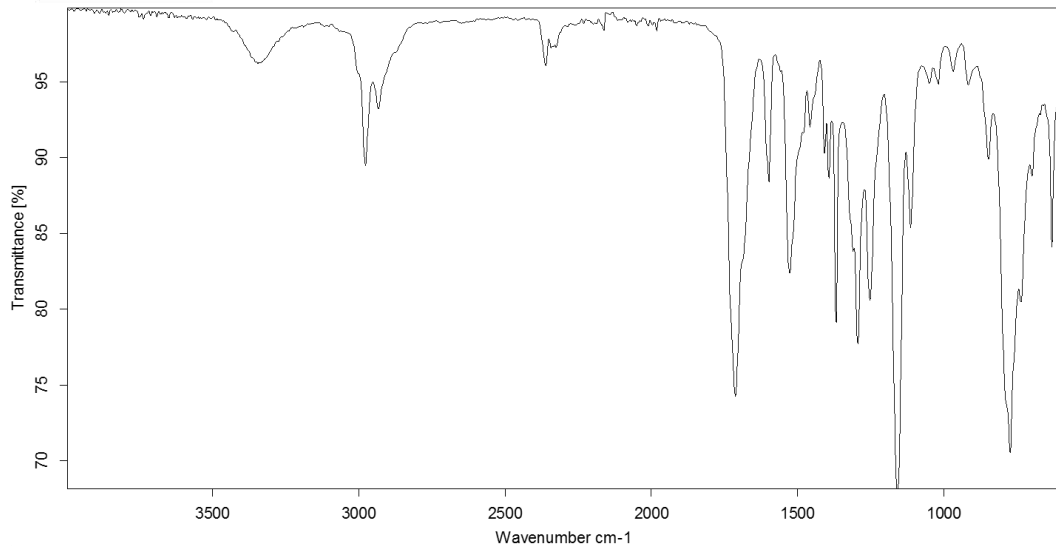
^1H NMR (400 MHz, CDCl_3)

 ^{13}C NMR (100.6 MHz, CDCl_3)

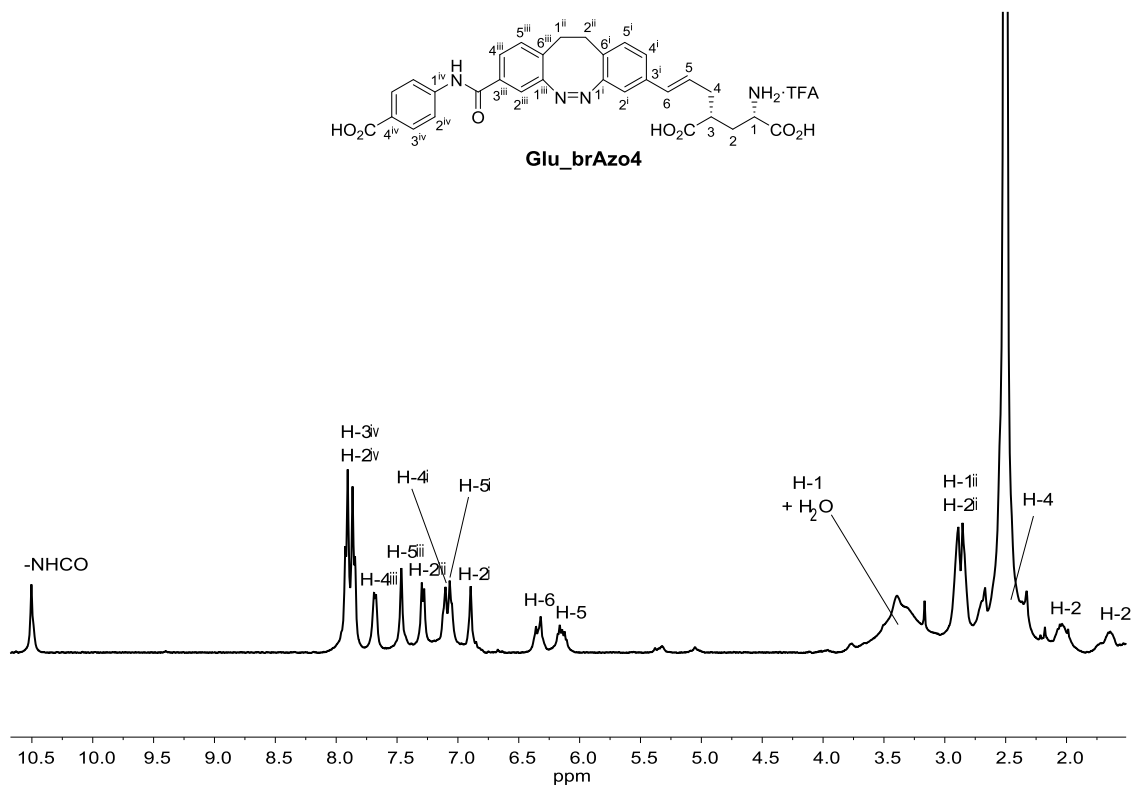
IR (ATR)

Spectra of selected compounds

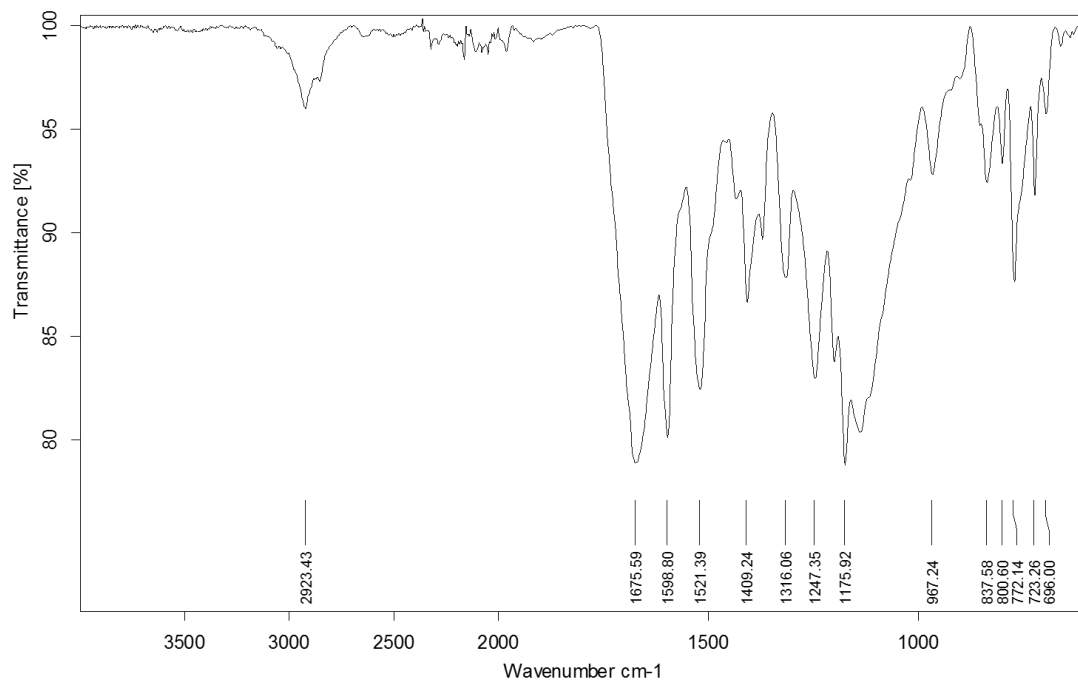
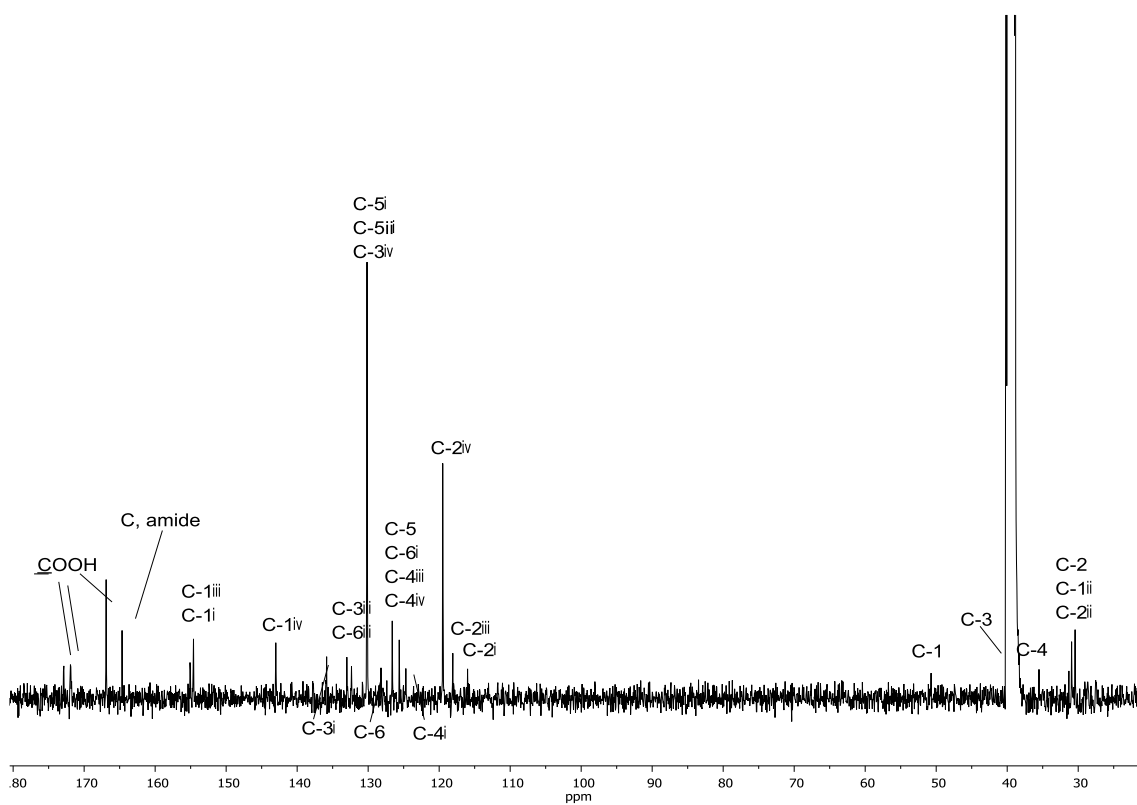


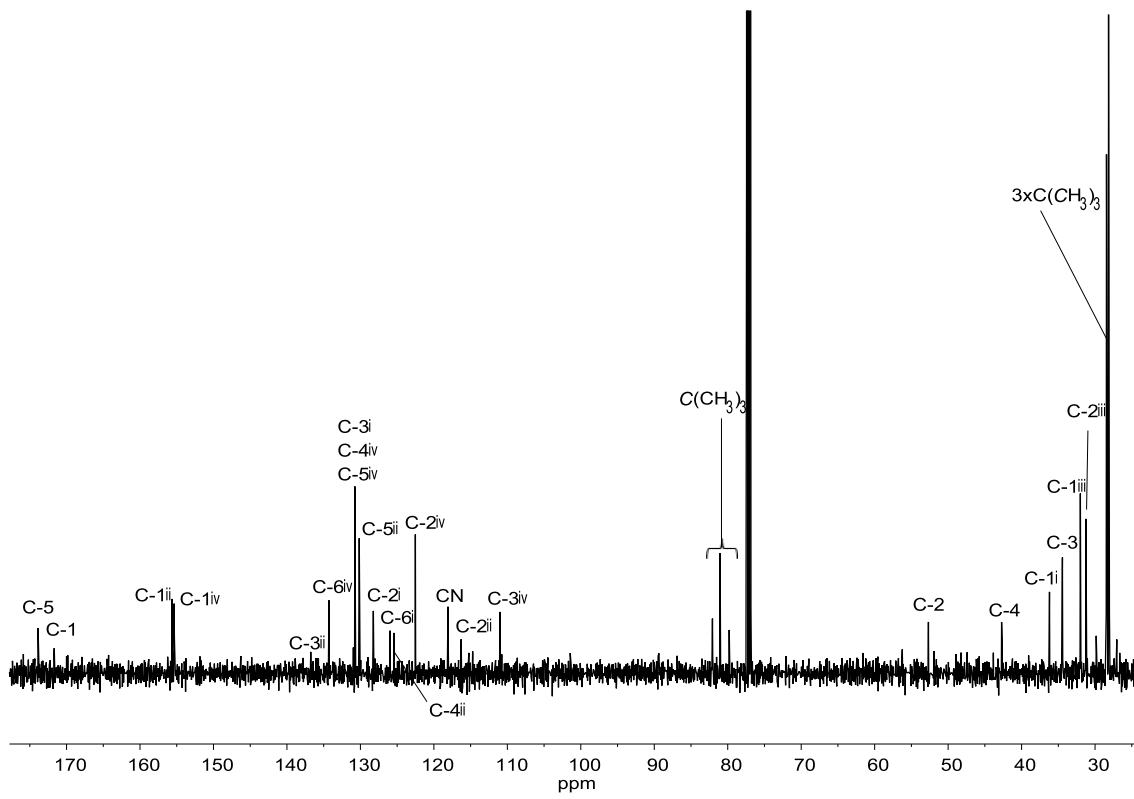
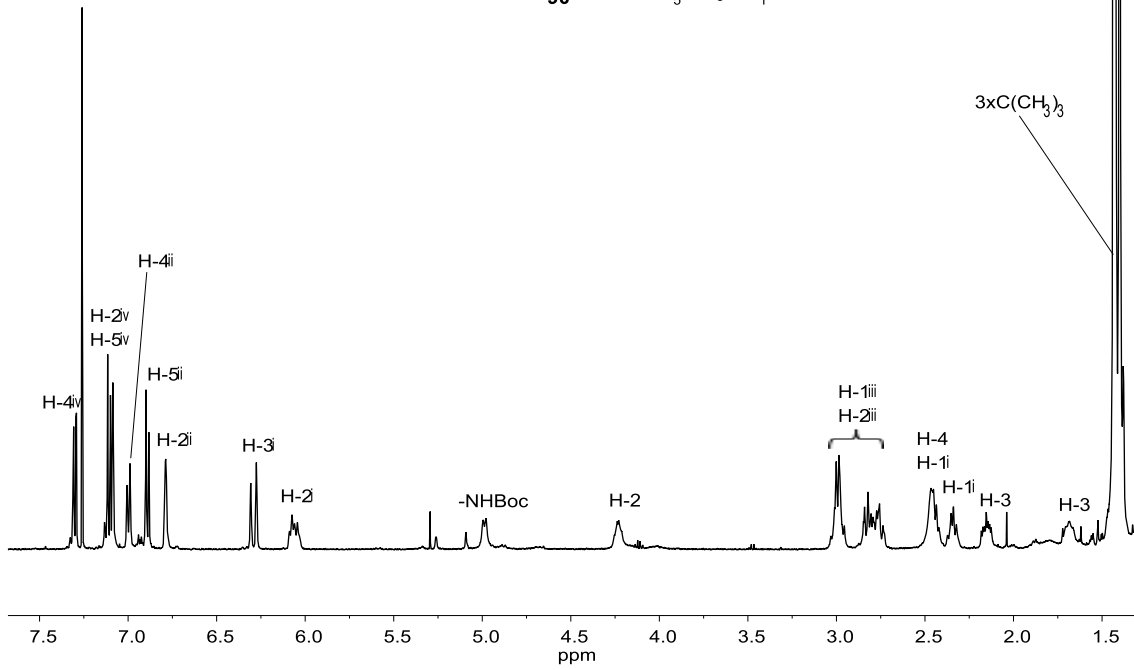
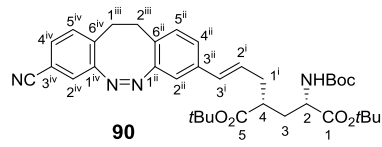


IR (ATR)

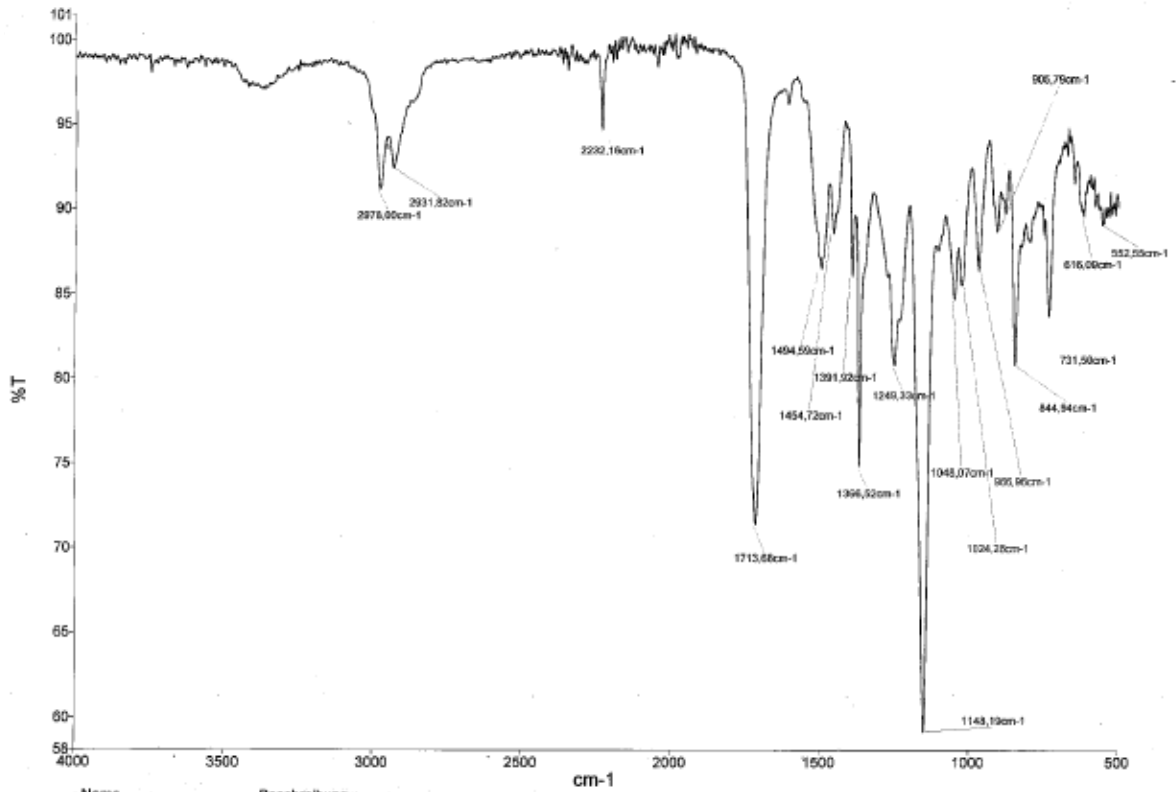
 ^1H NMR (400 MHz, $\text{DMSO-}d_6$)

Spectra of selected compounds

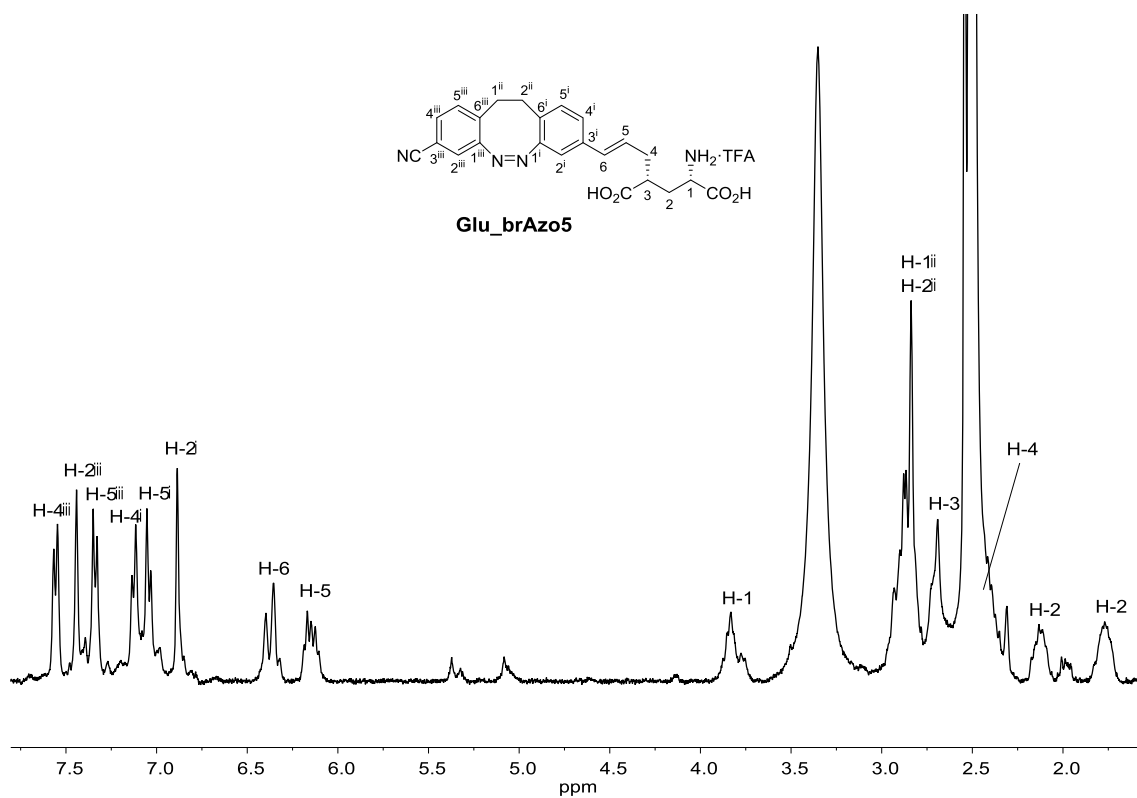




Spectra of selected compounds



IR (ATR)



^1H NMR (360 MHz, $\text{DMSO}-d_6$)

